

Old Dominion University

ODU Digital Commons

---

Civil & Environmental Engineering Theses & Dissertations

Civil & Environmental Engineering

---

Spring 2024

## Stability and Strength of Glass FRP Beam-Columns with Biaxial Bending and Torsion Including Shear and Warping Deformations

Emad M. Amin

*Old Dominion University*, [emadva@icloud.com](mailto:emadva@icloud.com)

Follow this and additional works at: [https://digitalcommons.odu.edu/cee\\_etds](https://digitalcommons.odu.edu/cee_etds)



Part of the [Civil Engineering Commons](#), and the [Scandinavian Studies Commons](#)

---

### Recommended Citation

Amin, Emad M.. "Stability and Strength of Glass FRP Beam-Columns with Biaxial Bending and Torsion Including Shear and Warping Deformations" (2024). Doctor of Philosophy (PhD), Thesis, Civil & Environmental Engineering, Old Dominion University, DOI: 10.25777/fkwj-tm57  
[https://digitalcommons.odu.edu/cee\\_etds/210](https://digitalcommons.odu.edu/cee_etds/210)

This Thesis is brought to you for free and open access by the Civil & Environmental Engineering at ODU Digital Commons. It has been accepted for inclusion in Civil & Environmental Engineering Theses & Dissertations by an authorized administrator of ODU Digital Commons. For more information, please contact [digitalcommons@odu.edu](mailto:digitalcommons@odu.edu).

**STABILITY AND STRENGTH OF GLASS FRP BEAM-COLUMNS WITH  
BIAXIAL BENDING AND TORSION INCLUDING SHEAR AND  
WARPING DEFORMATIONS**

by

Emad M. Amin

B.S. August 1991, University of Technology-Baghdad

MBA May 2010, South University

M.S. December 2015, Old Dominion University

A Dissertation Submitted to the Faculty of  
Old Dominion University in Partial Fulfillment of the  
Requirements for the Degree of

DOCTOR OF PHILOSOPHY

CIVIL ENGINEERING

OLD DOMINION UNIVERSITY

May 2024

Approved by:

Zia Razzaq (Director)

Mojtaba B. Sirjani (Member)

Shahin N. Amiri (Member)

Herish Hussein (Member)

## ABSTRACT

### STABILITY AND STRENGTH OF GLASS FRP BEAM-COLUMNS WITH BIAXIAL BENDING AND TORSION INCLUDING SHEAR AND WARPING DEFORMATIONS

Emad M. Amin  
Old Dominion University, 2024  
Director: Dr. Zia Razzaq

Presented herein is a study of the stability and strength of pultruded glass fiber reinforced polymer (Glass FRP) beam-columns with an I-shaped cross section subjected to biaxial bending and torsion including shear and warping deformations. Three coupled differential equations of equilibrium including second-order effects and geometric imperfections are formulated and solved using a finite-difference scheme. Laboratory experiments are also conducted on glass FRP members with applied torsion; axial load; combined axial load with biaxial bending; and combined axial load, biaxial bending and torsional moment, respectively, for comparison to the theoretical predictions. The theoretical results agreed well with the experiments for the cases of the axial load and applied torsion. The theory and experiments provided nearly the same stiffness characteristics for the members under combined axial load, bending moments, and torsional loading; however, the ultimate experimental loads were found to be controlled by excessive cracking and deformation of the bottom end connection. The theory is used to quantify the warping and shear deformation effects on the member strength. Finally, an interaction expression involving the axial load, biaxial bending, biaxial shear, and torsional moment is formulated for possible practical use.

## ACKNOWLEDGMENTS

The author would like to express deep appreciation to Dr. Zia Razzaq, who provided invaluable advice and encouragement throughout the completion of this dissertation. Without his guidance and assistance, this research would not have been possible. Special gratitude is extended to the dissertation committee members for their time and support. A heartfelt thanks goes to the author's colleague, George Kumi. His assistance in the laboratory significantly contributed to this work. Larson Lindberg from the Engineering Workshop also deserves thanks for his valuable contribution. Lastly, profound gratitude is owed to the author's family: his mother, wife Zainab, and children, Zane and Reema. Their unwavering support and encouragement throughout this academic journey. Their constant love has been a pillar of strength. Thank you all for standing by the author during this pursuit of knowledge and achievement.

## NOMENCLATURE

|                              |   |
|------------------------------|---|
| $A$                          | Area  |
| $A_i$                        | Element area  |
| $b$                          | Section width                                       |
| $d$                          | Section depth                                       |
| $dA$                         | Element Area  |
| $E$                          | Modulus of elasticity                               |
| $I_x, I_y$                   | Moment of inertia about x-axis and y-axis           |
| $I_{xy}$                     | Product moment of inertia                           |
| $I_{\omega x}, I_{\omega y}$ | Warping product of inertia about x-axis and y-axis. |
| $G$                          | Shear modulus of elasticity                         |
| $[K]$                        | Member global tangent stiffness matrix              |
| $K_T$                        | St. Venant torsion constant                         |
| $M_x, M_y$                   | Bending moments                                     |
| $M_z$                        | Torsional moment                                    |
| $M_{sv}$                     | St. Venant twisting resisting moment.               |

|               |                                    |
|---------------|------------------------------------|
| $M_\omega$    | Resisting warping twisting moment. |
| $\omega_n$    | Normalized unit warping            |
| $\{M\}$       | Moment vector                      |
| $P$           | Applied axial load.                |
| $W$           | Applied vertical load.             |
| $Q$           | Applied lateral load.              |
| $H$           | Nodal distance                     |
| $n$           | Number of nodes                    |
| $u_i$         | Nodal deflection in x-axis         |
| $v_i$         | Nodal deflection in y-axis         |
| $x, y, z$     | Global coordinates                 |
| $X, Y$        | Centroid coordinates               |
| $X_0, Y_0$    | Shear center coordinates           |
| $z_i$         | Nodal distance                     |
| $\Pi$         | Total energy                       |
| $\{\delta\}$  | Cross-sectional deformation vector |
| $\varepsilon$ | Normal Strain                      |

|                  |  |
|------------------|--|
| $\epsilon_t$     | Tensile strain                           |
| $\epsilon_c$     | Compression strain                       |
| $\epsilon_{ut}$  | Ultimate (fracture) tensile strain       |
| $\epsilon_{uc}$  | Ultimate (fracture) compression strain   |
| $\epsilon_{cr}$  | Tensile cracking strain                  |
| $\sigma$         | Stress                                   |
| $\sigma_{uT}$    | Ultimate (fracture) tensile strength     |
| $\sigma_{uC}$    | Ultimate (fracture) compression strength |
| $\emptyset$      | Angle of twist                           |
| $\Phi_x, \Phi_y$ | Bending curvature                        |
| $\{\Delta\}$     | Deformation vector                       |

## TABLE OF CONTENTS

|   | Page          |
|---|---------------|
| <b>LIST OF TABLES.....</b>  | <b>x</b>      |
| <b>LIST OF FIGURES.....</b>   | <b>xii</b>    |
| <br>Chapter   |               |
| <b>1. INTRODUCTION .....</b>  | <b>1</b>      |
| 1.1 Prelude .....   | 1             |
| 1.2 Literature Review.....  | 2             |
| 1.3 Problem Definition.....   | 10            |
| 1.4 Objectives and Scope.....   | 12            |
| 1.5 Assumptions and Conditions .....  | 13            |
| <br><b>2. THEORETICAL FORMULATION .....</b>   | <br><b>14</b> |
| 2.1 Governing Differential Equations Including Shear Effects and Warping .....  | 14            |
| 2.2 Boundary Conditions .....   | 38            |
| 2.2.1 Non-sway Members with Biaxial Partial Rotational and Lateral Restraints   | 38            |
| 2.2.2 Non-Sway Pinned Ends Members .....  | 39            |
| 2.2.3 Sway Pinned Member .....  | 39            |
| 2.2.4 Non-sway Fixed Ends Members .....   | 39            |
| 2.2.5 Sway Members with Biaxial Partial Rotational and Lateral Restraints.....  | 40            |
| 2.3 Finite-Difference Formulation.....  | 41            |
| 2.4 Solution Procedure.....   | 43            |
| 2.5 Equilibrium Equations for Simply Supported Sway Columns .....   | 44            |
| 2.6 Equilibrium Equations for Torsionally Free-Fixed Member .....   | 45            |
| 2.7 Equilibrium Equations for Simply Supported Sway Beam-Column for Combined Axial Load and Biaxial Bending Moment.....           | 45            |
| 2.8 Equilibrium Equations for Simply Supported Sway Beam-Columns for Combined Axial Load, Torsion and Biaxial Bending Moment..... | 46            |
| 2.9 Equilibrium Equations for Fixed-Pinned Sway Beam-Columns for Combined Axial Load, Biaxial Bending Moments, and Torsion.....   | 47            |



| Chapter  | Page      |
|--|-----------|
| 2.10 Numerical Results .....   | 48        |
| 2.10.1 Torsionally Loaded Member.....  | 48        |
| 2.10.2 Axially Loaded Member .....   | 49        |
| 2.10.3 Combined Axial Load and Biaxial Bending Moment .....  | 51        |
| 2.10.4 Combined Axial Load, Biaxial Bending Moment, and Torsion with Flexurally Pinned Ends .....  | 55        |
| 2.10.5 Combined Axial Load, Biaxial Bending Moment, and Torsion with Flexurally Fixed-Pinned ..... | 59        |
| <b>3. EXPERIMENTAL INVESTIGATION.....</b>  | <b>63</b> |
| 3.1 Experimental Study.....  | 63        |
| 3.1.1 Apparatus .....  | 64        |
| 3.1.2 Material properties .....  | 68        |
| 3.2 Experimental Results .....   | 69        |
| 3.2.1 Torsionally Loaded Member Test T-1 .....   | 71        |
| 3.2.2 Axially Loaded GFRP Column Test P-2 .....  | 74        |
| 3.2.3 Combined Axial Load and Biaxial Bending Moment Test PB-3 .....                               | 78        |
| 3.2.4 Combined Axial Load, Biaxial Bending Moment, and Torsional Moment Test PBT-p-4 .....         | 81        |
| 3.2.5 Combined Axial Load, Biaxial Bending Moment, and Torsional Moment Test PBT-fp-5 .....        | 86        |
| <b>4. THEORY VERSUS EXPERIMENTS.....</b>   | <b>92</b> |
| 4.1 For Test T-1 .....   | 92        |
| 4.2 For Test P-2.....  | 93        |
| 4.3 For Test PB-3 .....  | 95        |
| 4.4 For Test PBT-p-4 .....   | 97        |
| 4.5 For Test PBT-fp-5.....   | 101       |
| 4.6 Available Experimental Results.....  | 103       |
| 4.6.1 Stability of I-Beams .....   | 104       |
| 4.6.2 I-Beam Lateral Torsional Buckling .....  | 112       |
| 4.6.3 I-Beam Under Biaxial Bending .....   | 118       |
| 4.6.4 Uniaxial Loaded Beam-Column .....  | 121       |

| Chapter   | Page       |
|---|------------|
| <b>5. THRUST-MOMENT-TORSION INTERACTION RELATIONS .....</b>                                     | <b>128</b> |
| 5.1 .....Interaction Relation for Biaxially Loaded Beam-Column with Torsion                     | 137        |
| 5.2 Interaction Relation for Biaxially Loaded Beam-Column with Flexural Shear and Torsion ..... | 143        |
| 5.3 Interaction Relation Comparisons.....   | 145        |
| <b>6. CONCLUSIONS AND FUTURE RESEARCH .....</b>   | <b>156</b> |
| 6.1 Conclusions.....  | 156        |
| 6.2 Future Research .....   | 157        |
| <b>REFERENCES .....</b>   | <b>158</b> |
| <b>VITA AUCTORIS .....</b>  | <b>163</b> |

## LIST OF TABLES

| Table  | Page |
|--|------|
| 1. Theoretical Results for Torsionally Loaded Member.....  | 48   |
| 2. Theoretical Results for Axially Loaded Member .....   | 50   |
| 3. Combined Axial Load and Biaxial Bending Moment .....  | 52   |
| 4. Theoretical Results for Combined Axial Load, Biaxial Bending Moment, and Torsion with Flexurally Pinned Ends.....   | 56   |
| 5. Theoretical Results for Combined Axial Load, Biaxial Bending Moment, and Torsion with Flexurally Fixed-Pinned ..... | 60   |
| 6. Torsion Test T-1 Results .....  | 72   |
| 7. Loading Steps vs. Maximum Applied Torsional Moment for Test T-1 .....   | 72   |
| 8. Experimental Data for Axially Loaded Member Test P-2 Results.....   | 75   |
| 9. Experimental Results for Test PB-3 .....  | 79   |
| 10. Axial Load, Biaxial Bending Moment, and Torsion Test PBT-p-4 .....   | 82   |
| 11. Axial Load, Biaxial Bending Moment, and Torsion for Test PTB-fp-5 .....  | 87   |
| 12. Experimental Results for Test No. IFT3-1 [40] .....  | 105  |
| 13. MATLAB Results for Test No. IFT3-1 .....   | 105  |
| 14. Experimental Results for Test No. IFT3-2 [40] .....  | 107  |
| 15. MATLAB Results for Test No. IFT3-2.....  | 107  |
| 16. Experimental Results Test No. IFT3-3 [40] .....  | 109  |
| 17. MATLAB Test No. IFT3-3 .....   | 110  |
| 18. Experimental Vertical Deflections, $v$ (in.) for Investigation 1 [41].....   | 113  |
| 19. MATLAB Results for Investigation 1 .....   | 113  |
| 20. Experimental Results for Investigation 2 [41].....   | 116  |
| 21. MATLAB Results for Investigation 2 .....   | 116  |
| 22. Experimental Results for Case 1, $L = 64$ inches [42].....   | 118  |
| 23. MATLAB Results for Case 1, $L = 64$ inches .....   | 119  |
| 24. Experimental Results for Case 1, $L = 82$ inches [42].....   | 119  |
| 25. MATLAB Results for Case 1, $L = 82$ inches .....   | 120  |
| 26. Experimental Results for Case 1, $L = 100$ inches [42].....  | 120  |
| 27 Results for FRP I-beam 4x4x0.25" Case 1, $L = 100$ inches.....  | 121  |
| 28. Experimental Results for Major Axis Loading .....  | 122  |
| 29. MATLAB Results for Major Axis Loading .....  | 123  |
| 30. Experimental Results for Minor Axis Loading .....  | 125  |

| Table   | Page |
|---|------|
| 31. MATLAB Results for Minor Axis Loading.....                | 125  |
| 32. Normalized Applied Loads for L=1 ft. and $T = 0.1$ .....  | 138  |
| 33. Normalized Applied Loads for L=5 ft. and $T = 0.1$ .....  | 139  |
| 34. Normalized Applied Loads for L=9 ft. and $T = 0.1$ .....  | 140  |
| 35. Normalized Applied Loads for L= 13ft. and $T = 0.1$ ..... | 141  |
| 36. Normalized Applied Loads L=17 ft. and $T = 0.1$ .....     | 142  |
| 37. Normalized Applied Loads for L=17 ft. and $T = 0.5$ ..... | 143  |
| 38. Normalized Applied Loads for L=1 ft. and $T = 0.1$ .....  | 144  |
| 39. Normalized Applied Loads for L=5 ft. and $T = 0.1$ .....  | 144  |
| 40. Normalized Applied Load for L=9 ft. and $T = 0.1$ .....   | 145  |
| 41. Interaction Relation for $Lry = 17$ .....                 | 145  |
| 42. Interaction Relation for $Lry = 17$ .....                 | 146  |
| 43. Interaction Relation for $Lry = 17$ .....                 | 147  |
| 44. Interaction Relation for $Lry = 17$ .....                 | 148  |
| 45. Interaction Relation for $Lry = 51$ .....                 | 149  |
| 46. Interaction Relation for $Lry = 51$ .....                 | 150  |
| 47. Interaction Relation for $Lry = 51$ .....                 | 151  |
| 48. Interaction Relation for $Lry = 85$ .....                 | 152  |
| 49. Interaction Relation for $Lry = 85$ .....                 | 153  |
| 50. Interaction Relation for $Lry = 85$ .....                 | 154  |

## LIST OF FIGURES

| Figure   | Page |
|--|------|
| 1. Biaxially Loaded Beam-Column with Torsion .....                         | 11   |
| 2. Member Cross Section Before and After Deflection .....                  | 12   |
| 3. Tensile Stress-Strain Relationship.....                                 | 14   |
| 4. Sectorial Area $\omega$ .....   | 17   |
| 5. Coordinate Axes of an Open Section .....                                | 20   |
| 6. Geometry of Shear Stress Element.....                                   | 24   |
| 7. Torsion of Solid Section.....   | 24   |
| 8. Shear Stresses on Solid Element .....                                   | 25   |
| 9. Forces in the x-z and y-z Planes .....                                  | 26   |
| 10. $\xi - \eta$ Coordinate System .....                                   | 29   |
| 11. Twisting Due to Component of $M_x$ .....                               | 30   |
| 12. Twisting Due to Component of $M_y$ .....                               | 30   |
| 13. Twisting Due to Component of P in X-Z Plane .....                      | 31   |
| 14. Twisting Due to Component of P in Y-Z Plane .....                      | 31   |
| 15. Twisting Due to the Differential Warping of Two Adjacent Sections..... | 32   |
| 16. Twisting Due to the End Shears .....                                   | 33   |
| 17. Shear Bending and Deformation .....                                    | 34   |
| 18. Finite-Difference Nodes Along the Member.....                          | 43   |
| 19. Torsional Moment, $M_z$ , vs. Angle of Twist, $\phi$ .....             | 49   |
| 20. Axial Load, P, vs. Midspan Deflection, $u$ .....                       | 50   |
| 21. Axial Load, P, vs. Midspan Deflection, $v$ .....                       | 51   |
| 22. Axial Load, P, vs. Bottom End Angle of Twist, $\phi$ .....             | 51   |
| 23. Axial Load, P, vs. Midspan Deflection, $v$ .....                       | 52   |
| 24. Axial Load, P, vs. Midspan Deflection, $u$ .....                       | 53   |
| 25. Axial Load, P, vs. Midspan Angle of Twist, $\phi$ .....                | 53   |
| 26. Bending Moment, $M_x$ , vs. Midspan Deflection, $u$ .....              | 54   |
| 27. Bending Moment, $M_x$ , vs. Midspan Deflection, $u$ .....              | 54   |
| 28. Bending Moment, $M_x$ , vs. Bottom End Angle of Twist, $\phi$ .....    | 55   |
| 29. Axial Load, P, vs. Midspan Deflection, $u$ , $v$ .....                 | 57   |
| 30. Torsion, $M_z$ , vs. Midspan Deflection, $v$ and $u$ .....             | 57   |
| 31. Bending Moment, $M_x$ , vs. Midspan Deflection, $v$ .....              | 58   |

| Figure   | Page |
|--|------|
| 32. Bending Moment, $\mathbf{Mx}$ , vs. Midspan Deflection, $u$ .....  | 58   |
| 33. Bending Moment, $\mathbf{Mx}$ , vs. Bottom End Angle of Twist, $\phi$ .....  | 59   |
| 34. Axial Load, $P$ , vs. Midspan Deflections, $v$ , and $u$ .....   | 60   |
| 35. Bending Moment, $\mathbf{Mx}$ , vs. Midspan Deflection, $v$ .....  | 61   |
| 36. Bending Moment, $\mathbf{Mx}$ , vs. Midspan Deflection, $u$ .....  | 61   |
| 37. Bending Moment, $\mathbf{My}$ , vs. Bottom End Angle of Twist, $\phi$ .....  | 62   |
| 38. Experimental Applied Bending Moment.....   | 66   |
| 39. Apparatus.....   | 67   |
| 40. Hydraulic Jack and Load Cell C.....  | 68   |
| 41. Load, $W$ , vs. Vertical Displacement, $v$ , for Major Axis Test .....   | 70   |
| 42. Load, $Q$ , vs. Vertical Displacements, $u$ , for Minor Axis Test.....   | 70   |
| 43. Bottom End Connection of the Specimen .....  | 72   |
| 44. Specimen under Torsional Moment for Test T-1 .....   | 73   |
| 45. Applied Torsional Moment for Each Loading Step for Test T-1 .....  | 73   |
| 46. Experimental Torsional Moment, $\mathbf{Mz}$ , vs. Bottom End Angel of Twist, $\phi$ , Relationship for Test T-1 ..... | 74   |
| 47. Specimen Shape One Week after Torsion Test T-1 .....   | 74   |
| 48. Dial Gauges Numbering and Locations for Test P-2 .....   | 76   |
| 49. Axial Load, $P$ , vs. Midspan Deflection, $u$ , for Test P-2 .....   | 76   |
| 50. Axial Load, $P$ , vs. Midspan Deflection, $v$ , for Test P-2 .....   | 77   |
| 51. Axial Load, $P$ , vs. Bottom End Angle of Twist, $\phi$ , for Test P-2 .....   | 77   |
| 52. Axial Load, $P$ , vs. Midspan Deflections, $v$ , and $u$ , for Test PB3.....   | 79   |
| 53. Axial Load, $P$ , vs. Bottom End Angle of Twist, $\phi$ , for Test PB-3.....   | 80   |
| 54. Bending Moment, $\mathbf{Mx}$ , vs. Midspan Deflections, $v$ , and $u$ , for Test PB-3 .....                           | 80   |
| 55. Bending Moment, $\mathbf{Mx}$ , vs. Bottom End Angle of Twist, $\phi$ , for Test PB-3 .....                            | 81   |
| 56. Axial Load, $P$ , vs. Midspan Deflections, $v$ , and $u$ , for Test PBT-p-4 .....                                      | 83   |
| 57. Axial Load, $P$ , vs. Bottom End Angle of Twist, $\phi$ , for Test PBT-p-4.....  | 83   |
| 58. Torsion, $\mathbf{Mz}$ , vs. Midspan Deflections, $v$ , and $u$ , for Test PTB-p-4 .....                               | 84   |
| 59. Torsion, $\mathbf{Mz}$ , vs. Bottom End Angle of Twist, $\phi$ , for Test PTB-p-4 .....                                | 84   |
| 60. Bending Moment, $\mathbf{Mx}$ , vs. Midspan Deflection, $\phi$ , for Test PTB-p-4 .....                                | 85   |
| 61. Bending Moment, $\mathbf{Mx}$ , vs. Bottom Angle of Twist, $\phi$ , for Test PTB-p-4.....                              | 85   |
| 62. Axial Load, $P$ , vs. Midspan Deflections, $v$ , and $u$ , for Test PTB-fp-5 .....                                     | 88   |

| Figure   | Page |
|--|------|
| 63. Axial Load, $P$ , vs. Bottom End Angle of Twist, $\phi$ , for Test PTB-fp-5 .....        | 88   |
| 64. Torsion, $M_z$ , vs. Midspan Deflection, $v$ , and $u$ , for Test PTB-fp-5 .....         | 89   |
| 65. Torsion, $M_z$ , vs. Bottom End Angle of Twist, $\phi$ , for Test PTB-fp-5 .....         | 89   |
| 66. Bending Moment, $M_x$ , vs. Midspan Deflections, $v$ , and $u$ , for Test PTB-fp-5 ..... | 90   |
| 67. Bending Moment, $M_x$ , vs. Bottom End Angle of Twist, $\phi$ , for Test PTB-fp-5 .....  | 90   |
| 68. Cracks Due to Stress Concentration .....   | 91   |
| 69. Applied Torsion, $M_z$ , vs. Bottom End Angle of Twist, $\phi$ , for Test T-1 .....      | 92   |
| 70. Axial Load, $P$ , vs. Midspan Deflection, $u$ , for Test P-2 .....                       | 93   |
| 71. Axial Load, $P$ , vs. Midspan Deflection, $v$ , for Test P-2 .....                       | 94   |
| 72. Axial Load, $P$ , vs. Bottom End Angle of Twist, $\phi$ , for Test P-2 .....             | 94   |
| 73. Bending Moment, $M_x$ , vs. Midspan Deflection, $u$ , for Test PB-3 .....                | 95   |
| 74. Bending Moment, $M_x$ , vs. Midspan Deflection, $v$ , for Test PB-3 .....                | 96   |
| 75. Bending Moment, $M_x$ , vs. Bottom End Angle of Twist, $\phi$ , for Test PB-3 .....      | 96   |
| 76. Axial Load, $P$ , vs. Midspan Deflection, $u$ , for Test PTB-p-4 .....                   | 97   |
| 77. Axial Load, $P$ , vs. Midspan Deflection, $v$ , for Test PTB-p-4 .....                   | 98   |
| 78. Torsion, $M_z$ , vs. Midspan Deflection, $u$ , for Test PTB-p-4 .....                    | 98   |
| 79. Torsion, $M_z$ , vs. Midspan Deflection, $v$ , for Test PTB-p-4 .....                    | 99   |
| 80. Bending Moment, $M_x$ , vs. Midspan Deflection, $u$ , for Test PTB-p-4 .....             | 99   |
| 81. Bending Moment, $M_x$ , vs. Midspan Deflection, $v$ , for Test PTB-p-4 .....             | 100  |
| 82. Bending Moment, $M_x$ , vs. Bottom End Angle of Twist, $\phi$ , for Test PTB-p-4 .....   | 100  |
| 83. Axial Load, $P$ , vs. Midspan Deflections, $v$ , and $u$ , for Test PTB-fp-5 .....       | 101  |
| 84. Bending Moment, $M_x$ , vs. Midspan Deflection, $u$ , for Test PTB-fp-5 .....            | 102  |
| 85. Bending Moment, $M_x$ , vs. Midspan Deflection, $v$ , for Test PTB-fp-5 .....            | 102  |
| 86. Bending Moment, $M_x$ , vs. Bottom End Angle of Twist, $\phi$ , for Test PTB-fp-5 .....  | 103  |
| 87. Cross-Sectional Schematic View at Load Application Points for I-Section Beam             | 104  |
| 88. Load, $P$ , vs. Midspan Deflection, $vc$ , for Test No. IFT3-1 .....                     | 106  |
| 89. Load, $P$ , versus Midspan Deflection, $uc$ , for Test No. IFT3-1 .....                  | 106  |
| 90. Load, $P$ , versus Angle of Twist, $\phi$ , for Test No. IFT3-1 .....                    | 107  |
| 91. Load, $P$ , versus Midspan Deflection, $vc$ , for Test No. IFT3-2 .....                  | 108  |
| 92. Load, $P$ , versus Midspan Deflection, $uc$ , for Test No. IFT3-2 .....                  | 108  |
| 93. Load, $P$ , versus Angle of Twist, $\phi$ , for Test No. IFT3-2 .....                    | 109  |
| 94. Load, $P$ , versus Midspan Deflection, $vc$ , for Test No. IFT3-3 .....                  | 110  |

| Figure   | Page |
|--|------|
| 95. Load, P, versus Midspan Deflection, $uc$ , for Test No. IFT3-3 .....                                       | 111  |
| 96. Load, P, versus Angle of Twist, $\phi$ , for Test No. IFT3-3 .....   | 111  |
| 97. Load, Q, versus Vertical Deflection, $v$ , for 8 in. Distance from the Support for Investigation 1 .....   | 114  |
| 98. Load, Q, versus Vertical Deflection, $v$ , for 18 in. Distance from the Support for Investigation 1 .....  | 114  |
| 99. Load, Q, versus Vertical Deflection, $v$ , for 29 in. Distance from the Support for Investigation 1 .....  | 115  |
| 100. Applied Load, Q at 27 in. from the Support.....   | 115  |
| 101. Load, Q, versus Vertical Deflection, $v$ , for 6 in. Distance from the Support for Investigation 2 .....  | 116  |
| 102. Load, Q, versus Vertical Deflection, $v$ , for 21 in. Distance from the Support for Investigation 2 ..... | 117  |
| 103. Load, Q, versus Vertical Deflection, $v$ , for 36 in. Distance from the Support for Investigation 2 ..... | 117  |
| 104. Load, H, vs. Horizontal Lateral Deflection, $U$ , for Case 1, L = 64 inches.....                          | 119  |
| 105. Load, H, vs. Horizontal Deflection, $U$ for Case 1, L = 82 inches .....                                   | 120  |
| 106. Load, H, versus Horizontal Deflection, $U$ , for Case 1, L = 100 inches.....                              | 121  |
| 107. Load, P, versus Horizontal Deflection, $v$ , for Major Axis Loading .....                                 | 123  |
| 108. Load, P, versus Horizontal Deflection, $u$ , for Major Axis Loading .....                                 | 124  |
| 109. Load, P, versus Angle of Twist, $\phi$ for Major Axis Loading.....  | 124  |
| 110. Load, P, vs. Horizontal Deflection, $v$ , for Minor Axis Loading.....                                     | 126  |
| 111. Load, P, vs. Horizontal Deflection, $u$ , for Minor Axis Loading.....                                     | 126  |
| 112. Load, P, versus Angle of Twist, $\phi$ , for Minor Axis Loading.....                                      | 127  |
| 113. Axial Load, $Pc$ , vs. Slenderness Ratio, $Lbry$ .....  | 136  |
| 114. Bending Moment about x Axis, $Mcx$ , vs. Slenderness Ratio, $Lbry$ .....                                  | 136  |
| 115. Interaction Relation for $Lry = 17$ .....   | 146  |
| 116. Interaction Relation for $Lry = 17$ .....   | 147  |
| 117. Interaction Relation for $Lry = 17$ .....   | 148  |
| 118. Interaction Relation for $Lry = 17$ .....   | 149  |
| 119. Interaction Relation for $Lry = 51$ .....   | 150  |
| 120. Interaction Relation for $Lry = 51$ .....   | 151  |
| 121. Interaction Relation for $Lry = 51$ .....   | 152  |
| 122. Interaction Relation for $Lry = 85$ .....   | 153  |



| Figure  | Page |
|---|------|
| 123. Interaction Relation for <b><i>Lry</i></b> = <b>85</b> ..... | 154  |
| 124. Interaction Relation for <b><i>Lry</i></b> = <b>85</b> ..... | 155  |

# CHAPTER 1

## INTRODUCTION

### 1.1 Prelude

The use of pultruded Fiber Reinforced Polymer (FRP) structural products has gained considerable momentum during the past few decades. The primary advantages of FRP materials include absence of corrosion and magnetic effects and their light weight in comparison to traditional building materials such as steel and concrete. Although a considerable body of literature related to the structural performance of FRP beams, columns, beam-columns, and panels exists, several crucial areas related to the study of the behavior and strength of such members is still quite deficient. In 2023, the American Society of Civil Engineers (ASCE) published a Load and Resistance Design Factor (LRFD) Standard ASCE/SEI 74-23 for pultruded structural members. The ASCE/SEI 74-23 Standard has no interaction relationship for biaxially loaded FRP beam-columns with applied torsion for open sections.

This dissertation presents a comprehensive mathematical model to predict the behavior and strength of glass FRP beam-columns subjected to biaxial bending and torsion and to investigate the influence of both shear and warping deformations. To determine the validity of the theoretical study, an experimental investigation is also conducted on FRP members with various load combinations. A comparison of the theory is also made to some results available in the literature for a few special types of loading. Lastly, the theory presented is used for the development of a new interaction relationship between biaxial loading and torsion and flexural shear.

## 1.2 Literature Review

A sizeable body of literature exists on the subject matter of glass FRP with applications in civil engineering and other fields. However, presented in this section is a summary of the publications relevant to the problem considered in this dissertation.

Sirjani and Razzaq [1] presented an experimental and theoretical investigation of the load-carrying capacity of Fiber Reinforced Polymer (FRP) I-section beams subjected to four-point loading. The American Society of Civil Engineers' Load and Resistance Factor Design (ASCE-LRFD) Pre-Standard for FRP Structures was used to estimate the overall lateral-torsional buckling, web and flange local buckling, and material rupture load. For each of the studied beams, the Lateral-Torsional buckling failure mode was found to be the most critical failure mode. This study also found that the height of applied loads relative to the shear center highly influenced the Lateral-Torsional buckling load of the beams; therefore, the study concluded that the buckling load calculated using ASCE-LRFD equations lead to over-conservative results in a variety of cases.

Lin, Polyzois and Shah [2] used the finite element method with seven degrees of freedom at each node to study the stability problem of thin-walled fiber-reinforced plastic (FRP) structural members. The influence of the in-plane shear strain on the stability of the members is considered. The shape functions for the rotation and unit length rotation and unit length rotation induced by warping are derived. The static and geometric stiffness matrices of a general beam element are established based on the developed shape functions. The bifurcation buckling problem of thin-walled pultruded open-sections subjected to various loading and boundary conditions is examined through several examples. It is shown that the influence of the shear strain on the buckling capacity of the FRP structural members is significant and must be considered in the design of such members.

Cardoso, Harries and Batista [3] developed the strength equation for GFRP square tube pultruded columns, and this study assumed the ultimate column strength under axial load with uniaxial bending moment. Five GFRP square sections with different geometries on the stub and columns were considered to establish in situ properties. The development of a comprehensive strength equation was presented, and an experimental investigation for the behavior of the square GFRP tube columns was conducted. A relative slenderness factor was introduced to differentiate between tested sections; the factor was like that used in steel sections.

Ascione, Lamberti, and Razaqpur [4] presented a study of the axial-flexural-torsional response of pultruded GFRP slender beams to propose standard cross-sections and shapes to ultimately improve strength, stability, and deformational characteristics of the existing GFRP sections and shapes that are generally taken from a standard steel section. As GFRP sections are thin walled but are significantly less stiff than similar steel sections, the study focuses on enhancing the GFRP section's stiffness and buckling strength. A numerical model was used in this investigation that can trace the pre-buckling geometrically nonlinear response for both steel and GFRP sections. The buckling load is computed by the asymptotic value of the load-displacement curve. Different open and closed GFRP sections were tested with different boundary conditions. The investigation demonstrated that the existing GFRP sections do not have adequate stiffness and buckling strength; recommendations for new section proportions and modified shapes were made.

Razzaq et al. [5] presented a load and resistance factor design (LRFD) approach for lateral-torsional buckling based on experimental and theoretical study of the behavior of FRP channel section beams under the influence of gradually increasing static loads. Some experimental results for combined bending and torsion are also presented. Single span members with unrestrained end warping are considered with concentrated vertical loads passing through the shear center, the

geometric centroid, and location which is neither at the shear center nor at the centroid. A pair of concentrated loads are applied symmetrically about the beam midspan, through a system of loading plates and tie rods to allow an unrestrained deformation of the beam. The magnitude and significance of the warping stresses in comparison to the flexural stresses were identified. The predicted buckling load using suggested formula agrees with the experimental results.

Konate and Razzaq [6] presented a study of the failure modes for I-section Glass Fiber Reinforced Polymer (GFRP) beams with single mid-span web brace. The ASCE-LRFD Pre-Standard for FRP structures was used to calculate the theoretical predictions. For the considered member length, it was concluded that for small and medium I-sections lateral-torsional buckling is the governing failure mode and material rupture governed the failure mode for the bigger sections.

Nunes et al. [7] introduced experimental and numerical investigations about the structural behavior of GFRP pultruded columns subjected to small eccentric loadings about the strong axis. Long GFRP I-section columns were tested in compression applied with various eccentricity/height of the cross-section ratios. It was found that such small eccentricities very important for the behavior of GFRP pultruded columns. The initial stiffness of eccentrically loaded columns was like the concentrically loaded columns; however, for increasing loads the stiffness decreased due to the second-order effect. Results also showed that the load capacity of columns subjected to loads applied within the kern boundaries is reduced up to 40% at an approximately linear trend.

Barbero and DeVivo [8] presented theoretical design equations supported by data gathered during experimental testing of wide-flange and I-beam pultruded structural shapes. The design procedure accounts for axial load eccentricity and bending action induced by lateral loads and end-moments. Load and Resistance Factored Design (LRFD) method is used considering both strength and

serviceability. This paper addresses the methodology to determine the resistance factors, which should be used with load-factors accounting for the variability and uncertainty of the loads. The design equations use section-properties, such as the bending stiffness, which must be measured and supplied by the industry. It is found that the section-properties used in the design of beams and columns are sufficient for the design of beam-columns.

Davalos, Q. et al. [9] presents a comparison between experimental and analytical approaches to the flexural-torsional buckling behavior of pultruded fiber reinforced plastic I-beam. Two pultruded FRP I-beams were tested under mid-span concentrated loads to measure their flexural-torsional buckling responses. Non-linear elastic theory was used to derive total potential energy equations for the instability of the FRP I-beams. The Rayleigh-Ritz method was used to solve the equilibrium equation in terms of the total potential energy. Some engineering equations were formulated to predict the critical flexural-torsional buckling loads. The conclusions suggested a good agreement between the experimental results and finite-element analysis.

Using the Brooks and Turvey [10] method, several GRP pultruded I-section cantilever beams were selected to conduct a series of lateral buckling tests. The results of the theoretical loads calculated from approximate formulae and the numerical finite element eigenvalue method were compared. The study suggests that linear buckling analysis gives an inaccurate estimation for the critical load, and it is not recommended to be used in design. It is also suggested that initial out-of-straightness and pre-buckling deformation might be of value that must be included in the design formulas to get an accurate critical load for the pultruded GRP cantilever.

According to Yoon and Jang [11], FRP sections are suitable for the application in the construction field because they can be produced with different cross-sections and lengths. Their high corrosion

resistance makes FRP much appreciated when used in high corrosive environments. However, design criteria for this material are not fully developed. FRP tends to buckle easily because FRP members are composed of a thin plate component. For this reason, in design, buckling is one of the main governing limits. The analytical study results relate to the buckling behavior for the I-shape FRP compression member. Some studies adopted a design procedure like that used in AISC 360-10 with performing some minor modification.

Barbero et al. [12] noted that buckling is the main criteria in the design in Fiber-reinforced plastic (FRP) beams and columns which are being used for different structural applications. Their processes developed models using local buckling modes under axial and shear loading, considering the interaction between the flange and the web. For some available cross-sections, observed behaviors are presented and predicted some experimental data. Barbero developed failure envelopes for FRP I-shape and box shape beams and columns. This analysis method can be used to predict the behavior of any new pultruded material. To analyze anisotropic flanges of I-beams and box-shape, the Rayleigh-Ritz method was used in this paper. The conclusion suggests using 45-degree angle-ply layers to improve the buckling strength of the columns.

Tomasz, K. [13] presented a study of glass FRP beams with closed cross section subjected to pure bending using numerical calculations. The FEA model was developed using four node multi layered shell elements governed by first-order shear deformation theory. Linear buckling analysis and nonlinear static analysis including large displacements have been performed. A Newton-Rapson algorithm has been employed and ANSYS software was used in FEA. This study considered multiple load cases and initial geometrical out-of-straightness. Comparing results of tests and numerical calculations, it was observed that in some cases, the deflection of the beams

does not correspond to the bifurcation buckling mode but corresponds to the lowest buckling load; geometrical imperfection for higher buckling mode must be considered.

Smith and Bank [14] in this study, a modified beam theory for open-section, thin walled, composite beams were tested. Symmetric and antisymmetric glass/polyester I-beams were supported as cantilevers and tested under transverse loading and end moments. Induced twist and out-of-plane lateral deflection as well as in-plane transverse deflection (bending deflection) were measured. Comparisons with finite element analysis using a commercial software was also used. Out-of-plane deflections were found to be too small to be measured accurately.

Boscato et al. [15] introduced an experimental evaluation of the buckling behavior of built-up columns of pultruded profiles subjected to axial compression. Several columns are characterized with different configurations for the bolted connections joining the channel sections into built-up strut. The test results are compared with the closed-form equation predictions for flexural buckling resistance, with buckling resistance values established from both eigenvalue and geometric nonlinear finite element analyses. Results show that there is a significant role played by the end loading condition, the composite action, and imperfections. Simple closed form equations overestimate the flexural buckling strength, whereas the resistance provided by nonlinear analysis provides a reasonably reliable numerical approach to establishing the actual buckling behavior.

Zhan et al. [16] introduced a new closed-form equation using the Ayrton-Perry formula to determine the reduction factor for global flexural buckling of Pultruded Fiber Reinforced Polymer (PFRP) structural struts under axial compression. A second new empirical closed-form equation is derived based upon the experimental data and compared with validated numerical simulations. The accuracy of the two proposed equations is compared with those closed-forms solutions



available in the literature; both result in more accurate predictions than those from the extant equations.

Sirjani and Razzaq [17] presented the results of an experimental and theoretical study of I-section fiber reinforced plastic (FRP) beams subjected to a gradually increasing midspan load. The load is applied about the beam major axis from the compression flange side through a point below the shear center. The boundary conditions are flexurally and torsionally pinned. The flexural-torsional response of FRP beams is studied experimentally up to the maximum load-carrying capacity. The experimental loads are compared with those arrived at theoretically using an equilibrium approach and found to be in good agreement. An elastic buckling moment expression from the load and resistance factor design (LRFD) specification of the American Institute of Steel Construction is modified to obtain a design expression for estimating the beam buckling load.

Bank et al. [18] presented a paper focused on three issues related to the prediction of the buckling loads from experimental data and from analytical and numerical approaches: nonlinearity, anisotropy, and inhomogeneity. Experimental data obtained from full-scale buckling tests are reviewed, and a method is proposed for estimating the buckling stress in pultruded beams. Analytical studies based on classical orthotropic plate buckling theory are used to determine the edge restraint coefficient for pultruded beams and to show the influence of the in-plane material properties on the buckling loads. Numerical studies using the finite element method in which inhomogeneous material properties in the beam cross-section are considered are used to give predictions of buckling loads of the beams.

Vanevenhoven et al. [19] presented a study to provide appropriate resistance factor  $\phi$  factors for wide-flange pultruded columns that are compatible with ASCE 7 load factors and to provide a

unified analytical equation for local and global buckling of concentrically loaded axial members which may be appropriate for a future design code. The resistance factors are provided for different target levels of structural reliability,  $\beta$ , and for different nominal design properties of the pultruded materials. The resistance factors were determined using Monte Carlo simulation based on the results of 75 tests of full-scale pultruded columns that have been reported in the literature. In addition, resistance factors and structural reliabilities were calculated for the design equations provided by the manufacturers in their design codes. The paper demonstrated that a unified design equation for pultruded columns can be developed for LRFD with reliability indices that are similar to those used for conventional materials.

Barbero [20] presented a design equation for fiber reinforced plastic columns based on the interaction between local (flange) and global (Euler) buckling observed during testing of the FRP columns included in this investigation. An existing interaction equation is adapted to account for the modes of failure observed in columns made of fiber reinforced composite materials. Experimental data generated during this investigation is presented and used to validate the interaction equation and to obtain the interaction constant. A slenderness ratio is proposed and used to present a plot of buckling for all sections and column lengths.

To the best of the author's knowledge, the influence of the effects of shear and warping deformations on the strength of biaxially loaded GFRP beam-columns with or without applied torsion have not been published in the past.

### 1.3 Problem Definition

The problem addressed in this dissertation is to develop a theoretical behavior prediction model with the goal of determining the influence of shear and warping deformations on the strength and stability of glass FRP beam-columns under combined biaxial loading and torsion. Both biaxial sway and non-sway boundary conditions involving partial lateral and rotational restraints are considered. For the non-sway case, the governing stability equations of the beam-column were derived for partially restrained, pinned, and fixed ends boundary conditions, while the governing stability equations for the sway case are derived for partially restrained boundary conditions only. The beam-column is loaded by axial compressive force,  $P$ . Axial force,  $P$ , is assumed to maintain its original direction throughout the loading history. Applied bending moments at the ends of the member about the  $x$  and  $y$  axes,  $M_{Tx}$ ,  $M_{Bx}$ ,  $M_{Ty}$ , and  $M_{By}$ . Subscript B and T refer to the member bottom and top ends, respectively. These moments are shown positive according to the right-hand rule in Figure 1. Concentrated load is  $W$  and  $Q$  at any distance  $z$  in  $x$  and  $y$  axes directions, respectively, and applied torsion,  $M_z$ , at the bottom end of the member. Figure 1 shows a FRP member with  $z$  as its longitudinal axis.  $u$  is the displacement in the  $xz$  plane due to the applied bending moment  $M_y$  and concentrated load  $Q$ ,  $v$  is the displacement in the  $yz$  plane due to bending moment  $M_x$  and concentrated load  $W$ . Figure 2 shows the angle of twist,  $\phi$ , at any location  $z$  along the member's length due to the applied torsion  $M_z$ . Wide Flange Section IW-340 was considered in this dissertation analysis. The strength and the deflection of the members were calculated using a system of three simultaneous ordinary differential equations solved by the finite difference method. The ultimate result of the problem involves the development of new strength interaction expressions that can be used in future specifications.

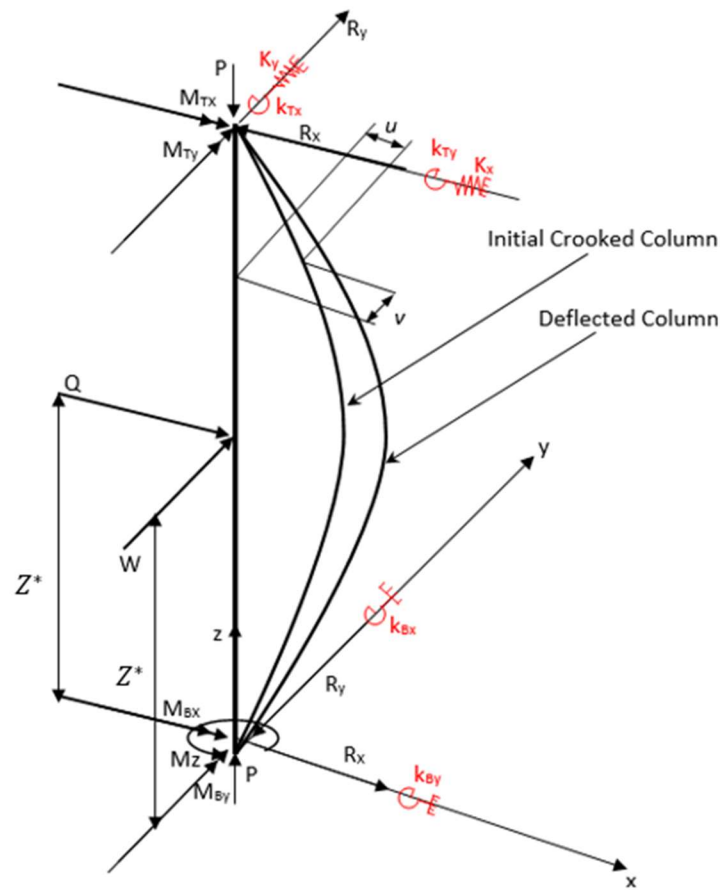
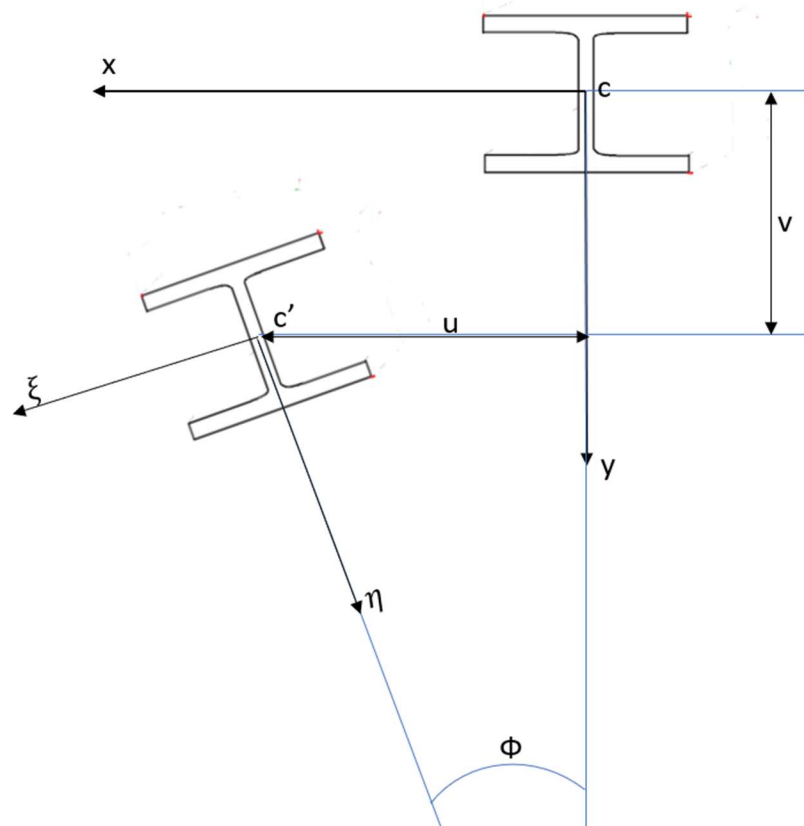


Figure 1. Biaxially Loaded Beam-Column with Torsion



**Figure 2. Member Cross Section Before and After Deflection**

#### 1.4 Objectives and Scope

The objectives of this dissertation are as follows:

- 1- Study the influence of shear and warping deformations on the strength and stability of a non-sway and sway single span beam-column involving partial lateral and rotational restraints.
- 2- Incorporate the influence of applied torsion into the governing nonlinear differential equations including both biaxial bending moments and axial thrust.
- 3- Develop new interaction relations for the I-section members that can be incorporated in the ASCE/SEI 74-23 standard.

## **1.5 Assumptions and Conditions**

The following assumptions are made in this dissertation:

1. All external loads are applied to the structural member in a quasi-static manner up to its ultimate strength.
2. The axial load is applied to the centroid of the cross section and retains its position until the member load-carrying capacity is reached.
3. Local buckling is not included in the theoretical analysis.
4. The members are linearly elastic.
5. The material compression and tension stress-strain relationships are identical.

## CHAPTER 2

### THEORETICAL FORMULATION

Presented in this chapter is the theoretical nonlinear analysis of a biaxially loaded beam-column with applied torsion; shear effects and initial out-of-straightness are also included. The geometrically nonlinear ordinary differential equations of equilibrium are formulated for the problem, and the finite difference method was used to obtain the solution for these differential equations.

#### 2.1 Governing Differential Equations Including Shear Effects and Warping

The adopted normal stress versus strain relationship for the GFRP is shown in Figure 3.

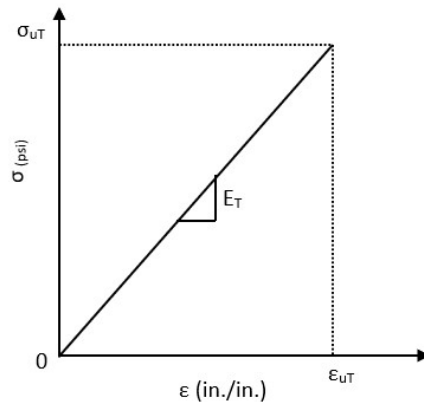


**Figure 3. Tensile Stress-Strain Relationship**

Assuming arbitrary coordinates  $x$ ,  $y$ , and  $z$  on the cross section, the normal strain,  $\epsilon_{\omega}$ , is related to the generalized strains: average axial strain,  $\epsilon_0$ , biaxial curvatures  $\phi_x$  and  $\phi_y$  about the coordinate axes  $x$  and  $y$ , and warping curvature,  $\phi''$  about  $z$  axis. At a point  $Q(x,y)$  of the cross section subjected to an axial load,  $P$ , as well as bending moments,  $M_x$  and  $M_y$ , about  $x$  and  $y$  axes, the normal strain due to restrained warping,  $\epsilon_{\omega}$ , is given by Chen et al. [21] as shown below.

$$\epsilon = \epsilon_0 + \phi_x y - \phi_y x - \omega_n \phi'' \quad (1)$$

$$\text{where: } \omega_n \phi'' = \epsilon_w \quad (1.a)$$

Since the stress-strain relation of elastic material is given by the following equations:

$$\sigma_w = E \epsilon_w \quad \text{for } 0 \leq \epsilon_w \leq \epsilon_{cr} \quad (2)$$

$$\sigma_w = 0 \quad \text{for } \epsilon_w > \epsilon_{cr} \quad (3)$$

The longitudinal strain,  $\epsilon_w$ , can be defined as presented below.

$$\epsilon_w = \frac{dw}{dz} \quad (4)$$

E is the Young's modulus and  $\sigma_w$  is the longitudinal stress due to restrained warping. The generalized stresses are related to the stress as presented below [21]:

$$P = \int_A \sigma_w dA \quad (5)$$

$$M_x = \int_A \sigma_w y dA \quad (6)$$

$$M_y = \int_A \sigma_w x dA \quad (7)$$

The generalized stress and generalized strain relations are obtained by combining Equations 1 through 7 as shown below.

$$P = EA\epsilon_0 + ES_y\phi_x - ES_x\phi_y - ES_\omega\phi'' \quad (8)$$

$$M_x = ES_y\epsilon_0 + EI_x\phi_x - EI_{xy}\phi_y - EI_{\omega y}\phi'' \quad (9)$$



$$M_y = -ES_x\epsilon_0 - EI_{xy}\phi_x + EI_y\phi_y + EI_{\omega x}\phi'' \quad (10)$$

$$M_w = ES_\omega\epsilon_0 + EI_{\omega y}\phi_x - EI_{\omega y}\phi_y - EI_\omega\phi'' \quad (11)$$

in which

$$A = \int_0^E t ds \quad (12)$$

$$S_x = \int x dA \quad (13)$$

$$S_y = \int y dA \quad (14)$$

$$S_\omega = \int \omega_n dA \quad (15)$$

$$I_x = \int y^2 dA \quad (16)$$

$$I_y = \int x^2 dA \quad (17)$$

$$I_\omega = \int \omega_n^2 dA \quad (18)$$

$$I_{xy} = \int xy dA \quad (19)$$

$$I_{\omega x} = \int \omega x dA \quad (20)$$

$$I_{\omega y} = \int \omega y dA \quad (21)$$

where  $\omega$  as shown in Figure 4 is the double sectorial area also known as the unit warping with respect to the centroid, and it is defined by the equation below [22].

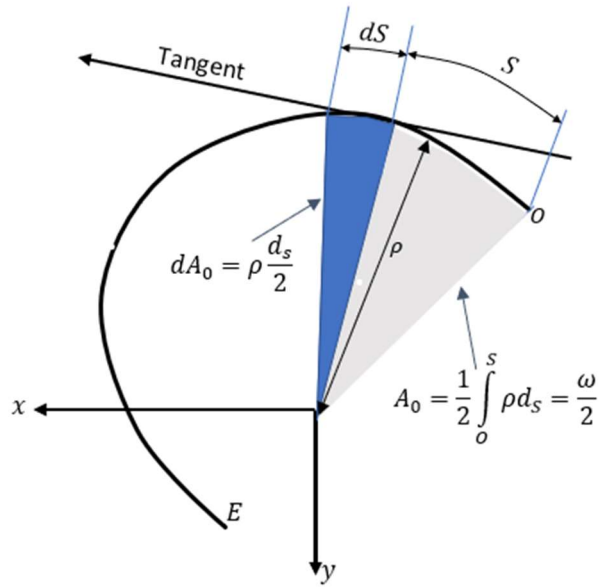


**Figure 4. Sectorial Area  $\omega$**

$$\omega = \int_0^s \rho ds \quad (22)$$

in which  $\rho$  is the perpendicular distance from the centroid of the section to a tangent drawn at an arbitrary point  $Q(x,y)$ , and  $\omega_n$ , is the normalized unit warping defined as shown in Equation 23 below [22].

$$\omega_n = \frac{1}{A} \int_0^E \omega_0 t ds - \omega_0 \quad (23)$$

where  $\omega_0$  is the double sectorial area or the unit warping with respect to the shear center and defined as:

$$\omega_0 = \int_0^E \rho_0 ds \quad (24)$$

in which  $\rho_0$  is the distance between the tangent of a general point  $Q$  and the torsion center, as shown in Figure 5. The location of the shear center,  $S(X_0, Y_0)$ , is computed by [23]:

$$X_0 = \frac{I_{xy}I_{\omega x} - I_y I_{\omega y}}{I_{xy}^2 - I_x I_y} \quad (25)$$

$$Y_0 = \frac{I_x I_{\omega x} - I_{xy} I_{\omega y}}{I_{xy}^2 - I_x I_y} \quad (26)$$

The unit warping term  $\omega_0$  in Equation 24 can be found by examining the geometrical relationships of the arbitrary point Q(x,y). This examination gives the following equation [23]

$$\rho_0 = \rho + Y_0 \frac{dx}{ds} - X_0 \frac{dy}{ds} \quad (27)$$

Substituting Equation 27 into Equation 24 gives

$$\omega_0 = \int_0^s \rho ds + Y_0 \int_{x_1}^x dx - X_0 \int_{y_1}^y dy \quad (28)$$

where  $x_1, y_1$  are the coordinate distance to the starting surface of the section, referenced to the centroid. If the warping is not restrained, Equation 28 gives:

$$\omega_0 = \omega + Y_0 x - Y_0 x_1 - X_0 y + X_0 y_1 \quad (29)$$

The warping with respect to the shear center S is given as [22]

$$w = w_0 - \phi' \omega_0 \quad (30)$$

Therefore, Equation 4 and 2 become:

$$\epsilon_w = w'_0 - \phi'' \omega_0 \quad (31)$$

$$\sigma_w = E w'_0 - E \omega_0 \phi'' \quad (32)$$

The horizontal shearing stress flow  $\tau_w t$  must be in equilibrium with the  $\sigma_w$  stresses. Starting at the free edge, which requires  $\tau_w t = 0$  and a  $\tau_w t dz$  at a distance  $s$ , gives

$$\tau_w t = - \int_0^s t \frac{d\sigma_w}{dz} ds \quad (33)$$

The stresses  $\sigma_w$  and  $\tau_w t$  are induced by torsional conditions and not bending.  $M_w$  in Equation 11 is the warping moment, also known as the bimoment. The warping moment,  $M_w$ , is related to the twisting moment,  $T_w$ , as shown in the following steps [22]

$$T_w = \int_0^E \rho_0 \tau_w t ds \quad (34)$$

The shear flow equation is [22]

$$\tau_w t = -ES\omega\phi''' \quad (35)$$

Substituting Equation 15 and 35 into Equation 34,

$$T_w = -E\phi''' \int_0^E \rho_0 \left( \int_0^s \omega_n t ds \right) ds \quad (36)$$

The twisting moment of the cross-section,  $T_w$ , can be written as presented below.

$$T_w = -EI_\omega \phi''' \quad (37)$$

Therefore,

$$T_w = M'_w \quad (38)$$

The general warping stress  $\sigma_w$  can also be written in another form.

$$\sigma_w = \frac{M'_w \omega_n}{I_\omega} = E\omega_n \phi'' \quad (39)$$

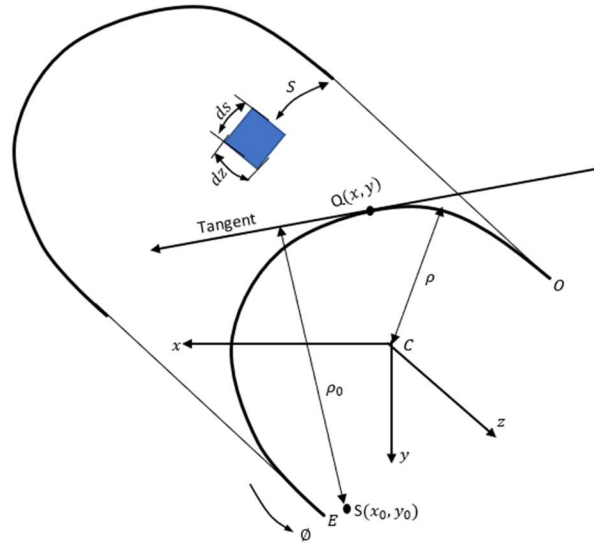


**Figure 5. Coordinate Axes of an Open Section**

The state of stress on a section induced by only a torsional moment applied at the center of twist or shear center as seen in Figure 6 and negating any stresses due to bending can be described as pure torsion or St. Venant contribution  $T_{sv}$ . The element in Figure 6 has undergone a rotation,  $\phi$ , due to the applied torque,  $T_{sv}$ , and thus a vertical displacement,  $v$ , and horizontal displacement,  $u$ . In addition to these in-plane distortions, the element will displace out-of-plane of the section in the  $z$  direction an amount  $w$ . The in-plane distortions are related to the rotation and coordinates  $x$  and  $y$  as presented in the following equations [25]

$$v = x\phi \quad (40)$$

$$u = -y\phi \quad (41)$$

Examining the element in the  $x$ - $z$  plane indicates that the element changes position with respect to the  $x$  and  $z$  axes. This change in position will create a shear strain  $\gamma_{xz}$  equal to [24]

$$\gamma_{xz} = \frac{\partial u}{\partial z} + \frac{\partial w}{\partial x} \quad (42)$$

Similarly, the change in position of the element with respect to the Y and Z axes creates a shear strain  $\gamma_{yz}$ , and it is equal to

$$\gamma_{yz} = \frac{\partial v}{\partial z} + \frac{\partial w}{\partial y} \quad (43)$$

Differentiating Equations 40 and 41

$$\frac{\partial v}{\partial z} = x\phi' \quad (44)$$

$$\frac{\partial u}{\partial z} = -y\phi' \quad (45)$$

Substituting Equations 44 and 45 into Equations 42 and 43,

$$\gamma_{xz} = -y\phi' + \frac{\partial w}{\partial x} \quad (46)$$

$$\gamma_{yz} = x\phi' + \frac{\partial w}{\partial y} \quad (47)$$

Considering a linear elastic material, the strain  $\gamma$  is related to the shear stress,  $\tau$ , by the modulus of rigidity,  $G$ , Equations 46 and 47 can be rewritten as follows:

$$\frac{\tau_{xz}}{G} = -y\phi' + \frac{\partial w}{\partial x} \quad (48)$$

$$\frac{\tau_{yz}}{G} = x\phi' + \frac{\partial w}{\partial y} \quad (49)$$

Differentiating Equations 48 and 49 conveys the following equations:

$$\frac{\partial \tau_{xz}}{\partial y} = -G\phi' \quad (50)$$

$$\frac{\partial \tau_{yz}}{\partial x} = G\phi' \quad (51)$$

Subtracting Equation 51 from 50 results in the following equation:

$$\frac{\partial \tau_{xz}}{\partial y} - \frac{\partial \tau_{yz}}{\partial x} = -2G\phi' \quad (52)$$

Assuming that the stresses  $\tau_{xz}$  and  $\tau_{yz}$  are related by a function  $\psi(x,y)$ , known as the Airy's Stress Function [24]

$$\tau_{xz} = \frac{\partial \psi}{\partial y} \quad \text{and} \quad \tau_{yz} = -\frac{\partial \psi}{\partial x} \quad (53)$$

The state of the stress on one face of an element subjected to shearing stresses is shown in Figure

7. Then the resulting torque about the shear center  $T_{sv}$  is [24]

$$T_{sv} = \int_0^A (\tau_{xz}y - \tau_{yz}x) dA \quad (54)$$

The entire state of stress for the element on all faces as shown in Figure 8 must be in equilibrium,

so  $\Sigma f_z = 0$

$$\frac{\partial \tau_{xz}}{\partial x} + \frac{\partial \tau_{yz}}{\partial y} = 0 \quad (55)$$

Deriving Equation 53 and substituting into 52 conveys

$$\frac{\partial^2 \psi}{\partial x^2} + \frac{\partial^2 \psi}{\partial y^2} = -2G\phi' \quad (56)$$

Equation 54 will convey:

$$T_{sv} = \int_0^A \left( \frac{\partial \psi}{\partial y} y - \left( -\frac{\partial \psi}{\partial x} \right) x \right) dA \quad (57)$$

Therefore,

$$T_{sv} = 2 \iint \psi dx dy \quad (58)$$

Equation 58 suggests that the applied torque is equal to twice the area under the  $\Psi$  function. To find a solution for Equation 58, Timoshenko [24] and Galambos [22] propose the use of a membrane analogy, this technique permits visualizing the  $\Psi$  function inflated as a thin membrane over the exact cross section. The relationship between the applied twisting moment  $T_{sv}$  and the resulting twisting angle per unit length,  $\phi$ . is shown below [22].

$$T_{sv} = GK_T \phi' \quad (59)$$

in which  $K_T$  is the torsion constant and it is equal to the sum of the  $K_T$  values for each element

$$K_T = \frac{1}{3} \sum_{i=1}^{i=n} b_{ij} t_{ij}^3 \quad (60)$$

in which  $b_{ij}$  and  $t_{ij}$  are the length and the thickness of an element, respectively. The total twisting moment  $M_\zeta$  is the sum of the warping contribution  $T_w$  from Equation 37 and St. Venant contribution  $T_{sv}$  from Equation 59 [22]:

$$M_\zeta = -EI_\omega \phi''' + GK_T \phi' \quad (61)$$



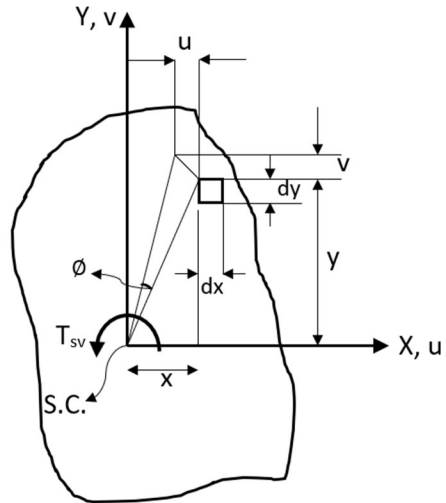


**Figure 6. Geometry of Shear Stress Element**

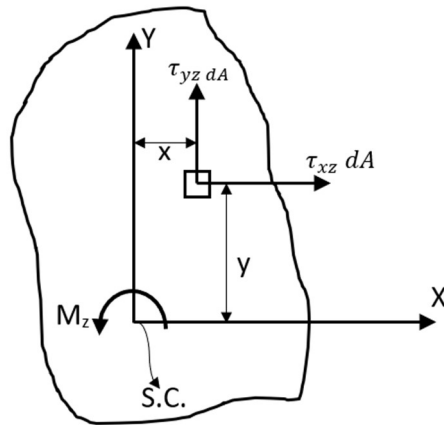


**Figure 7. Torsion of Solid Section**

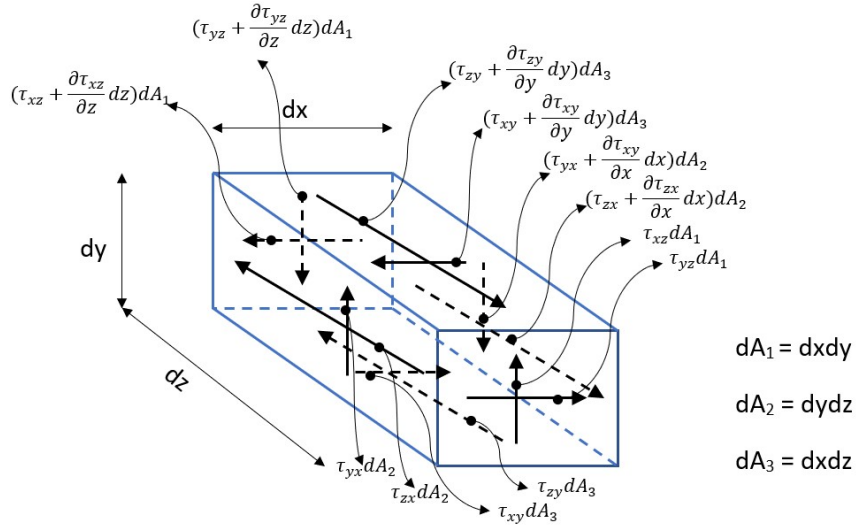


**Figure 8. Shear Stresses on Solid Element**

The member in Figures 1 and 9 are assumed to have initial out-of-straightness,  $\delta_x$  and  $\delta_y$ , in the  $x$  and  $y$  axes respectively, and to be prismatic. The bending restraints of the member and connections at the ends, B and T, are depicted by partial rotational springs with stiffnesses,  $k_{Tx}$ ,  $k_{Bx}$ ,  $k_{Ty}$ , and  $k_{By}$ . The forces consist of a compressive axial force  $P$  assumed to retain its original direction throughout the loading history moments  $M_{Tx}$ ,  $M_{Bx}$ ,  $M_{Ty}$ , and  $M_{By}$  are shown positive according to the right-hand rule, concentrated loads  $W$  and  $Q$  in the  $x$  and  $y$  axes respectively, and a torque  $M_z$  at the midspan of the member.  $M_x$  and  $M_y$  are the internal resisting bending moments.  $R_x$  and  $R_y$  are the reactions at the ends of the member computed from equilibrium.

$$R_{Tx} = \frac{1}{L} (M_{By} - m_{By} + M_{Ty} - m_{Ty} - k_x \Delta_x L + WZ^*) \quad (62)$$

$$R_{Bx} = R_{Tx} + K_x \Delta_x - W \quad (62 \text{ a})$$

$$R_{Ty} = \frac{1}{L} (M_{Bx} - m_{Bx} + M_{Tx} - m_{Tx} + K_y \Delta_y L - QZ^*) \quad (63)$$

$$R_{By} = R_{Ty} + Q - K_y \Delta_y \quad (63 \text{ a})$$

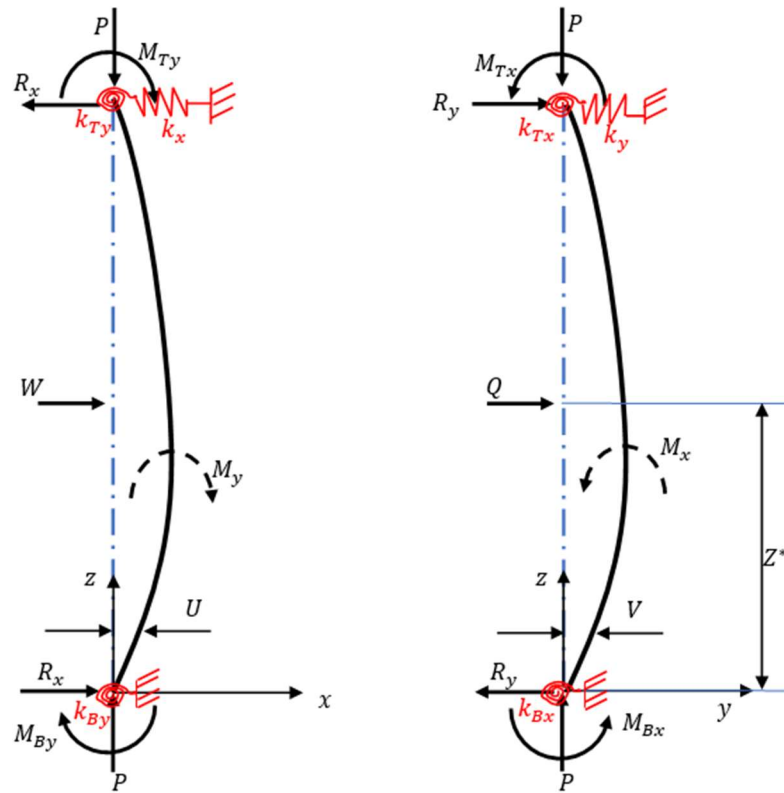


**Figure 9. Forces in the x-z and y-z Planes**

$m_{By}$ ,  $m_{Ty}$ ,  $m_{Bx}$  and  $m_{Tx}$  are the induced bending moments at the member ends due to partial rotational end restraints and are calculated as shown:

$$m_{Bx} = k_{Bx} \theta_{Bx} \quad (64)$$

$$m_{By} = k_{By} \theta_{By} \quad (65)$$

$$m_{Tx} = k_{Tx} \theta_{Tx} \quad (66)$$

$$m_{Ty} = k_{Ty} \theta_{Ty} \quad (67)$$

Internal bending moments  $M_x$  and  $M_y$  are obtained from the flexural equilibrium equation for  $Z^* \leq z \leq L$

$$M_x = -M_{Bx} + m_{Bx} + \frac{z}{L}(M_{Bx} - m_{Bx} + M_{Tx} - m_{Tx} + k_y \Delta_y L - QZ^*) + QZ^* - zk_y \Delta_y + PV \quad (68)$$

$$M_y = -M_{By} + m_{By} + \frac{z}{L}(M_{By} - m_{By} + M_{Ty} + m_{Ty} - k_x \Delta_x L + WZ^*) - WZ^* + zk_x \Delta_x - PU \quad (69)$$

Internal bending moments  $M_x$  and  $M_y$  for  $0 \leq z \leq Z^*$  can be written as follows:

$$M_x = -M_{Bx} + m_{Bx} + \frac{z}{L}(M_{Bx} - m_{Bx} + M_{Tx} - m_{Tx} + k_y \Delta_y L - QZ^*) + Qz - zk_y \Delta_y + PV \quad (70)$$

$$M_y = -M_{By} + m_{By} + \frac{z}{L}(M_{By} - m_{By} + M_{Ty} - m_{Ty} - k_x \Delta_x L + WZ^*) - Wz + zk_x \Delta_x - PU \quad (71)$$

where:

$$V = v_i + v_c \quad (72)$$

$$U = u_i + u_c \quad (73)$$

in which:

$$u_c = u + \phi Y_0 \quad \text{and} \quad v_c = v - \phi X_0 \quad (74)$$

$$u_i = \delta_{0x} \sin\left(\frac{\pi z}{L}\right) \quad \text{and} \quad v_i = \delta_{0y} \sin\left(\frac{\pi z}{L}\right) \quad (75)$$

Within the span of the member the cross section will no longer be in the original undeformed x-y-z coordinate system after the deformations have taken place. Rotation and translation of the cross section will occur as shown in Figure 10, and the principle set of new axes are  $\xi$  and  $\eta$ . The internal bending moments  $M_x$  and  $M_y$  will transform to the new axes; the angle  $\phi$  is small, therefore:

$$\tan \phi = \phi, \sin \phi = \phi, \text{ and } \cos \phi = 1 \quad (76)$$

The internal moment after deformations have taken place is obtained from the following equations:

$$M_{\xi} = M_x + \phi M_y \quad (77)$$

and

$$M_{\eta} = M_y - \phi M_x \quad (78)$$

Knowing that, the internal moments acting at any location along the z axis are obtained from [27]:

$$M_{\xi} = -EI_x v'' - EI_{xy} u'' \quad (79)$$

and

$$M_{\eta} = EI_y u'' + EI_{xy} v'' \quad (80)$$

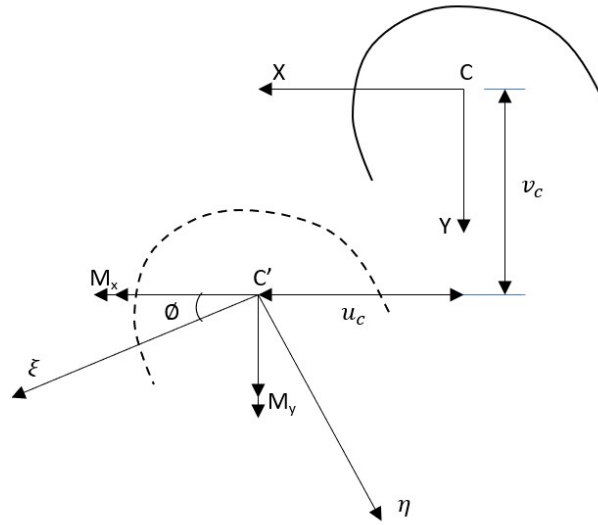


**Figure 10.  $\xi - \eta$  Coordinate System**

In addition to the components of  $M_x$  and  $M_y$  along the principal axes  $\xi$  and  $\eta$  due to the rotation of  $x$  and  $y$  axes, another component will occur along the axial principal axis  $\zeta$  within the span; it is perpendicular to the cross section and inclined from the  $z$  axis as seen in Figures 11 and 12.

The resultant of both components will make the first contribution for the twisting moment [22]

$$M_{\zeta 1} = M_x \frac{du}{dz} + M_y \frac{dv}{dz} \quad (81)$$

$$M_{\zeta 2} = P(Y_0 \frac{du}{dz} - X_0 \frac{dv}{dz}) \quad (82)$$

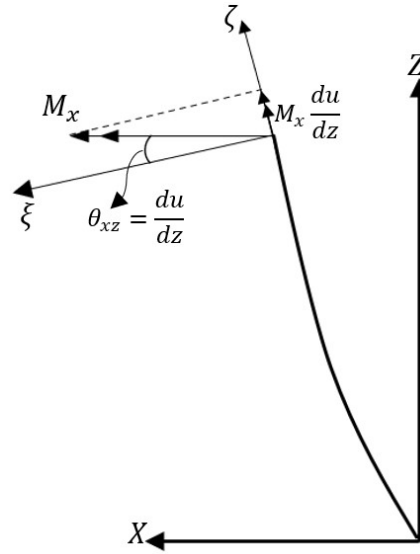


**Figure 11. Twisting Due to Component of  $M_x$**

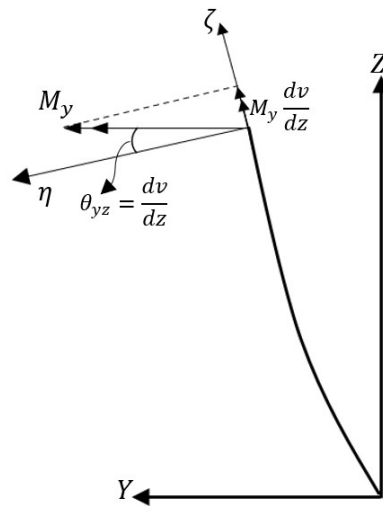


**Figure 12. Twisting Due to Component of  $M_y$**

The second contribution to the torque component results from axial load  $P$ .  $P$  will retain its original direction; therefore, it will have two components acting through the centroid of the cross section; the first component is the contribution of  $P$  in the  $x$ - $z$  plane, and the second contribution is from the  $y$ - $z$  plane as seen in Figures 13 and 14 [22].

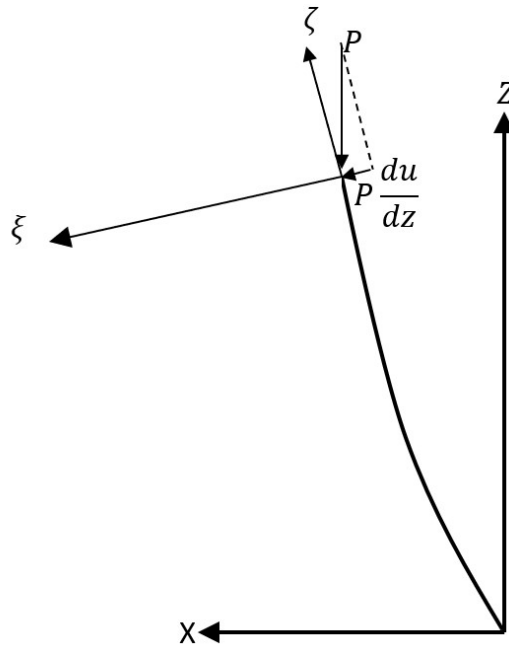


**Figure 13. Twisting Due to Component of P in X-Z Plane**

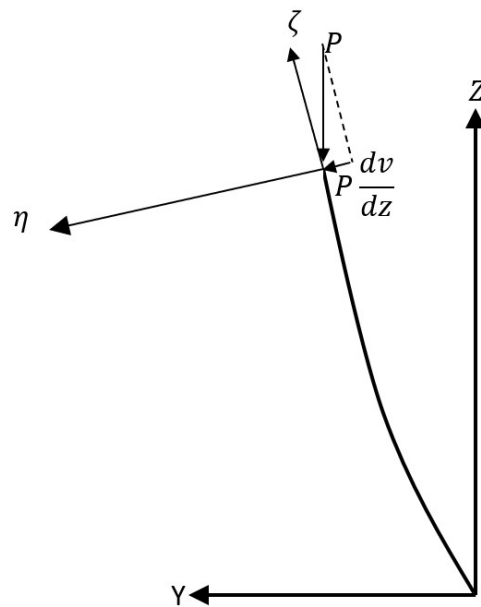


**Figure 14. Twisting Due to Component of P in Y-Z Plane**



Figure 15 illustrates the third contribution to the torque component caused by the warping of two adjacent cross sections to each other. The direction of the normal stress  $\sigma$  is inclined by the angle  $a \frac{d\phi}{d\zeta}$  to the  $\zeta$  axis. The component of this stress is  $\sigma dA a \frac{d\phi}{d\zeta}$ , and it causes a twist about the shear center equal to

$$dM_{\zeta 3} = -a \int (\sigma dA) \left( a \frac{d\phi}{d\zeta} \right) \quad (83)$$

Integrating Equation 83 over the cross-section results in

$$M_{\zeta 3} = -\frac{d\phi}{d\zeta} \int \sigma a^2 dA \quad (84)$$

The integration term of Equation 84 is known as the Wagner effect  $\bar{K}$  which is defined by:

$$\bar{K} = \int \sigma a^2 dA \quad (85)$$

$a$  is the distance from a point on the cross section to the shear center. Noting that  $d\zeta = dz$ , Equation 84 can be rewritten as shown below.

$$M_{\zeta 3} = -\bar{K} \frac{d\phi}{dz} \quad (86)$$

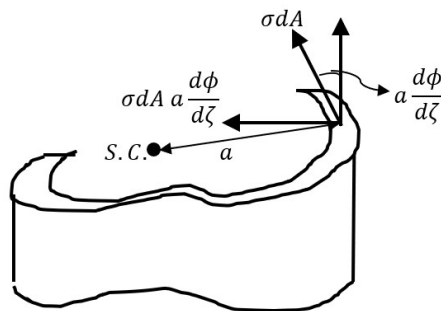


**Figure 15. Twisting Due to the Differential Warping of Two Adjacent Sections**

The last contribution to the torque is due to the end shears as can be seen in Figure 16.

$$M_{\zeta_4} = -R_y u - R_x v \quad (87)$$

Therefore, the total twisting moment is the sum of the four components in Equations 81, 82, 86, and 87.

$$M_{\zeta} = M_x \frac{du}{dz} + M_y \frac{dv}{dz} + P \left( Y_0 \frac{du}{dz} - X_0 \frac{dv}{dz} \right) - \bar{K} \frac{d\phi}{dz} - R_y u - R_x v \quad (88)$$

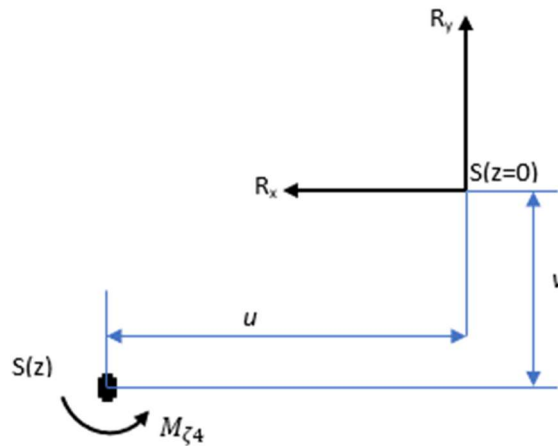


**Figure 16. Twisting Due to the End Shears**

An additional deflection will be produced by the shearing force, in the form of a mutual sliding of adjacent cross sections along each other as presented in Figure 17. For a simply supported beam with an in-span concentrated force case, Timoshenko [37] applies the conjugate beam method to superimpose the bending moment produced from the uniformly distributed load over a short portion,  $e$ , of the beam. Wang et al. [38] utilized the energy method to derive the bending solutions for different beam theories. The relationship between deflection, rotation, bending moment, and shear force of the Timoshenko beam theory (TBT) in terms of the corresponding quantities of Euler-Bernoulli beam theory (EBT) was established for different boundary conditions. The results

show that for statically determinate beams, the shear force, bending moment, and slope in the two theories remain the same, while the deflection differs. For statically indeterminate beams, the solutions for shear force, bending moment, slope, and deflection predicted by the two theories are not the same. In this dissertation the effects of shear for the Timoshenko beam will be incorporated in the stability equations for the applicable case as shown below.

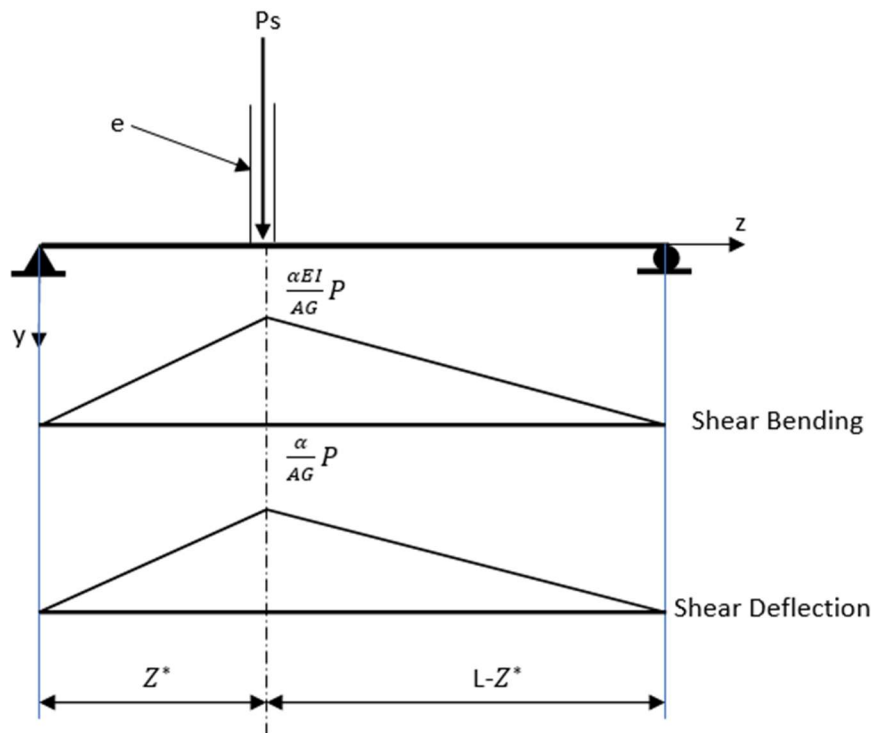


**Figure 17. Shear Bending and Deformation**

Equations 68 through 71 will be modified to incorporate the shear effect as shown below.

$$M_{t_x} = M_x + M_{sx} \quad (89)$$

$$M_{t_y} = M_y + M_{sy} \quad (90)$$

Similarly, Equations 72 and 73 will be modified as follows:

$$V_t = V + v^T \quad (91)$$

$$U_t = U + u^T \quad (92)$$

where:  $M_{sx}$  and  $M_{sy}$  are moments due to shear effect about the x and y axis respectively, and  $v^T$  and  $u^T$  are the deflections due to shear effect in the y and x axes, respectively. Timoshenko [37] introduced numerical factors  $\alpha_x$  and  $\alpha_y$  with which the average shearing stress must be multiplied to obtain the shearing stress at the centroid of the cross sections. Numerical factors,  $\alpha_x$  and  $\alpha_y$ , for I-sections can be calculated from the following equations:

$$\alpha_x = \frac{A}{8I_x t_w} \left[ b_f d^2 - (b_f - t_w)(d - 2t_f)^2 \right] \quad (93)$$

$$\alpha_y = \frac{A b_f^2}{4I_y} \quad (94)$$

Equations 77 and 78 will be adjusted to incorporate the shear effects as presented below.

$$M_\xi = M_{t_x} + \phi M_{t_y} \quad (95)$$

$$M_\eta = M_{t_y} - \phi M_{t_x} \quad (96)$$

Substitute Equations 89 and 90 into Equation 95. After rearranging and commensurate with the small deflection assumption, terms involving the products of quantities  $u\phi, v\phi, \phi^2, uv, v^2, u^2, v'\phi, u'\phi, \dots etc.$  are ignored. The first general stability governing equation is presented below.

$$\begin{aligned}
EI_x v'' + EI_{xy} u'' + Pv + m_{Bx} \left(1 - \frac{z}{L}\right) - \frac{z}{L} m_{Tx} + \phi \left[-M_{By} + \frac{z}{L} (M_{By} + M_{Ty} - k_x \Delta_x L + \right. \\
\left. WZ^*) + W(z - Z^*) + z(k_x \Delta_x - W) - M_{sy} - PX_0\right] = M_{Bx} - \frac{z}{L} (M_{Bx} + M_{Tx} + k_y \Delta_y L - \\
QZ^*) + Q(z - Z^*) + z(k_y \Delta_y - Q) - P(\delta_{0y} \sin\left(\frac{\pi z}{L}\right) + v^T) - M_{sx} \quad (97)
\end{aligned}$$

Furthermore, substituting Equations 89 and 90 into Equation 96 and following the small deflections assumption will lead to the second general stability equation presented below.

$$\begin{aligned}
EI_y u'' + EI_{xy} v'' - m_{By} \left(1 - \frac{z}{L}\right) - \frac{z}{L} m_{Ty} + Pu + \phi \left[-M_{Bx} + \frac{z}{L} (M_{Bx} + M_{Tx} + k_y \Delta_y L - QZ^*) - \right. \\
\left. Q(z - Z^*) + z(Q - k_y \Delta_y) + M_{sx} + PY_0\right] = -M_{By} + \frac{z}{L} (M_{By} + M_{Ty} - k_x \Delta_x L + WZ^*) + \\
W(z - Z^*) + z(k_x \Delta_x - W) - P\left(\delta_{0x} \sin\left(\frac{\pi z}{L}\right) + u^T\right) - M_{sy} \quad (98)
\end{aligned}$$

For  $0 \leq z \leq Z^*$ , the term  $W(z - Z^*)$  and  $Q(z - Z^*)$  in Equations 97 and 98 must be set to zero.

Finally, equating Equation 61 to Equation 88 will construct the last general stability equation. The third general stability equation is presented below.

$$\begin{aligned}
EI_\omega \phi''' - (GK_T + \bar{K})\phi' + u' \left(-M_{Bx} + \frac{z}{L} (M_{Bx} + M_{Tx} + k_y \Delta_y L - QZ^*) - Q(z - Z^*) + z(Q - \right. \\
\left. k_y \Delta_y) + M_{sx} + PY_0\right) + v' \left(-M_{By} + \frac{z}{L} (M_{By} + M_{Ty} - k_x \Delta_x L + WZ^*) + W(z - Z^*) + \right. \\
\left. z(k_x \Delta_x - W) - M_{sy} - PX_0\right) - \frac{u}{L} (M_{Bx} + M_{Tx} + k_y \Delta_y L - QZ^*) - \frac{v}{L} (M_{By} + M_{Ty} - k_x \Delta_x L + \\
WZ^*) = M_z \quad (99)
\end{aligned}$$

Setting the external applied moments at the top and bottom of the member equals the values shown below.

$$M_{Bx} = -M_{0x1} \quad \text{and} \quad M_{Tx} = M_{0x2} \quad (100)$$

$$M_{By} = M_{0y1} \quad \text{and} \quad M_{Ty} = -M_{0y2} \quad (101)$$

Equations 97, 98, and 99 can be rewritten as follows:

$$EI_x v'' + EI_{xy} u'' + Pv - m_{Bx} \left(1 - \frac{z}{L}\right) - m_{Tx} \frac{z}{L} - \phi \left[ M_{0y1} - \frac{z}{L} (M_{0y1} - M_{0y2} - k_x \Delta_x L + WZ^*) - W(z - Z^*) - z(k_x \Delta_x - W) + M_{sy} + PX_0 \right] = -M_{0x1} + \frac{z}{L} (M_{0x1} - M_{0x2} - k_y \Delta_y L + QZ^*) + Q(z - Z^*) + z(k_y \Delta_y - Q) - M_{sx} - P \left( \delta_{0y} \sin\left(\frac{\pi z}{L}\right) + v^T \right) \quad (102)$$

$$EI_y u'' + EI_{xy} v'' + Pu - m_{By} \left(1 - \frac{z}{L}\right) - m_{Ty} \frac{z}{L} + \phi \left[ M_{0x1} - \frac{z}{L} (M_{0x1} - M_{0x2} - k_y \Delta_y L + QZ^*) - Q(z - Z^*) + z(Q - k_y \Delta_y) + M_{sx} + PY_0 \right] = -M_{0y1} + \frac{z}{L} (M_{0y1} - M_{0y2} - k_x \Delta_x L + WZ^*) + W(z - Z^*) + z(k_x \Delta_x - W) - M_{sy} - P \left( \delta_{0x} \sin\left(\frac{\pi z}{L}\right) + u^T \right) \quad (103)$$

$$EI_\omega \phi'''' - (GK_T + \bar{K}) \phi' + u' \left[ M_{0x1} - \frac{z}{L} (M_{0x1} - M_{0x2} - k_y \Delta_y L + QZ^*) - Q(z - Z^*) + z(Q - k_y \Delta_y) + M_{sx} + PY_0 \right] - v' \left[ M_{0y1} - \frac{z}{L} (M_{0y1} - M_{0y2} - k_x \Delta_x L + WZ^*) - W(z - Z^*) - z(k_x \Delta_x - W) + M_{sy} + PX_0 \right] + \frac{u}{L} (M_{0x1} - M_{0x2} - k_y \Delta_y L + QZ^*) - \frac{v}{L} (M_{0y1} - M_{0y2} - k_x \Delta_x L + WZ^*) = M_z \quad (104)$$

Equations 102, 103, and 104 present the general stability governing equations that can be adjusted to accommodate different boundary conditions presented in the following sections.

## 2.2 Boundary Conditions

### 2.2.1 Non-sway Members with Biaxial Partial Rotational and Lateral Restraints

$$u(0) = u(L) = v(0) = v(L) = 0 \quad (105)$$

$$\Delta_x = \Delta_y = 0 \quad (106)$$

$$u'(0) = \theta_{Bx} \quad (107)$$

$$u'(L) = \theta_{Tx} \quad (108)$$

$$v'(0) = \theta_{By} \quad (109)$$

$$v'(L) = \theta_{Ty} \quad (110)$$

$$u''(0) = \frac{M_{0y1} - m_{By}}{EI_y} \quad (111)$$

$$u''(L) = \frac{-M_{0y2} + m_{Ty}}{EI_y} \quad (112)$$

$$v''(0) = \frac{-M_{0x1} + m_{Bx}}{EI_x} \quad (113)$$

$$v''(L) = \frac{M_{0x2} - m_{Bx}}{EI_x} \quad (114)$$

For restrained warping, boundary and symmetry conditions are written as:

$$\phi(0) = \phi'(0) = \phi(L) = \phi'(L) = 0 \quad (115)$$

While for unrestrained warping boundary conditions, Equation 115 will be written as follows:

$$\phi(0) = \phi''(0) = \phi(L) = \phi''(L) = 0 \quad (115 \text{ a})$$

### 2.2.2 Non-Sway Pinned Ends Members

In addition to Equations 105, 106, and 115 the following boundary conditions must be forced:

$$u''(0) = \frac{M_{0y1}}{EI_y} \quad (116)$$

$$u''(L) = \frac{-M_{0y2}}{EI_y} \quad (117)$$

$$v''(0) = \frac{-M_{0x1}}{EI_x} \quad (118)$$

$$v''(L) = \frac{M_{0x2}}{EI_x} \quad (119)$$

### 2.2.3 Sway Pinned Member

The following boundary conditions must be forced for this case:

$$u(0) = v(0) = 0 \quad (119 \text{ a})$$

$$u(L) = \Delta_x \text{ and } v(L) = \Delta_y \quad (119 \text{ b})$$

$$u''(0) = \frac{M_{0y1}}{EI_y} \text{ and } v''(0) = -\frac{M_{0x1}}{EI_x} \quad (119 \text{ c})$$

$$u'''(L) = \frac{R_x - k_x \Delta_x}{EI_y} \text{ and } v'''(L) = \frac{R_y - K_y \Delta_y}{EI_x} \quad (119 \text{ d})$$

### 2.2.4 Non-sway Fixed Ends Members

In addition to Equations 105, 106, 115 and 115a the following boundary conditions must be forced:

$$u'(0) = u'(L) = v'(0) = v'(L) = 0 \quad (120)$$

$$\theta_{Bx} = \theta_{Tx} = \theta_{By} = \theta_{Ty} = 0 \quad (121)$$



$$u''(0) = \frac{M_{0y1} - m_{By}}{EI_y} \quad (122)$$

$$u''(L) = \frac{-M_{0y2} + m_{Ty}}{EI_y} \quad (123)$$

$$v''(0) = \frac{-M_{0x1} + m_{Bx}}{EI_x} \quad (124)$$

$$v''(L) = \frac{M_{0x2} - m_{Tx}}{EI_x} \quad (125)$$

### 2.2.5 Sway Members with Biaxial Partial Rotational and Lateral Restraints

In addition to Equations 111 through 116 the following boundary conditions must be forced:

$$u(0) = v(0) = 0 \quad (126)$$

$$u(L) = \Delta_x \quad (127)$$

$$v(L) = \Delta_y \quad (128)$$

$$u'''(L) = \frac{R_x - k_x \Delta_x}{EI_y} \quad (129)$$

$$v'''(L) = \frac{R_y - k_y \Delta_y}{EI_x} \quad (130)$$

### 2.3 Finite-Difference Formulation

The central difference method, which involves pivotal points symmetrically located with respect to  $i$ , this method is more accurate than backward or forward differences and is particularly useful in the solution of boundary value problems. The differential equations using this method are shown below [28].

$$y_i' = \frac{-y_{i-1} + y_{i+1}}{2h} \quad (131)$$

$$y_i'' = \frac{y_{i-1} - 2y_i + y_{i+1}}{h^2} \quad (132)$$

$$y_i''' = \frac{-y_{i-2} + 2y_{i-1} - 2y_{i+1} + y_{i+2}}{2h^3} \quad (133)$$

$$y_i^{IV} = \frac{y_{i-2} - 4y_{i-1} + 6y_i - 4y_{i+1} + y_{i+2}}{h^4} \quad (134)$$

in which  $h$  is the grid step along the total span.

The next step is using the above finite differential formulations to solve three-stability differential Equations 102, 103, and 104 for I-sections numerically. These equations represent the governing equations for a single span beam-column member under axial load,  $P$ , biaxial bending moments applied at both ends of the member  $M_{0x}$  and  $M_{0y}$ , concentrated loads  $Q$  and  $W$ , and a torque at the midspan,  $M_z$ . Equation 88 assumed the only variables with respect to  $z$  are  $u$ ,  $v$ , and  $\phi$ . The finite differential formulation for Equations 102, 103, and 104 after rearranging are shown below.

$$\begin{aligned}
& \frac{B_x}{h^2} v_{i-1} + \left( P - 2 \frac{B_x}{h^2} \right) v_i + \frac{B_x}{h^2} v_{i+1} - m_{Bx} \left( 1 - \frac{z}{L} \right) - \frac{z}{L} m_{Tx} + \frac{B_{xy}}{h^2} u_{i-1} - 2 \frac{B_{xy}}{h^2} u_i + \frac{B_{xy}}{h^2} u_{i+1} - \\
& \phi_i \left[ M_{0y1} - \frac{z}{L} ( M_{0y1} - M_{0y2} - k_x \Delta_x L + WZ^* ) - W(z - Z^*) - z(k_x \Delta_x - W) + M_{sy} + PX_0 \right] = \\
& -M_{0x1} + \frac{z}{L} ( M_{0x1} - M_{0x2} - k_y \Delta_y L + QZ^* ) + Q(z - Z^*) + z(k_y \Delta_y - Q) - M_{sx} - \\
& P \left( \delta_{0y} \sin \left( \frac{\pi z}{L} \right) + v^T \right) \tag{135}
\end{aligned}$$

$$\begin{aligned}
& \frac{B_y}{h^2} u_{i-1} + \left( P - 2 \frac{B_y}{h^2} \right) u_i + \frac{B_y}{h^2} u_{i+1} - m_{By} \left( 1 - \frac{z}{L} \right) - \frac{z}{L} m_{Ty} + \frac{B_{xy}}{h^2} v_{i-1} - 2 \frac{B_{xy}}{h^2} v_i + \frac{B_{xy}}{h^2} v_{i+1} + \\
& \phi_i \left[ M_{0x1} - \frac{z}{L} ( M_{0x1} - M_{0x2} - k_y \Delta_y L + QZ^* ) - Q(z - Z^*) + z(Q - k_y \Delta_y) + M_{sx} + PY_0 \right] = \\
& -M_{0y1} + \frac{z}{L} ( M_{0y1} - M_{0y2} - k_x \Delta_x L + WZ^* ) + W(z - Z^*) + z(k_x \Delta_x - W) - M_{sy} - \\
& P \left( \delta_{0x} \sin \left( \frac{\pi z}{L} \right) + u^T \right) \tag{136}
\end{aligned}$$

$$\begin{aligned}
& -\frac{C_w}{2h^3} \phi_{i-2} + \left( \frac{C_w}{h^3} + \frac{(GK_T + K)}{2h} \right) \phi_{i-1} - \left( \frac{C_w}{h^3} + \frac{(GK_T + K)}{2h} \right) \phi_{i+1} + \frac{C_w}{2h^3} \phi_{i+2} - \frac{M_{tx}^*}{2h} u_{i-1} + M_{tx}^{**} u_i + \\
& \frac{M_{tx}^*}{2h} u_{i+1} + \frac{M_{ty}^*}{2h} v_{i-1} - M_{ty}^{**} v_i - \frac{M_{ty}^*}{2h} v_{i+1} = M_z \tag{137}
\end{aligned}$$

Where:

$$M_{tx}^* = M_{0x1} - \frac{z}{L} ( M_{0x1} - M_{0x2} - k_y \Delta_y L + QZ^* ) - Q(z - Z^*) + z(Q - k_y \Delta_y) + M_{sx} + PY_0 \tag{138}$$

$$M_{ty}^* = M_{0y1} - \frac{z}{L} ( M_{0y1} - M_{0y2} - k_x \Delta_x L + WZ^* ) - W(z - Z^*) - z(k_x \Delta_x - W) + M_{sy} + PX_0 \tag{139}$$

$$M_{tx}^{**} = \frac{1}{L} ( M_{0x1} - M_{0x2} - k_y \Delta_y L + QZ^* ) \tag{140}$$

$$M_{ty}^{**} = \frac{1}{L} ( M_{0y1} - M_{0y2} - k_x \Delta_x L + WZ^* ) \tag{141}$$

By applying equations 135, 136, and 137 at the number of nodes along the member, as shown in Figure 18, and utilizing the matrix form, these equations can be written as:

$$\{F\} = [K(P)]\{\Delta\} \quad (142)$$

where  $\{F\}$  is the nodal loading vector,  $[K(P)]$  is a stiffness matrix as a function of the applied axial load  $P$ , and  $\{\Delta\}$  is the nodal displacement vector.

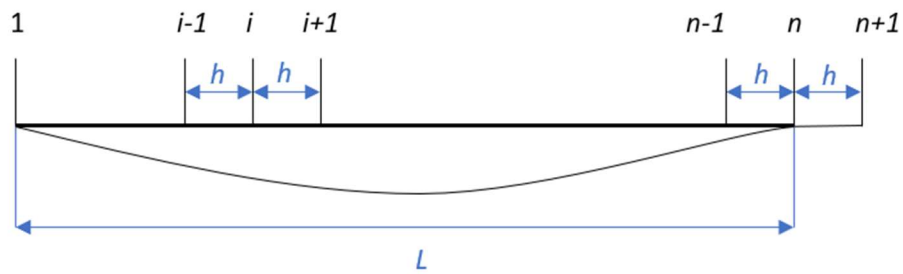


**Figure 18. Finite-Difference Nodes Along the Member**

## 2.4 Solution Procedure

The solution scheme of solving the nonlinear governing Equations 135 to 137 is developed and presented below.

1. Define geometric and material properties for the member.
2. Specify external loads.
3. Apply Equations 135 to 137 at discrete points along the member.
4. Generate the global stiffness matrix  $[K]$ .
5. Compute determinant  $D_p = |[K_p]|$  of matrix  $K$ .
6. Compute determinant  $D_0 = |[K_0]|$  of matrix  $K$ .

7. Compute dimensionless determinant  $\bar{D} = \frac{D_p}{D_o}$ .
8. Determine the instability load  $P_{cr}$ .
9. Compute deflections at each node using equation  $\{F\}=[K(P)]\{\Delta\}$ .
10. Compute  $\sigma\left(\frac{L}{2}\right)$  and  $\tau\left(\frac{L}{2}\right)$ .
11. Compute the Interaction Ratio and compare to that from Reference [33].
12. Increase the external loads and go to Step 3.
13. Stop.

The above iteration algorithm is programmed to obtain numerical results. Regression analysis is used to adjust the interaction ratio expression to include the second-order effects. The second-order normal stresses and shear stresses are computed using the following equations. The suggested Interaction Ratio expression will be discussed later in this dissertation:

$$\sigma = \frac{P}{A} + \frac{I_{xy}X - I_yY}{I_{xy}^2 - I_xI_y} (M_{tx} + \phi M_{ty}) + \frac{I_{xy}Y - I_xX}{I_{xy}^2 - I_xI_y} (M_{ty} - \phi M_{tx}) + \frac{PV}{S_x} + \frac{PU}{S_y} + E\omega_n\phi'' \quad (143)$$

$$\tau = \frac{V_y \int_0^s yt ds}{tI_x} + \frac{V_x \int_0^s xt ds}{tI_y} + \frac{ES_w\phi'''}{t} + Gt\phi' \quad (144)$$

Equations 143 and 144 will be used to determine initiation of cracking in members.

## 2.5 Equilibrium Equations for Simply Supported Sway Columns

If an axial compressive load is applied on a sway simply supported column, stability Equations 135-137 reduce to the following expressions:

$$\begin{aligned} \frac{B_x}{h^2} v_{i-1} + \left(P - 2\frac{B_x}{h^2}\right) v_i + \frac{B_x}{h^2} v_{i+1} + \frac{B_{xy}}{h^2} u_{i-1} - 2\frac{B_{xy}}{h^2} u_i + \frac{B_{xy}}{h^2} u_{i+1} - \phi_i P X_0 = \\ -P \left( \delta_{0y} \sin\left(\frac{\pi z}{L}\right) \right) \end{aligned} \quad (145)$$

$$\begin{aligned} & \frac{B_y}{h^2} u_{i-1} + \left(P - 2 \frac{B_y}{h^2}\right) u_i + \frac{B_y}{h^2} u_{i+1} + \frac{B_{xy}}{h^2} v_{i-1} - 2 \frac{B_{xy}}{h^2} v_i + \frac{B_{xy}}{h^2} v_{i+1} + \phi_i P Y_0 = \\ & -P \left( \delta_{0x} \sin\left(\frac{\pi z}{L}\right) \right) \end{aligned} \quad (146)$$

$$\begin{aligned} & -\frac{C_w}{2h^3} \phi_{i-2} + \left(\frac{C_w}{h^3} + \frac{GK_T + \bar{K}}{2h}\right) \phi_{i-1} - \left(\frac{C_w}{h^3} + \frac{GK_T + \bar{K}}{2h}\right) \phi_{i+1} + \frac{C_w}{2h^3} \phi_{i+2} - \frac{P Y_0}{2h} u_{i-1} - k_y \Delta_y u_i + \\ & \frac{P Y_0}{2h} u_{i+1} + \frac{P X_0}{2h} v_{i-1} + k_x \Delta_x v_i - \frac{P X_0}{2h} v_{i+1} = 0 \end{aligned} \quad (147)$$

## 2.6 Equilibrium Equations for Torsionally Free-Fixed Member

If a torsion is applied at the bottom end of a member, stability Equations 135-137 reduce to the following expression:

$$-\frac{C_w}{2h^3} \phi_{i-2} + \left(\frac{C_w}{h^3} + \frac{GK_T + \bar{K}}{2h}\right) \phi_{i-1} - \left(\frac{C_w}{h^3} + \frac{GK_T + \bar{K}}{2h}\right) \phi_{i+1} + \frac{C_w}{2h^3} \phi_{i+2} = M_z \quad (148)$$

## 2.7 Equilibrium Equations for Simply Supported Sway Beam-Column for Combined Axial Load and Biaxial Bending Moment

If an axial load and biaxial bending moment are applied concurrently, Equations 135-141 reduce to the following:

$$\begin{aligned} & \frac{B_x}{h^2} v_{i-1} + \left(P - 2 \frac{B_x}{h^2}\right) v_i + \frac{B_x}{h^2} v_{i+1} + \frac{B_{xy}}{h^2} u_{i-1} - 2 \frac{B_{xy}}{h^2} u_i + \frac{B_{xy}}{h^2} u_{i+1} - \phi_i \left[ M_{0y1} - \frac{z}{L} (M_{0y1} - \right. \\ & \left. M_{0y2} - k_x \Delta_x L) + M_{sy} + P X_0 \right] = -M_{0x1} + \frac{z}{L} (M_{0x1} - M_{0x2} - k_y \Delta_y L) - M_{sx} - \\ & P \left( \delta_{0y} \sin\left(\frac{\pi z}{L}\right) + v^T \right) \end{aligned} \quad (149)$$

$$\begin{aligned} & \frac{B_y}{h^2} u_{i-1} + \left(P - 2 \frac{B_y}{h^2}\right) u_i + \frac{B_y}{h^2} u_{i+1} + \frac{B_{xy}}{h^2} v_{i-1} - 2 \frac{B_{xy}}{h^2} v_i + \frac{B_{xy}}{h^2} v_{i+1} + \phi_i \left[ M_{0x1} - \frac{z}{L} (M_{0x1} - \right. \\ & \left. M_{0x2} - k_y \Delta_y L) + M_{sx} + P Y_0 \right] = -M_{0y1} + \frac{z}{L} (M_{0y1} - M_{0y2} - k_x \Delta_x L) - M_{sy} - \\ & P \left( \delta_{0x} \sin\left(\frac{\pi z}{L}\right) + u^T \right) \end{aligned} \quad (150)$$

$$\begin{aligned}
& -\frac{C_w}{2h^3} \phi_{i-2} + \left( \frac{C_w}{h^3} + \frac{(GK_T + \bar{K})}{2h} \right) \phi_{i-1} - \left( \frac{C_w}{h^3} + \frac{(GK_T + \bar{K})}{2h} \right) \phi_{i+1} + \frac{C_w}{2h^3} \phi_{i+2} - \frac{M_{tx}^*}{2h} u_{i-1} + M_{tx}^{**} u_i + \\
& \frac{M_{tx}^*}{2h} u_{i+1} + \frac{M_{ty}^*}{2h} v_{i-1} - M_{ty}^{**} v_i - \frac{M_{ty}^*}{2h} v_{i+1} = 0
\end{aligned} \tag{151}$$

where:

$$M_{tx}^* = M_{0x1} - \frac{z}{L} (M_{0x1} - M_{0x2}) + M_{sx} + PY_0 \tag{152}$$

$$M_{ty}^* = M_{0y1} - \frac{z}{L} (M_{0y1} - M_{0y2}) + M_{sy} + PX_0 \tag{153}$$

$$M_{tx}^{**} = \frac{1}{L} (M_{0x1} - M_{0x2} - k_y \Delta_y L) \tag{154}$$

$$M_{ty}^{**} = \frac{1}{L} (M_{0y1} - M_{0y2} - k_x \Delta_x L) \tag{155}$$

Equations 149-155 are the governing differential equations for a simply supported beam-column under axial load, biaxial bending moments, and torsion.

## 2.8 Equilibrium Equations for Simply Supported Sway Beam-Columns for Combined Axial Load, Torsion and Biaxial Bending Moment

If an axial compressive load, biaxial bending moment, and torsional moment are applied concurrently, Equations 149-155 are applicable except Equation 151 reduces to the following expressions:

$$\begin{aligned}
& -\frac{C_w}{2h^3} \phi_{i-2} + \left( \frac{C_w}{h^3} + \frac{(GK_T + \bar{K})}{2h} \right) \phi_{i-1} - \left( \frac{C_w}{h^3} + \frac{(GK_T + \bar{K})}{2h} \right) \phi_{i+1} + \frac{C_w}{2h^3} \phi_{i+2} - \frac{M_{tx}^*}{2h} u_{i-1} + M_{tx}^{**} u_i + \\
& \frac{M_{tx}^*}{2h} u_{i+1} + \frac{M_{ty}^*}{2h} v_{i-1} - M_{ty}^{**} v_i - \frac{M_{ty}^*}{2h} v_{i+1} = M_z
\end{aligned} \tag{156}$$

Equations 145-156 are the governing differential equations for a simply supported beam-column under axial load, biaxial bending moments, and torsion.

## 2.9 Equilibrium Equations for Fixed-Pinned Sway Beam-Columns for Combined Axial Load, Biaxial Bending Moments, and Torsion

If an axial compressive load, biaxial bending moment, and torsional moment are applied concurrently, Equations 135-141 reduce to the following expressions:

$$\frac{B_x}{h^2} v_{i-1} + \left( P - 2 \frac{B_x}{h^2} \right) v_i + \frac{B_x}{h^2} v_{i+1} + \frac{B_{xy}}{h^2} u_{i-1} - 2 \frac{B_{xy}}{h^2} u_i + \frac{B_{xy}}{h^2} u_{i+1} - \phi_i \left[ \frac{z}{L} M_{0y2} + M_{sy} + P X_0 \right] = - \frac{z}{L} M_{0x2} - M_{sx} - P \left( \delta_{0y} \sin \left( \frac{\pi z}{L} \right) + v^T \right) \quad (157)$$

$$\frac{B_y}{h^2} u_{i-1} + \left( P - 2 \frac{B_y}{h^2} \right) u_i + \frac{B_y}{h^2} u_{i+1} + \frac{B_{xy}}{h^2} v_{i-1} - 2 \frac{B_{xy}}{h^2} v_i + \frac{B_{xy}}{h^2} v_{i+1} + \phi_i \left[ \frac{z}{L} M_{0x2} + M_{sx} + P Y_0 \right] = - \frac{z}{L} M_{0y2} - M_{sy} - P \left( \delta_{0x} \sin \left( \frac{\pi z}{L} \right) + u^T \right) \quad (158)$$

$$- \frac{C_w}{2h^3} \phi_{i-2} + \left( \frac{C_w}{h^3} + \frac{(GK_T + \bar{K})}{2h} \right) \phi_{i-1} - \left( \frac{C_w}{h^3} + \frac{(GK_T + \bar{K})}{2h} \right) \phi_{i+1} + \frac{C_w}{2h^3} \phi_{i+2} - \frac{M_{tx}^*}{2h} u_{i-1} + M_{tx}^{**} u_i + \frac{M_{tx}^*}{2h} u_{i+1} + \frac{M_{ty}^*}{2h} v_{i-1} - M_{ty}^{**} v_i - \frac{M_{ty}^*}{2h} v_{i+1} = M_z \quad (159)$$

Where:

$$M_{tx}^* = \frac{z}{L} M_{0x2} + M_{sx} + P Y_0 \quad (160)$$

$$M_{ty}^* = \frac{z}{L} M_{0y2} + M_{sy} + P X_0 \quad (161)$$

$$M_{tx}^{**} = - \frac{1}{L} M_{0x2} \quad (162)$$

$$M_{ty}^{**} = - \frac{1}{L} M_{0y2} \quad (163)$$



Equations 157-163 are the governing differential equations for a sway beam column fixed at the bottom end and pinned at the top end under axial load, biaxial bending moments, and torsion.

## 2.10 Numerical Results

Numerical results based on the theoretical formulation are presented below.

### 2.10.1 Torsionally Loaded Member

Table 1 presents the theoretical results extracted from the MATLAB code developed in this dissertation. The first column in this table shows the applied torsion,  $M_z$ , while the second column presents the angle of twist,  $\phi$ , at the bottom end of the member. Figure 19 presents the applied torsion versus the angle of twist at the bottom end of the member.

**Table 1. Theoretical Results for Torsionally Loaded Member**

| $\Phi$<br>deg. | $M_z$<br>lb.in. |
|----------------|-----------------|
| 0              | 0               |
| 2.5961         | 406.25          |
| 4.673          | 731.25          |
| 5.112          | 800             |
| 5.7514         | 900             |
| 6.39           | 1000            |
| 12.78043       | 2000            |
| 159.7547       | 25000           |
| 20.22499       | 3165            |

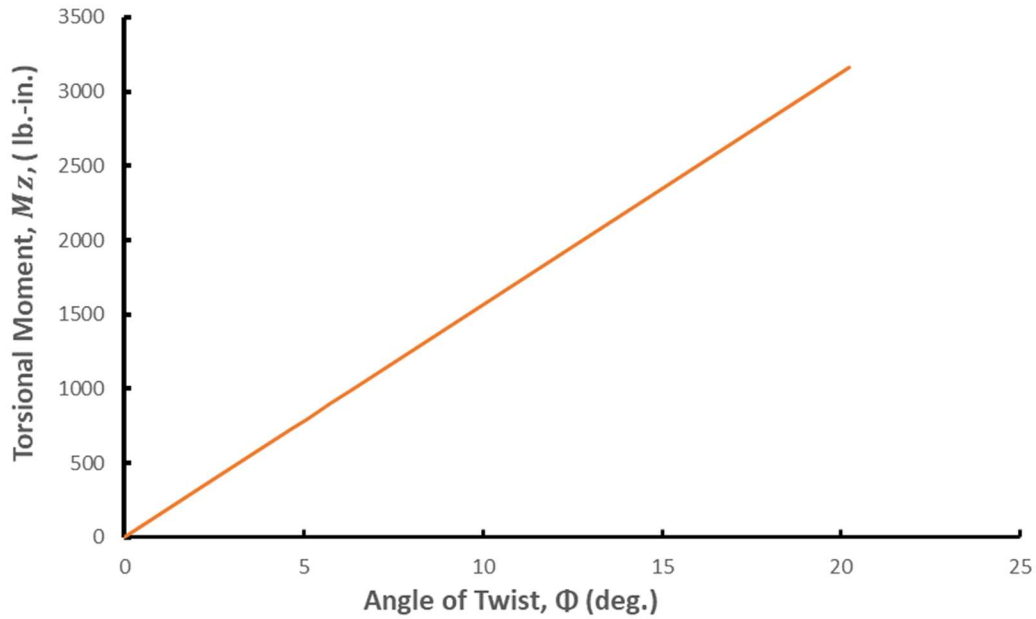


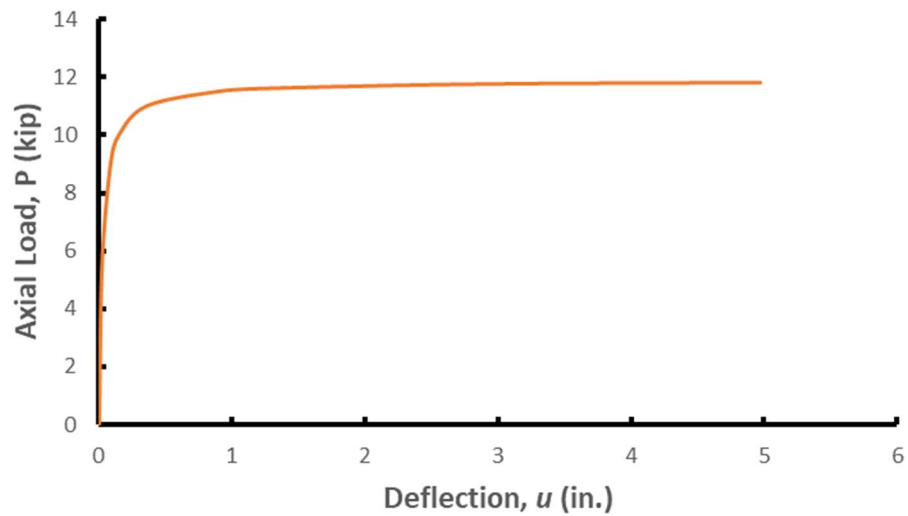
**Figure 19. Torsional Moment,  $M_z$ , vs. Angle of Twist,  $\phi$**

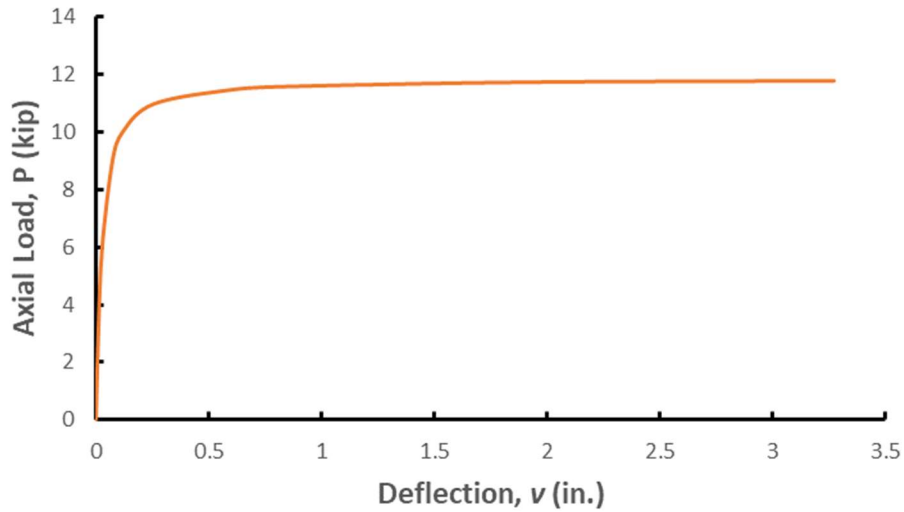
### 2.10.2 Axially Loaded Member

Table 2 presents the theoretical results from the MATLAB code. The first column in this table shows the applied axial load,  $P$ . The deflections in the  $y$  axis;  $v$ ,  $x$  axes;  $u$ , and the angle of twist,  $\phi$ , are shown in the second, third, and fourth column of this table, respectively. Figures 20, 21, and 22 show the axial Load,  $P$ , versus the midspan deflection in the  $y$  axis,  $v$ , in the  $x$  axis  $u$ , and the angle of twist,  $\phi$ , respectively.

**Table 2. Theoretical Results for Axially Loaded Member**

| <b>P</b>   | <b><i>v</i></b> | <b><i>u</i></b> | <b><math>\Phi</math></b> |
|------------|-----------------|-----------------|--------------------------|
| <b>kip</b> | <b>in.</b>      | <b>in.</b>      | <b>deg.</b>              |
| 0          | 0               | 0               | 0                        |
| 3          | 0.010098        | 0.007967        | 0                        |
| 6          | 0.027321        | 0.025788        | 0                        |
| 9          | 0.07252         | 0.085174        | 0                        |
| 10         | 0.116582        | 0.149061        | 0                        |
| 11         | 0.25806         | 0.362044        | 0                        |
| 11.5       | 0.612366        | 0.903032        | 0                        |
| 11.6       | 0.840661        | 1.252494        | 0                        |
| 11.75      | 1.899903        | 2.875197        | 0                        |
| 11.8       | 3.271223        | 4.976575        | 0                        |
| 11.85      | 11.73559        | 17.94823        | 0                        |

**Figure 20. Axial Load,  $P$ , vs. Midspan Deflection,  $u$**



**Figure 21. Axial Load,  $P$ , vs. Midspan Deflection,  $v$**

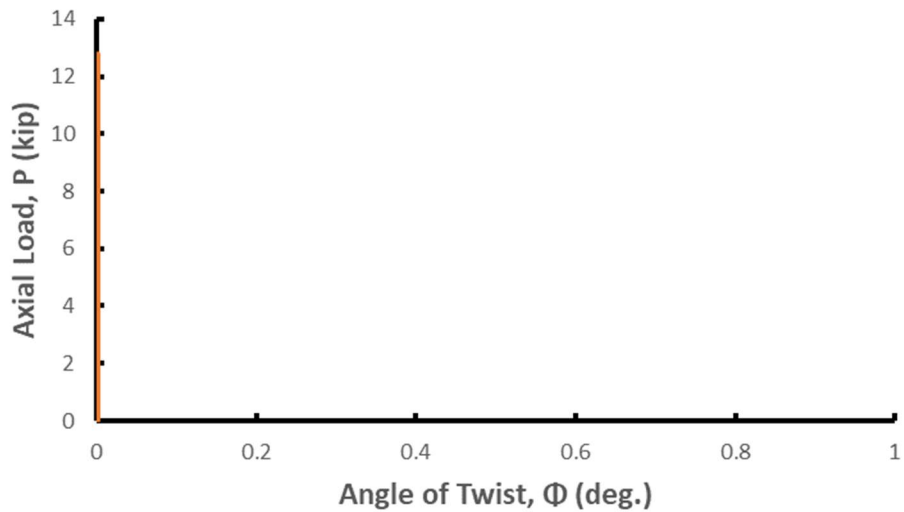


**Figure 22. Axial Load,  $P$ , vs. Bottom End Angle of Twist,  $\phi$**

### 2.10.3 Combined Axial Load and Biaxial Bending Moment

Table 3 summarizes the theoretical results for this test. Figures 23 through 25 present the applied axial load,  $P$ , versus the midspan deflection,  $v$ ,  $u$ , and the bottom end angle of twist,  $\phi$ , respectively.

Figures 26 through 28 present the applied bending moment,  $M_x$ , versus the midspan deflections.

Table 3. Combined Axial Load and Biaxial Bending Moment

| $M_x$ , kip.in. | $v$ , in. | $u$ , in. | $\Phi$ , deg. |
|-----------------|-----------|-----------|---------------|
| 0               | 0         | 0         | 0             |
| 1               | 0.03708   | 0.098039  | 0.013471      |
| 2               | 0.07415   | 0.196078  | 0.05379       |
| 2.5             | 0.09268   | 0.245098  | 0.083936      |
| 3               | 0.1112    | 0.294118  | 0.120675      |
| 3.5             | 0.12972   | 0.343137  | 0.163943      |
| 4               | 0.14824   | 0.392157  | 0.213664      |
| 4.5             | 0.16675   | 0.441176  | 0.269755      |
| 5               | 0.18525   | 0.490196  | 0.332121      |
| 6               | 0.22223   | 0.588235  | 0.475245      |
| 9               | 0.33294   | 0.882353  | 1.042506      |
| 10              | 0.36974   | 0.980392  | 1.273589      |
| 11              | 0.40649   | 1.078431  | 1.523454      |
| 12              | 0.44318   | 1.176471  | 1.790673      |
| 12.5            | 0.46151   | 1.22549   | 1.930333      |

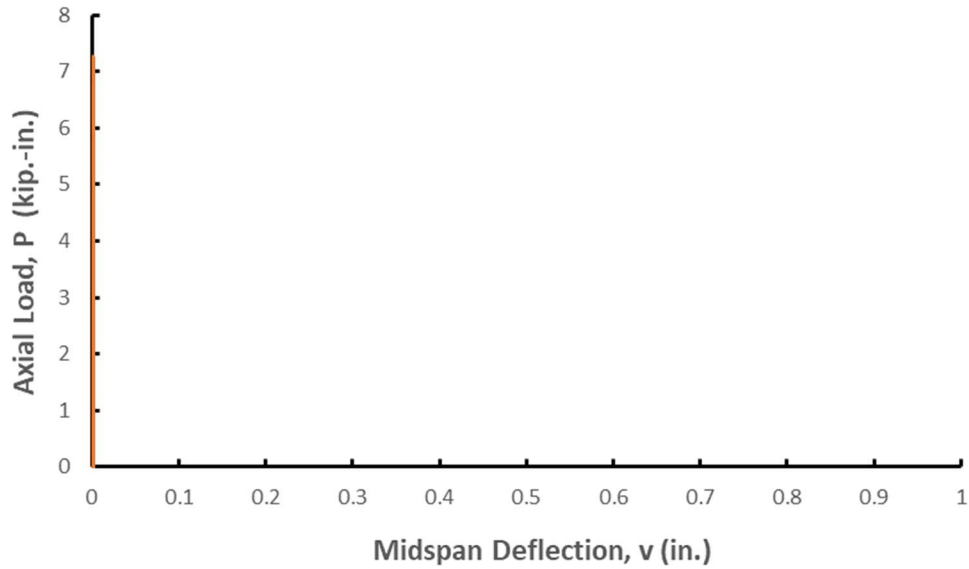
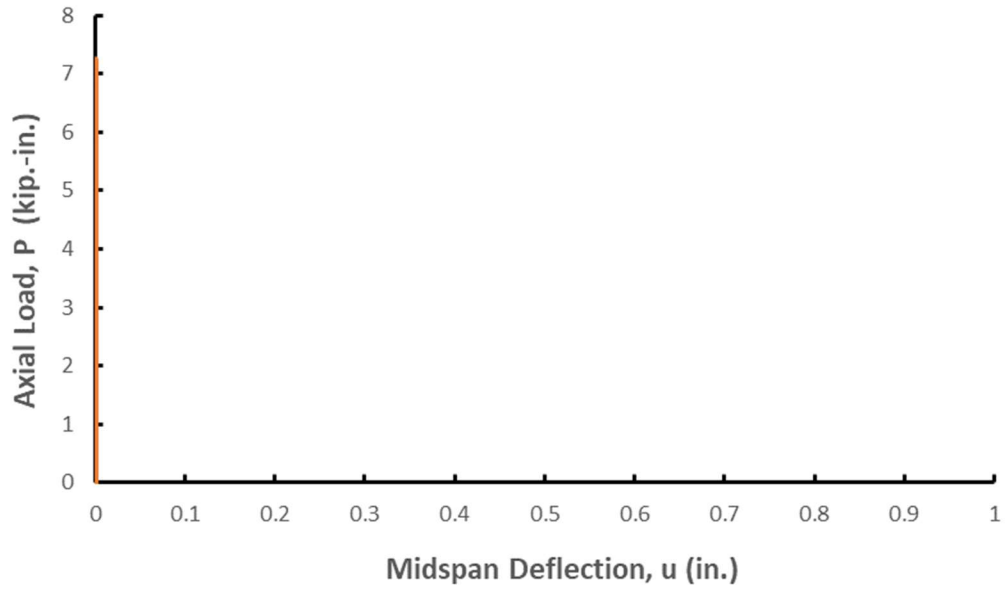
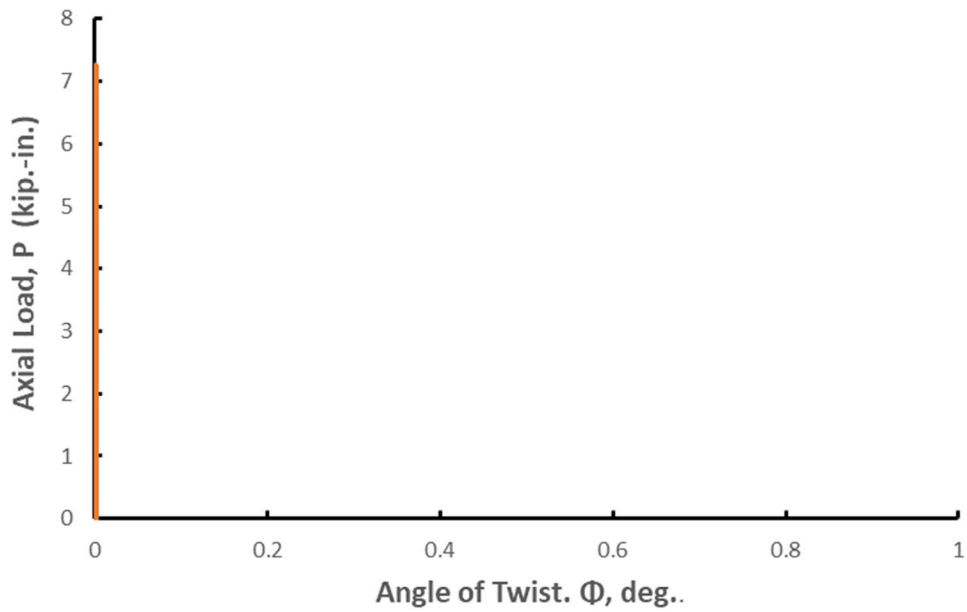


Figure 23. Axial Load, P, vs. Midspan Deflection, v



**Figure 24. Axial Load, P, vs. Midspan Deflection,  $u$**



**Figure 25. Axial Load, P, vs. Midspan Angle of Twist,  $\phi$**

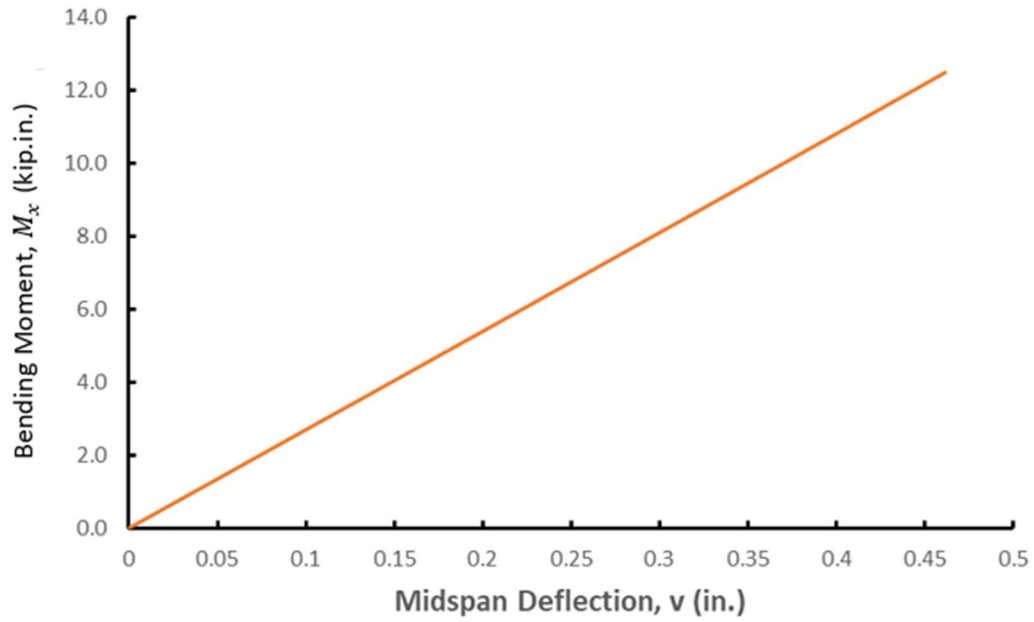


Figure 26. Bending Moment,  $M_x$ , vs. Midspan Deflection,  $v$

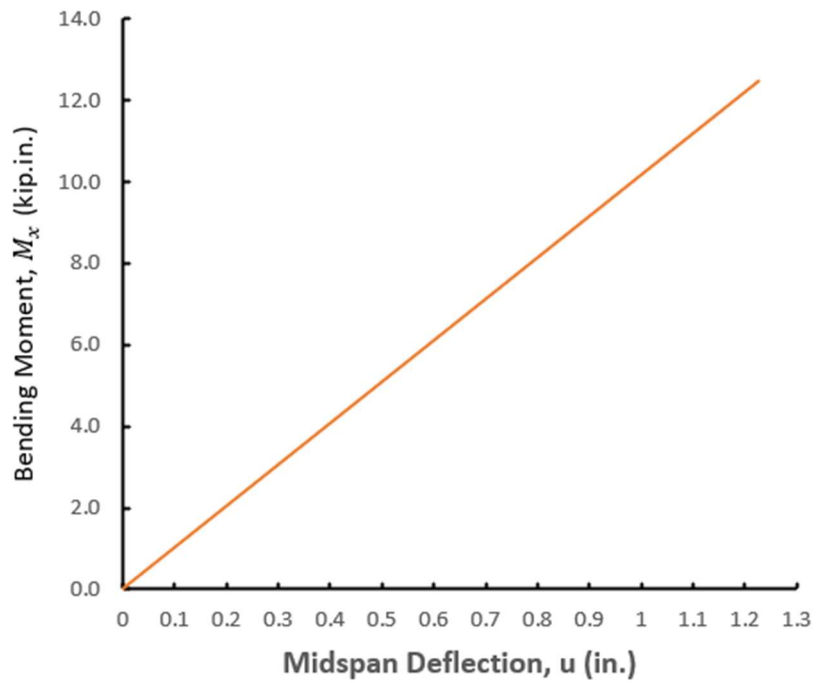
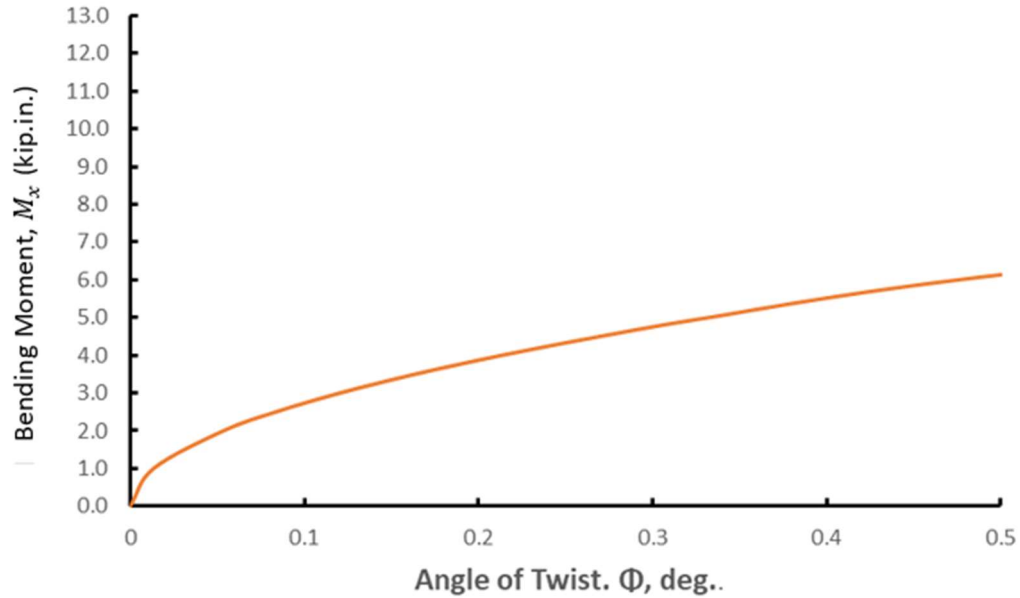


Figure 27. Bending Moment,  $M_x$ , vs. Midspan Deflection,  $u$



**Figure 28. Bending Moment,  $M_x$ , vs. Bottom End Angle of Twist,  $\phi$**

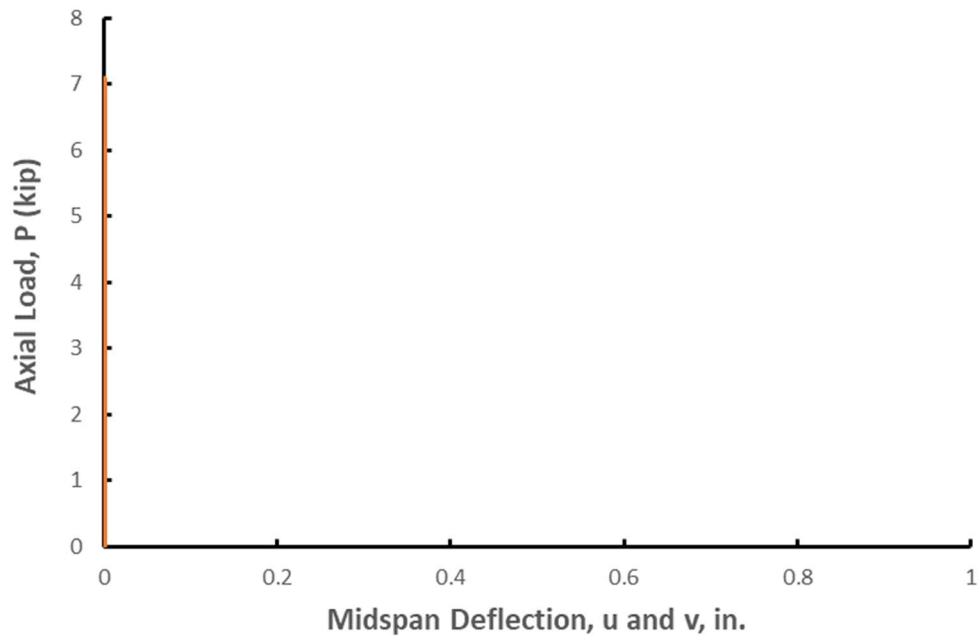
#### **2.10.4 Combined Axial Load, Biaxial Bending Moment, and Torsion with Flexurally Pinned Ends**

Table 4 summarizes the theoretical results for this test. The first column of this table shows the applied bending moment,  $M_x$ . The second through the third columns represent the deflection  $v$ ,  $u$ , and the bottom end angle of twist,  $\phi$  respectively. Figures 29 through 33 show the axial load,  $P$ , torsion,  $M_z$ , and bending moment,  $M_x$  vs. deflection  $v$ ,  $u$ , and  $\phi$  respectively.



**Table 4. Theoretical Results for Combined Axial Load, Biaxial Bending Moment, and Torsion with Flexurally Pinned Ends**

| $M_x$ , kip.in. | $v$ , in. | $u$ , in. | $\Phi$ , deg. |
|-----------------|-----------|-----------|---------------|
| 0               | 0         | 0         | 0.101463      |
| 0.76875         | 0.017384  | 0.048652  | 0.10349       |
| 0.873214        | 0.019746  | 0.055263  | 0.10456       |
| 1.048929        | 0.02372   | 0.066384  | 0.116         |
| 1.222500        | 0.027645  | 0.077369  | 0.1194        |
| 1.315179        | 0.02974   | 0.083234  | 0.121         |
| 1.366071        | 0.030891  | 0.086455  | 0.123         |
| 1.429821        | 0.032333  | 0.090489  | 0.1253        |
| 1.714821        | 0.038778  | 0.108526  | 0.1279        |
| 1.994464        | 0.045101  | 0.126224  | 0.130928      |
| 2.378036        | 0.053775  | 0.150499  | 0.13345       |
| 2.645893        | 0.059832  | 0.167451  | 0.1361        |
| 2.751964        | 0.062231  | 0.174164  | 0.1405        |
| 2.883214        | 0.065199  | 0.18247   | 0.1447        |
| 3.036964        | 0.068675  | 0.192201  | 0.1478        |
| 3.188036        | 0.072092  | 0.201762  | 0.1579        |
| 3.357857        | 0.075932  | 0.212509  | 0.163928      |
| 3.493929        | 0.079009  | 0.221121  | 0.167         |
| 3.631607        | 0.082122  | 0.229834  | 0.1831        |
| 3.846429        | 0.08698   | 0.243429  | 0.191         |
| 4.043571        | 0.091438  | 0.255906  | 0.2068        |
| 4.177500        | 0.094467  | 0.264382  | 0.2155        |
| 4.595893        | 0.103928  | 0.290861  | 0.225         |
| 4.824107        | 0.109088  | 0.305304  | 0.239         |
| 4.956429        | 0.112081  | 0.313678  | 0.247         |
| 5.490536        | 0.124158  | 0.34748   | 0.257         |
| 5.740179        | 0.129804  | 0.363279  | 0.2789        |
| 6.211607        | 0.140464  | 0.393115  | 0.33          |
| 6.454821        | 0.145964  | 0.408507  | 0.2655        |
| 6.722679        | 0.152021  | 0.425459  | 0.275         |
| 7.069821        | 0.159871  | 0.447429  | 0.289         |
| 7.258393        | 0.164135  | 0.459363  | 0.297         |
| 7.499464        | 0.169587  | 0.47462   | 0.307         |
| 8.0             | 0.180905  | 0.506297  | 0.3289        |
| 9.0             | 0.203519  | 0.569584  | 0.38          |
| 10.0            | 0.226132  | 0.632871  | 0.432         |
| 10.5            | 0.237438  | 0.664515  | 0.4618        |



**Figure 29. Axial Load,  $P$ , vs. Midspan Deflection,  $u$ ,  $v$**

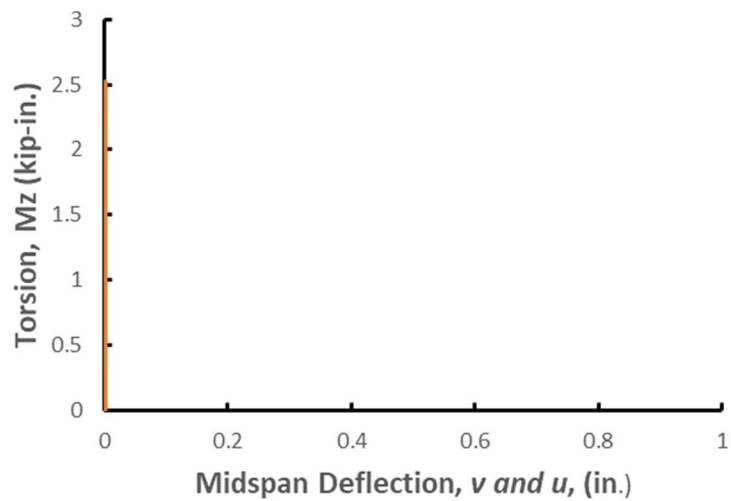


**Figure 30. Torsion,  $M_z$ , vs. Midspan Deflection,  $v$  and  $u$**

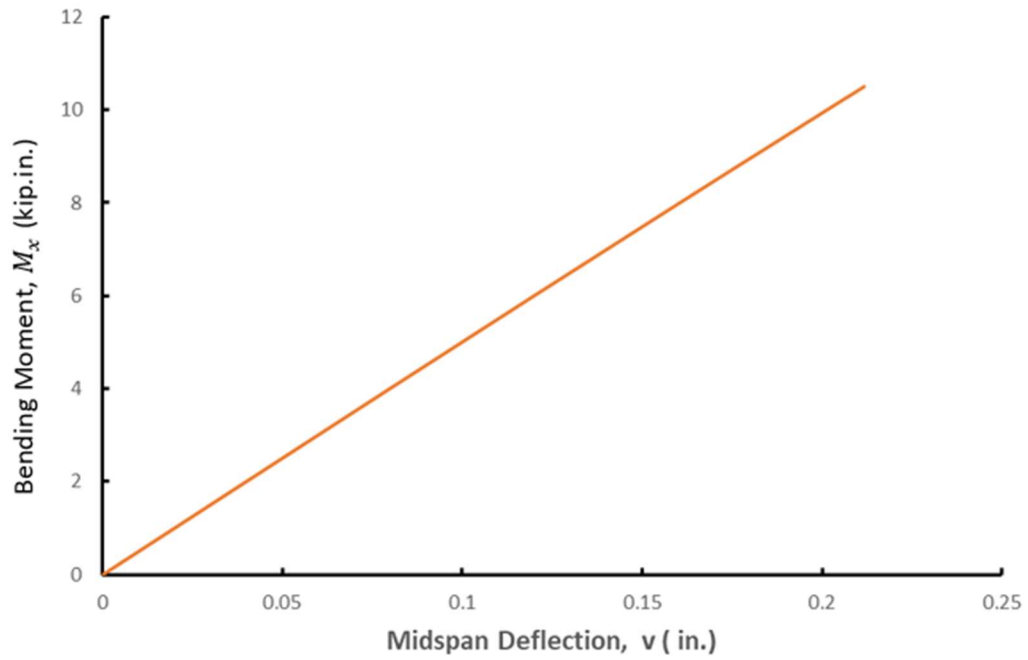


**Figure 31. Bending Moment,  $M_x$ , vs. Midspan Deflection,  $v$**

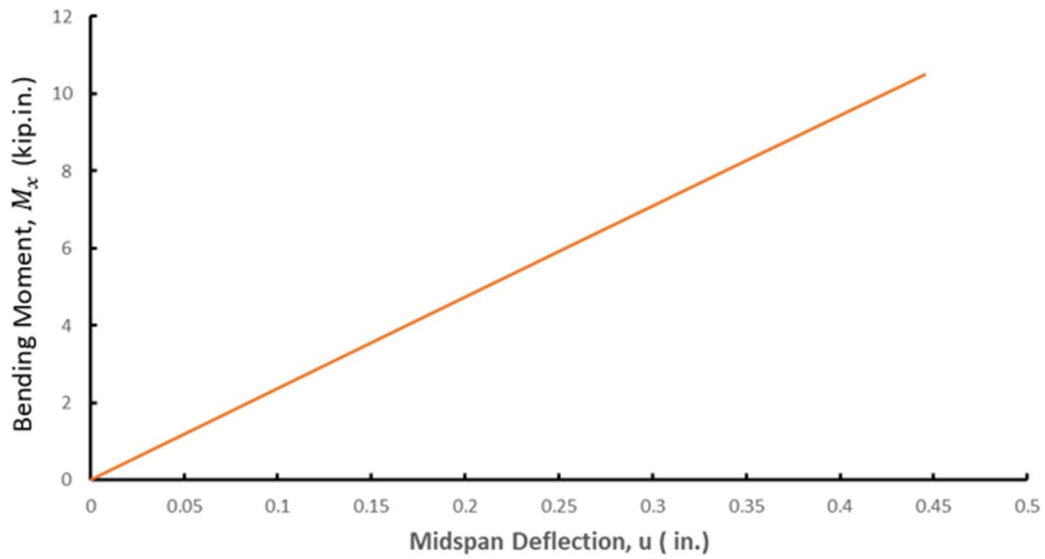


**Figure 32. Bending Moment,  $M_x$ , vs. Midspan Deflection,  $u$**

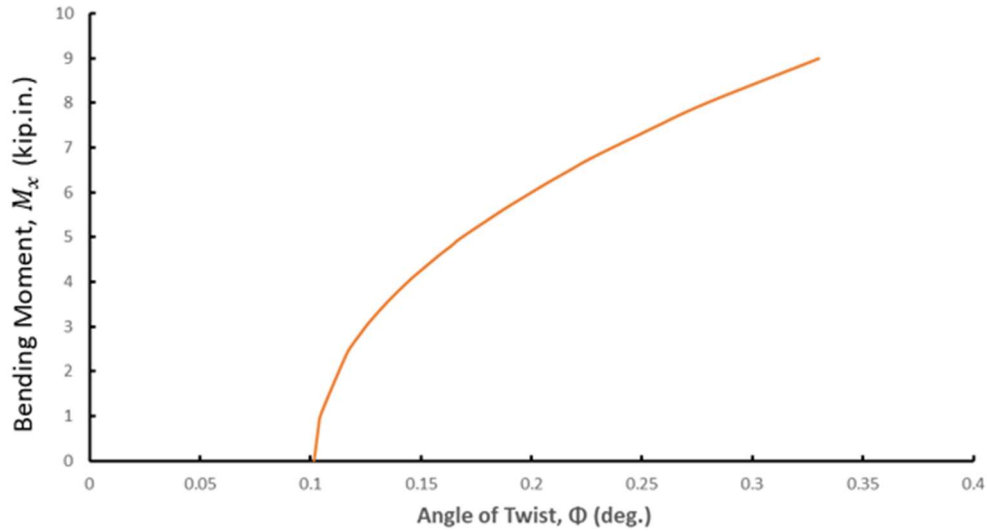


**Figure 33. Bending Moment,  $M_x$ , vs. Bottom End Angle of Twist,  $\phi$**

### **2.10.5 Combined Axial Load, Biaxial Bending Moment, and Torsion with Flexurally Fixed-Pinned**

Table 5 summarizes the theoretical results for this test. The first column of this table shows the applied bending moment. The second through the third column represent the deflection  $v$ ,  $u$ , and the bottom end angle of twist,  $\phi$  respectively. Figures 34 through 37 show the axial load,  $P$ , and bending moment,  $M_x$ , vs. deflection  $v$ ,  $u$ , and  $\phi$  respectively.

**Table 5. Theoretical Results for Combined Axial Load, Biaxial Bending Moment, and Torsion with Flexurally Fixed-Pinned**

| $M_x$ , kip.in. | $v$ , in. | $u$ , in. | $\Phi$ , deg. |
|-----------------|-----------|-----------|---------------|
| 0               | 0         | 0         | -0.0122       |
| 2.4567857       | 0.084021  | 0.116094  | -0.01578      |
| 3.0953571       | 0.10586   | 0.14627   | -0.01398      |
| 3.58875         | 0.122734  | 0.169585  | -0.00793      |
| 4.1191071       | 0.140872  | 0.194646  | 0.002896      |
| 4.6548214       | 0.159194  | 0.219961  | 0.015623      |
| 5.175           | 0.176984  | 0.244542  | 0.028604      |
| 5.7123214       | 0.19536   | 0.269933  | 0.04566       |
| 6.2496429       | 0.213736  | 0.295324  | 0.065867      |
| 6.7992857       | 0.232534  | 0.321297  | 0.087378      |
| 7.2691071       | 0.248601  | 0.343498  | 0.109573      |
| 7.4458929       | 0.254647  | 0.351852  | 0.119795      |
| 7.5369643       | 0.257762  | 0.356156  | 0.124754      |
| 7.6548214       | 0.261793  | 0.361725  | 0.129534      |
| 7.7458929       | 0.264907  | 0.366028  | 0.13653       |
| 7.8744643       | 0.269305  | 0.372104  | 0.147349      |
| 8.2173214       | 0.28103   | 0.388306  | 0.168516      |

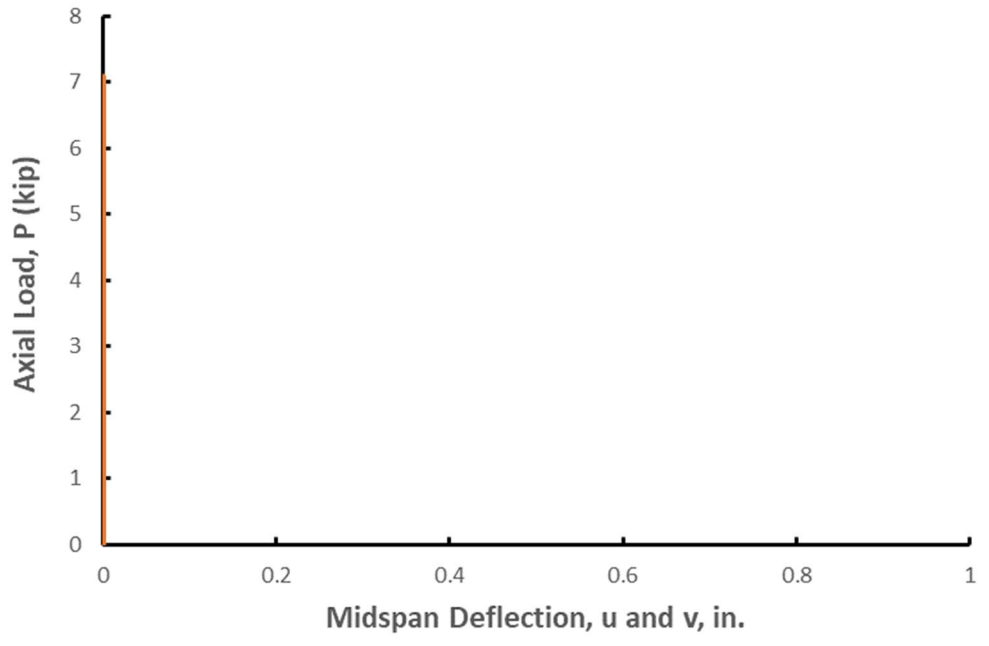


**Figure 34. Axial Load, P, vs. Midspan Deflections, v, and u**

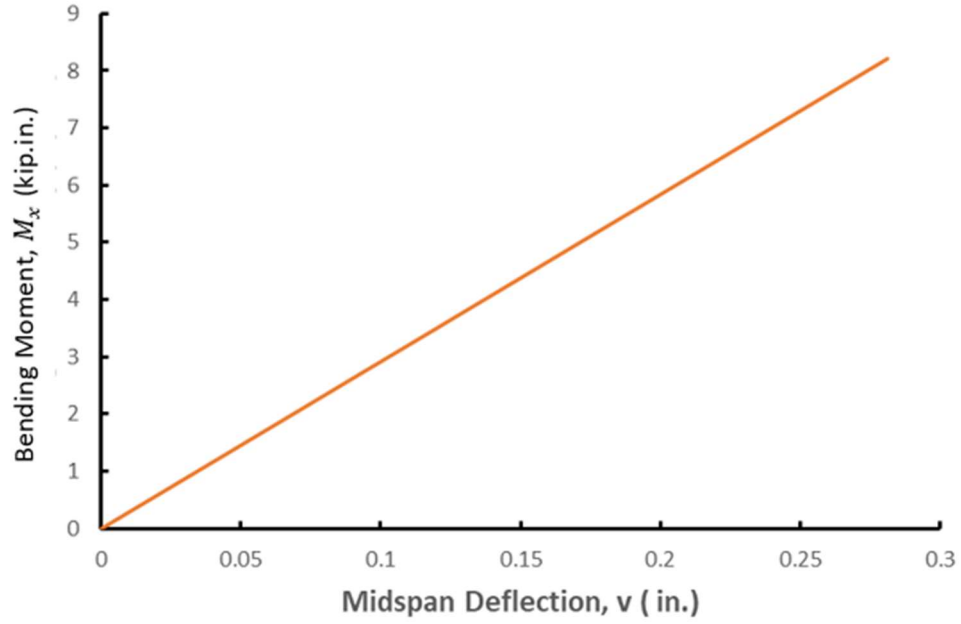


**Figure 35. Bending Moment,  $M_x$ , vs. Midspan Deflection,  $v$**

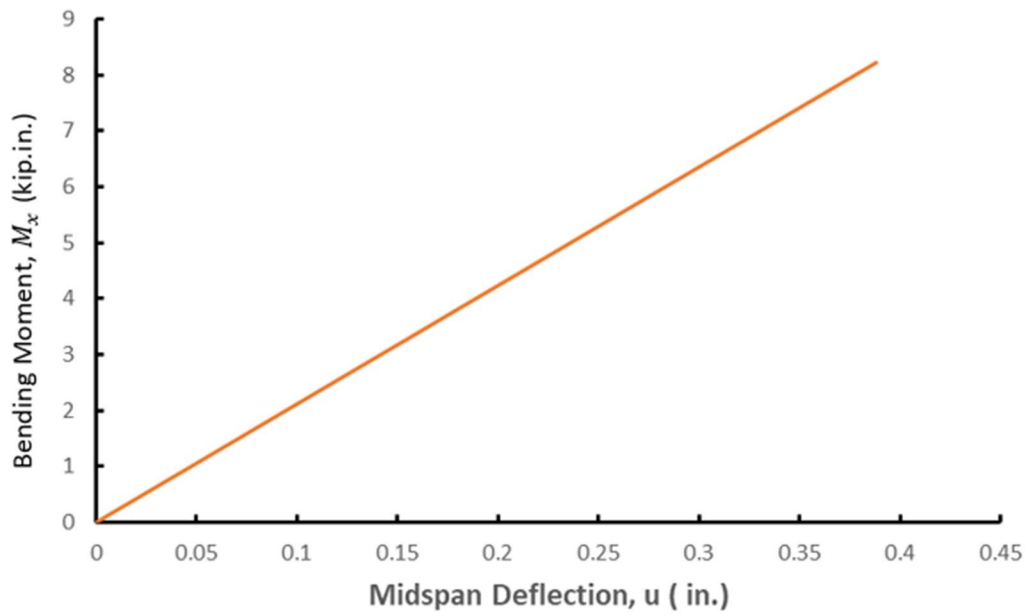


**Figure 36. Bending Moment,  $M_x$ , vs. Midspan Deflection,  $u$**

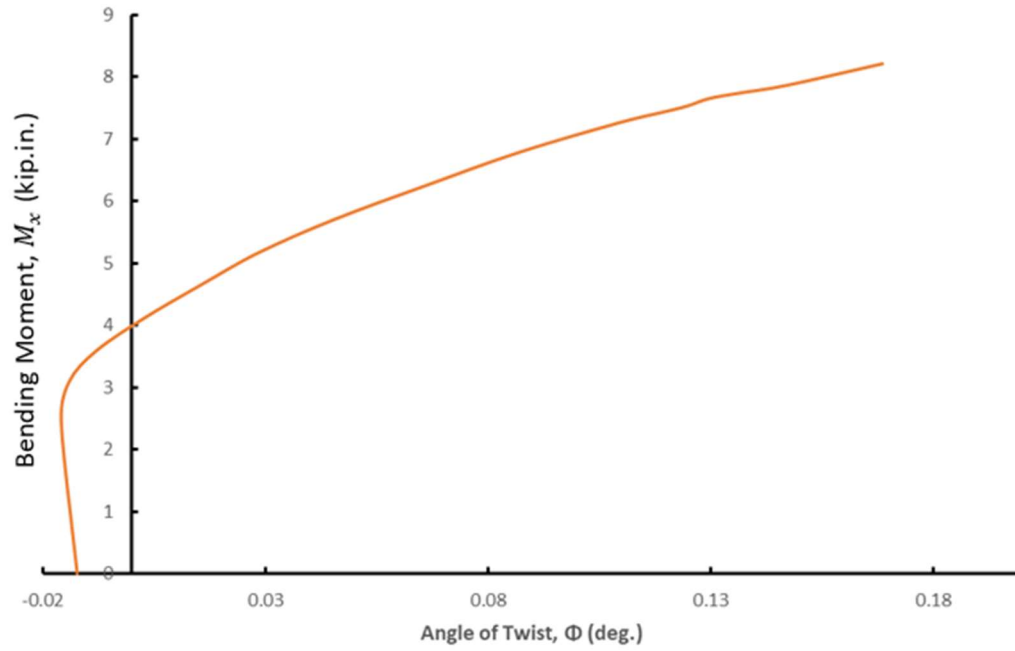


**Figure 37. Bending Moment,  $M_y$ , vs. Bottom End Angle of Twist,  $\phi$**

## CHAPTER 3

### EXPERIMENTAL INVESTIGATION

#### 3.1 Experimental Study

A total of five experiments are conducted in the laboratory with a 30-degree orientation of the cross section relative to the principal axes. That is, each experiment is conducted about the non-principal axes as depicted in Figure 19. Each member is torsionally end restrained. That is, both the angle of twist and its first derivative are zero at the upper boundaries and the first derivative of the angle of twist is zero at the bottom end of the member. The following test designations and type of loading and boundary conditions are used.

**Test T-1:** Torsionally end-restrained and flexurally pinned member subjected to a gradually increasing torsional moment,  $M_z$ , applied at the bottom end of the member about its z axis, until large torsional deflection is developed.

**Test P-2:** Flexurally pinned-end member subjected to a gradually increasing axial load, P, until the maximum load-carrying capacity is reached.

**Test PB-3:** Flexurally pinned-end member at both ends subjected to a gradually increasing axial load, P, first and then held constant, followed by a gradually increasing bending moment at the member top end about the non-principal x axis which resulted in biaxial bending about the cross-sectional principal axes. This member experienced cracking around the bolt holes in its end connections.

**Test PTB-p-4:** With the member flexurally pinned at both ends, an axial load P is applied first and then held constant, followed by a torsional moment applied at the bottom end of the member



about the z axis, then also held constant, and finally subjected to a gradually increasing bending moment at the member top end about the non-principal x axis which resulted in biaxial bending about the cross-sectional principal axes. This member experienced cracking around the holes in its bottom end connection.

**Test PTB-pf-5:** With the member flexurally pinned at the top end and fixed at its bottom end, it is subjected to the same loading sequence as that used for PTB-p-4.

In the above designations, P, T, and B refer to the axial load, torsion, and bending, respectively. Also, p refers to a flexurally pinned boundary condition whereas f indicates a flexurally fixed boundary condition.

Unavoidable eccentricities and imperfections of the support were encountered during testing due to the upper end gimble significant out-of-plane displacements in addition to minor in-plane displacements. The displacements of the support frame are captured by adding a lateral spring in the corresponding direction at the upper end of the member.

### **3.1.1 Apparatus**

IW340 FRP beam-columns were tested using a specially designed and developed apparatus capable of applying biaxial bending moments, axial load, and torsion. This apparatus has been utilized previously in numerous research lab investigations at Old Dominion University. The setup includes lower and upper end gimbals at the ends of the test specimen along with a steel casing with Hydraulic Jack A and Load Cell A.

The lower end gimbal consists of a four-sided steel gimbal outer box. The gimbal inner box is supported by a pair of inner bearings and a shaft along the x-axis. These inner bearings are housed in two opposite walls of the gimbal outer box. The opposing walls of the gimbal outer box contain

a pair of shafts and outer bearings along the y-axis. The lower end gimbal is attached to a steel plate, beneath which is a gliding steel chamber. The gliding steel chamber rides on the outer surface of a steel casing that houses a compression load cell mounted on a hydraulic jack. The steel casing is welded to a floor steel plate, which in turn is anchored to the laboratory test bed.

The upper end gimbal is identical to the lower end gimbal; however, it is mounted in an upside-down position. The upper end gimbal is attached to a steel crossbeam, which is bolted at its ends to steel columns. These end columns are anchored to the laboratory test bed, forming a large reaction frame, while the crossbeam supports the upper end gimbal. The axial load is applied using a Hydraulic Jack A and measured with a Load Cell A. The load cell pushes a steel plate which in turn transmits the axial load to the lower gimbal outer box through a pair of outer bearings and shafts. The load is finally transferred to the test specimen through the gimbal inner box. The bending moment is applied at the top end of the member by means of a moment arm bolted to the upper gimbal inner box as shown in Figure 20. The moment arm is a 1.0x2.0x24.0 in. solid rectangular steel section. Load W is applied through two 0.75 in. diameter tie rods. These rods are 75 inches long each and separated by 12 inch long 0.5 in. thick steel plates forming a closed ring at the top and bottom. By means of ball and socket arrangement, the top plate B sits on the machined arm. Using a similar arrangement, the Bottom Plate A is attached to a compression Load Cell B. Load Cell B is mounted on Hydraulic Jack B, which is bolted to a small reaction frame in an upside-down position. The small steel reaction frame is mounted to the laboratory test bed. Load W can finally be produced by manually controlling Hydraulic Jack B. The biaxial bending moments  $M_{x^*}$  and  $M_{y^*}$  are generated by applying a resultant bending moment  $M_x$  about  $x$  axis with an angle  $\theta = 30^\circ$  as shown in Figure 20. The biaxial bending moments  $M_{Tx}$  and  $M_{Ty}$  are equal to  $M_x(\cos 30^\circ)$  and  $M_x(\sin 30^\circ)$  respectively. The torsional moment is applied at the bottom

end by means of an eccentric force  $F$  applied with Hydraulic Jack C and transmitted to the member by means of chain. The bottom end gimbal rests on a steel plate and rides on solid steel spheres arranged in a circle as schematically shown in Figure 38 below.

IW430 glass FRP members are used for this experimental study. Each test member has a clear length of 32 inches. The distance between the centerlines of the end gimbals, including both the actual member length and the solid portions of the end fixture, is 37.0 inches, which is the length that will be used in the analysis. The axial load and both bending and torsional moments are applied slowly and incrementally with regular stops to manually record the output data in the elastic range. The member load-carrying capacity is observed when the applied load starts dropping while at the same time the deformations keep increasing.

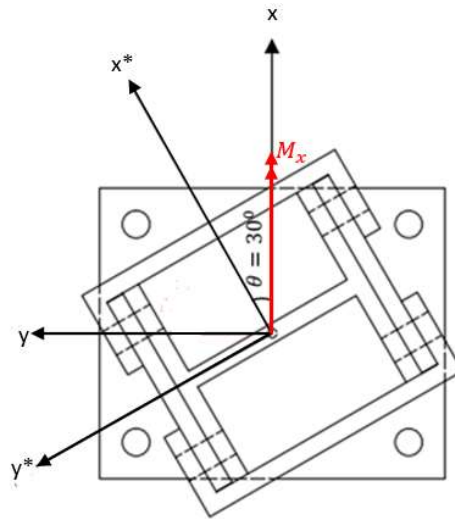


**Figure 38. Experimental Applied Bending Moment**



**Figure 39. Apparatus**

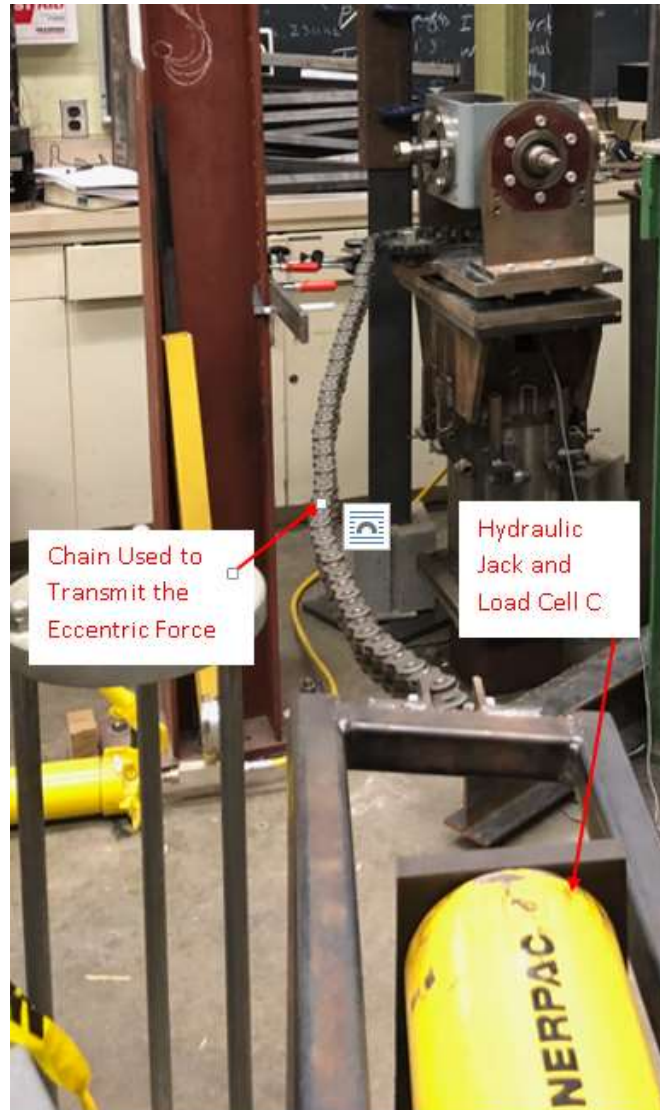


**Figure 40. Hydraulic Jack and Load Cell C**

### 3.1.2 Material properties

Based on the ASTM 3-Point Bending Test, two specimens were tested about the x and y axes to verify the experimental values of Young's modulus,  $E_x$  and  $E_y$ . These are within the manufacturer's recommended range. The cracking stress  $\sigma_{crx}$  and  $\sigma_{cry}$  for the GFRP specimens were also calculated. The values of Young's modulus and the cracking stresses are listed below.

$$E_x = 1.4624 \times 10^6 \text{ psi}$$

$$E_y = 2.66 \times 10^6 \text{ psi}$$

$$\sigma_{crx} = 19977.214 \text{ psi}$$

$$\sigma_{cry} = 36336.983 \text{ psi}$$

The shear modulus,  $G$ , for the GFRP was found using a torsion test conducted on an IW430 member. The value was found to be as follows:

$$G = 0.429 \times 10^6 \text{ psi}$$

In this dissertation, the above material properties mentioned are used in the analysis.

## **3.2 Experimental Results**

### **Cracking Limit Test Results**

The cracking limit loading is defined as the set of external loads that cause initiation of cracking at any point in a member. For cracking limit tests, the relation between the applied load,  $W$ , vs. displacements at the midspan of the member is graphically presented in Figures 41 and 42.

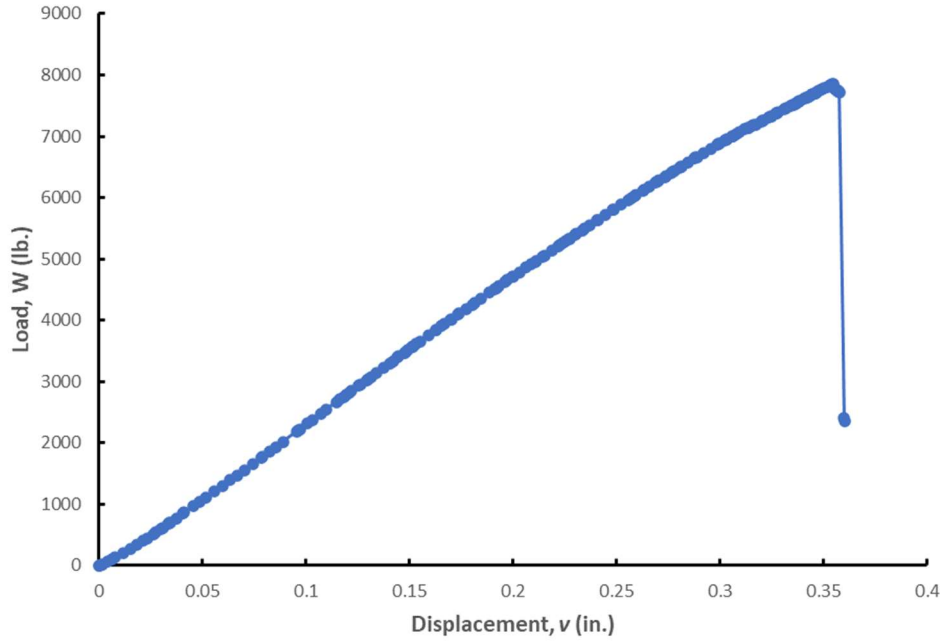


**Figure 41. Load,  $W$ , vs. Vertical Displacement,  $v$ , for Major Axis Test**

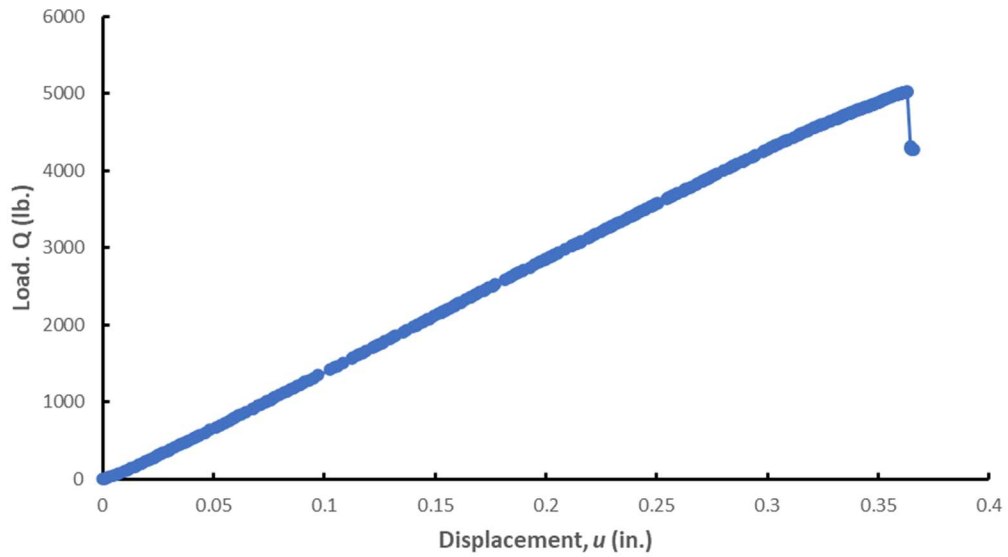


**Figure 42. Load,  $Q$ , vs. Vertical Displacements,  $u$ , for Minor Axis Test**

### 3.2.1 Torsionally Loaded Member Test T-1

This test was conducted by installing the glass FRP specimen in the apparatus. The top and the bottom ends of the specimen were restrained against warping as shown in Figure 43 below. The torsional moment was applied and gradually increased at the bottom end of the specimen via a chain connected to the hydraulic jack from one end and engaged with a gear on the other end. The force developed in the chain applied the torsional moment by an arm of 8.125 in. The angle of twist was measured at the bottom end of the member for each load increment. Table 6 summarizes the test results; the first column shows the measured angle of twist at the bottom end of the specimen in degree unit while the second column shows the applied torsional moment in lb.-in. units. The piston of the hydraulic jack reached the maximum available length without initiating a crack in the member. Four cycles of loading/unloading of the member were repeated. No cracks were initiated in the member from all four cycles; however, the member underwent significant angle of twist indicating that the member failed in serviceability as shown in Figure 44. For each reloading step, the member had the capacity to withstand a higher value of the applied torsional moment than the loading step before; hence, the member maintained its strength throughout the test and did not fail. Table 7 summarizes the applied load for each loading step. The relationship between loading step numbers vs. the applied torsional moment is shown in Figure 45. The torsional moment,  $M_z$ , vs. angle of twist at the bottom end of the member,  $\phi$ , is presented in Figure 46. The glass FRP member elastically recovered its original shape and did not show any permanent deformation after it was taken off the testing apparatus as shown in Figure 47.



**Table 6. Torsion Test T-1 Results**

| $\Phi$   | $M_z$  |
|----------|--------|
| deg.     | lb.in. |
| 0        | 0      |
| 2.682452 | 406.25 |
| 7.754286 | 731.25 |
| 17.33811 | 1137.5 |
| 28.97393 | 1625   |
| 40.00875 | 1950   |

**Table 7. Loading Steps vs. Maximum Applied Torsional Moment for Test T-1**

| Loading Cycles | $M_z$   |
|----------------|---------|
|                | lb.in.  |
| 1              | 1950    |
| 2              | 3168.75 |
| 3              | 4387.5  |
| 4              | 4631.25 |

**Figure 43. Bottom End Connection of the Specimen**



**Figure 44. Specimen under Torsional Moment for Test T-1**

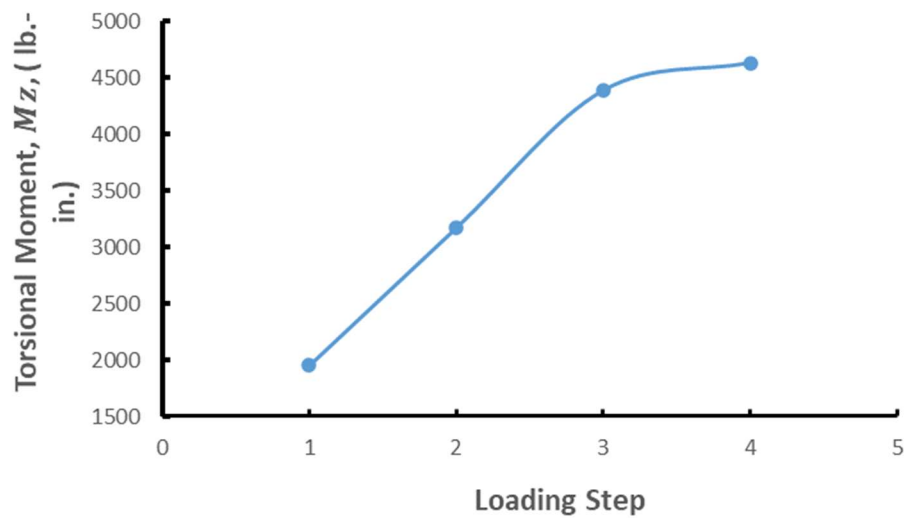


**Figure 45. Applied Torsional Moment for Each Loading Step for Test T-1**

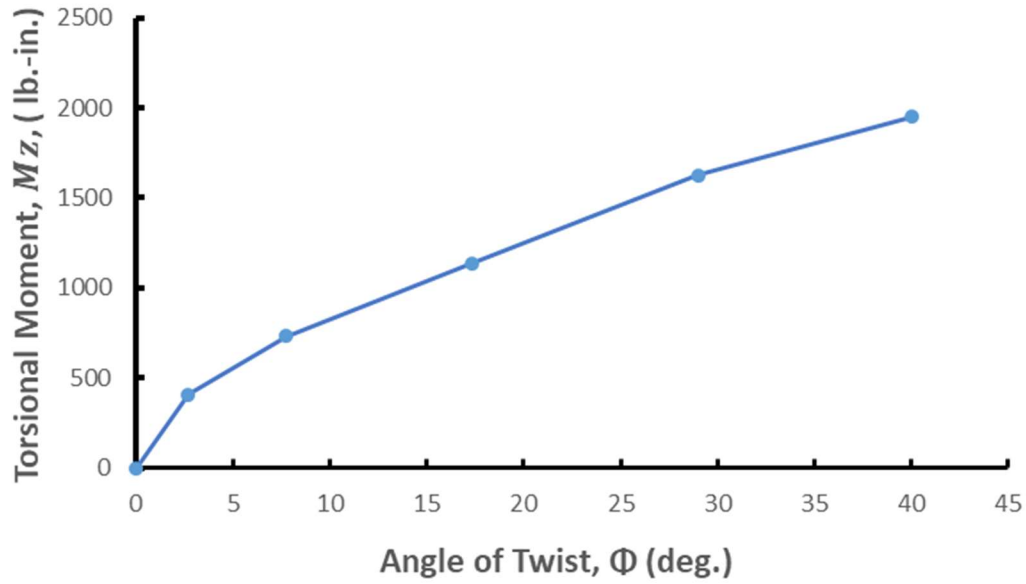


**Figure 46. Experimental Torsional Moment,  $M_z$ , vs. Bottom End Angel of Twist,  $\phi$ , Relationship for Test T-1**



**Figure 47. Specimen Shape One Week after Torsion Test T-1**

### 3.2.2 Axially Loaded GFRP Column Test P-2

The experimental results presented in this section are for the glass FRP column under axial loading. The top and the bottom of the member were pinned in the x and y axes directions. The axial load was applied using Hydraulic Jack A and increased gradually. The bottom base plate of the apparatus was restrained against rotation by applying four clamps. Three dial gauges were installed at the midspan of the member to measure the lateral deflections, and a fourth dial gauge was installed at the bottom plate of the apparatus to measure the angle of the twist at the bottom end of

the member. Figure 48 presents the location and the numbering of the installed dial gauges for this test. Table 8 summarizes the processed data for these test results. In this table the first column represents the applied axial load,  $P$ ; the second column represents the displacement in the  $y$  axis direction,  $v$ ; the third column represents the displacement in the  $x$  axis direction,  $u$ ; the fourth column represents the angle of twist,  $\phi$ , at the bottom end of the member. Figures 49 to 51 present the relationship between the applied axial load,  $P$ , and the member deformations,  $v$ ,  $u$ , and  $\phi$ , respectively. In these figures, the change to the slope of the curves between axial load 4 kip to 10 kip is observable indicating a fictitious increase of the stiffness of the tested member. This increase is attributed to the unavoidable eccentricities and deformations discussed in Section 3.1.

**Table 8. Experimental Data for Axially Loaded Member Test P-2 Results**

| <b>Load</b> | <b><math>v</math></b> | <b><math>u</math></b> | <b><math>\Phi</math></b> |
|-------------|-----------------------|-----------------------|--------------------------|
| <b>kip</b>  | <b>in.</b>            | <b>in.</b>            | <b>deg.</b>              |
| 0           | 0                     | 0                     | 0                        |
| 1.95        | 0.074                 | 0.075                 | 0.0008                   |
| 3.97        | 0.105                 | 0.175                 | 0.005867                 |
| 5.92        | 0.188                 | 0.208                 | 0.0064                   |
| 8.13        | 0.193                 | 0.246                 | 0.006667                 |
| 10.12       | 0.198                 | 0.3                   | 0.0072                   |
| 11.86       | 0.03                  | 0.48                  | 0.008                    |
| 12.07       | 0.675                 | 0.675                 | 0.079                    |
| 11.92       | 0.71                  | 0.71                  | 0.065                    |

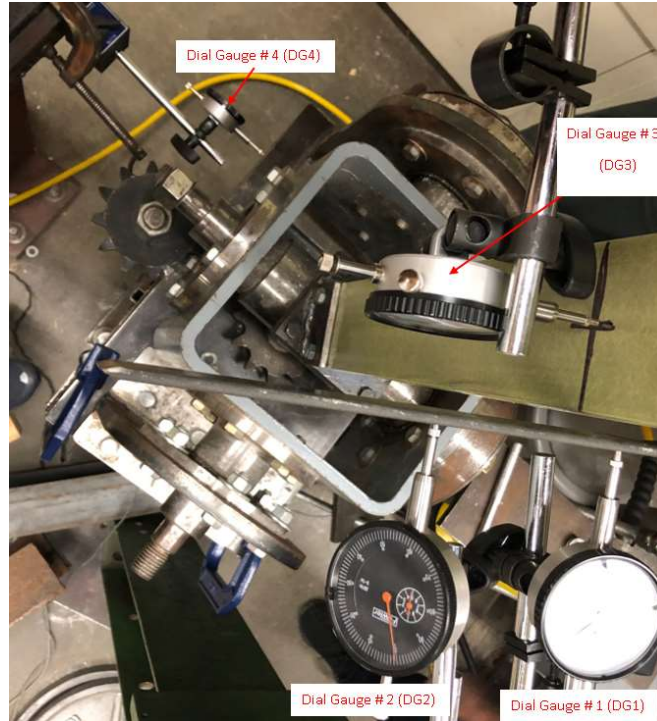


**Figure 48. Dial Gauges Numbering and Locations for Test P-2**

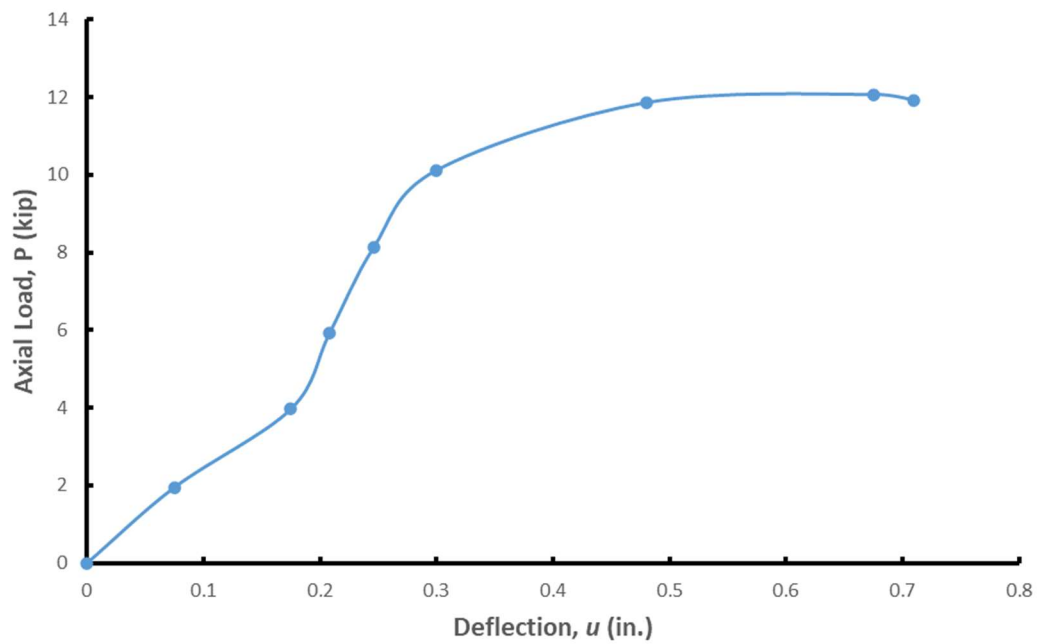


**Figure 49. Axial Load,  $P$ , vs. Midspan Deflection,  $u$ , for Test P-2**

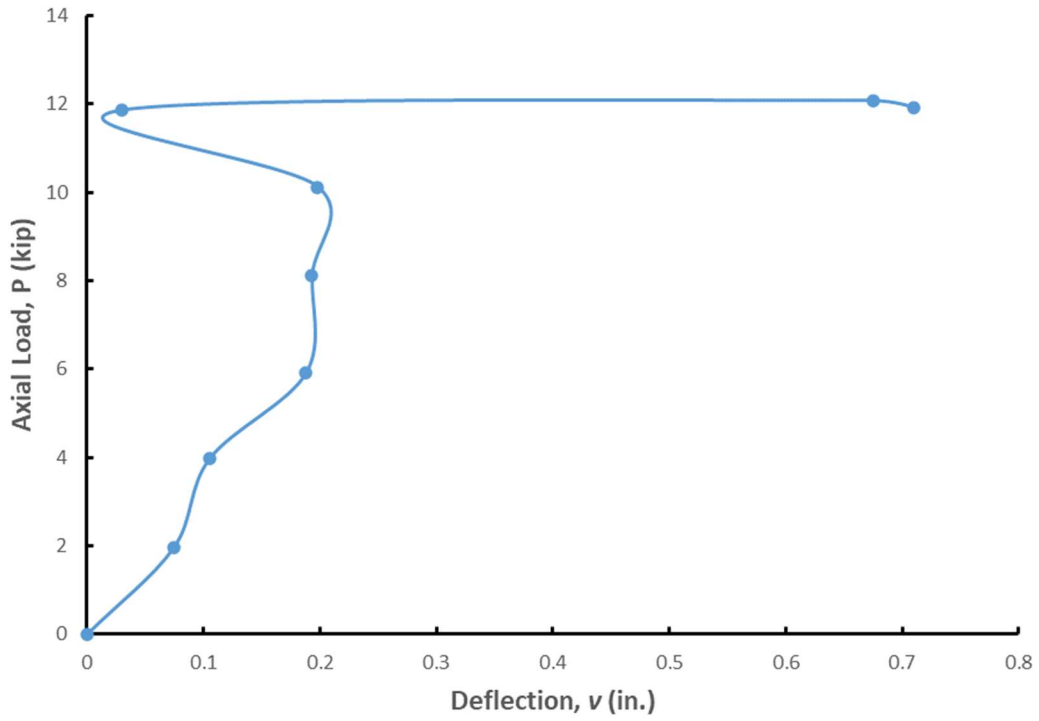


Figure 50. Axial Load,  $P$ , vs. Midspan Deflection,  $v$ , for Test P-2

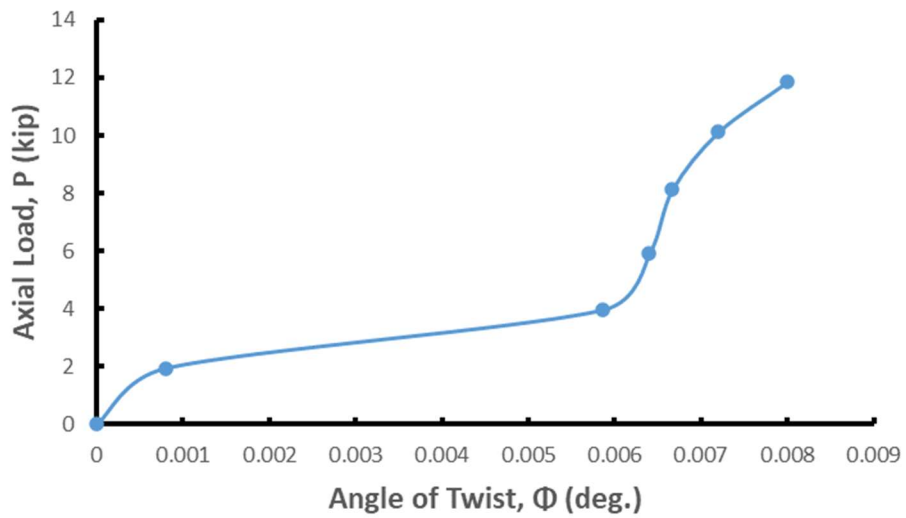


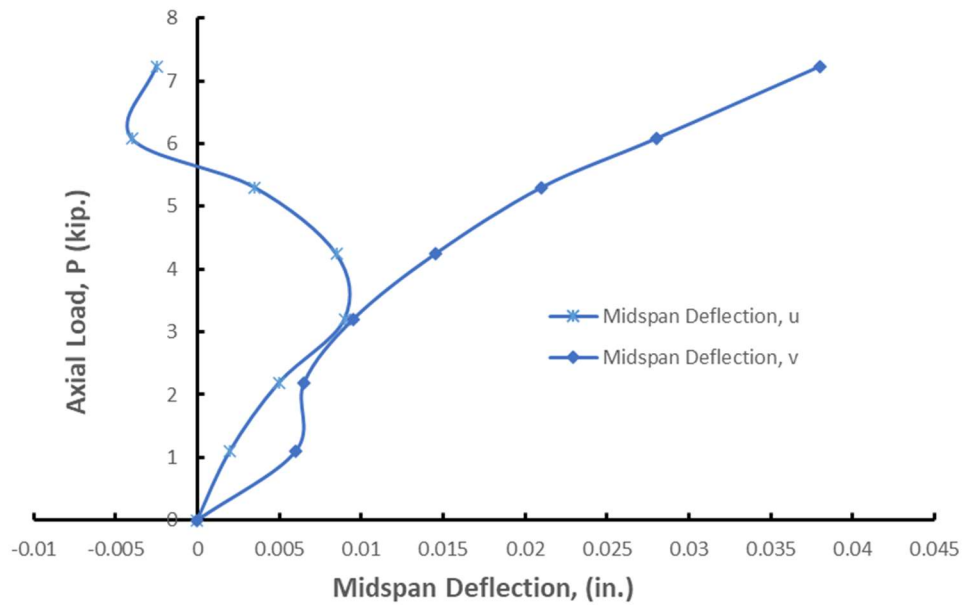
Figure 51. Axial Load,  $P$ , vs. Bottom End Angle of Twist,  $\phi$ , for Test P-2

### 3.2.3 Combined Axial Load and Biaxial Bending Moment Test PB-3

This test was conducted by installing the glass FRP specimen into the apparatus using the same boundary conditions and dial gauge locations previously mentioned. The axial load is first applied using the hydraulic jack and increased gradually then held constant followed by a gradually increasing biaxial bending moment up to the maximum load. Table 9 summarizes the processed data results of this test. The first column presents the applied axial load,  $P$ , and the bending moment  $M_x$ , the second, third, fourth, and fifth columns present the deformations,  $v$ ,  $u$ , and  $\phi$ , respectively. Figure 52 shows the midspan deflections  $u$  and  $v$  versus applied axial load,  $P$ . Figure 54 shows the bottom end angle of twist,  $\phi$ , versus applied axial load,  $P$ . Figure 54 shows the midspan deflections  $u$  and  $v$  versus bending moment,  $M_x$ . Finally, Figure 55 shows the angle of twist at the bottom end of the member,  $\phi$ , versus applied bending moment  $M_x$  for this test.

Table 9. Experimental Results for Test PB-3

| P, kip          | $u$ , in. | $v$ , in. | $\Phi$ , deg. |
|-----------------|-----------|-----------|---------------|
| 0               | 0         | 0         | 0             |
| 1.1             | 0.002     | 0.006     | 0.00038       |
| 2.19            | 0.005     | 0.0065    | 0.00057       |
| 3.2             | 0.009     | 0.0095    | 0.0019        |
| 4.24            | 0.0085    | 0.0145    | 0.00286       |
| 5.3             | 0.0035    | 0.021     | 0.00343       |
| 6.08            | -0.004    | 0.028     | 0.00343       |
| 7.23            | -0.0025   | 0.038     | 0.00381       |
| $M_x$ , kip.in. | $u$ , in. | $v$ , in. | $\Phi$ , deg. |
| 0               | -0.0025   | 0.038     | 0.00381       |
| 1.3291          | -0.0235   | 0.079     | 0.00838       |
| 1.5798          | -0.0095   | 0.087     | 0.01333       |
| 1.8236          | 0.0065    | 0.093     | 0.01905       |
| 2.1048          | 0.023     | 0.0995    | 0.02514       |
| 3.0595          | 0.081     | 0.124     | 0.03389       |
| 4.0854          | 0.243     | 0.149     | 0.04606       |
| 5.2013          | 0.35      | 0.189     | 0.06258       |
| 6.2191          | 0.432     | 0.216     | 0.0838        |
| 7.2959          | 0.511     | 0.248     | 0.11022       |
| 1.3655          | 0.611     | 0.339     | 0.13648       |

Figure 52. Axial Load,  $P$ , vs. Midspan Deflections,  $v$ , and  $u$ , for Test PB3



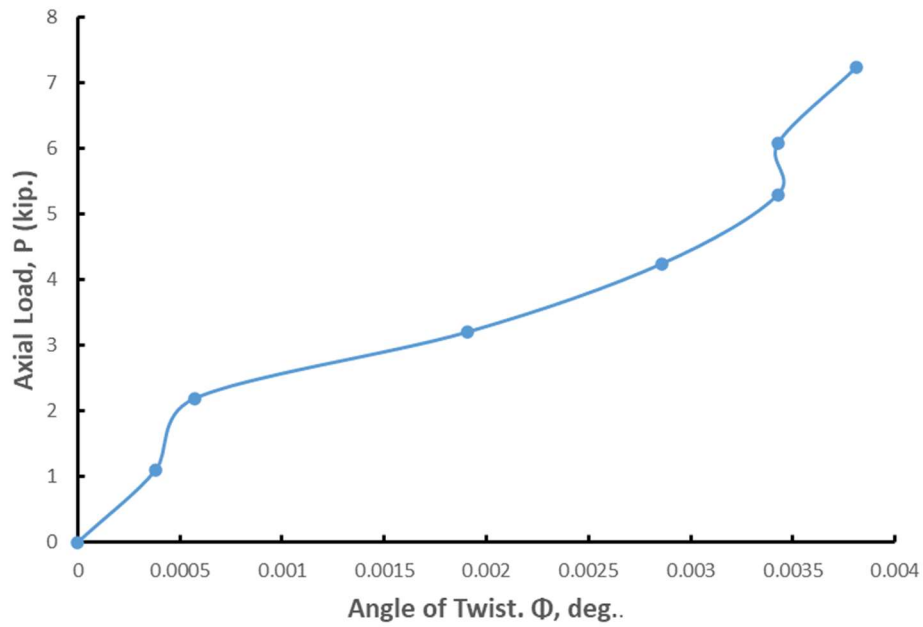


Figure 53. Axial Load,  $P$ , vs. Bottom End Angle of Twist,  $\phi$ , for Test PB-3

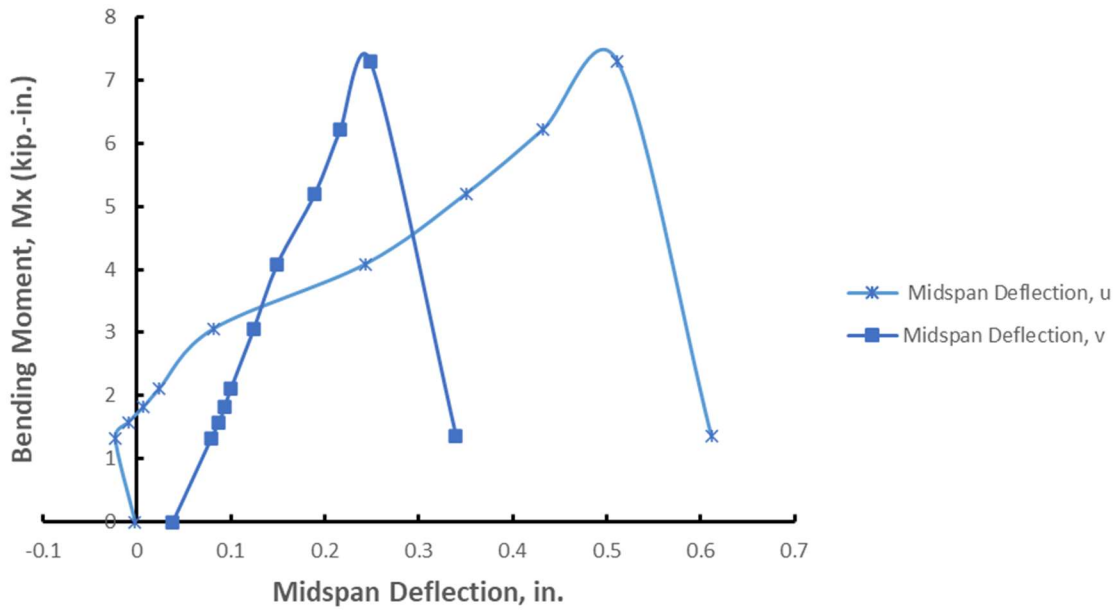
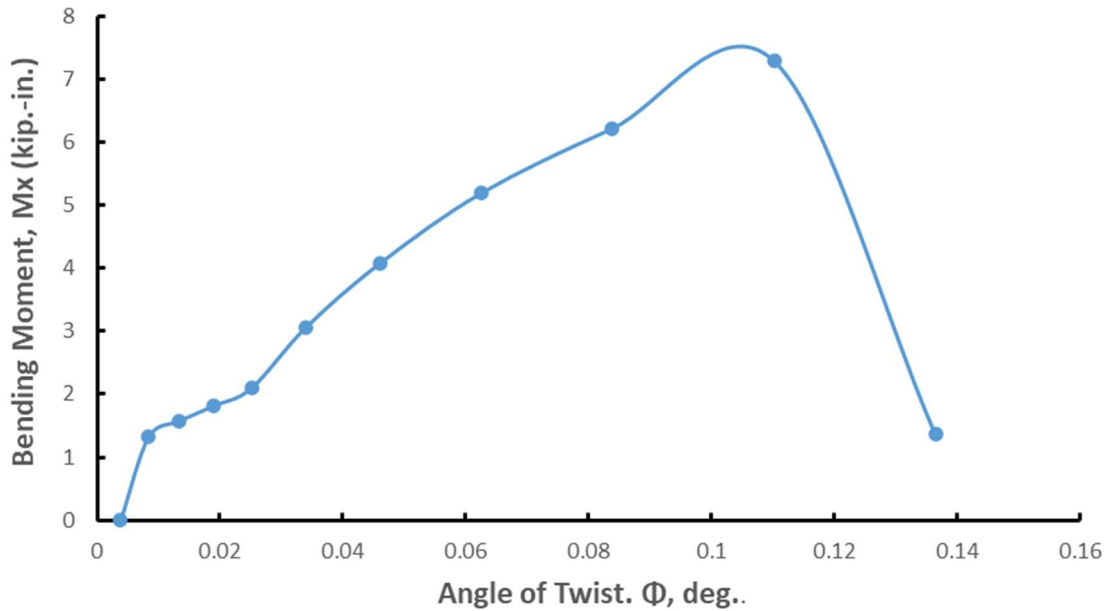


Figure 54. Bending Moment,  $M_x$ , vs. Midspan Deflections,  $v$ , and  $u$ , for Test PB-3



**Figure 55. Bending Moment,  $M_x$ , vs. Bottom End Angle of Twist,  $\phi$ , for Test PB-3**

### 3.2.4 Combined Axial Load, Biaxial Bending Moment, and Torsional Moment Test PBT-p-4

This test is performed by gradually applying the axial load up to approximately 7 kip then holding constant followed by applying a gradually increasing torsion up to approximately 2.5 kip-in. Finally, the bending moment,  $M_x$ , was applied and gradually increased until the maximum load was reached. The member is flexurally pinned and constrained against warping at both the top and the bottom ends. Table 10 summarizes the results for this case. The first column represents the applied load while the second through the fifth columns represent the deformations,  $u$ ,  $v$ , and  $\phi$ , respectively. Figures 56 through 61 present the applied load versus the deflections.

Table 10. Axial Load, Biaxial Bending Moment, and Torsion Test PBT-p-4

| <b>P, kip</b>                    | <b>u, in.</b> | <b>v, in.</b> | <b><math>\Phi</math>, deg.</b> |
|----------------------------------|---------------|---------------|--------------------------------|
| 0                                | 0             | 0             | 0                              |
| 1.05                             | 0.001         | -0.003        | 0.013217                       |
| 2.17                             | 0.004         | -0.005        | 0.047443                       |
| 3.18                             | 0.008         | -0.0055       | 0.047443                       |
| 4.15                             | 0.015         | -0.005        | 0.04831                        |
| 5.18                             | 0.028         | 0.001         | 0.049004                       |
| 7.07                             | 0.068         | 0.0155        | 0.050184                       |
| <b><math>M_z</math>, kip.in.</b> | <b>u, in.</b> | <b>v, in.</b> | <b><math>\Phi</math>, deg.</b> |
| 0                                | 0.068         | 0.0155        | 0.050184                       |
| 0.975                            | 0.069         | 0.0165        | 0.050878                       |
| 1.4625                           | 0.07          | 0.0175        | 0.051398                       |
| 2.35625                          | 0.0735        | 0.0205        | 0.054693                       |
| 2.51875                          | 0.075         | 0.0205        | 0.104625                       |
| <b><math>M_x</math>, kip.in.</b> | <b>u, in.</b> | <b>v, in.</b> | <b><math>\Phi</math>, deg.</b> |
| 0                                | 0.075         | 0.0205        | 0.104625                       |
| 0.76875                          | 0.087         | 0.025         | 0.15896                        |
| 0.873214286                      | 0.092         | 0.0275        | 0.15913                        |
| 1.048928571                      | 0.102         | 0.0325        | 0.159639                       |
| 1.2225                           | 0.111         | 0.0375        | 0.159978                       |
| 1.315178571                      | 0.116         | 0.0405        | 0.160317                       |
| 1.366071429                      | 0.1185        | 0.0415        | 0.160486                       |
| 1.429821429                      | 0.124         | 0.0455        | 0.160994                       |
| 1.714821429                      | 0.1385        | 0.0505        | 0.161672                       |
| 1.994464286                      | 0.1545        | 0.0555        | 0.16472                        |
| 2.378035714                      | 0.175         | 0.0655        | 0.165904                       |
| 2.645892857                      | 0.19          | 0.0715        | 0.16675                        |
| 2.751964286                      | 0.1965        | 0.0745        | 0.166919                       |
| 2.883214286                      | 0.205         | 0.078         | 0.167427                       |
| 3.036964286                      | 0.214         | 0.082         | 0.168103                       |
| 3.188035714                      | 0.224         | 0.0855        | 0.168441                       |
| 3.357857143                      | 0.235         | 0.0905        | 0.169117                       |
| 3.493928571                      | 0.2435        | 0.0935        | 0.171819                       |
| 3.631607143                      | 0.2535        | 0.0975        | 0.172495                       |
| 3.846428571                      | 0.266         | 0.1035        | 0.17317                        |
| 4.043571429                      | 0.279         | 0.109         | 0.173845                       |
| 4.1775                           | 0.289         | 0.1125        | 0.174351                       |
| 4.595892857                      | 0.319         | 0.1255        | 0.176037                       |
| 4.824107143                      | 0.337         | 0.1315        | 0.17688                        |
| 4.956428571                      | 0.357         | 0.1385        | 0.179575                       |
| 5.490535714                      | 0.392         | 0.2675        | 0.254173                       |
| 5.740178571                      | 0.409         | 0.2725        | 0.254824                       |
| 6.211607143                      | 0.466         | 0.2795        | 0.254661                       |
| 6.454821429                      | 0.49          | 0.2895        | 0.254661                       |
| 6.722678571                      | 0.512         | 0.2945        | 0.254661                       |
| 7.069821429                      | 0.547         | 0.3105        | 0.254661                       |
| 7.258392857                      | 0.565         | 0.3115        | 0.254694                       |
| 7.499464286                      | 0.59          | 0.3185        | 0.254661                       |

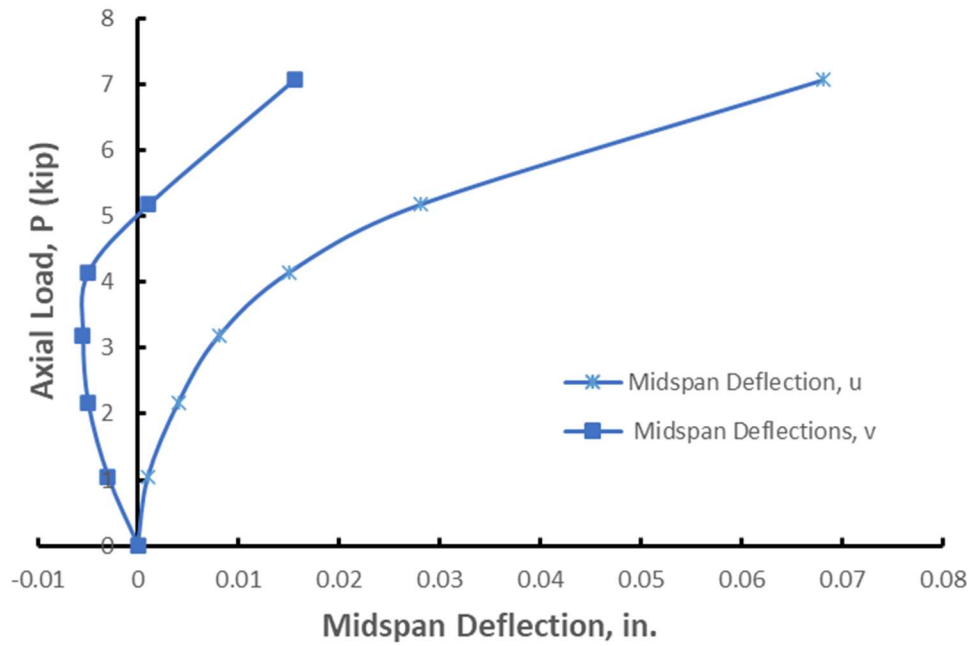


Figure 56. Axial Load,  $P$ , vs. Midspan Deflections,  $v$ , and  $u$ , for Test PBT-p-4

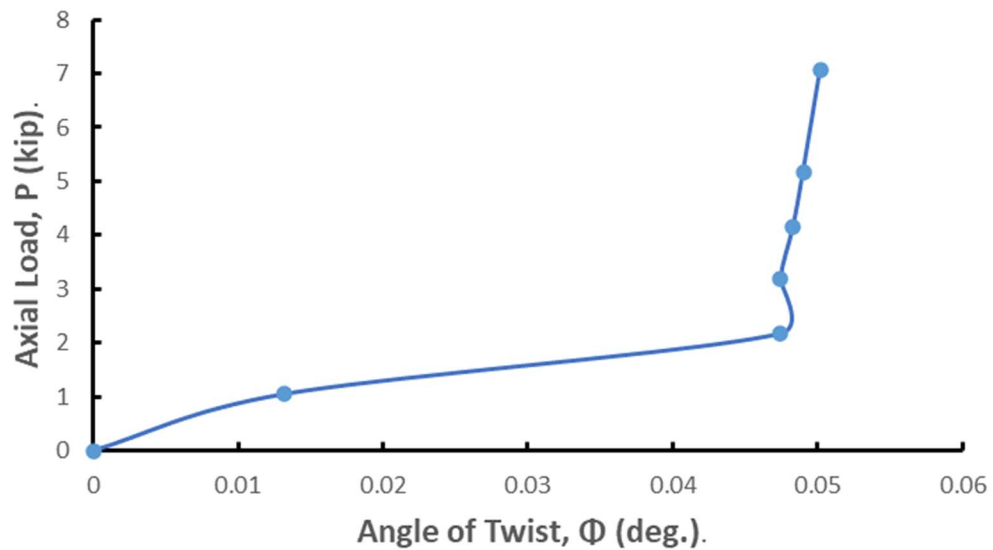


Figure 57. Axial Load,  $P$ , vs. Bottom End Angle of Twist,  $\phi$ , for Test PBT-p-4

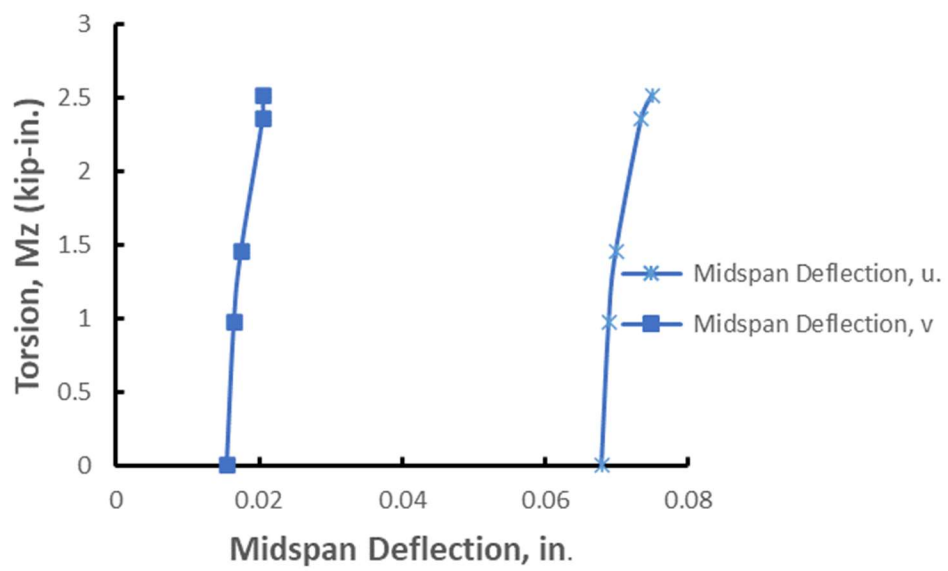


Figure 58. Torsion,  $M_z$ , vs. Midspan Deflections,  $v$ , and  $u$ , for Test PTB-p-4

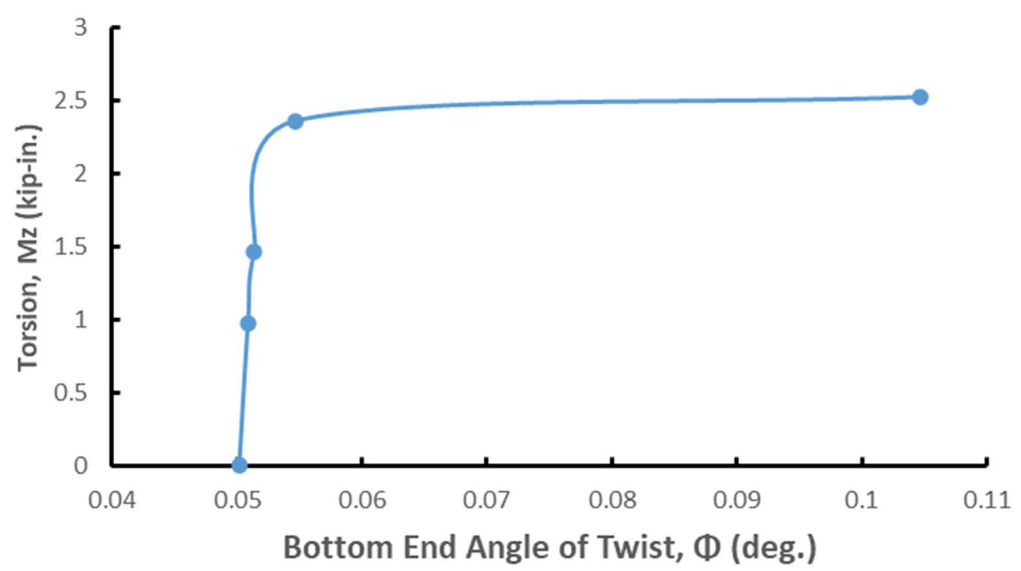


Figure 59. Torsion,  $M_z$ , vs. Bottom End Angle of Twist,  $\phi$ , for Test PTB-p-4

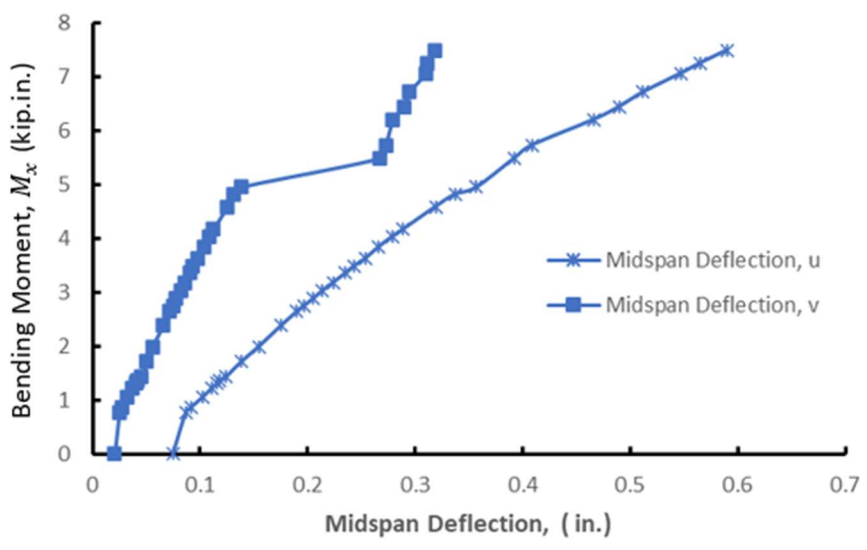


Figure 60. Bending Moment,  $M_x$ , vs. Midspan Deflection,  $\phi$ , for Test PTB-p-4

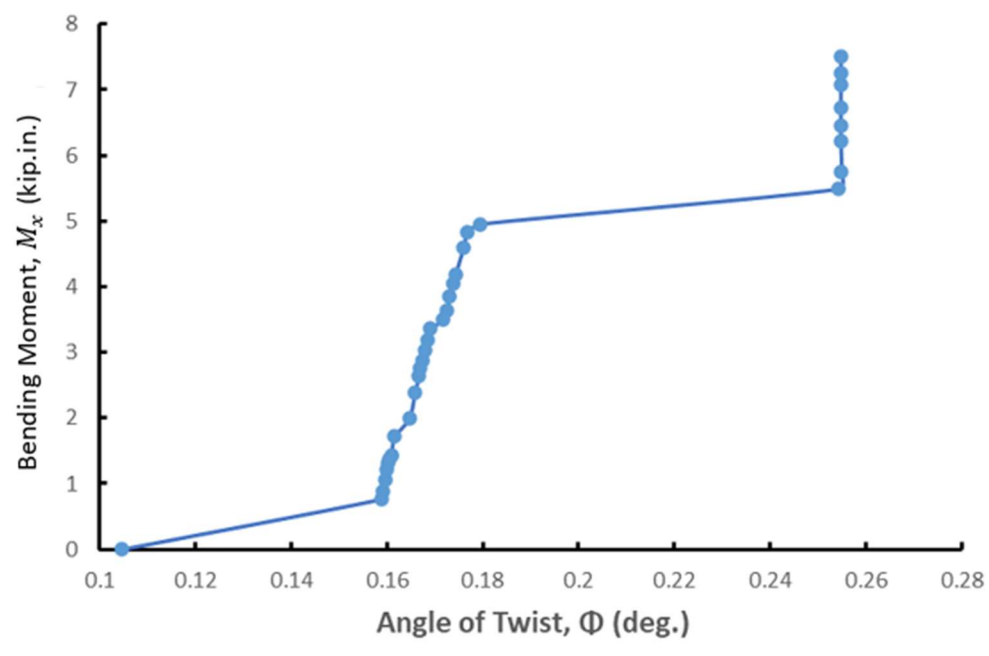


Figure 61. Bending Moment,  $M_x$ , vs. Bottom Angle of Twist,  $\phi$ , for Test PTB-p-4

### **3.2.5 Combined Axial Load, Biaxial Bending Moment, and Torsional Moment Test PBT-fp-5**

With the member flexurally pinned at the top end and fixed at its bottom end, it is subjected to the same loading sequence as that used for PTB-p-4. Table 11 summarizes the processed results for this case. The first column represents the applied loads while the second through the fifth columns represent the deflections. Figures 62 through 67 present the applied load versus the deflection relationship.

Table 11. Axial Load, Biaxial Bending Moment, and Torsion for Test PTB-fp-5

| <b>P, kip</b>                    | <b>u, in.</b> | <b>v, in.</b> | <b><math>\Phi</math>, deg.</b> |
|----------------------------------|---------------|---------------|--------------------------------|
| 0                                | 0             | 0             | 0                              |
| 0.8                              | 0.01775       | 0.078         | -0.0044                        |
| 1.91                             | 0.0165        | 0.043         | -0.0064                        |
| 2.95                             | 0.02775       | 0.026         | -0.0066                        |
| 3.88                             | 0.04725       | 0.12          | -0.0098                        |
| 4.96                             | 0.064         | 0.201         | -0.0202                        |
| 5.96                             | 0.0925        | 0.248         | -0.0202                        |
| 6.95                             | 0.115         | 0.306         | -0.0214                        |
| <b><math>M_z</math>, kip.in.</b> | <b>u, in.</b> | <b>v, in.</b> | <b><math>\Phi</math>, deg.</b> |
| 0                                | 0.115         | 0.306         | -0.0214                        |
| 0.05                             | 0.115         | 0.306         | -0.0206                        |
| 0.1                              | 0.1165        | 0.306         | -0.019                         |
| 0.17                             | 0.123         | 0.307         | -0.0158                        |
| 0.21                             | 0.1275        | 0.3085        | -0.0134                        |
| 0.24                             | 0.1305        | 0.309         | -0.0122                        |
| <b><math>M_x</math>, kip.in.</b> | <b>u, in.</b> | <b>v, in.</b> | <b><math>\Phi</math>, deg.</b> |
| 0                                | 0.1305        | 0.309         | -0.0122                        |
| 2.456785714                      | 0.148         | 0.3245        | -0.0102                        |
| 3.095357143                      | 0.1765        | 0.348         | -0.007                         |
| 3.58875                          | 0.203         | 0.368         | -0.0022                        |
| 4.119107143                      | 0.234         | 0.39          | 0.007001                       |
| 4.654821429                      | 0.268         | 0.412         | 0.019792                       |
| 5.175                            | 0.306         | 0.433         | 0.036165                       |
| 5.712321429                      | 0.3345        | 0.453         | 0.061668                       |
| 6.249642857                      | 0.404         | 0.469         | 0.077561                       |
| 6.799285714                      | 0.446         | 0.494         | 0.079941                       |
| 7.269107143                      | 0.481         | 0.519         | 0.080338                       |
| 7.403035714                      | 0.5445        | 0.514         | 0.081924                       |
| 7.445892857                      | 0.5445        | 0.514         | 0.081924                       |
| 7.536964286                      | 0.5505        | 0.517         | 0.081924                       |
| 7.654821429                      | 0.5595        | 0.5225        | 0.082324                       |
| 7.745892857                      | 0.5685        | 0.527         | 0.082324                       |
| 7.874464286                      | 0.583         | 0.534         | 0.082324                       |
| 8.217321429                      | 0.5775        | 0.548         | 0.081924                       |



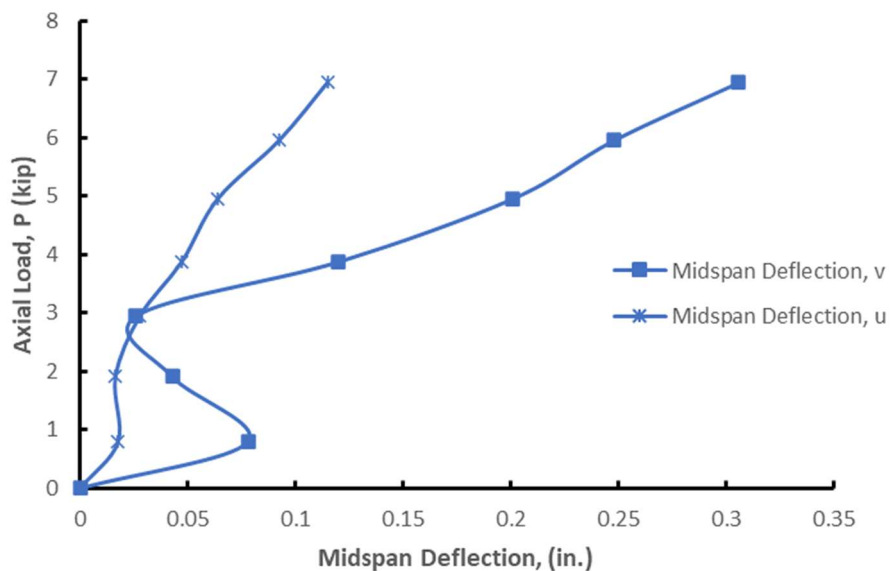


Figure 62. Axial Load,  $P$ , vs. Midspan Deflections,  $v$ , and  $u$ , for Test PTB-fp-5

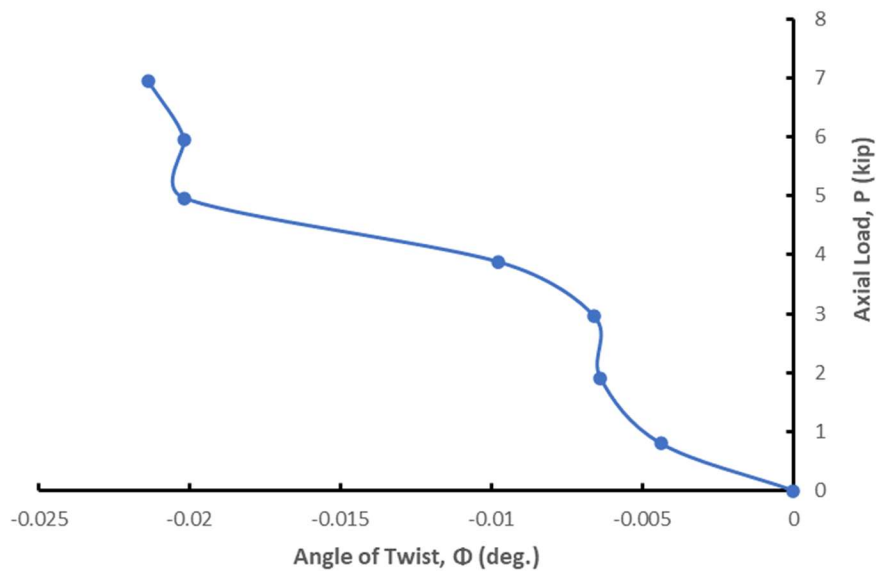


Figure 63. Axial Load,  $P$ , vs. Bottom End Angle of Twist,  $\phi$ , for Test PTB-fp-5

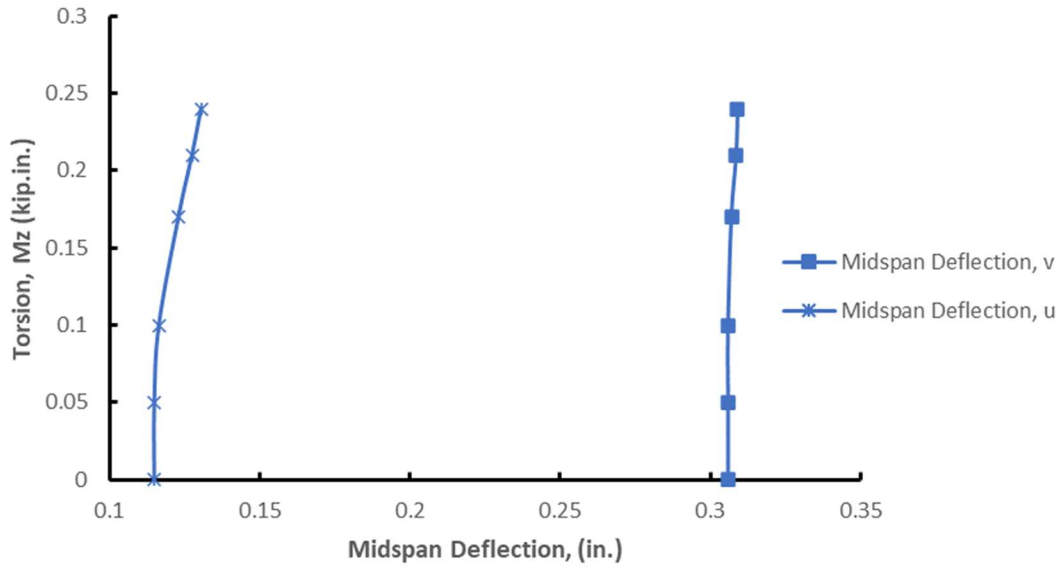


Figure 64. Torsion,  $M_z$ , vs. Midspan Deflection,  $v$ , and  $u$ , for Test PTB-fp-5

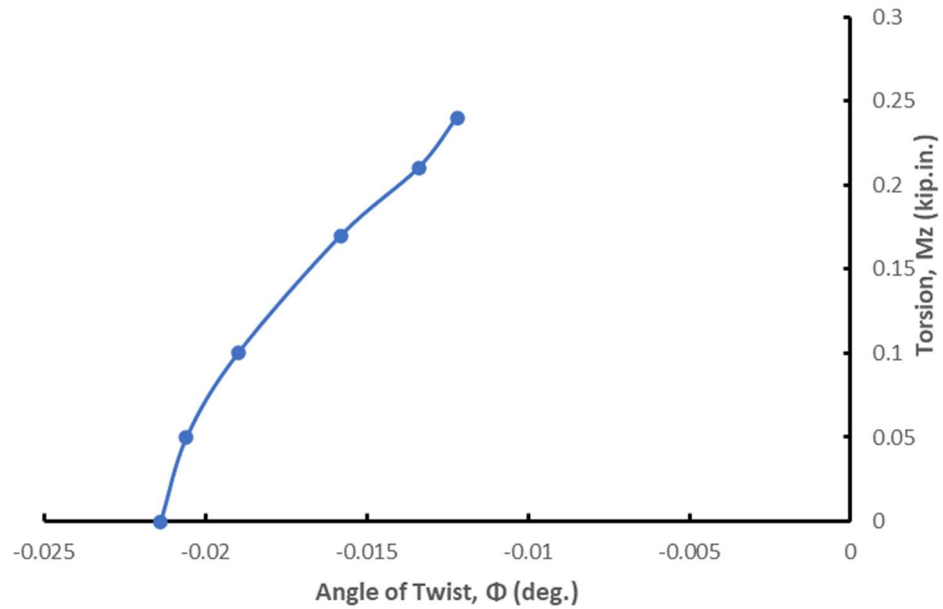


Figure 65. Torsion,  $M_z$ , vs. Bottom End Angle of Twist,  $\phi$ , for Test PTB-fp-5

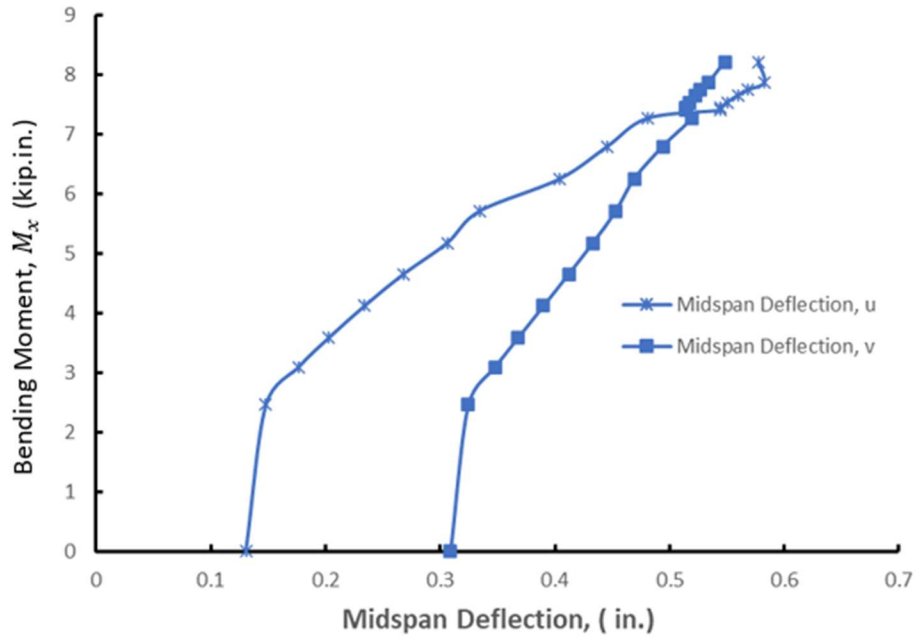


Figure 66. Bending Moment,  $M_x$ , vs. Midspan Deflections,  $v$ , and  $u$ , for Test PTB-fp-5

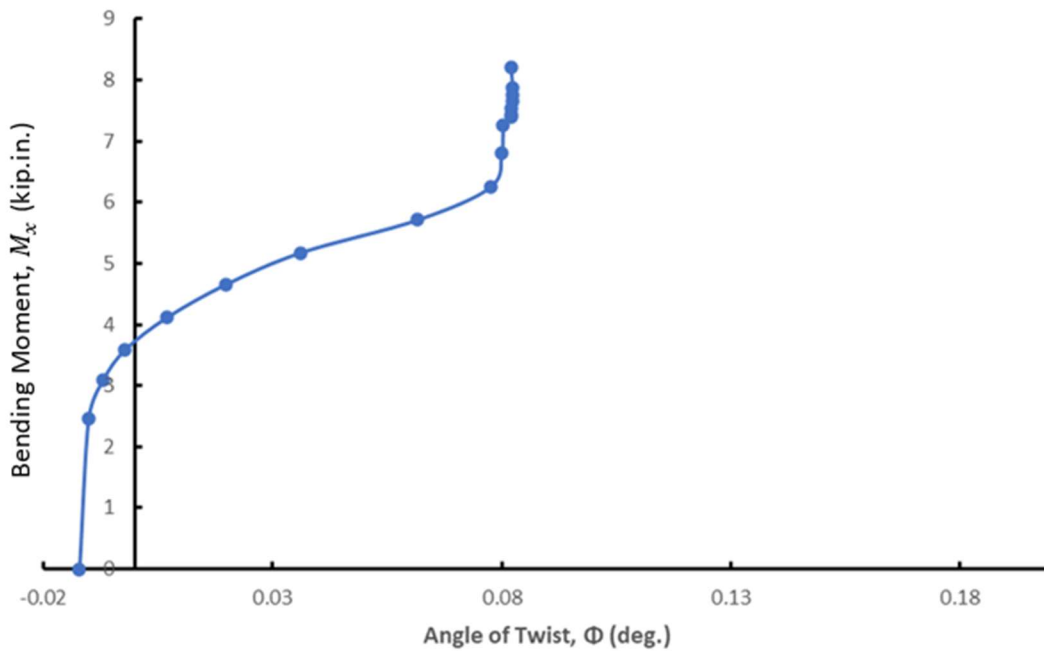


Figure 67. Bending Moment,  $M_x$ , vs. Bottom End Angle of Twist,  $\phi$ , for Test PTB-fp-5

In Tests PB-3, PTB-p-4, and PTB-fp-5 the tested members developed excessive cracking in and around the flange connection-holes at the member bottom end as can be seen in the following figure.



**Figure 68. Cracks Due to Stress Concentration**

## CHAPTER 4

### THEORY VERSUS EXPERIMENTS

This chapter presents numerical results based on the theoretical formulation presented in Chapter 2, as well as a comparison of experimental load-deflection from Chapter 3.

#### 4.1 For Test T-1

Figure 69 illustrates the predicted relationship between the applied torsional moment,  $M_z$ , and the angle of twist,  $\phi$  at the bottom end of the member. This prediction is compared with the experimental results. Both the predicted and experimental curves align well up to about 2.6 degrees. Beyond this point, the member exhibits substantial angle of twists, indicating that the condition exceeds the assumption of the small deflection theory.

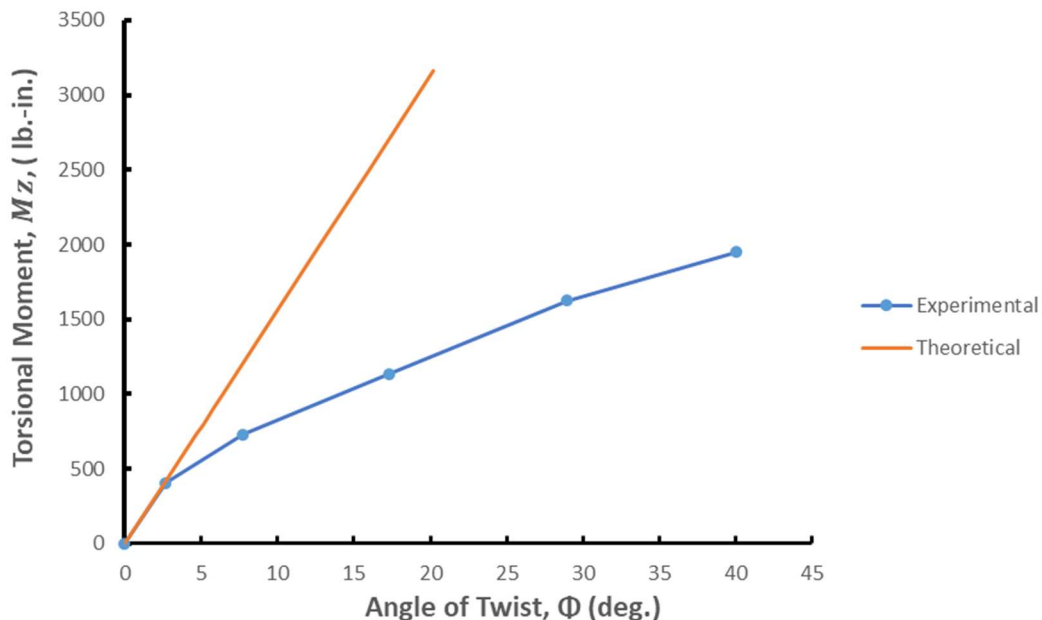
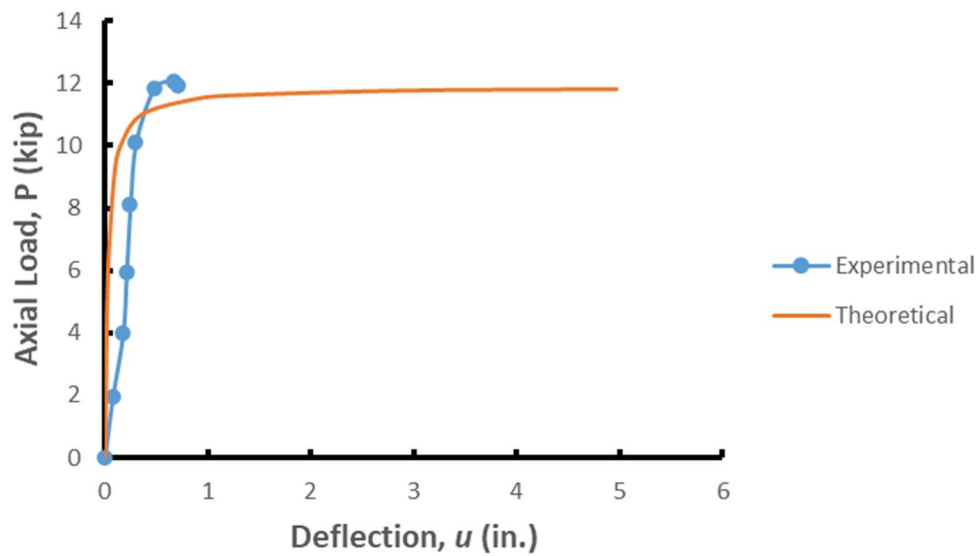


Figure 69. Applied Torsion,  $M_z$ , vs. Bottom End Angle of Twist,  $\phi$ , for Test T-1

#### 4.2 For Test P-2

For this test, Figures 70 to 72 illustrate the predicted relationship between the applied axial load,  $P$ , and deflections  $u$ ,  $v$ , and  $\phi$ . The theoretical axial load-carrying capacity agrees well with that observed experimentally and is found to be only 1.8 percent less than that found experimentally.



**Figure 70. Axial Load,  $P$ , vs. Midspan Deflection,  $u$ , for Test P-2**

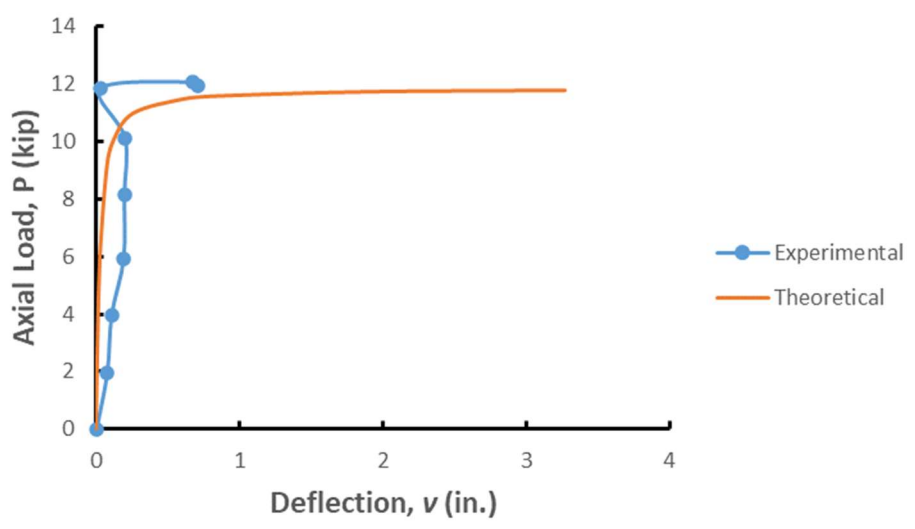


Figure 71. Axial Load,  $P$ , vs. Midspan Deflection,  $v$ , for Test P-2

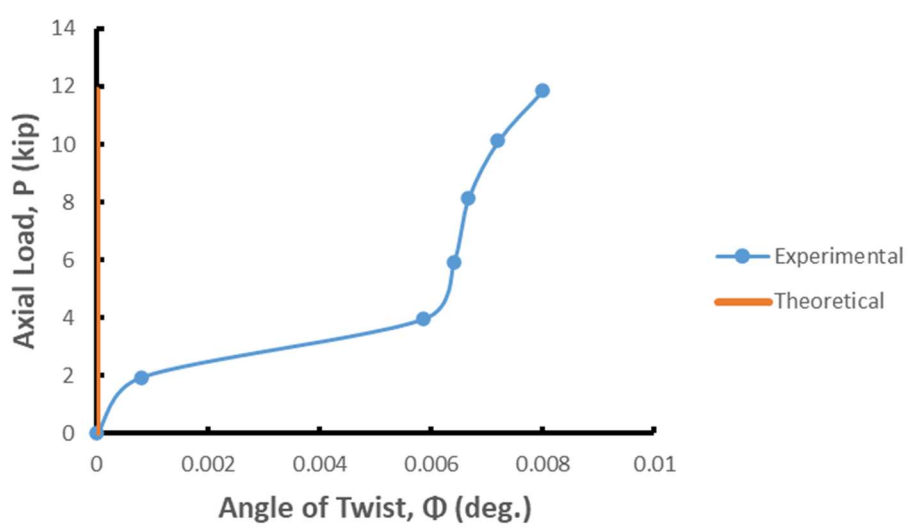


Figure 72. Axial Load,  $P$ , vs. Bottom End Angle of Twist,  $\phi$ , for Test P-2

### 4.3 For Test PB-3

Figure 73 through 75 present the applied bending moment,  $M_x$ , versus the midspan deflection,  $v$ ,  $u$ , and the bottom end angle of twist,  $\phi$ , respectively. It should be noted that the specimen developed cracks at the top and bottom connections as can be seen in Figure 56. No other cracks developed in the member.

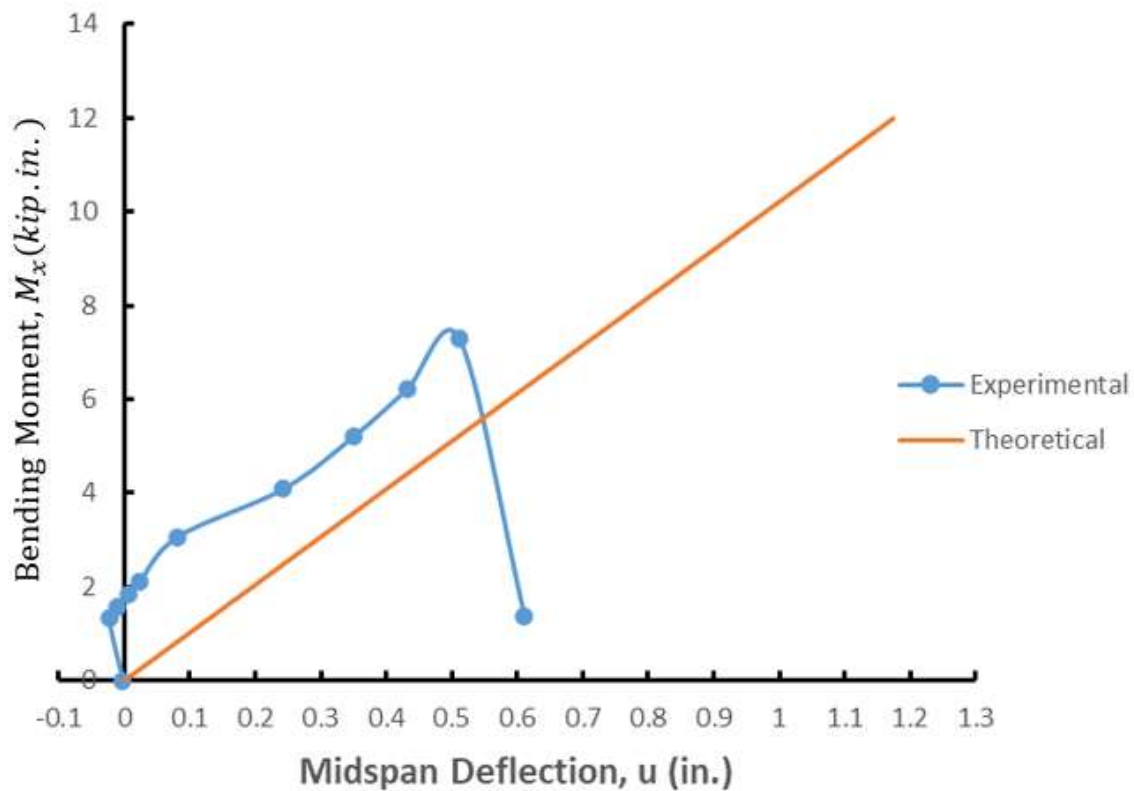


Figure 73. Bending Moment,  $M_x$ , vs. Midspan Deflection,  $u$ , for Test PB-3



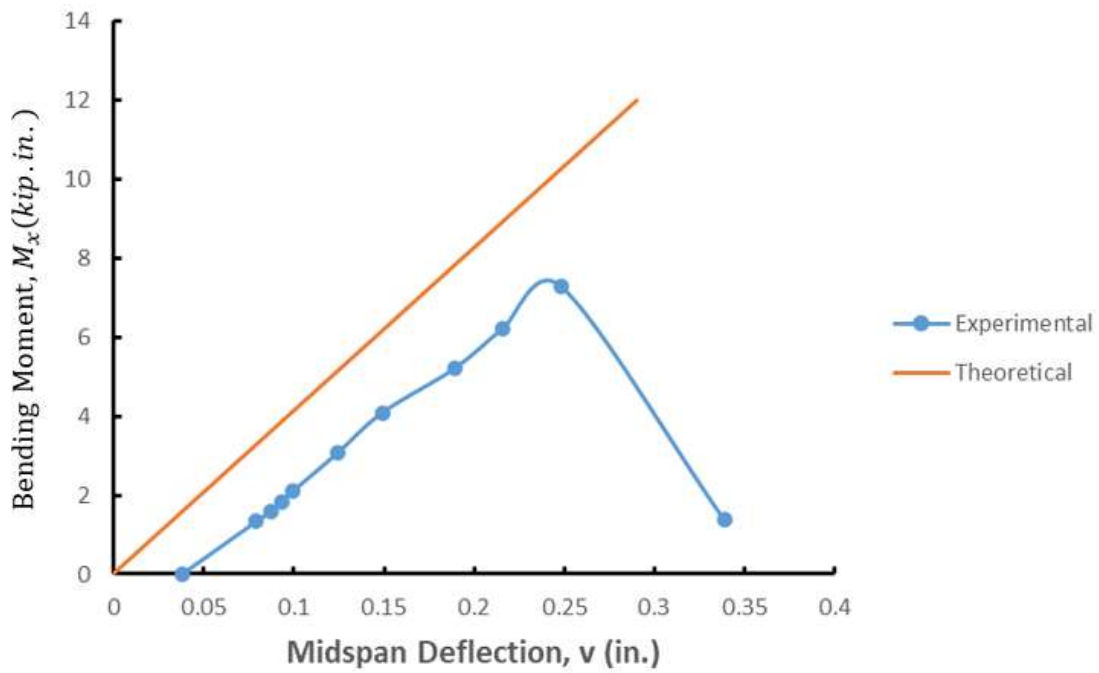


Figure 74. Bending Moment,  $M_x$ , vs. Midspan Deflection,  $v$ , for Test PB-3

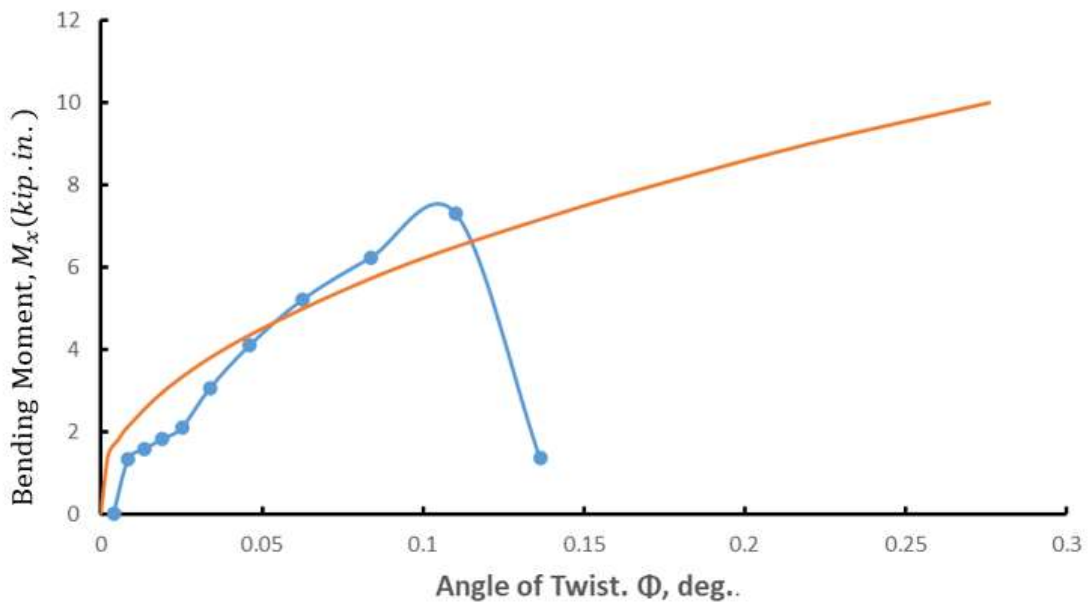
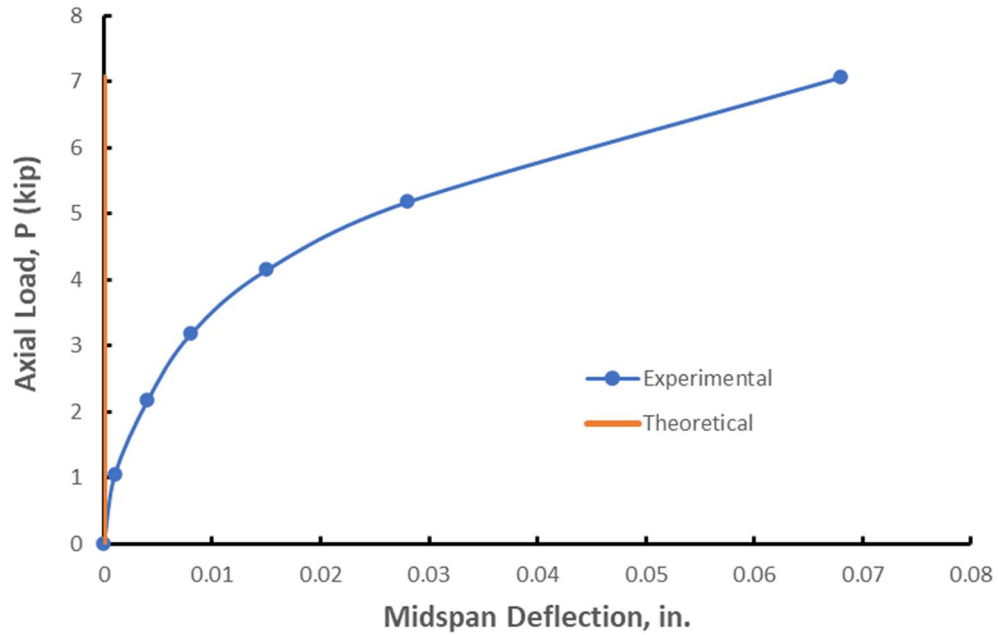


Figure 75. Bending Moment,  $M_x$ , vs. Bottom End Angle of Twist,  $\phi$ , for Test PB-3

#### 4.4 For Test PBT-p-4

Figures 76 through 82 show the relationship of the axial load,  $P$ , torsion,  $M_z$ , and bending moment,  $M_x$  vs. deflection  $v$ ,  $u$ , and  $\phi$ , respectively for this test.



**Figure 76. Axial Load,  $P$ , vs. Midspan Deflection,  $u$ , for Test PTB-p-4**

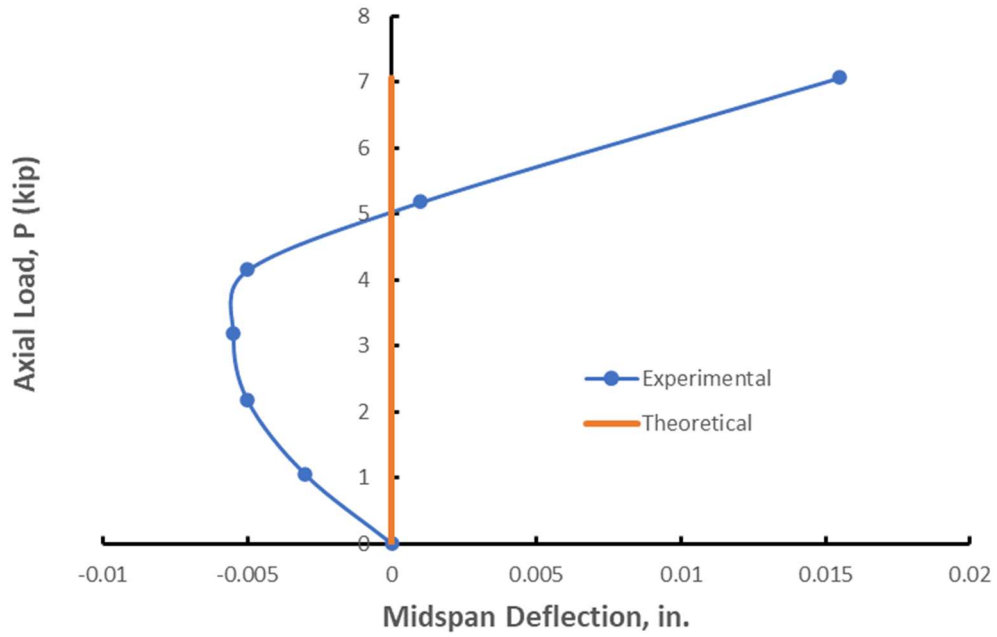


Figure 77. Axial Load,  $P$ , vs. Midspan Deflection,  $v$ , for Test PTB-p-4

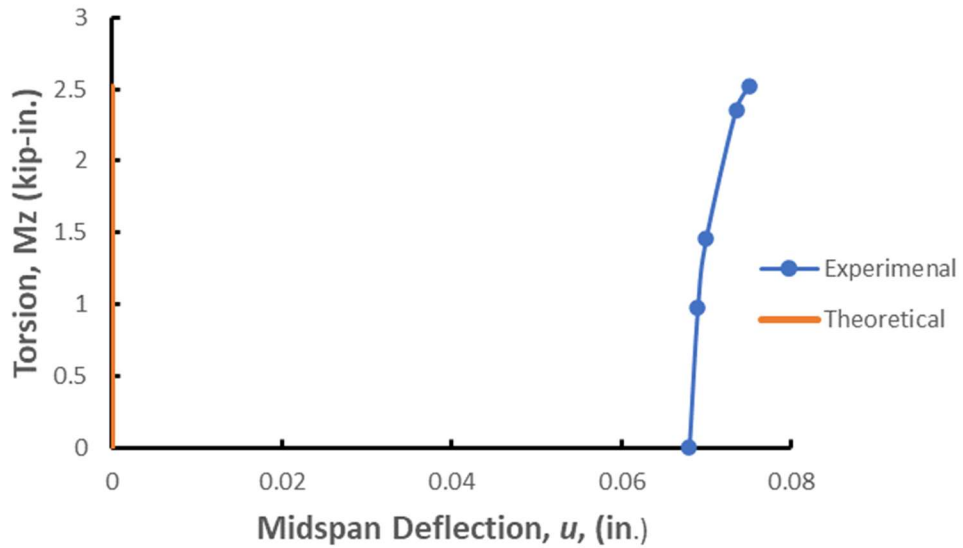


Figure 78. Torsion,  $M_z$ , vs. Midspan Deflection,  $u$ , for Test PTB-p-4

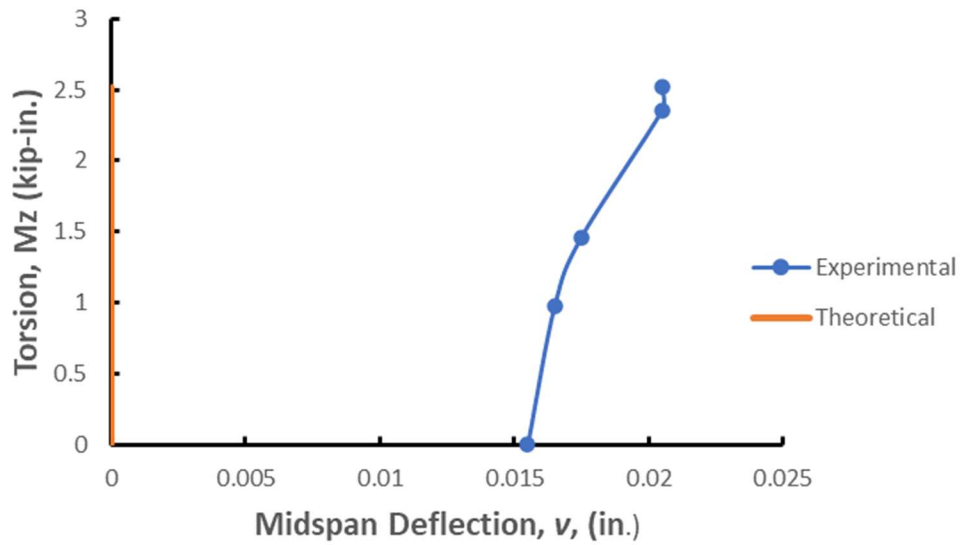


Figure 79. Torsion,  $M_z$ , vs. Midspan Deflection,  $v$ , for Test PTB-p-4

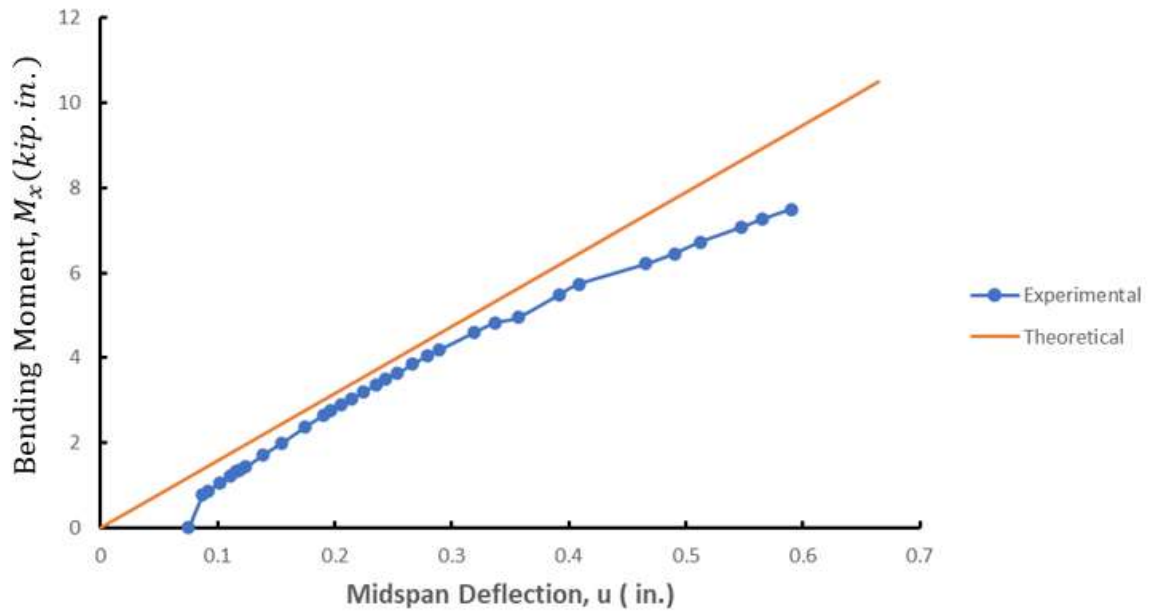


Figure 80. Bending Moment,  $M_x$ , vs. Midspan Deflection,  $u$ , for Test PTB-p-4

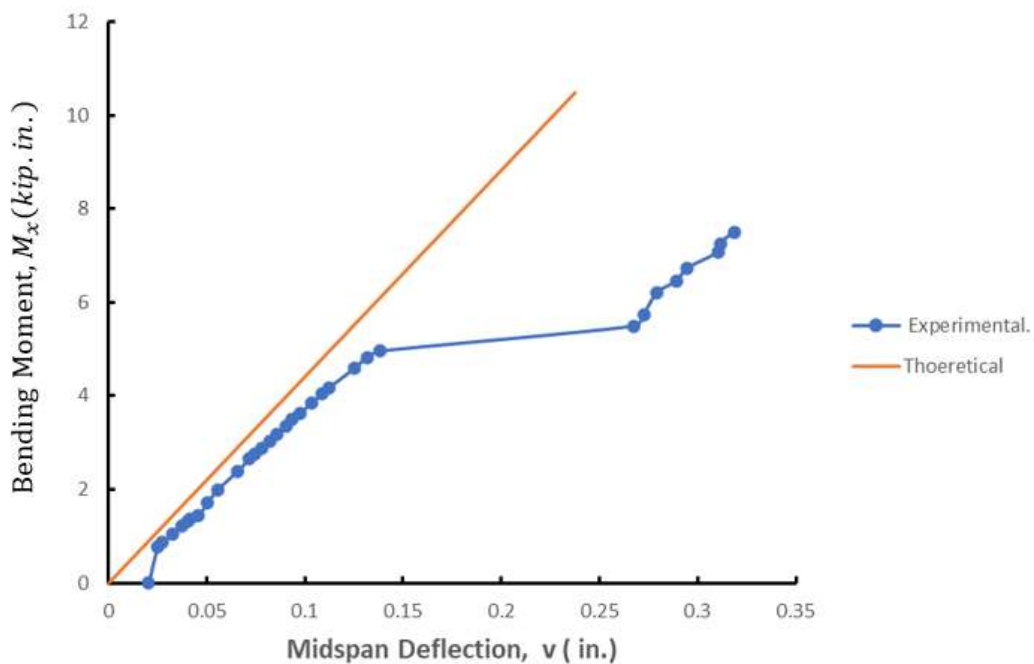


Figure 81. Bending Moment,  $M_x$ , vs. Midspan Deflection,  $v$ , for Test PTB-p-4

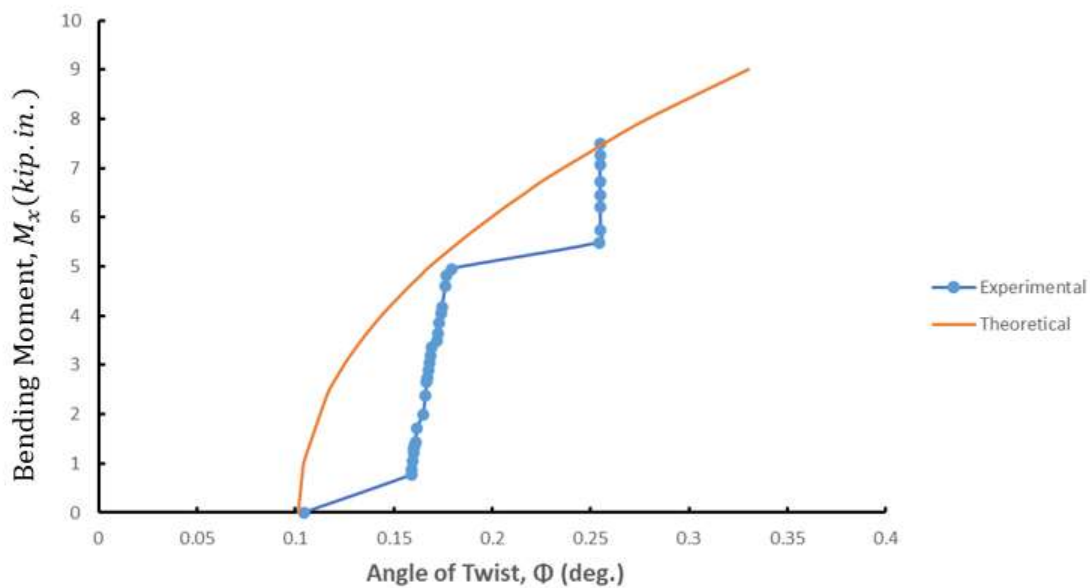


Figure 82. Bending Moment,  $M_x$ , vs. Bottom End Angle of Twist,  $\phi$ , for Test PTB-p-4

#### 4.5 For Test PBT-fp-5

For this test, Figures 83 through 67 show the axial load,  $P$ , and bending moment,  $M_x$ , vs. deflection  $v$ ,  $u$ , and  $\phi$  respectively.

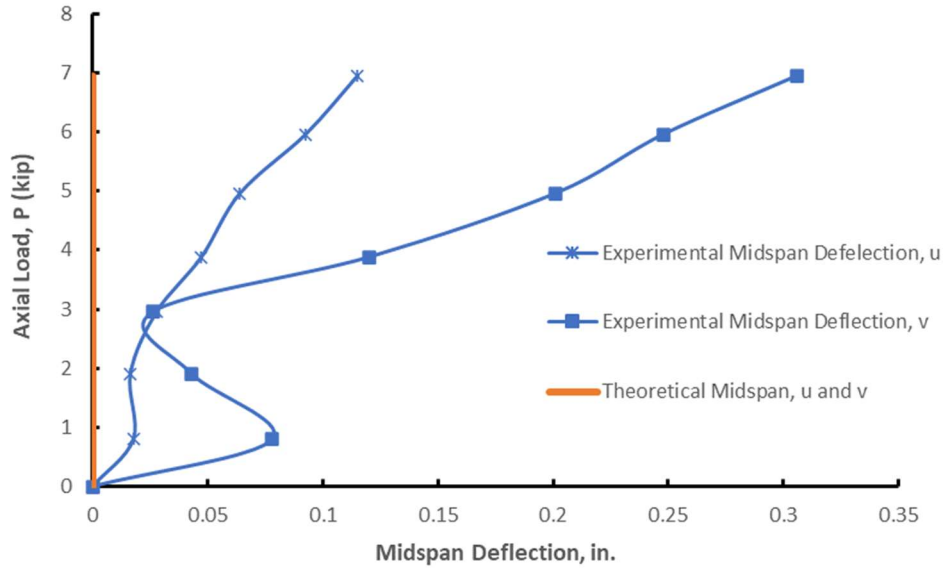


Figure 83. Axial Load,  $P$ , vs. Midspan Deflections,  $v$ , and  $u$ , for Test PTB-fp-5

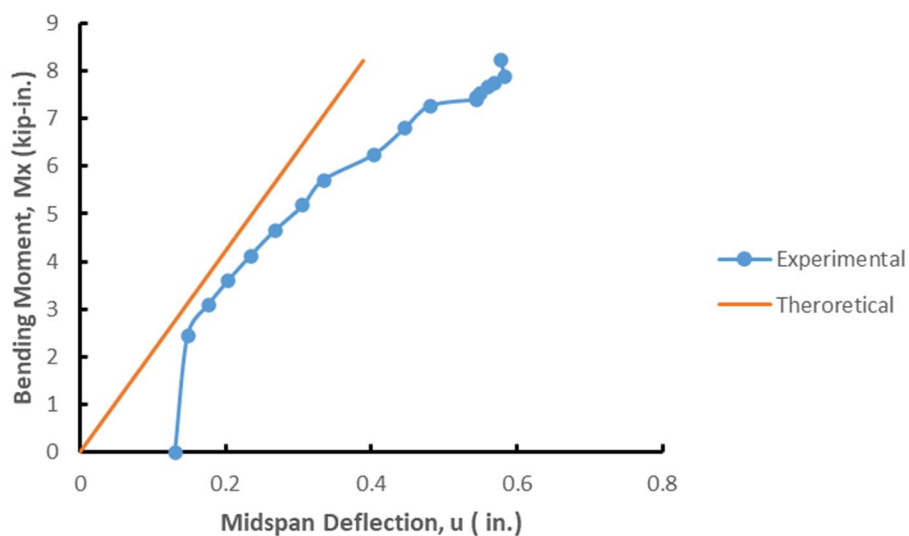


Figure 84. Bending Moment,  $M_x$ , vs. Midspan Deflection,  $u$ , for Test PTB-fp-5

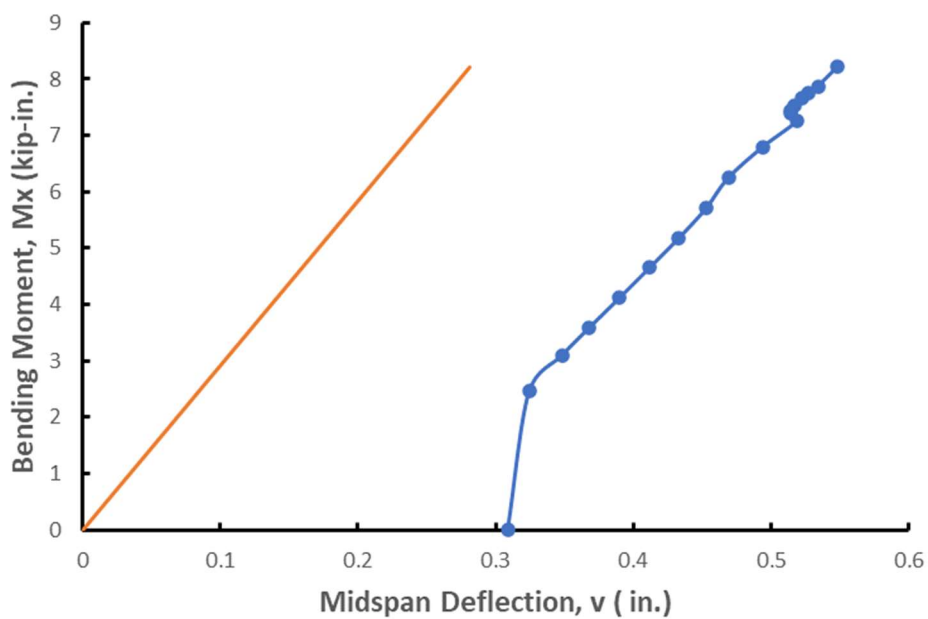
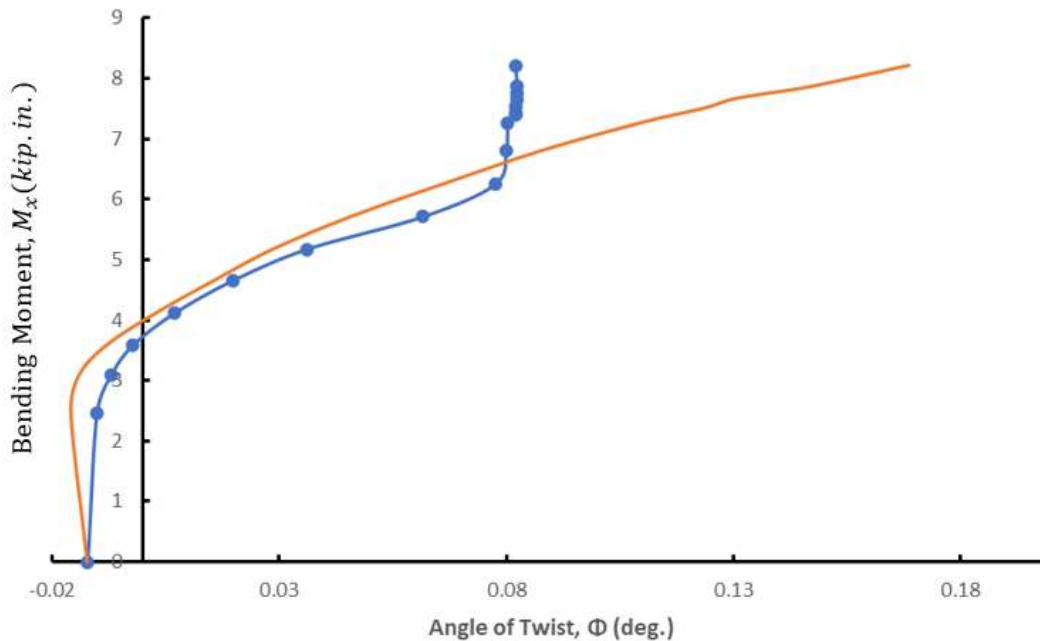


Figure 85. Bending Moment,  $M_x$ , vs. Midspan Deflection,  $v$ , for Test PTB-fp-5



**Figure 86. Bending Moment,  $M_x$ , vs. Bottom End Angle of Twist,  $\phi$ , for Test PTB-fp-5**

The following sections present the comparison between the available experimental results with the prediction using the MATLAB code. Each section contains a table that identifies the corresponding applied load and the calculated deflections. The table is then followed by figures showing the graphical relationship between the applied load and the related deflections.

#### 4.6 Available Experimental Results

As an additional validation and verification of the theoretical formulation solutions presented in Chapter 2, the output of the used MATLAB code developed in this dissertation proposal is compared to the laboratory experimental studies summarized below.



### 4.6.1 Stability of I-Beams

#### Three-Point Loading through Shear Center [40]

Sirjani [40] conducted three-point loading tests using the load application setup shown schematically in Figure 68. In this experimental study, a simply supported FRP  $4 \times 2 \times \frac{1}{2}$  in. cross section was adopted for the I-beam. A pair of steel tie rods were used to apply upward vertical loads ( $Q$ ) placed symmetrically about the shear center,  $S$ , which coincides with the centroid,  $C$ . The resultant,  $P=2Q$ , shown in Figure 87 acts at a distance  $y_0 = -3.5$  in. above the  $x$  axis but passes through the  $S$  and  $C$ .

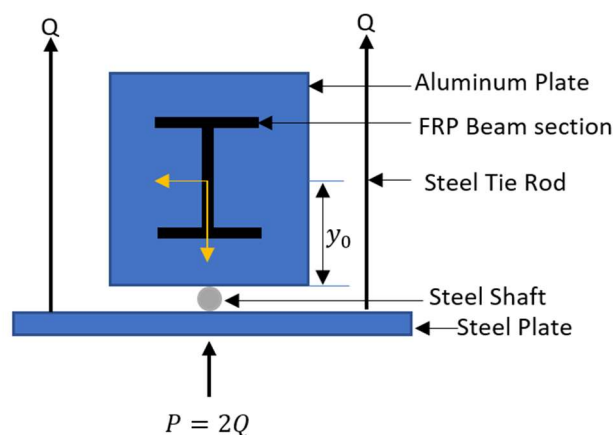


**Figure 87. Cross-Sectional Schematic View at Load Application Points for I-Section Beam**

Table 12 summarizes the experimental results for a 108-inch span I-beam for test No. IFT3-1. The first column of this table shows the observation number. The second column through the fifth column present the applied load,  $P$ ; the midspan vertical deflection,  $v_c$ ; the midspan horizontal deflection,  $u_c$ ; and the midspan angle of twist,  $\phi$  respectively. Figure 88 shows the experimental load,  $P$ , versus midspan vertical,  $v_c$ . Figure 89 shows the experimental load,  $P$ , versus midspan

deflection,  $u_c$ , and Figure 90 shows the experimental load,  $P$ , versus midspan angle of twist,  $\phi$ . Tables 14 and 16 present the experimental results for I-beam test No., IFT3-2, and IFT3-3 with a clear span  $L = 96$  and  $84$  in., respectively. Figures 91 through 96 show the midspan load,  $P$ , versus deflection curves from the corresponding tables. Tables 13, 15, and 17 present the theoretical results from the MATLAB code for each case.

**Table 12. Experimental Results for Test No. IFT3-1 [40]**

| Obesrvation | Load, P | Midspan Vertical Deflection | Midspan Lateral Deflection | Midspan Angle of Twist |
|-------------|---------|-----------------------------|----------------------------|------------------------|
| No.         | lbs.    | $v_{c,in.}$                 | $u_{c,in.}$                | $\phi$ , rad.          |
| 0           | 0       | 0                           | 0                          | 0                      |
| 1           | 35      | 0.09156                     | -0.01464                   | 0.009472               |
| 2           | 62      | 0.15541                     | -0.03947                   | 0.014323               |
| 3           | 78      | 0.21328                     | -0.08306                   | 0.012616               |
| 4           | 99      | 0.312                       | 0.65102                    | -0.014029              |

**Table 13. MATLAB Results for Test No. IFT3-1**

| Obesrvation | Load, P | Midspan Vertical Deflection | Midspan Lateral Deflection | Midspan Angle of Twist |
|-------------|---------|-----------------------------|----------------------------|------------------------|
| No.         | lbs     | $v_{c,in.}$                 | $u_{c,in.}$                | $\phi$ , rad.          |
| 0           | 0       | 0                           | 0                          | 0                      |
| 1           | 35      | 0.082089076                 | -0.02363887                | 0.006978913            |
| 2           | 62      | 0.145414934                 | -0.03397233                | 0.010183054            |
| 3           | 78      | 0.182941369                 | -0.037881176               | 0.011406436            |
| 4           | 99      | 0.232194814                 | -0.041584072               | 0.012551841            |
| 5           | 124     | 0.290829868                 | -0.044609061               | 0.01346171             |

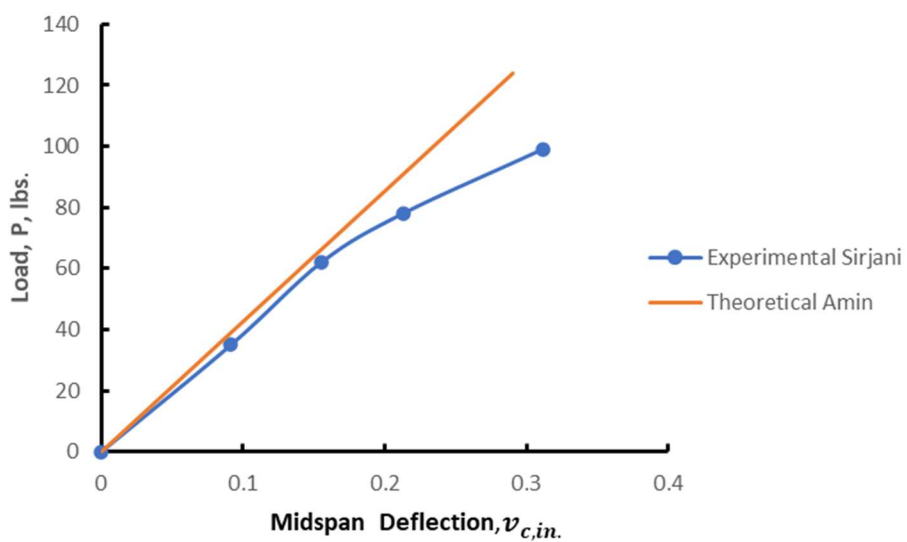


Figure 88. Load, P, vs. Midspan Deflection,  $v_c$ , for Test No. IFT3-1

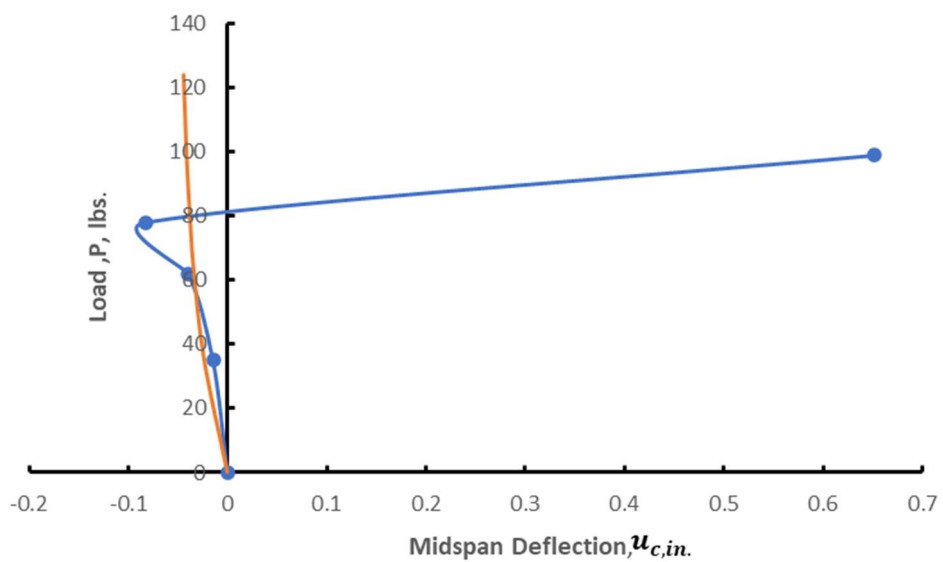


Figure 89. Load, P, versus Midspan Deflection,  $u_c$ , for Test No. IFT3-1

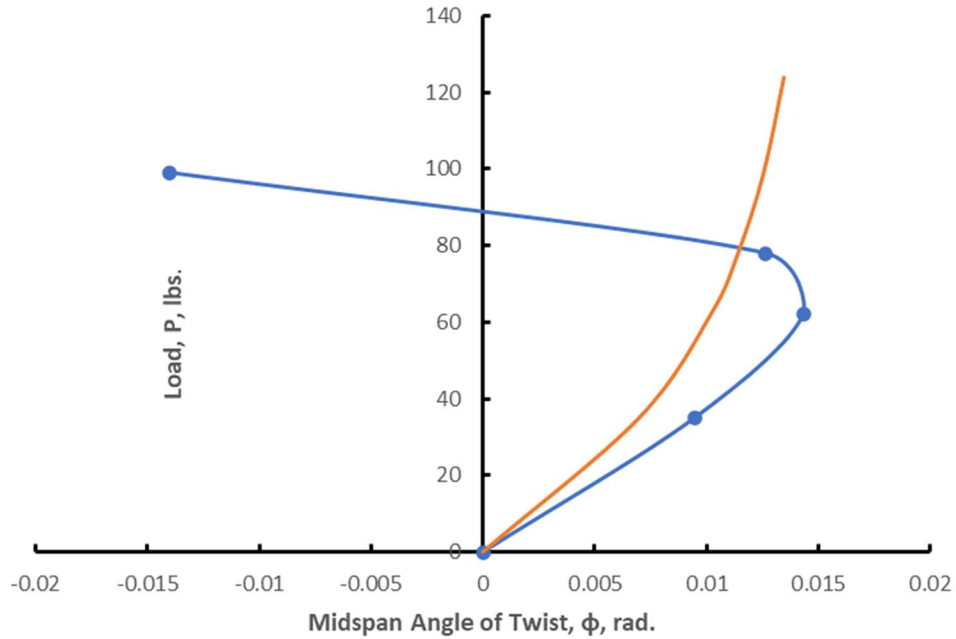


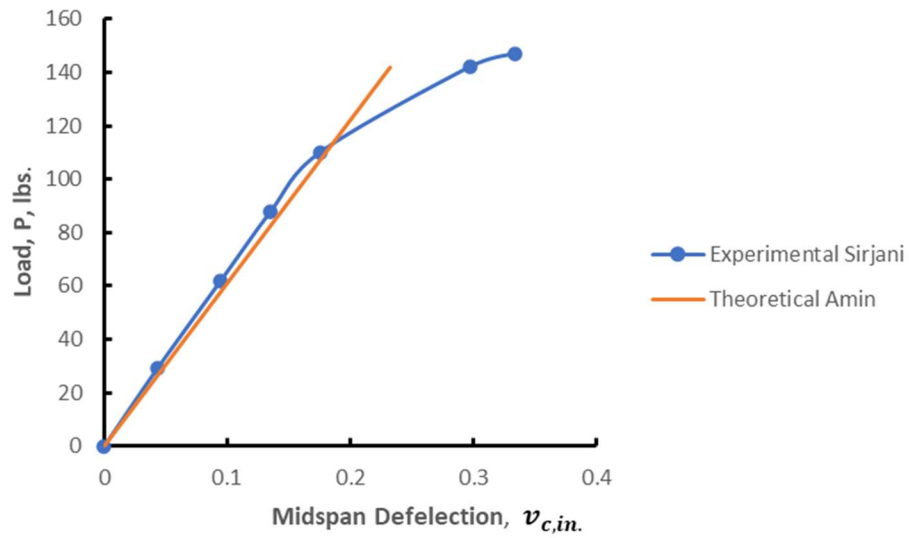
Figure 90. Load,  $P$ , versus Angle of Twist,  $\phi$ , for Test No. IFT3-1

Table 14. Experimental Results for Test No. IFT3-2 [40]

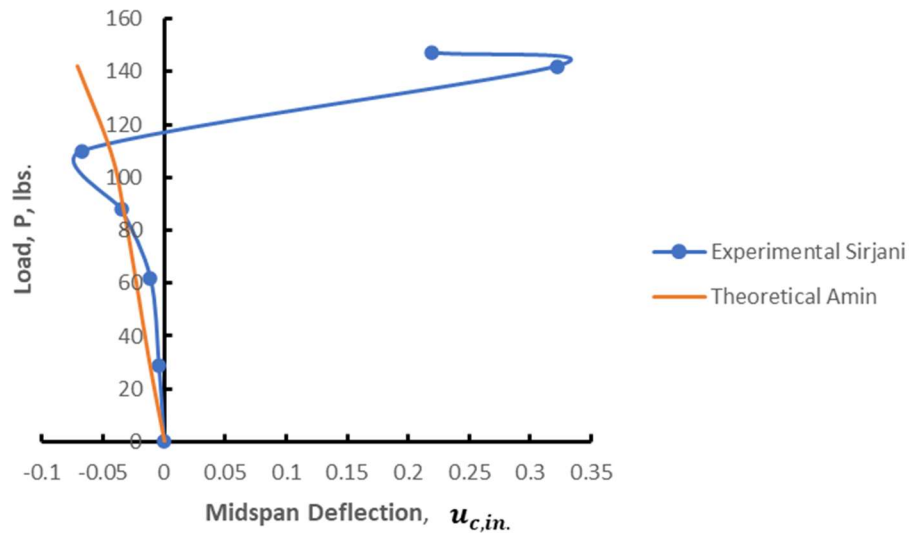
| Observation No. | Load, $P$ lbs. | Midspan Vertical Deflection $v_{c,in.}$ | Midspan Lateral Deflection $u_{c,in.}$ | Midspan Angle of Twist $\phi$ , rad. |
|-----------------|----------------|---|--|--------------------------------------|
| 0               | 0              | 0                                       | 0                                      | 0                                    |
| 1               | 29             | 0.04309                                 | -0.0043                                | 0.005318                             |
| 2               | 62             | 0.09491                                 | -0.01136                               | 0.011125                             |
| 3               | 88             | 0.13554                                 | -0.03534                               | 0.015454                             |
| 4               | 110            | 0.17556                                 | -0.06694                               | 0.013825                             |
| 5               | 142            | 0.29745                                 | 0.32178                                | -0.037071                            |
| 6               | 147            | 0.33352                                 | 0.21938                                | -0.06072                             |

Table 15. MATLAB Results for Test No. IFT3-2

| Observation No. | Load, $P$ lbs. | Midspan Vertical Deflection $v_{c,in.}$ | Midspan Lateral Deflection $u_{c,in.}$ | Midspan Angle of Twist $\phi$ , rad. |
|-----------------|----------------|---|--|--------------------------------------|
| 0               | 0              | 0                                       | 0                                      | 0                                    |
| 1               | 29             | 0.04754212                              | -0.01187515                            | 0.003809489                          |
| 2               | 62             | 0.101641773                             | -0.023658081                           | 0.008712837                          |
| 3               | 88             | 0.144265742                             | -0.033411715                           | 0.013676933                          |
| 4               | 110            | 0.180332178                             | -0.043943438                           | 0.019530552                          |
| 5               | 142            | 0.232792448                             | -0.070785133                           | 0.034869785                          |



**Figure 91. Load, P, versus Midspan Deflection,  $v_c$ , for Test No. IFT3-2**



**Figure 92. Load, P, versus Midspan Deflection,  $u_c$ , for Test No. IFT3-2**

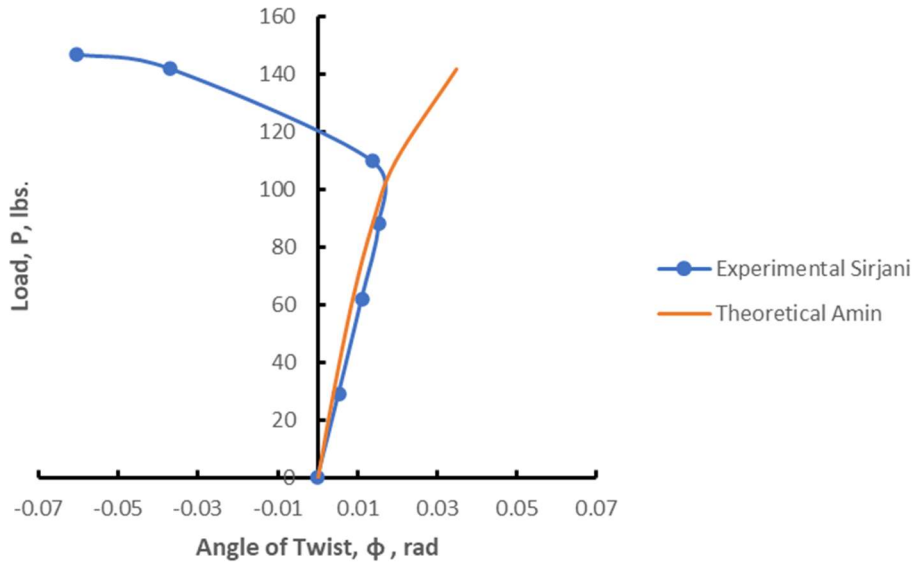


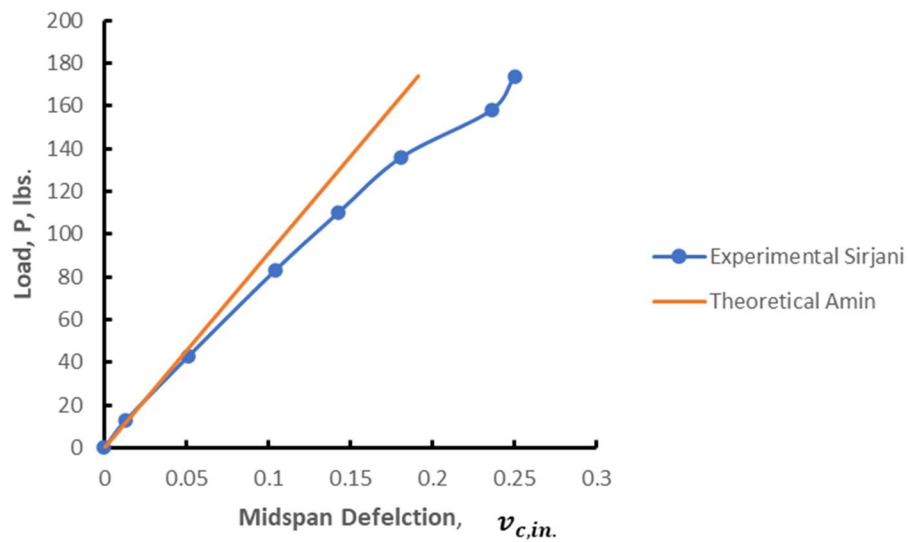
Figure 93. Load,  $P$ , versus Angle of Twist,  $\phi$ , for Test No. IFT3-2

Table 16. Experimental Results Test No. IFT3-3 [40]

| Observation No. | Load, $P$ lbs. | Midspan Vertical Deflection $v_{c,in.}$ | Midspan Lateral Deflection $u_{c,in.}$ | Midspan Angle of Twist $\phi$ , rad. |
|-----------------|----------------|---|--|--------------------------------------|
| 0               | 0              | 0                                       | 0                                      | 0                                    |
| 1               | 13             | 0.013123                                | -5.5E-05                               | 0.00202                              |
| 2               | 43             | 0.051392                                | 0.003076                               | 0.005665                             |
| 3               | 83             | 0.10405                                 | -0.02061                               | 0.010482                             |
| 4               | 110            | 0.142537                                | -0.040332                              | 0.011079                             |
| 5               | 136            | 0.181047                                | -0.059414                              | 0.009088                             |
| 6               | 158            | 0.235874                                | 0.844613                               | -0.002814                            |
| 7               | 174            | 0.249995                                | 0.865044                               | -0.025282                            |

Table 17. MATLAB Test No. IFT3-3

| Observation No. | Load, P lbs | Midspan Vertical Deflection $v_{c,in.}$ | Midspan Lateral Deflection $u_{c,in.}$ | Midspan Angle of Twist $\phi, rad.$ |
|-----------------|-------------|---|--|-------------------------------------|
| 0               | 0           | 0                                       | 0                                      | 0                                   |
| 1               | 13          | 0.014275224                             | -0.004071877                           | 0.001212095                         |
| 2               | 43          | 0.047218047                             | -0.012304135                           | 0.004048399                         |
| 3               | 83          | 0.091141812                             | -0.021272964                           | 0.008071215                         |
| 4               | 110         | 0.120790353                             | -0.02650723                            | 0.011105764                         |
| 5               | 136         | 0.1493408                               | -0.03136444                            | 0.014456413                         |
| 6               | 158         | 0.173498871                             | -0.035649346                           | 0.017790975                         |
| 7               | 174         | 0.191068376                             | -0.039058041                           | 0.020627939                         |

Figure 94. Load, P, versus Midspan Deflection,  $v_c$ , for Test No. IFT3-3

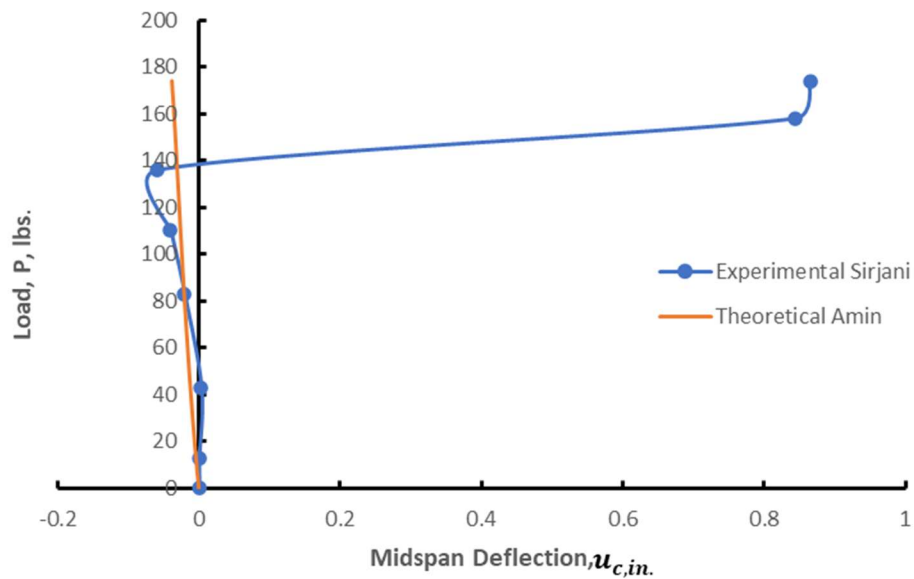


Figure 95. Load,  $P$ , versus Midspan Deflection,  $u_c$ , for Test No. IFT3-3

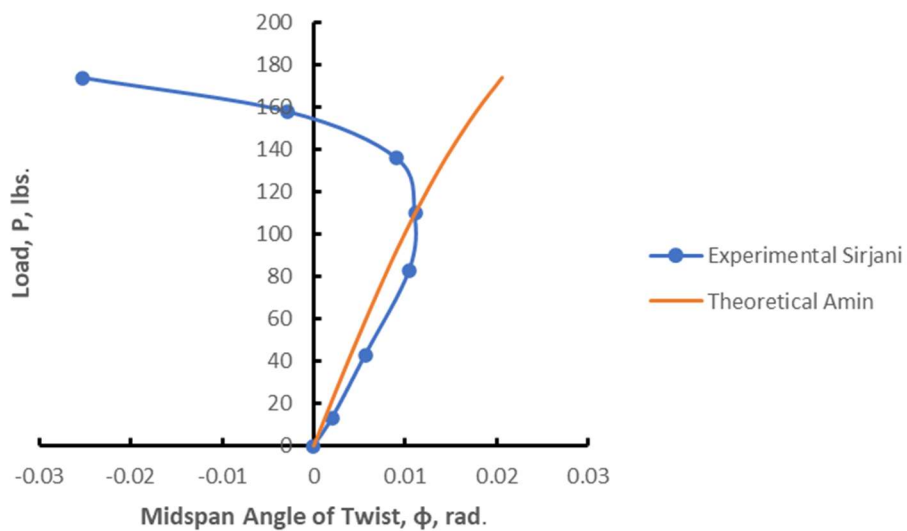


Figure 96. Load,  $P$ , versus Angle of Twist,  $\phi$ , for Test No. IFT3-3



#### 4.6.2 I-Beam Lateral Torsional Buckling

Hampton [41] conducted laboratory experiments on single, two and three span glass FRP beams subjected to in-plane gradually increasing quasi-static loading eventually resulting in lateral-torsional instability. The following sections describe part of the experimental testing included in this study.

##### Investigation 1

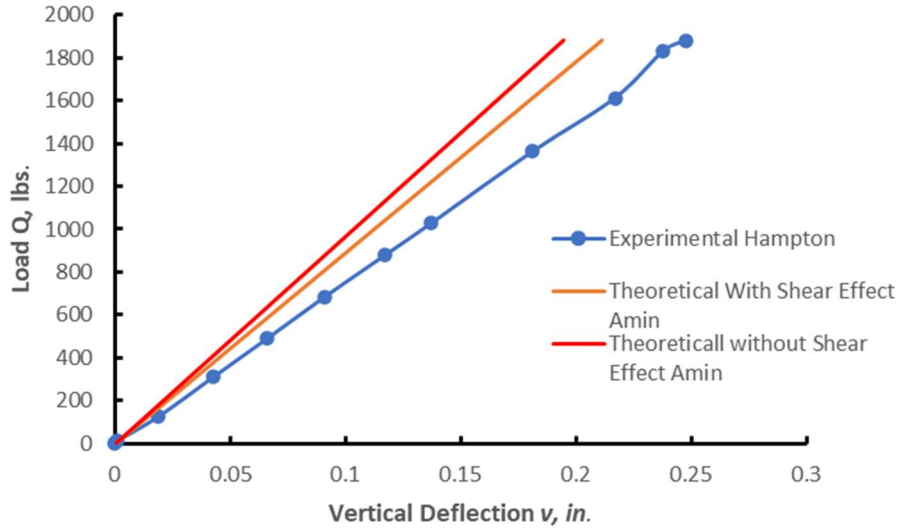
These experiments investigated the translational and rotational deflections of a single span beam with a point load at midspan using a 4x4x0.25" cross section. A GFRP beam of length  $L = 75''$  was placed in a beam testing apparatus then in-plane vertical load,  $Q$ , was applied to the beam until it reached lateral-torsional buckling failure. The objective of this investigation is to identify the shear effect on the in-plane and out of plane deflections. These typically unaddressed deflections often lead to premature buckling failure of the beam. Table 18 summarizes the experimental vertical deflections for investigation 1. Figures 97 through 99 show the relation between the applied load,  $Q$ , versus the vertical deflections with and without the shear effect for number of points along the span of the beam. Because there is no load in the x axis direction,  $W = 0$ , and for zero applied torsion,  $M_z = 0$ , the theoretical values of the horizontal deflection,  $u$ , and the angle of twist,  $\phi$  within the elastic range will be zero for Finite Difference Method calculations; however, the tested specimens will undergo lateral and rotational distortions. Table 19 presents the output of the MATLAB code for this case.

Table 18. Experimental Vertical Deflections,  $\nu$  (in.) for Investigation 1 [41]

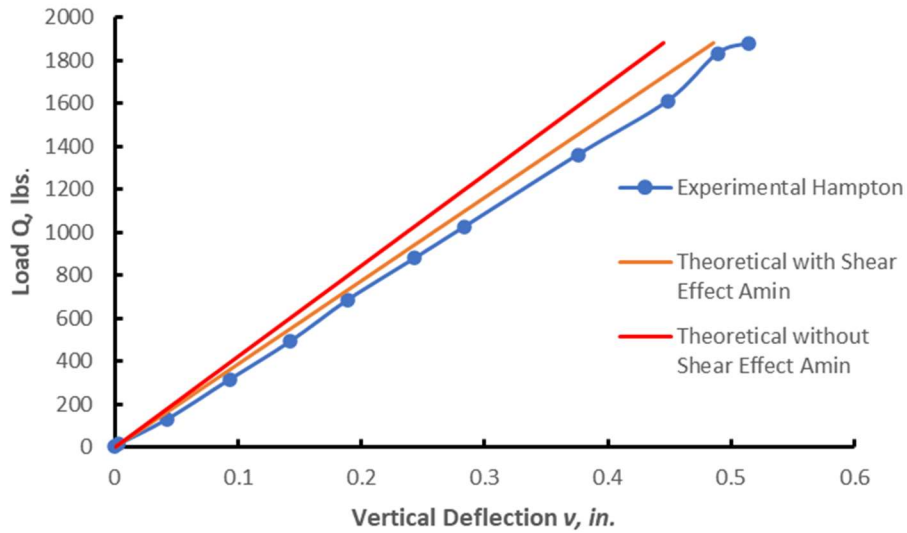
| Vertical Load<br>Q, lbs | Distance from Support |        |        |
|-------------------------|-----------------------|--------|--------|
|                         | 8 in.                 | 18 in. | 29 in. |
| 0                       | 0                     | 0      | 0      |
| 14.078                  | -0.001                | 0.003  | 0.004  |
| 129.25                  | -0.019                | 0.042  | 0.053  |
| 314.89                  | -0.043                | 0.093  | 0.121  |
| 491.298                 | -0.066                | 0.142  | 0.178  |
| 685.838                 | -0.091                | 0.189  | 0.258  |
| 878.73                  | -0.117                | 0.243  | 0.329  |
| 1027.1                  | -0.137                | 0.284  | 0.386  |
| 1361.8                  | -0.181                | 0.376  | 0.509  |
| 1612.4                  | -0.217                | 0.449  | 0.607  |
| 1831.6                  | -0.238                | 0.489  | 2.1    |
| 1880                    | -0.248                | 0.514  | 2.7    |

Table 19. MATLAB Results for Investigation 1

| With Shear Effect |                       |          |          | Without Shear Effect |                       |          |          |
|-------------------|-----------------------|----------|----------|----------------------|-----------------------|----------|----------|
| Vertical Load     | Distance from Support |          |          | Vertical Load        | Distance from Support |          |          |
| Q, lbs            | 8 in.                 | 18 in.   | 29 in.   | Q, lbs               | 8 in.                 | 18 in.   | 29 in.   |
| 0                 | 0                     | 0        | 0        | 0                    | 0                     | 0        | 0        |
| 14.078            | 0.001585              | 0.003639 | 0.005282 | 14.078               | 0.001459257           | 0.003334 | 0.00478  |
| 129.25            | 0.014549              | 0.03341  | 0.048493 | 129.25               | 0.013397426           | 0.030613 | 0.043886 |
| 314.89            | 0.035446              | 0.081397 | 0.118144 | 314.89               | 0.032639964           | 0.074582 | 0.106918 |
| 491.298           | 0.055304              | 0.126998 | 0.184331 | 491.298              | 0.050925558           | 0.116364 | 0.166816 |
| 685.838           | 0.077203              | 0.177285 | 0.257321 | 685.838              | 0.071090627           | 0.16244  | 0.23287  |
| 878.73            | 0.098917              | 0.227147 | 0.329692 | 878.73               | 0.091084873           | 0.208127 | 0.298365 |
| 1027.1            | 0.115618              | 0.265499 | 0.385359 | 1027.1               | 0.106464184           | 0.243268 | 0.348743 |
| 1361.8            | 0.153295              | 0.352017 | 0.510936 | 1361.8               | 0.141157557           | 0.322542 | 0.462388 |
| 1612.4            | 0.181504              | 0.416796 | 0.604959 | 1612.4               | 0.167133532           | 0.381896 | 0.547477 |
| 1831.6            | 0.206179              | 0.473458 | 0.687201 | 1831.6               | 0.189854737           | 0.433813 | 0.621904 |
| 1880              | 0.211627              | 0.485969 | 0.70536  | 1880                 | 0.194871645           | 0.445277 | 0.638338 |



**Figure 97. Load, Q, versus Vertical Deflection,  $v$ , for 8 in. Distance from the Support for Investigation 1**



**Figure 98. Load, Q, versus Vertical Deflection,  $v$ , for 18 in. Distance from the Support for Investigation 1**

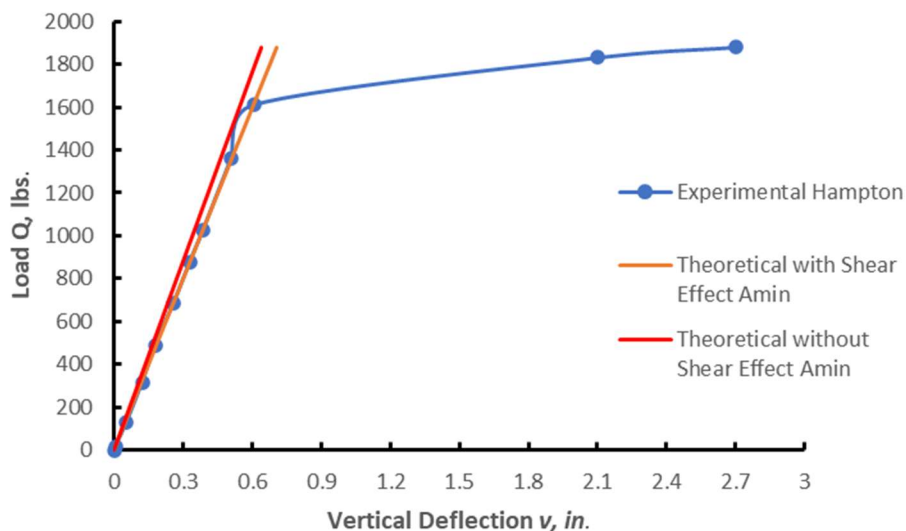


**Figure 99. Load,  $Q$ , versus Vertical Deflection,  $v$ , for 29 in. Distance from the Support for Investigation 1**

### Investigation 2

These experiments were conducted to predict the vertical deflections of a single span using 3x3x0.25" GFRP I-beam of length  $L = 79.5''$  with an off-center point load. In this case, the vertical load,  $Q$ , is applied at distance 27in as shown in Figure 100 from the support. Table 20 summarizes the experimental vertical deflections for Investigation 2. The relation between the applied load,  $Q$ , versus the vertical deflections,  $v$ , for several points on the beam is presented in Figures 101 through 103. The MATLAB output of the theoretical vertical deflections,  $v$ , for different values of applied load,  $Q$ , is summarized in Table 21.



**Figure 100. Applied Load,  $Q$  at 27 in. from the Support**

**Table 20. Experimental Results for Investigation 2 [41]**

| Vertical Load<br>Q, lbs | Distance from Support |        |        |
|-------------------------|-----------------------|--------|--------|
|                         | 6 in.                 | 21 in. | 36 in. |
| 0                       | 0                     | 0      | 0      |
| 182.6                   | 0.074                 | 0.23   | 0.181  |
| 424.4                   | 0.132                 | 0.309  | 0.399  |
| 651.4                   | 0.206                 | 0.476  | 0.593  |
| 865.3                   | 0.338                 | 0.64   | 0.792  |
| 910                     | 0.41                  | 0.794  | 0.966  |

**Table 21. MATLAB Results for Investigation 2**

| With Shear Effect |                       |          |          | Without Shear Effect |                       |          |          |
|-------------------|-----------------------|----------|----------|----------------------|-----------------------|----------|----------|
| Vertical Load     | Distance from Support |          |          | Vertical Load        | Distance from Support |          |          |
| Q, lbs            | 6 in.                 | 21 in.   | 36 in.   | Q, lbs               | 6 in.                 | 21 in.   | 36 in.   |
| 0                 | 0                     | 0        | 0        | 0                    | 0                     | 0        | 0        |
| 182.6             | 0.047759              | 0.149109 | 0.186985 | 182.6                | 0.04528               | 0.140429 | 0.17772  |
| 424.4             | 0.111003              | 0.346559 | 0.434591 | 424.4                | 0.105239              | 0.326386 | 0.413058 |
| 651.4             | 0.170375              | 0.531924 | 0.667042 | 651.4                | 0.161529              | 0.500961 | 0.633992 |
| 865.3             | 0.226321              | 0.706592 | 0.886078 | 865.3                | 0.21457               | 0.665462 | 0.842176 |
| 910               | 0.238013              | 0.743094 | 0.931851 | 910                  | 0.225654              | 0.699838 | 0.885681 |

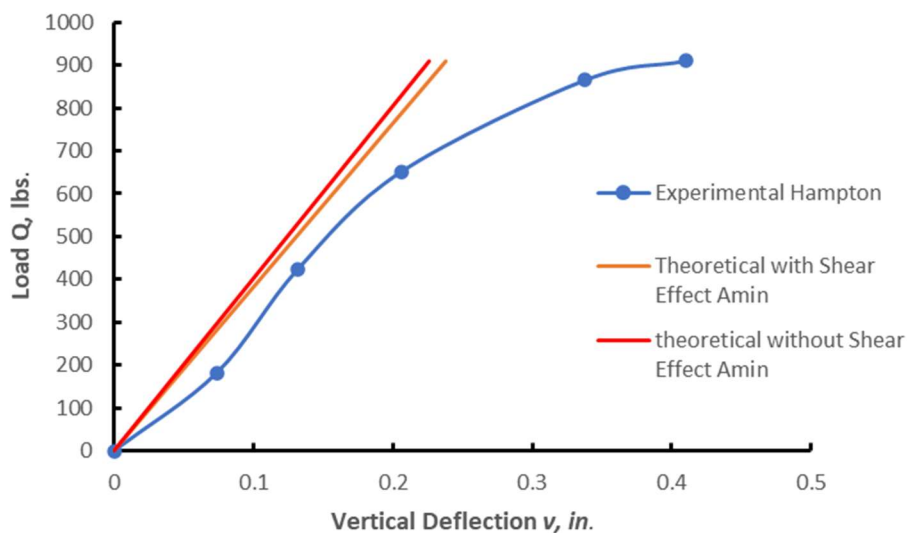


**Figure 101. Load, Q, versus Vertical Deflection,  $v$ , for 6 in. Distance from the Support for Investigation 2**

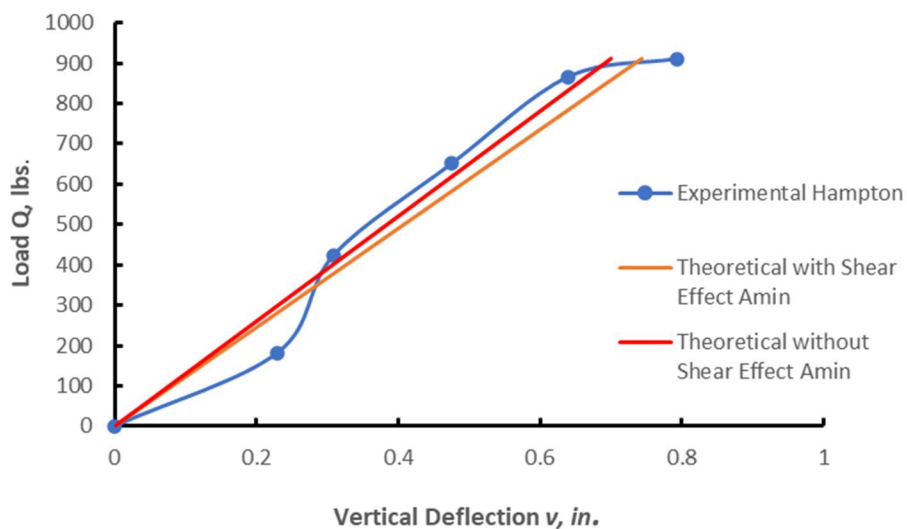


**Figure 102. Load,  $Q$ , versus Vertical Deflection,  $v$ , for 21 in. Distance from the Support for Investigation 2**

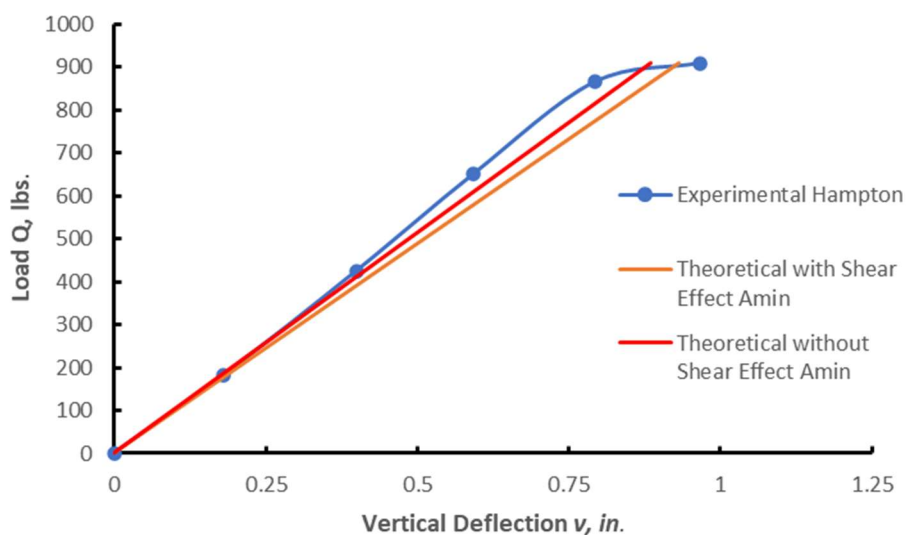


**Figure 103. Load,  $Q$ , versus Vertical Deflection,  $v$ , for 36 in. Distance from the Support for Investigation 2**

### 4.6.3 I-Beam Under Biaxial Bending

#### Case 1: Minor Axis Bending Due to Single Point at Midspan of the Member

Knorowski [42] conducted an experimental minor axis bending of FRP 4x4x1/4" I-beam by applying a single point load at the midspan through its shear center using a pulley system. Incremental load was applied to the I-beam by adding weights to the fabricated steel container. Unsupported beam lengths of 64 inches, 82 inches, and 100 inches were tested. Tables 22, 24, and 26 summarize the experimental horizontal deflections,  $U$ , for Case 1. The relation between the applied load,  $H$ , versus the horizontal deflections,  $U$ , for the midspan of the member is presented in Figures 104 through 106. Tables 23, 25, and 27 present the MATLAB output for this experiment.

**Table 22. Experimental Results for Case 1, L = 64 inches [42]**

| <b>Lateral Load</b> | <b>Experimental Deflection</b> |
|---------------------|--------------------------------|
| <b>H (lbs.)</b>     | <b>U (in.)</b>                 |
| 0                   | 0                              |
| 50                  | 0.0397                         |
| 100                 | 0.0783                         |
| 150                 | 0.112                          |
| 200                 | 0.1557                         |
| 250                 | 0.1931                         |
| 300                 | 0.2281                         |

Table 23. MATLAB Results for Case 1, L = 64 inches

| Lateral Load<br>H (lbs.) | Experimental Deflection<br>U (in.) |
|--------------------------|------------------------------------|
| 0                        | 0                                  |
| 50                       | 0.038231074                        |
| 100                      | 0.074091779                        |
| 150                      | 0.109952483                        |
| 200                      | 0.145813187                        |
| 250                      | 0.181673891                        |
| 300                      | 0.217534595                        |

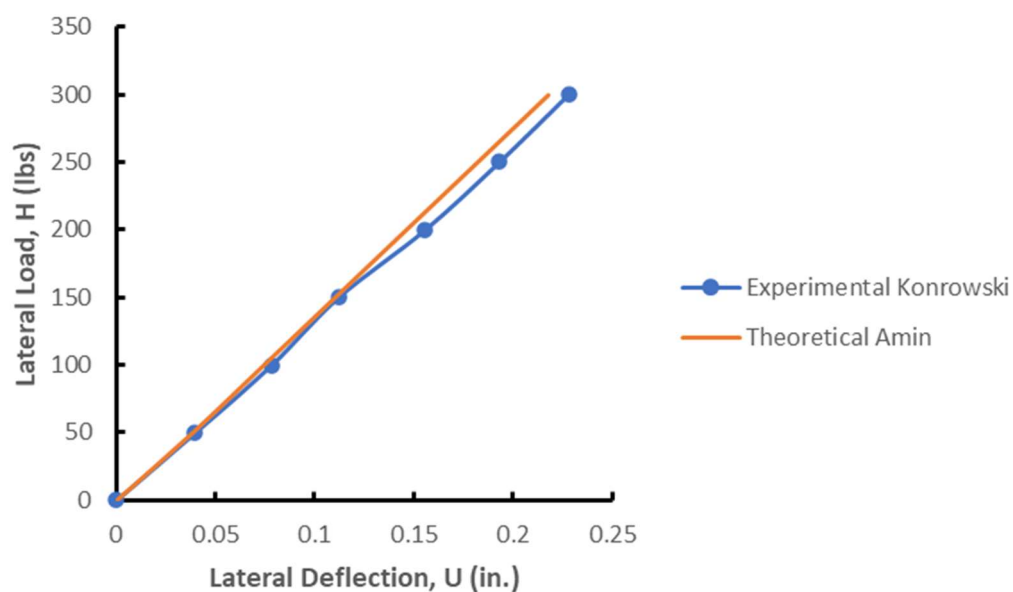


Figure 104. Load, H, vs. Horizontal Lateral Deflection, U, for Case 1, L = 64 inches

Table 24. Experimental Results for Case 1, L = 82 inches [42]

| Lateral Load<br>H (lbs.) | Experimental Deflection<br>U (in.) |
|--------------------------|------------------------------------|
| 0                        | 0                                  |
| 50                       | 0.0817                             |
| 100                      | 0.1603                             |
| 150                      | 0.2327                             |
| 200                      | 0.319                              |
| 250                      | 0.3987                             |
| 300                      | 0.4744                             |



Table 25. MATLAB Results for Case 1, L = 82 inches

| Lateral Load<br>H (lbs.) | Experimental Deflection<br>U (in.) |
|--------------------------|------------------------------------|
| 0                        | 0                                  |
| 50                       | 0.076103898                        |
| 100                      | 0.149170758                        |
| 150                      | 0.222237619                        |
| 200                      | 0.295304479                        |
| 250                      | 0.36837134                         |
| 300                      | 0.4414382                          |

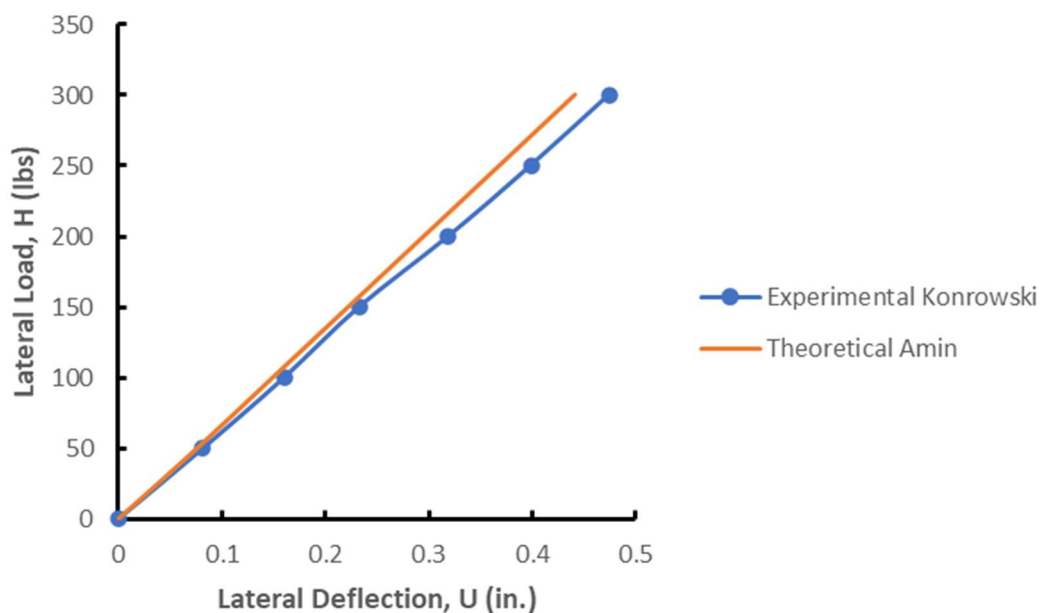


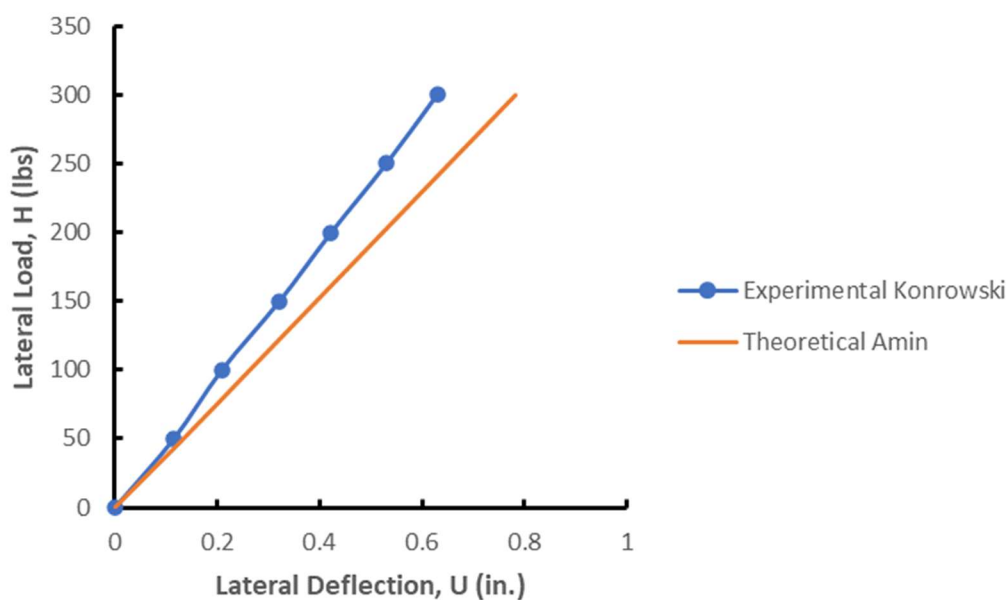
Figure 105. Load, H, vs. Horizontal Deflection, U for Case 1, L = 82 inches

Table 26. Experimental Results for Case 1, L = 100 inches [42]

| Lateral Load<br>H (lbs.) | Experimental Deflection<br>U (in.) |
|--------------------------|------------------------------------|
| 0                        | 0                                  |
| 50                       | 0.1153                             |
| 100                      | 0.209                              |
| 150                      | 0.3214                             |
| 200                      | 0.4224                             |
| 250                      | 0.5301                             |
| 300                      | 0.6291                             |

**Table 27 Results for FRP I-beam 4x4x0.25" Case 1, L = 100 inches**

| Lateral Load | Experimental Deflection |
|--------------|-------------------------|
| H (lbs.)     | U (in.)                 |
| 0            | 0                       |
| 50           | 0.133560967             |
| 100          | 0.263418231             |
| 150          | 0.393275495             |
| 200          | 0.523132758             |
| 250          | 0.652990022             |
| 300          | 0.782847286             |



**Figure 106. Load, H, versus Horizontal Deflection, U, for Case 1, L = 100 inches**

#### 4.6.4 Uniaxial Loaded Beam-Column

Al-Huazi [43] conducted an experimental investigation for the FRP beam-column channel section under uniaxial bending moment about the major and the minor axes for pinned-fixed boundary conditions among other FRP sections including initial geometric imperfection.

### I-Beam with Major Axis Loading [43]

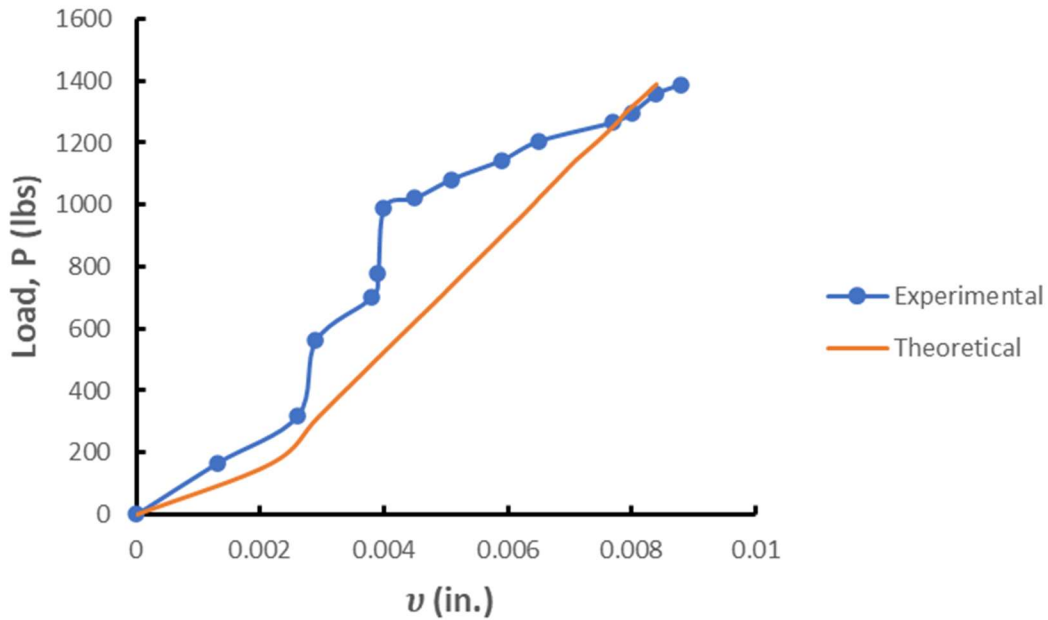
This investigation is for the I-Beam under uniaxial bending moment about the major axis for pinned-fixed boundary conditions. Table 28 summarizes the experimental results for this test. The first column represents the applied load,  $P$ , while the second through the third columns represent the midspan deflections; the deflection in the  $y$  axis,  $v$ ; the deflection in the  $x$  axis,  $u$ ; and the angle of rotation,  $\phi$ , respectively. Figures 107 through 109 represent the applied load,  $P$ , versus the midspan deflection,  $v$ ; the midspan deflection,  $u$ ; and the angle of twist,  $\phi$  respectively. The MATLAB output for this experiment can be found in Table 29.

**Table 28. Experimental Results for Major Axis Loading**

| Loads, $P$ (lbs) | $v$ (in.) | $u$ (in.) | $\Phi$ (Rad.) |
|------------------|-----------|-----------|---------------|
| 0                | 0         | 0         | 0             |
| 165.238          | 0.0013    | 0.0029    | 0.0005        |
| 317.928          | 0.0026    | 0.0044    | 0.0008        |
| 562.232          | 0.0029    | 0.006     | 0.0011        |
| 699.653          | 0.0038    | 0.0081    | 0.0014        |
| 775.998          | 0.0039    | 0.0107    | 0.0019        |
| 989.764          | 0.004     | 0.0119    | 0.0021        |
| 1020.302         | 0.0045    | 0.0133    | 0.0024        |
| 1081.378         | 0.0051    | 0.0159    | 0.0028        |
| 1142.454         | 0.0059    | 0.0174    | 0.0031        |
| 1203.53          | 0.0065    | 0.0193    | 0.0034        |
| 1264.606         | 0.0077    | 0.0204    | 0.0036        |
| 1295.144         | 0.008     | 0.0219    | 0.0039        |
| 1356.22          | 0.0084    | 0.023     | 0.0041        |
| 1386.758         | 0.0088    | 0.0237    | 0.0042        |

**Table 29. MATLAB Results for Major Axis Loading**

| Loads, P (lbs) | $v$ (in.) | $u$ (in.) | $\Phi$ (Rad.) |
|----------------|-----------|-----------|---------------|
| 0              | 0         | 0         | 0             |
| 165.238        | 0.00218   | 0.0014500 | 0.00120967    |
| 317.928        | 0.00295   | 0.0014585 | 0.00120966    |
| 562.232        | 0.00419   | 0.0014710 | 0.00120963    |
| 699.653        | 0.0049    | 0.0014780 | 0.00120961    |
| 775.998        | 0.00528   | 0.0014820 | 0.00120959    |
| 989.764        | 0.00636   | 0.0014938 | 0.00120953    |
| 1020.302       | 0.0065    | 0.0014954 | 0.00120953    |
| 1081.378       | 0.0068    | 0.0014990 | 0.00120951    |
| 1142.454       | 0.0071    | 0.0015020 | 0.00120949    |
| 1203.53        | 0.00745   | 0.0015050 | 0.00120947    |
| 1264.606       | 0.00777   | 0.0015080 | 0.00120944    |
| 1295.144       | 0.0079    | 0.0015100 | 0.00120943    |
| 1356.22        | 0.00824   | 0.0015134 | 0.00120941    |
| 1386.758       | 0.0084    | 0.0015150 | 0.00120940    |

**Figure 107. Load, P, versus Horizontal Deflection, v, for Major Axis Loading**

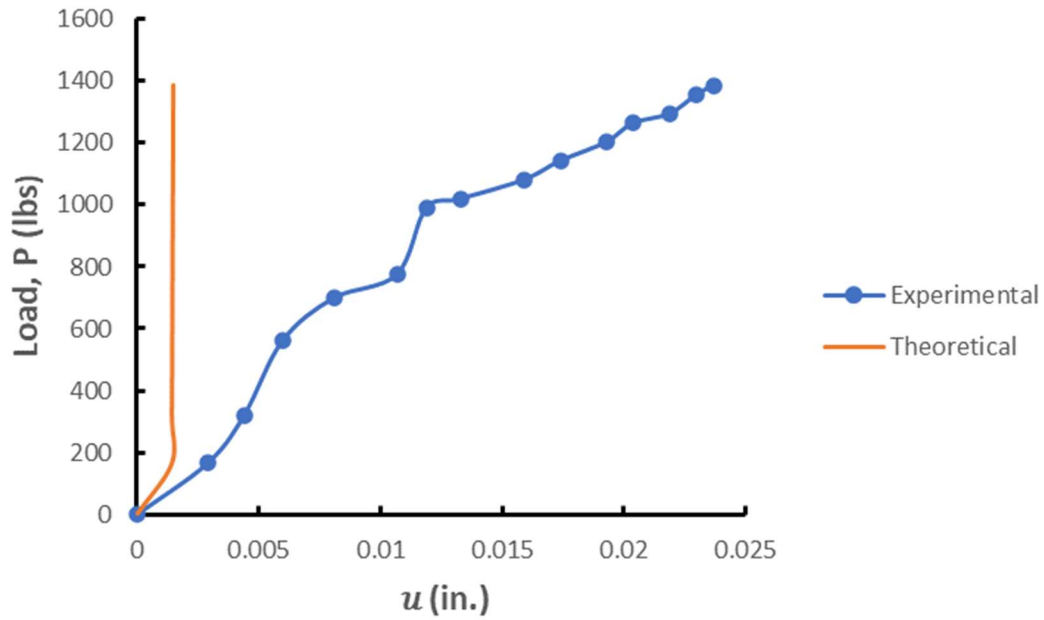


Figure 108. Load,  $P$ , versus Horizontal Deflection,  $u$ , for Major Axis Loading

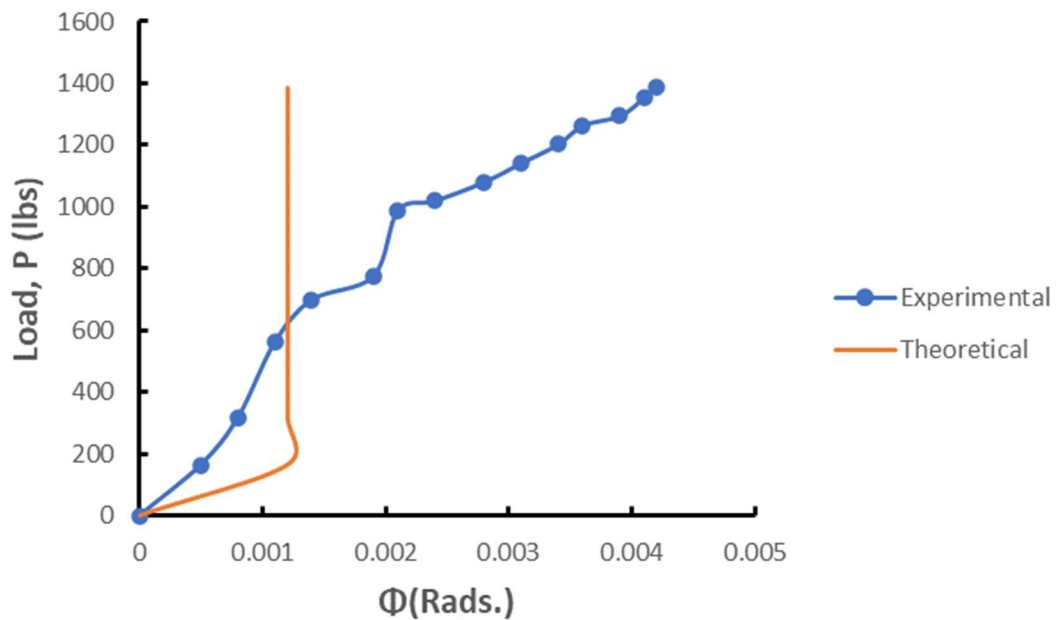


Figure 109. Load,  $P$ , versus Angle of Twist,  $\phi$  for Major Axis Loading

### I-Beam Minor Axis Loading [43]

This investigation is for the I-Beam under uniaxial bending moment about the minor axis for pinned-fixed boundary conditions. Table 30 summarizes the experimental results for this test. The first column represents the applied load,  $P$ , while the second through the third column represents the midspan deflections; the deflection in the  $y$  axis,  $v$ ; the deflection in the  $x$  axis,  $u$ ; and the angle of rotation,  $\phi$ , respectively. Figures 110 through 112 represent the applied load,  $P$ , versus the midspan deflection,  $v$ , the midspan deflection,  $u$ , and the angle of twist,  $\phi$  respectively. MATLAB output for this experiment is summarized in Table 31.

**Table 30. Experimental Results for Minor Axis Loading**

| Loads, $P$ (lbs) | $v$ (in.) | $u$ (in.) | $\Phi$ (Rad.) |
|------------------|-----------|-----------|---------------|
| 0                | 0         | 0         | 0             |
| 1111.916         | 0.0563    | 0.0148    | 0.0109        |
| 1447.837         | 0.0609    | 0.0176    | 0.0118        |
| 1686.53          | 0.0628    | 0.0185    | 0.0122        |
| 1814             | 0.0648    | 0.0207    | 0.0126        |
| 1944.664         | 0.0678    | 0.0259    | 0.0132        |

**Table 31. MATLAB Results for Minor Axis Loading**

| Loads, $P$ (lbs) | $v$ (in.) | $u$ (in.) | $\Phi$ (Rad.) |
|------------------|-----------|-----------|---------------|
| 0                | 0         | 0         | 0             |
| 1111.916         | 0.0028    | 0.051467  | 0.0024        |
| 1447.837         | 0.0028    | 0.067556  | 0.0024        |
| 1686.53          | 0.0028    | 0.079283  | 0.0024        |
| 1814             | 0.0028    | 0.0856    | 0.0024        |
| 1944.664         | 0.0028    | 0.09225   | 0.0024        |

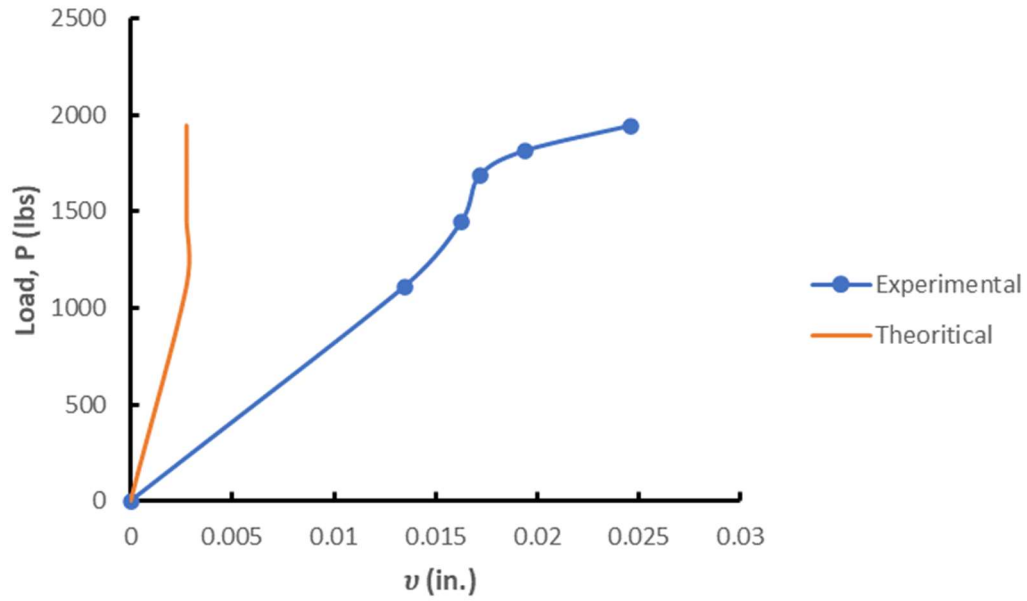


**Figure 110. Load,  $P$ , vs. Horizontal Deflection,  $v$ , for Minor Axis Loading**

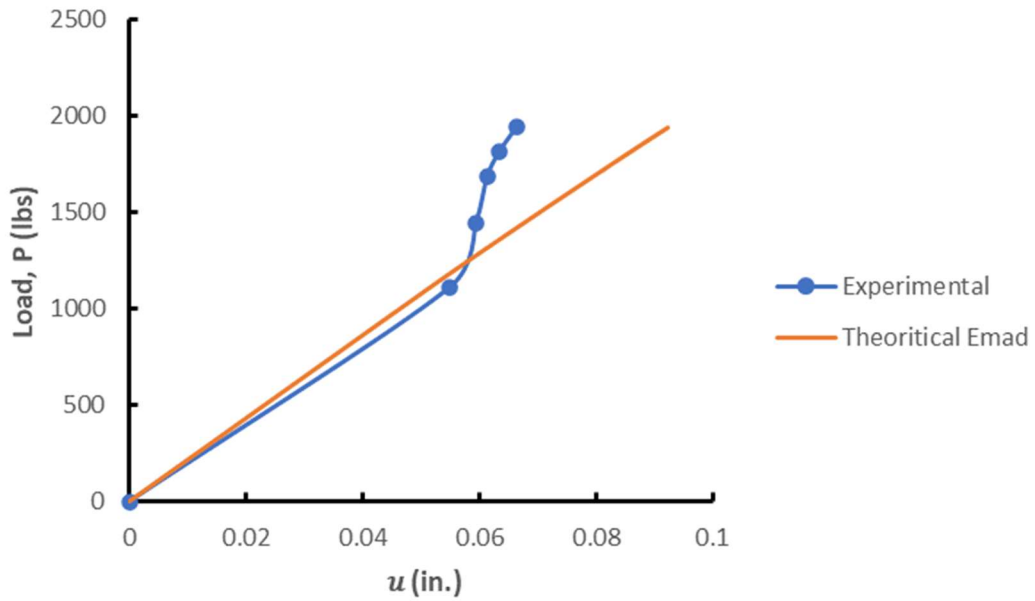


**Figure 111. Load,  $P$ , vs. Horizontal Deflection,  $u$ , for Minor Axis Loading**

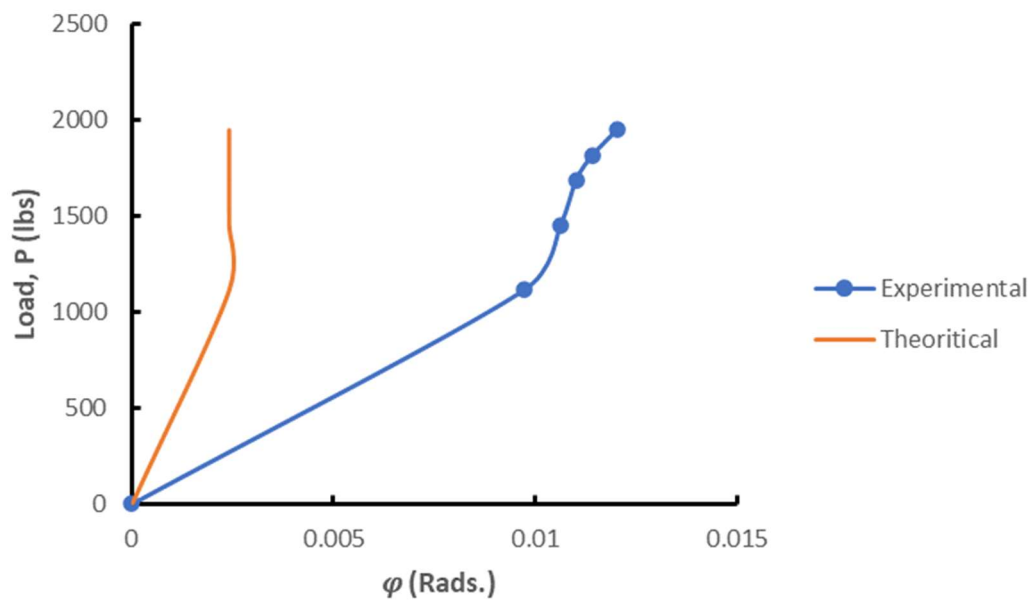


**Figure 112. Load, P, versus Angle of Twist,  $\phi$ , for Minor Axis Loading**



## CHAPTER 5

### THRUST-MOMENT-TORSION INTERACTION RELATIONS

Presented in this chapter is a new ultimate strength interaction relation for biaxially loaded beam-column with applied torsion. The ASCE 74-23 Standard for Load and Resistance Factor Design (LRFD) of Pultruded Fiber Reinforced Polymer (FRP) Structures, Reference 33, has an interaction expression without the shear effects and is for only round and hollow rectangular sections although the title of the section includes the doubly symmetric members subjected to torsion and combined torsion, flexure, and axial load. ASCE 74-23 uses the following dimensionless normal stress expression:

$$\frac{P_u}{P_c} + \frac{M_{ux}}{M_{cx}} + \frac{M_{uy}}{M_{cy}} + \left(\frac{T_u}{T_c}\right)^2 \leq 1.0 \quad (164)$$

Terms  $P_c$ ,  $M_c$ , and  $T_c$  in Equation 164 are defined in Reference 33 as the available axial compressive strength, available flexural strength about x and y axes, available design torsional strength, respectively.  $P_u$ ,  $M_u$ , and  $T_u$  are the applied axial load, bending moment about x and y axes, and torsional moment, respectively.

The design compression strength from Reference 33 is the minimum of the four buckling formulas 165 to 168 and a cracking/crushing term calculated from Equation 169.

$$F_{crx} = \frac{\pi^2 E_L}{\left(\frac{K_x L_x}{r_x}\right)^2} \text{ and } \phi_c = 0.7 \quad (165)$$

$$F_{cry} = \frac{\pi^2 E_L}{\left(\frac{K_y L_y}{r_y}\right)^2} \text{ and } \phi_c = 0.7 \quad (166)$$

$$F_{crf} = \frac{G_{LT}}{\left(\frac{b_f}{2t_f}\right)^2} \text{ and } \phi_c = 0.8 \quad (167)$$

$$F_{crw} = \frac{\pi^2 [\sqrt{E_{L,w}E_{T,w}} + \nu_{LT}E_{T,w} + 2G_{LT}]}{\left(\frac{h}{t_w}\right)^2} \text{ and } \phi_c = 0.8 \quad (168)$$

$$0.7\lambda F_L^c \quad (169)$$

where:

$F_{crx}$  = the elastic flexural buckling stress about the x-axis

$F_{cry}$  = the elastic flexural buckling stress about the y-axis

$F_{crf}$  = local flange buckling

$F_{crw}$  = local web buckling

$k_x$  = the effective length factor corresponding to the x-axis

$k_y$  = the effective length factor corresponding to the y-axis

L = laterally unbraced length of member

r = governing radius of gyration about the axis of buckling

$E_L$  = characteristic value of longitudinal compression elastic modulus of the flange or web, whichever is smaller

$E_{T,w}$  = characteristic value of the compression elastic modulus of the web in the direction perpendicular to the pultrusion direction

$\nu_{LT}$  = Poisson's ratio of the web plate element associated with transverse deformation when compression is applied in the longitudinal direction

$\lambda$  = time effect factor

$F_L^c$  = minimum longitudinal compression material strength of all elements comprising the cross section

The minimum member compression strength from equations 165 through 169 is then compared to the compression strength for the member serviceability from equation 170

$$P_s = \phi_0 \frac{\pi^2 E_L}{\left(\frac{kL_e}{r}\right)^2} \leq 0.3 F_L^c \quad (170)$$

Where:

$\frac{kL_e}{r}$  = the governing effective slenderness ratio

$\phi_0$  = reduction factor to account for the initial out-of-straightness of the member. This is defined as follows:

$$\phi_0 = 1 - 500 \frac{\delta_0}{L} \quad (171)$$

In the above equation the initial out-of-straightness,  $\frac{\delta_0}{L}$ , is limited to a maximum acceptable limit of  $\frac{1}{500}$ ; otherwise, the member is rejected.

To calculate the design flexural strength of a doubly symmetrical member when the longitudinal elastic moduli in the flanges and webs are within 15% of each other, Reference 33 suggests the use of the minimum of the following equations:

a. Nominal Strength of Members due to Material Rupture

$$M_n = \frac{F_L I}{y} \text{ and } \phi = 0.65 \quad (172)$$

where:

$F_L$  = characteristic longitudinal strength (in tension or compression) of the member

$I$  = moment of inertia of the member about the axis of bending

$y$  = distance from the neutral axis to the extreme fiber of the member

b. Nominal Strength of Members due to Local Instability

$$M_n = \frac{f_{cr} I}{y} \text{ and } \phi = 0.8 \quad (173)$$

where:

$f_{cr}$  = characteristic buckling stress taken as the minimum of compression flange local buckling and web local buckling. For doubly symmetric I-shaped bent about their strong axis, local buckling for the flange and the web can be calculated from Equations 174 and 177, respectively. For members bent about their weak axis,  $f_{cr}$  is calculated from Equation 178.

$$f_{cr} = \frac{4t_f^2}{b_f^2} \left[ \frac{7}{12} \sqrt{\frac{E_{L,f} E_{T,f}}{1+4.1\xi}} + G_{LT} \right] \quad (174)$$

where:

$$\xi = \frac{E_{T,f} t_f^3}{B_f k_r 6} \quad (175)$$

$$k_r = \frac{E_{T,w} t_w^3}{6h} \left( 1 - \left[ \left( \frac{48 t_f^2 h^2 E_{L,w}}{11.1 \pi^2 t_w^2 b_f^2 E_{L,f}} \right) \left( \frac{G_{LT}}{1.25 \sqrt{E_{L,w} E_{T,w}} + E_{T,w} v_{LT} + 2 G_{LT}} \right) \right] \right) \quad (176)$$

$$f_{cr} = \frac{11.1 \pi^2 t_w^2}{12 h^2} \left( 1.25 \sqrt{E_{L,w} E_{T,w}} + E_{T,w} v_{LT} + 2 G_{LT} \right) \quad (177)$$

$$f_{cr} = \frac{4 t_f^2}{b_f^2} G_{LT} \quad (178)$$

c. Nominal Strength of Members due to Lateral-Torsional Buckling

Members are bent about their strong axis:

$$M_n = C_b \sqrt{\frac{\pi^2 E_{L,f} I_y D_J}{L_b^2} + \frac{\pi^4 E_{L,f}^2 I_y C_w}{L_b^4}}, \text{ and } \phi = 0.7 \quad (179)$$

where:

$$D_J = \text{Torsional rigidity for open section} = G_{LT} \sum \frac{1}{3} b_i t_i^3$$

$$C_w = \text{warping constant} = \frac{t_f h^2 b_f^3}{24}$$

$C_b$  = Moment modification factor for unsupported span with both ends braced. It is permitted to conservatively assume a value of unity.

The shear design strength of a member shall be taken as the smaller strength obtained from the limit states of material rupture in shear and local web buckling from Equations 180 and 181, respectively.

$$V_n = F_{LT} A_s \text{ and } \phi = 0.65 \quad (180)$$

$$V_n = f_{cr} A_s \text{ and } \phi = 0.8 \quad (181)$$

where:

$F_{LT}$ =characteristic in-plane shear strength

$A_s$ = shear area

$f_{cr}$  = critical shear buckling stress depending on  $2G_{LT} + E_{T,w}v_{LT}$  and  $\sqrt{E_{L,w}E_{T,w}}$ .

$$\text{Case 1: } 2G_{LT} + E_{T,w}v_{LT} \leq \sqrt{E_{L,w}E_{T,w}}$$

$$f_{cr} = \frac{t_w^2 k_{LT1}^4 \sqrt{E_{L,w}(E_{T,w})^3}}{3h^2} \quad (182)$$

where:

$$k_{LT1} = 8.1 + \frac{5(2G_{LT} + E_{T,w}v_{LT})}{\sqrt{E_{L,w}E_{T,w}}} \quad (183)$$

$$\text{Case 2: } 2G_{LT} + E_{T,w}v_{LT} \geq \sqrt{E_{L,w}E_{T,w}}$$

$$f_{cr} = \frac{k_{LT2} E_{T,w} t_w^2}{3h^2} \sqrt{v_{LT} + \frac{2G_{LT}}{E_{T,w}}} \quad (184)$$

where:

$$k_{LT2} = 11.7 + 1.4 \left( \frac{\sqrt{E_{L,w}E_{T,w}}}{2G_{LT} + E_{T,w}v_{LT}} \right)^2 \quad (185)$$

Finally, the torsional strength for a wide flange beam can be taken as the minimum of the limit states of torsional rupture and torsional buckling from Equations 186 and 187.

$$T_n = F_n \hat{J} \quad (186)$$

$$T_n = F_{cr} C \quad (187)$$

where:

$$F_n = \gamma G_{LT} \quad (188)$$

$\gamma$  = nominal coupon specimen shear strain per unit length as defined in ASTM D5379-05. Reference 33 gives minimal details for calculating or estimating this limit. The commentary of Reference 33 suggests that the products of shear strain times the gage length of a specimen subjected to torque divided by the wall thickness in a wide flange beam may be taken as 4.0.

$$\hat{J} = \text{St. Venant torsion constant} = \frac{2b_f t_f^3 + d_w t_w^3}{3}$$

$$C = \text{torsional constant} = \frac{\hat{J}}{t_f}$$

For wide flange beams

$$F_{cr} = \frac{G_{LT}}{3I_0} (2b_f t_f^3 + d_w t_w^3) + \frac{E_L^c}{24I_0} \left(\frac{\pi}{l_b}\right)^2 (t_f b_f^3 d_w^2) \quad (189)$$

where:

$I_0$  = sum of moments of inertia about the strong axis of bending and the weak axis of bending

$l_b$  = lengths between points that are braced against twist

It is worth emphasizing that all of the experimental attempts to fail the tested member in torsion were unsuccessful. A large angle of rotations of the member was observed.

The following notes were concluded from the MATLAB code which was prepared for this dissertation:

1. Lateral-Torsional Buckling is the controlling failure mode in bending about the strong axis for long members. For noticeably short members (around 1 foot long), Local-Buckling failure mode governs in bending about the strong axis.
2. Flexural capacity of members about the weak axis is governed by the Local-Buckling failure mode limit which is significantly greater than that for strong axis in long members (longer than 10 ft).
3. Biaxially loaded long members tend to develop an angle of twist greater than 6 degrees when subjected to torques less than the calculated capacity from Equations 186 and 187. This contradicts the small deformations assumption used in deriving stability Equations 102 through 104.

Keeping the linear dimensionless normal stress of expressions 164, a new dimensionless shear and torsion expressions will be introduced in the following more comprehensive interaction expression. The expression proposed herein is relating dimensionless axial load, bending moments about the x and y axes, shear force, and torsional moment. The graphical relationship between the critical axial load and critical moment about the x axis,  $M_{cx}$ , vs. the slenderness ratio,  $\frac{L_b}{r_y}$ , is presented in the following figures and based on the experimental findings in section 3.1.2. Values from these figures will be used hereafter in determining the axial capacity and the flexural capacity of the member about the x axis.



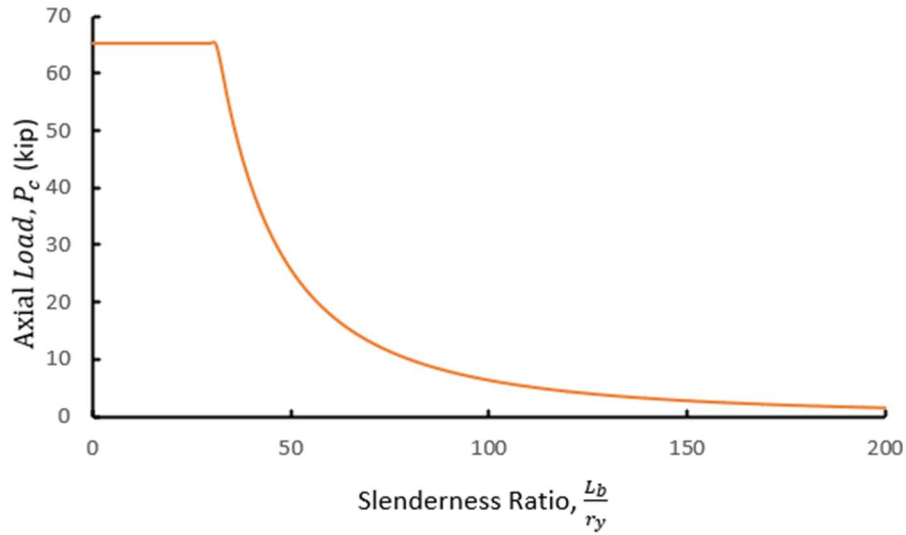


**Figure 113. Axial Load,  $P_c$ , vs. Slenderness Ratio,  $\frac{L_b}{r_y}$**

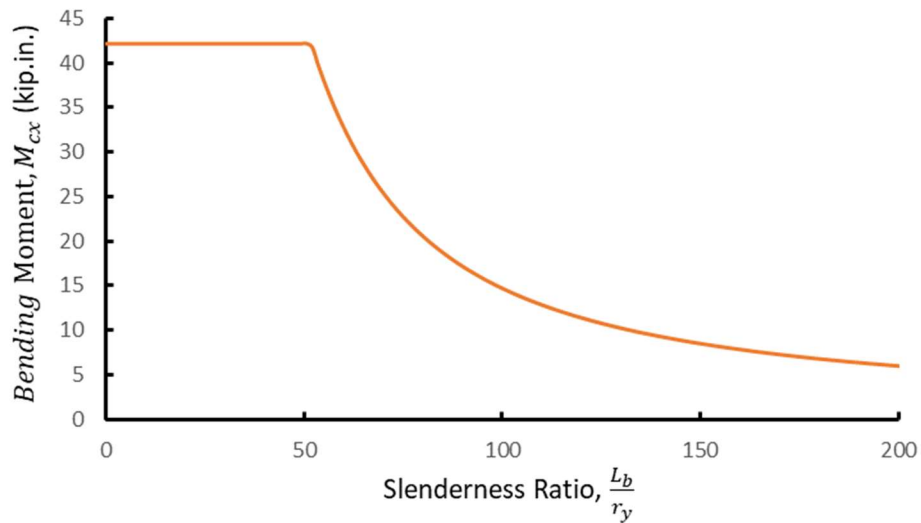


**Figure 114. Bending Moment about x Axis,  $M_{cx}$ , vs. Slenderness Ratio,  $\frac{L_b}{r_y}$**

From Section 3.1.2, the available flexural strength about the y axis can be estimated as  $M_{cy} = 27.3 \text{ kip.in.}$

To account for the presence of the shear stress, a new shear strength term,  $V_c$ , is introduced in the proposed interaction expression based on the material rupture limit state  $V_c = 13 \text{ kip}$ .

Lastly, the available torsional strength of the member,  $T_c$ , is calculated from Equation 187, Reference [33] when the stiffness of the member governs. The proposed interaction expression is presented as follows:

$$\left(\frac{P_u}{P_c} + \frac{M_{ux}}{M_{cx}} + \frac{M_{uy}}{M_{cy}}\right) + \left(\frac{V_u}{V_c} + \frac{T_u}{T_c}\right)^\alpha \leq 1.0 \quad (191)$$

where:

$V_u$  is the flexural shear and constants  $\alpha$  will be evaluated using the curve fitting technique for the following load combinations.

### 5.1 Interaction Relation for Biaxially Loaded Beam-Column with Torsion

Interaction relation for this case is presented below for different member lengths using the following expression:

$$\left(\frac{P_u}{P_c} + \frac{M_{ux}}{M_{cx}} + \frac{M_{uy}}{M_{cy}}\right) + \left(\frac{T_u}{T_c}\right)^\alpha \leq 1.0 \quad (192)$$

Table 32 represents the data for a 1 ft long biaxially loaded beam column with a torsion at the midspan. The member was subjected to equal applied bending moment at the top and bottom end about both the x and y axes. The first column in Table 32 shows the normalized torsional ratio,  $\bar{T}$ , of 10%. The second column is the normalized axial load,  $\bar{P}$ , which varies from 0 to 80%. The third and the fourth columns are the second order bending moment about the x and the y axes,  $\bar{M}_x$  and  $\bar{M}_y$ , respectively, and the fifth column represents the angle of twist,  $\phi$ , in degrees. The rest of the

columns, hereafter, represent a repetition of the previous columns calculated based on Reference

33. Using the curve fitting technique, the term  $\alpha$  in Equation 192 was found to be 1.9.

**Table 32. Normalized Applied Loads for L=1 ft. and  $\bar{T} = 0.1$**

| $\bar{T}$ | $\bar{P}$ | $\bar{M}_x$ | $\bar{M}_y$ | $\phi, rad.$ | $\phi, deg.$ | $\bar{T}$ | $\bar{P}$ | $\bar{M}_x$ | $\bar{M}_y$ | $IR_{ASCE}$ |
|-----------|-----------|-------------|-------------|--------------|--------------|-----------|-----------|-------------|-------------|-------------|
| 0.1       | 0         | 0.889854    | 0.010147    | 0.001871     | 0.107228     | 0.1       | 0         | 0.9         | 0           | 0.91        |
|           |           | 0.403329    | 0.496704    | 0.002216     | 0.126988     |           |           | 0.403137    | 0.491244    | 0.904381    |
|           |           | 0.221889    | 0.678162    | 0.002125     | 0.121771     |           |           | 0.221654    | 0.675242    | 0.906895    |
|           |           | 0.170735    | 0.729275    | 0.002078     | 0.119063     |           |           | 0.170487    | 0.727116    | 0.907603    |
|           |           | 0.00027     | 0.899726    | 0.001852     | 0.10613      |           |           | 0           | 0.9         | 0.91        |
| $\bar{T}$ | $\bar{P}$ | $\bar{M}_x$ | $\bar{M}_y$ | $\phi, rad.$ | $\phi, deg.$ | $\bar{T}$ | $\bar{P}$ | $\bar{M}_x$ | $\bar{M}_y$ | $IR_{ASCE}$ |
| 0.1       | 0.2       | 0.692049    | 0.007951    | 0.001886     | 0.108044     | 0.1       | 0.2       | 0.7         | 0           | 0.91        |
|           |           | 0.313796    | 0.386205    | 0.002087     | 0.119557     |           |           | 0.313665    | 0.382218    | 0.905883    |
|           |           | 0.1726      | 0.527401    | 0.002026     | 0.116062     |           |           | 0.172425    | 0.525273    | 0.907698    |
|           |           | 0.1328      | 0.567207    | 0.001995     | 0.114312     |           |           | 0.132615    | 0.565595    | 0.90821     |
|           |           | 0.000213    | 0.69979     | 0.001852     | 0.10613      |           |           | 0           | 0.9         | 0.91        |
| $\bar{T}$ | $\bar{P}$ | $\bar{M}_x$ | $\bar{M}_y$ | $\phi, rad.$ | $\phi, deg.$ | $\bar{T}$ | $\bar{P}$ | $\bar{M}_x$ | $\bar{M}_y$ | $IR_{ASCE}$ |
| 0.1       | 0.4       | 0.494309    | 0.005691    | 0.00189      | 0.108275     | 0.1       | 0.4       | 0.5         | 0           | 0.91        |
|           |           | 0.224204    | 0.275804    | 0.001983     | 0.113624     |           |           | 0.224115    | 0.273096    | 0.907211    |
|           |           | 0.12332     | 0.376776    | 0.001947     | 0.111553     |           |           | 0.1232      | 0.375314    | 0.908514    |
|           |           | 0.094861    | 0.405144    | 0.00193      | 0.110567     |           |           | 0.094733    | 0.40403     | 0.908763    |
|           |           | 0.000152    | 0.4999      | 0.00185      | 0.106023     |           |           | 0           | 0.5         | 0.91        |
| $\bar{T}$ | $\bar{P}$ | $\bar{M}_x$ | $\bar{M}_y$ | $\phi, rad.$ | $\phi, deg.$ | $\bar{T}$ | $\bar{P}$ | $\bar{M}_x$ | $\bar{M}_y$ | $IR_{ASCE}$ |
| 0.1       | 0.6       | 0.2966      | 0.003403    | 0.001883     | 0.107897     | 0.1       | 0.6       | 0.3         | 0           | 0.91        |
|           |           | 0.13455     | 0.165457    | 0.001898     | 0.108754     |           |           | 0.134499    | 0.163894    | 0.908393    |
|           |           | 0.07399     | 0.22604     | 0.001891     | 0.108327     |           |           | 0.07392     | 0.225189    | 0.909109    |
|           |           | 0.056925    | 0.243114    | 0.001883     | 0.107905     |           |           | 0.05685     | 0.242462    | 0.909312    |
|           |           | 9.11E-05    | 0.29991     | 0.001851     | 0.10603      |           |           | 0           | 0.3         | 0.91        |
| $\bar{T}$ | $\bar{P}$ | $\bar{M}_x$ | $\bar{M}_y$ | $\phi, rad.$ | $\phi, deg.$ | $\bar{T}$ | $\bar{P}$ | $\bar{M}_x$ | $\bar{M}_y$ | $IR_{ASCE}$ |
| 0.1       | 0.8       | 0.09888     | 0.001124    | 0.001865     | 0.10688      | 0.1       | 0.8       | 0.1         | 0           | 0.91        |
|           |           | 0.044857    | 0.055149    | 0.001863     | 0.106719     |           |           | 0.04484     | 0.05464     | 0.90948     |
|           |           | 0.024662    | 0.075339    | 0.001859     | 0.106487     |           |           | 0.024639    | 0.07506     | 0.909699    |
|           |           | 0.018975    | 0.081035    | 0.001857     | 0.106405     |           |           | 0.01895     | 0.080821    | 0.909771    |
|           |           | 3.04E-05    | 0.09999     | 0.001851     | 0.106079     |           |           | 0           | 0.1         | 0.91        |

The following tables and figures repeat what was described above but for different lengths as indicated below.

Table 33. Normalized Applied Loads for L=5 ft. and  $\bar{T} = 0.1$ 

| $\bar{T}$ | $\bar{P}$ | $\bar{M}_x$ | $\bar{M}_y$ | $\phi, rad.$ | $\phi, deg.$ | $\bar{T}$ | $\bar{P}$ | $\bar{M}_x$ | $\bar{M}_y$ | $IR_{ASCE}$ |
|-----------|-----------|-------------|-------------|--------------|--------------|-----------|-----------|-------------|-------------|-------------|
| 0.1       | 0         | 0.818       | 0.08237     | 0.04374      | 2.506        | 0.1       | 0         | 0.9         | 0           | 0.91        |
|           |           | 0.557       | 0.34306     | 0.07127      | 4.083        |           |           | 0.549       | 0.2529      | 0.81209     |
|           |           | 0.396       | 0.50366     | 0.07152      | 4.098        |           |           | 0.383       | 0.4406      | 0.83329     |
|           |           | 0.335       | 0.5653      | 0.06852      | 3.926        |           |           | 0.319       | 0.5149      | 0.84429     |
|           |           | 0.01        | 0.8899      | 0.02616      | 1.499        |           |           | 0           | 0.9         | 0.91        |
| $\bar{T}$ | $\bar{P}$ | $\bar{M}_x$ | $\bar{M}_y$ | $\phi, rad.$ | $\phi, deg.$ | $\bar{T}$ | $\bar{P}$ | $\bar{M}_x$ | $\bar{M}_y$ | $IR_{ASCE}$ |
| 0.1       | 0.2       | 0.637       | 0.06271     | 0.04272      | 2.448        | 0.1       | 0.2       | 0.7         | 0           | 0.91        |
|           |           | 0.439       | 0.26101     | 0.06133      | 3.514        |           |           | 0.434       | 0.1998      | 0.84342     |
|           |           | 0.311       | 0.38942     | 0.06107      | 3.499        |           |           | 0.301       | 0.347       | 0.85841     |
|           |           | 0.261       | 0.43864     | 0.05854      | 3.354        |           |           | 0.251       | 0.4048      | 0.86588     |
|           |           | 0.008       | 0.69244     | 0.02514      | 1.44         |           |           | 0           | 0.7         | 0.91        |
| $\bar{T}$ | $\bar{P}$ | $\bar{M}_x$ | $\bar{M}_y$ | $\phi, rad.$ | $\phi, deg.$ | $\bar{T}$ | $\bar{P}$ | $\bar{M}_x$ | $\bar{M}_y$ | $IR_{ASCE}$ |
| 0.1       | 0.4       | 0.457       | 0.04295     | 0.0408       | 2.338        | 0.1       | 0.4       | 0.5         | 0           | 0.91        |
|           |           | 0.318       | 0.18205     | 0.05117      | 2.932        |           |           | 0.315       | 0.145       | 0.86969     |
|           |           | 0.224       | 0.2764      | 0.05023      | 2.878        |           |           | 0.218       | 0.2512      | 0.87929     |
|           |           | 0.187       | 0.31253     | 0.04821      | 2.762        |           |           | 0.181       | 0.2924      | 0.88376     |
|           |           | 0.005       | 0.4948      | 0.02455      | 1.406        |           |           | 0           | 0.5         | 0.91        |
| $\bar{T}$ | $\bar{P}$ | $\bar{M}_x$ | $\bar{M}_y$ | $\phi, rad.$ | $\phi, deg.$ | $\bar{T}$ | $\bar{P}$ | $\bar{M}_x$ | $\bar{M}_y$ | $IR_{ASCE}$ |
| 0.1       | 0.6       | 0.276       | 0.0238      | 0.03742      | 2.144        | 0.1       | 0.6       | 0.3         | 0           | 0.91        |
|           |           | 0.194       | 0.10646     | 0.04077      | 2.336        |           |           | 0.192       | 0.0884      | 0.89042     |
|           |           | 0.135       | 0.16475     | 0.03928      | 2.251        |           |           | 0.133       | 0.1527      | 0.8954      |
|           |           | 0.113       | 0.18703     | 0.03788      | 2.17         |           |           | 0.11        | 0.1774      | 0.89748     |
|           |           | 0.003       | 0.2969      | 0.02443      | 1.4          |           |           | 0           | 0.3         | 0.91        |
| $\bar{T}$ | $\bar{P}$ | $\bar{M}_x$ | $\bar{M}_y$ | $\phi, rad.$ | $\phi, deg.$ | $\bar{T}$ | $\bar{P}$ | $\bar{M}_x$ | $\bar{M}_y$ | $IR_{ASCE}$ |
| 0.1       | 0.8       | 0.093       | 0.00667     | 0.03103      | 1.778        | 0.1       | 0.8       | 0.1         | 0           | 0.91        |
|           |           | 0.065       | 0.03453     | 0.03032      | 1.737        |           |           | 0.065       | 0.03        | 0.90507     |
|           |           | 0.045       | 0.0546      | 0.0292       | 1.673        |           |           | 0.045       | 0.0516      | 0.90639     |
|           |           | 0.038       | 0.06221     | 0.02863      | 1.641        |           |           | 0.037       | 0.0598      | 0.90683     |
|           |           | 0.001       | 0.099       | 0.02487      | 1.425        |           |           | 0           | 0.1         | 0.91        |

Table 34. Normalized Applied Loads for L=9 ft. and  $\bar{T} = 0.1$ 

| $\bar{T}$ | $\bar{P}$ | $\bar{M}_x$ | $\bar{M}_y$ | $\phi, rad.$ | $\phi, deg.$ | $\bar{T}$ | $\bar{P}$ | $\bar{M}_x$ | $\bar{M}_y$ | $IR_{ASCE}$ |
|-----------|-----------|-------------|-------------|--------------|--------------|-----------|-----------|-------------|-------------|-------------|
| 0.1       | 0.2       | 0.838295    | 0.0617058   | 0.0719374    | 4.1217086    | 0.1       | 0         | 0.9         | 0           | 0.91        |
|           |           | 0.6810652   | 0.2189354   | 0.1218154    | 6.9795065    |           |           | 0.664867    | 0.1360627   | 0.8109297   |
|           |           | 0.5585806   | 0.3414198   | 0.1388076    | 7.9530919    |           |           | 0.522329    | 0.2672321   | 0.7995611   |
|           |           | 0.5047344   | 0.3952744   | 0.1407689    | 8.0654624    |           |           | 0.45946     | 0.3290941   | 0.7985541   |
|           |           | 0.0399523   | 0.86005     | 0.0475327    | 2.7234222    |           |           | 0           | 0.9         | 0.91        |
| $\bar{T}$ | $\bar{P}$ | $\bar{M}_x$ | $\bar{M}_y$ | $\phi, rad.$ | $\phi, deg.$ | $\bar{T}$ | $\bar{P}$ | $\bar{M}_x$ | $\bar{M}_y$ | $IR_{ASCE}$ |
| 0.1       | 0.2       | 0.6548685   | 0.0451316   | 0.0673523    | 3.8590006    | 0.1       | 0.2       | 0.7         | 0           | 0.91        |
|           |           | 0.5373833   | 0.1626169   | 0.1017567    | 5.830227     |           |           | 0.526665    | 0.1077802   | 0.8444452   |
|           |           | 0.4388549   | 0.2611452   | 0.1149839    | 6.5880923    |           |           | 0.414996    | 0.2123187   | 0.8373147   |
|           |           | 0.3949252   | 0.305075    | 0.1165307    | 6.6767174    |           |           | 0.3651402   | 0.2615364   | 0.8366766   |
|           |           | 0.02798     | 0.67202     | 0.042603     | 2.4409712    |           |           | 0           | 0.7         | 0.91        |
| $\bar{T}$ | $\bar{P}$ | $\bar{M}_x$ | $\bar{M}_y$ | $\phi, rad.$ | $\phi, deg.$ | $\bar{T}$ | $\bar{P}$ | $\bar{M}_x$ | $\bar{M}_y$ | $IR_{ASCE}$ |
| 0.1       | 0.4       | 0.4698661   | 0.030134    | 0.062677     | 3.5911255    | 0.1       | 0.4       | 0.5         | 0           | 0.91        |
|           |           | 0.3892013   | 0.1107991   | 0.0828283    | 4.7457142    |           |           | 0.382859    | 0.0783508   | 0.8712098   |
|           |           | 0.3167481   | 0.183252    | 0.0911838    | 5.2244566    |           |           | 0.3029366   | 0.1549873   | 0.8679239   |
|           |           | 0.283869    | 0.2161312   | 0.0920187    | 5.2722809    |           |           | 0.2666906   | 0.1910206   | 0.8677112   |
|           |           | 0.0186371   | 0.481363    | 0.0396169    | 2.26988      |           |           | 0           | 0.5         | 0.91        |
| $\bar{T}$ | $\bar{P}$ | $\bar{M}_x$ | $\bar{M}_y$ | $\phi, rad.$ | $\phi, deg.$ | $\bar{T}$ | $\bar{P}$ | $\bar{M}_x$ | $\bar{M}_y$ | $IR_{ASCE}$ |
| 0.1       | 0.6       | 0.283503    | 0.0164972   | 0.0568693    | 3.2583698    | 0.1       | 0.6       | 0.3         | 0           | 0.91        |
|           |           | 0.2366696   | 0.0633308   | 0.064911     | 3.7191286    |           |           | 0.2336365   | 0.0478129   | 0.8914494   |
|           |           | 0.192046    | 0.1079541   | 0.068057     | 3.899376     |           |           | 0.185726    | 0.0950205   | 0.8907465   |
|           |           | 0.1714133   | 0.1285868   | 0.1636201    | 0.117195     |           |           | 0.1636201   | 0.117195    | 0.8908151   |
|           |           | 0.0108726   | 0.289128    | 0.0384784    | 2.2046499    |           |           | 0           | 0.3         | 0.91        |
| $\bar{T}$ | $\bar{P}$ | $\bar{M}_x$ | $\bar{M}_y$ | $\phi, rad.$ | $\phi, deg.$ | $\bar{T}$ | $\bar{P}$ | $\bar{M}_x$ | $\bar{M}_y$ | $IR_{ASCE}$ |
| 0.1       | 0.8       | 0.095333    | 0.0046672   | 0.0478452    | 2.7413275    | 0.1       | 0.8       | 0.1         | 0           | 0.91        |
|           |           | 0.0799059   | 0.0200947   | 0.0481351    | 2.75794      |           |           | 0.079144    | 0.0161965   | 0.9053405   |
|           |           | 0.0646252   | 0.0353748   | 0.0477199    | 2.7341514    |           |           | 0.0631192   | 0.0322928   | 0.905412    |
|           |           | 0.0574673   | 0.0425343   | 0.0472866    | 2.7093246    |           |           | 0.055626    | 0.0398428   | 0.9054688   |
|           |           | 0.0036951   | 0.09631     | 0.09631      | 0.0392577    |           |           | 0           | 0.1         | 0.91        |

Table 35. Normalized Applied Loads for L= 13ft. and  $\bar{T} = 0.1$ 

| $\bar{T}$ | $\bar{P}$ | $\bar{M}_x$ | $\bar{M}_y$ | $\phi, rad.$ | $\phi, deg.$ | $\bar{T}$ | $\bar{P}$ | $\bar{M}_x$ | $\bar{M}_y$ | $IR_{ASCE}$ |
|-----------|-----------|-------------|-------------|--------------|--------------|-----------|-----------|-------------|-------------|-------------|
| 0.1       | 0         | 0.8516      | 0.0484      | 0.08605792   | 4.930756     | 0.1       | 0         | 0.9         | 0           | 0.91        |
|           |           | 0.735       | 0.165       | 0.15012295   | 8.601412     |           |           | 0.71        | 0.09        | 0.8178      |
|           |           | 0.63738     | 0.2626      | 0.1801084    | 10.31945     |           |           | 0.58        | 0.19        | 0.7878      |
|           |           | 0.59288     | 0.3071      | 0.18714363   | 10.72254     |           |           | 0.52        | 0.24        | 0.7765      |
|           |           | 0.08612     | 0.8139      | 0.06987948   | 4.003799     |           |           | 0           | 0.9         | 0.91        |
| $\bar{T}$ | $\bar{P}$ | $\bar{M}_x$ | $\bar{M}_y$ | $\phi, rad.$ | $\phi, deg.$ | $\bar{T}$ | $\bar{P}$ | $\bar{M}_x$ | $\bar{M}_y$ | $IR_{ASCE}$ |
| 0.1       | 0.2       | 0.66521     | 0.0348      | 0.07919047   | 4.53728      | 0.1       | 0.2       | 0.7         | 0           | 0.91        |
|           |           | 0.57939     | 0.1206      | 0.12297182   | 7.045766     |           |           | 0.57        | 0.07        | 0.8502      |
|           |           | 0.50075     | 0.1993      | 0.14672878   | 8.40694      |           |           | 0.47        | 0.15        | 0.8306      |
|           |           | 0.46396     | 0.236       | 0.15265983   | 8.746764     |           |           | 0.42        | 0.24        | 0.8229      |
|           |           | 0.05497     | 0.645       | 0.05627807   | 3.224496     |           |           | 0           | 0.7         | 0.91        |
| $\bar{T}$ | $\bar{P}$ | $\bar{M}_x$ | $\bar{M}_y$ | $\phi, rad.$ | $\phi, deg.$ | $\bar{T}$ | $\bar{P}$ | $\bar{M}_x$ | $\bar{M}_y$ | $IR_{ASCE}$ |
| 0.1       | 0.4       | 0.47702     | 0.023       | 0.07293952   | 4.179127     | 0.1       | 0.4       | 0.5         | 0           | 0.91        |
|           |           | 0.41899     | 0.081       | 0.09853909   | 5.645874     |           |           | 0.41        | 0.05        | 0.8752      |
|           |           | 0.36135     | 0.1386      | 0.11413605   | 6.539514     |           |           | 0.34        | 0.11        | 0.8647      |
|           |           | 0.33354     | 0.1665      | 0.11820831   | 6.772837     |           |           | 0.31        | 0.14        | 0.8605      |
|           |           | 0.0342      | 0.4658      | 0.04849252   | 2.778417     |           |           | 0           | 0.5         | 0.91        |
| $\bar{T}$ | $\bar{P}$ | $\bar{M}_x$ | $\bar{M}_y$ | $\phi, rad.$ | $\phi, deg.$ | $\bar{T}$ | $\bar{P}$ | $\bar{M}_x$ | $\bar{M}_y$ | $IR_{ASCE}$ |
| 0.1       | 0.6       | 0.28749     | 0.0125      | 0.06589576   | 3.775549     | 0.1       | 0.6       | 0.3         | 0           | 0.91        |
|           |           | 0.25428     | 0.0457      | 0.07641962   | 4.378522     |           |           | 0.25        | 0.03        | 0.8935      |
|           |           | 0.21901     | 0.081       | 0.08321799   | 4.76804      |           |           | 0.21        | 0.07        | 0.8897      |
|           |           | 0.20144     | 0.0986      | 0.08493425   | 4.866374     |           |           | 0.19        | 0.09        | 0.888       |
|           |           | 0.01921     | 0.2808      | 0.04517418   | 2.58829      |           |           | 0           | 0.3         | 0.91        |
| $\bar{T}$ | $\bar{P}$ | $\bar{M}_x$ | $\bar{M}_y$ | $\phi, rad.$ | $\phi, deg.$ | $\bar{T}$ | $\bar{P}$ | $\bar{M}_x$ | $\bar{M}_y$ | $IR_{ASCE}$ |
| 0.1       | 0.8       | 0.09645     | 0.0035      | 0.05569918   | 3.191328     | 0.1       | 0.8       | 0.1         | 0           | 0.91        |
|           |           | 0.08565     | 0.0143      | 0.05650873   | 3.237712     |           |           | 0.08        | 0.01        | 0.9059      |
|           |           | 0.07366     | 0.0263      | 0.05675215   | 3.251659     |           |           | 0.07        | 0.02        | 0.9053      |
|           |           | 0.06754     | 0.0325      | 0.05661183   | 3.243619     |           |           | 0.06        | 0.03        | 0.905       |
|           |           | 0.00648     | 0.0935      | 0.04578292   | 2.623168     |           |           | 0           | 0.1         | 0.91        |

Table 36. Normalized Applied Loads L=17 ft. and  $\bar{T} = 0.1$ 

| $\bar{T}$ | $\bar{P}$ | $\bar{M}_x$ | $\bar{M}_y$ | $\phi, rad.$ | $\phi, deg.$ | $\bar{T}$ | $\bar{P}$ | $\bar{M}_x$ | $\bar{M}_y$ | $IR_{ASCE}$ |
|-----------|-----------|-------------|-------------|--------------|--------------|-----------|-----------|-------------|-------------|-------------|
| 0.1       | 0         | 0.86035     | 0.03965324  | 0.09401      | 5.3862       | 0.1       | 0         | 0.9         | 0           | 0.91        |
|           |           | 0.76623     | 0.13377153  | 0.16806      | 9.6289       |           |           | 0.7413      | 0.073       | 0.824       |
|           |           | 0.68479     | 0.21521262  | 0.20752      | 11.89        |           |           | 0.6204      | 0.152       | 0.7825      |
|           |           | 0.64722     | 0.25278279  | 0.2184       | 12.514       |           |           | 0.5614      | 0.193       | 0.76406     |
|           |           | 0.15331     | 0.746693    | 0.74669      | 5.7676       |           |           | 0           | 0.9         | 0.91        |
| $\bar{T}$ | $\bar{P}$ | $\bar{M}_x$ | $\bar{M}_y$ | $\phi, rad.$ | $\phi, deg.$ | $\bar{T}$ | $\bar{P}$ | $\bar{M}_x$ | $\bar{M}_y$ | $IR_{ASCE}$ |
| 0.1       | 0.2       | 0.67178     | 0.02821968  | 0.08568      | 4.9091       | 0.1       | 0.2       | 0.7         | 0           | 0.91        |
|           |           | 0.60332     | 0.0966844   | 0.13573      | 7.777        |           |           | 0.5874      | 0.058       | 0.85497     |
|           |           | 0.53769     | 0.16231356  | 0.16718      | 9.5785       |           |           | 0.4962      | 0.122       | 0.82785     |
|           |           | 0.50633     | 0.19366772  | 0.17656      | 10.116       |           |           | 0.4506      | 0.155       | 0.8153      |
|           |           | 0.0893      | 0.610697    | 0.0717       | 4.1079       |           |           | 0           | 0.7         | 0.91        |
| $\bar{T}$ | $\bar{P}$ | $\bar{M}_x$ | $\bar{M}_y$ | $\phi, rad.$ | $\phi, deg.$ | $\bar{T}$ | $\bar{P}$ | $\bar{M}_x$ | $\bar{M}_y$ | $IR_{ASCE}$ |
| 0.1       | 0.4       | 0.48147     | 0.01852906  | 0.07849      | 4.4974       | 0.1       | 0.4       | 0.5         | 0           | 0.91        |
|           |           | 0.43568     | 0.06431679  | 0.10757      | 6.1635       |           |           | 0.4265      | 0.042       | 0.87833     |
|           |           | 0.38774     | 0.11225512  | 0.1284       | 7.3566       |           |           | 0.3644      | 0.089       | 0.86367     |
|           |           | 0.36389     | 0.13611425  | 0.13508      | 7.7394       |           |           | 0.3325      | 0.114       | 0.85655     |
|           |           | 0.05118     | 0.44882121  | 0.05591      | 3.2032       |           |           | 0           | 0.449       | 0.85882     |
| $\bar{T}$ | $\bar{P}$ | $\bar{M}_x$ | $\bar{M}_y$ | $\phi, rad.$ | $\phi, deg.$ | $\bar{T}$ | $\bar{P}$ | $\bar{M}_x$ | $\bar{M}_y$ | $IR_{ASCE}$ |
| 0.1       | 0.6       | 0.28994     | 0.01005969  | 0.07077      | 4.0546       | 0.1       | 0.6       | 0.3         | 0           | 0.91        |
|           |           | 0.26399     | 0.03600886  | 0.08282      | 4.7451       |           |           | 0.2597      | 0.025       | 0.89515     |
|           |           | 0.23482     | 0.06517706  | 0.09222      | 5.2837       |           |           | 0.2245      | 0.055       | 0.8895      |
|           |           | 0.2197      | 0.08031151  | 0.09537      | 5.4641       |           |           | 0.206       | 0.071       | 0.88663     |
|           |           | 0.02736     | 0.2726385   | 0.04921      | 2.8192       |           |           | 0           | 0.3         | 0.91        |
| $\bar{T}$ | $\bar{P}$ | $\bar{M}_x$ | $\bar{M}_y$ | $\phi, rad.$ | $\phi, deg.$ | $\bar{T}$ | $\bar{P}$ | $\bar{M}_x$ | $\bar{M}_y$ | $IR_{ASCE}$ |
| 0.1       | 0.8       | 0.09714     | 0.00285629  | 0.05997      | 3.4361       | 0.1       | 0.8       | 0.1         | 0           | 0.91        |
|           |           | 0.08877     | 0.01122674  | 0.06109      | 3.5004       |           |           | 0.0877      | 0.009       | 0.9063      |
|           |           | 0.07891     | 0.02108546  | 0.06182      | 3.5418       |           |           | 0.0765      | 0.019       | 0.90531     |
|           |           | 0.07364     | 0.02636486  | 0.06194      | 3.5488       |           |           | 0.0706      | 0.024       | 0.9048      |
|           |           | 0.00912     | 0.09089     | 0.04919      | 2.8186       |           |           | 0           | 0.1         | 0.91        |

**Table 37. Normalized Applied Loads for L=17 ft. and  $\bar{T} = 0.5$** 

| $\bar{T}$ | $\bar{P}$ | $\bar{M}_x$ | $\bar{M}_y$ | $\phi, rad.$ | $\phi, deg.$ | $\bar{T}$ | $\bar{P}$ | $\bar{M}_x$ | $\bar{M}_y$ | $IR_{ASCE}$ |
|-----------|-----------|-------------|-------------|--------------|--------------|-----------|-----------|-------------|-------------|-------------|
| 0.5       | 0         | 0.43765     | 0.062388    | 0.2907513    | 16.65882     | 0.5       | 0         | 0.44        | 0           | 0.68765     |
|           |           | 0.40617     | 0.093884    | 0.2997098    | 17.17211     |           |           | 0.38        | 0.04        | 0.670775    |
|           |           | 0.372448    | 0.127631    | 0.3058209    | 17.52225     |           |           | 0.32        | 0.08        | 0.652243    |
|           |           | 0.355535    | 0.144519    | 0.3075681    | 17.62235     |           |           | 0.29        | 0.1         | 0.642953    |
|           |           | 0.182803    | 0.318       | 0.2818417    | 16.14834     |           |           | 0           | 0.32        | 0.568       |
| $\bar{T}$ | $\bar{P}$ | $\bar{M}_x$ | $\bar{M}_y$ | $\phi, rad.$ | $\phi, deg.$ | $\bar{T}$ | $\bar{P}$ | $\bar{M}_x$ | $\bar{M}_y$ | $IR_{ASCE}$ |
| 0.5       | 0.2       | 0.26455     | 0.035483    | 0.2735652    | 15.67413     | 0.5       | 0.2       | 0.26        | 0           | 0.71455     |
|           |           | 0.245608    | 0.054462    | 0.2773628    | 15.89172     |           |           | 0.23        | 0.02        | 0.705518    |
|           |           | 0.225156    | 0.075534    | 0.3058209    | 17.52225     |           |           | 0.2         | 0.05        | 0.695916    |
|           |           | 0.214012    | 0.086002    | 0.2806659    | 16.08097     |           |           | 0.18        | 0.06        | 0.690258    |
|           |           | 0.105357    | 0.19465     | 0.2653732    | 15.20476     |           |           | 0           | 0.19        | 0.64465     |
| $\bar{T}$ | $\bar{P}$ | $\bar{M}_x$ | $\bar{M}_y$ | $\phi, rad.$ | $\phi, deg.$ | $\bar{T}$ | $\bar{P}$ | $\bar{M}_x$ | $\bar{M}_y$ | $IR_{ASCE}$ |
| 0.5       | 0.4       | 0.08865     | 0.01137     | 0.2615981    | 14.98847     | 0.5       | 0.2       | 0.09        | 0           | 0.73865     |
|           |           | 0.085275    | 0.014739    | 0.2617668    | 14.99813     |           |           | 0.08        | 0           | 0.737174    |
|           |           | 0.079707    | 0.02036     | 0.2619327    | 15.00764     |           |           | 0.07        | 0.01        | 0.73477     |
|           |           | 0.075777    | 0.025031    | 0.2620078    | 15.01194     |           |           | 0.07        | 0.02        | 0.733425    |
|           |           | 0.034718    | 0.066       | 0.2579061    | 14.77693     |           |           | 0           | 0.07        | 0.716       |

## 5.2 Interaction Relation for Biaxially Loaded Beam-Column with Flexural Shear and Torsion

Presented below is the more comprehensive interaction relation for the biaxially loaded beam-column including the normalized flexural shear and torsion.

$$\left( \frac{P_u}{P_c} + \frac{M_{ux}}{M_{cx}} + \frac{M_{uy}}{M_{cy}} \right) + \left( \frac{V_{ux}}{V_{cx}} + \frac{V_{uy}}{V_{cy}} + \frac{T_u}{T_c} \right)^\alpha \leq 1.0 \quad (193)$$

Table 43 represents the data for a 1 ft long biaxially loaded beam column with applied torsion at the midspan. The member was subjected to an applied bending moment at the top end about both the x and y axes. The first column in Table 43 shows the normalized torsion,  $\bar{T}$ , of 10%. The second column is the normalized axial load,  $\bar{P}$ . The third and the fourth columns are the normalized



bending moment including the second order effects about the x and the y axes,  $\overline{M}_x$  and  $\overline{M}_y$ , respectively. The fifth and sixth columns represent the normalized flexural shear in the x and y axis directions,  $\overline{V}_x$  and  $\overline{V}_y$ , respectively. The seventh column is the angle of twist,  $\phi$ , in degrees at the midspan. The rest of the columns, hereafter, represent a repetition of the previous columns calculated based on Reference 33. Using the curve fitting technique, the term  $\alpha$  in Equation 193 was found to be 2.0.

**Table 38. Normalized Applied Loads for L=1 ft. and  $\overline{T} = 0.1$**

| $\overline{T}$ | $\overline{P}$ | $\overline{M}_x$ | $\overline{M}_y$ | $\overline{V}_x$ | $\overline{V}_y$ | $\phi, deg.$ | $\overline{T}$ | $\overline{P}$ | $\overline{M}_x$ | $\overline{M}_y$ | $IR_{ASCE}$ |
|----------------|----------------|------------------|------------------|------------------|------------------|--------------|----------------|----------------|------------------|------------------|-------------|
| 0.1            | 0              | 0.336            | 0.0038           | 0                | 0.288            | 0.106226     | 0.1            | 0              | 0.33637          | 0                | 0.34637     |
| 0.1            | 0              | 0.315            | 0.3873           | 0.0269           | 0.269449         | 0.114956     | 0.1            | 0              | 0.31465          | 0.383419         | 0.708069    |
| 0.1            | 0              | 0.287            | 0.8776           | 0.0614           | 0.245634         | 0.124363     | 0.1            | 0              | 0.28684          | 0.873827         | 1.170667    |
| $\overline{T}$ | $\overline{P}$ | $\overline{M}_x$ | $\overline{M}_y$ | $\overline{V}_x$ | $\overline{V}_y$ | $\phi, deg.$ | $\overline{T}$ | $\overline{P}$ | $\overline{M}_x$ | $\overline{M}_y$ | $IR_{ASCE}$ |
| 0.1            | 0.2            | 0.31             | 0.0982           | 0.0066           | 0.26581          | 0.10913      | 0.1            | 0.2            | 0.3104           | 0.09456          | 0.61496     |
| 0.1            | 0.2            | 0.305            | 0.1896           | 0.0131           | 0.261383         | 0.111175     | 0.1            | 0.2            | 0.30523          | 0.18597          | 0.7012      |
| 0.1            | 0.2            | 0.3              | 0.278            | 0.0193           | 0.257092         | 0.113084     | 0.1            | 0.2            | 0.30022          | 0.274376         | 0.784596    |
| $\overline{T}$ | $\overline{P}$ | $\overline{M}_x$ | $\overline{M}_y$ | $\overline{V}_x$ | $\overline{V}_y$ | $\phi, deg.$ | $\overline{T}$ | $\overline{P}$ | $\overline{M}_x$ | $\overline{M}_y$ | $IR_{ASCE}$ |
| 0.1            | 0.3            | 0.305            | 0.0035           | 0                | 0.261571         | 0.107271     | 0.1            | 0.3            | 0.30545          | 0                | 0.61545     |
| 0.1            | 0.3            | 0.295            | 0.1834           | 0.0126           | 0.252849         | 0.111293     | 0.1            | 0.3            | 0.295265         | 0.179899         | 0.785164    |
| 0.1            | 0.3            | 0.291            | 0.2689           | 0.0187           | 0.2487           | 0.113106     | 0.1            | 0.3            | 0.29042          | 0.26542          | 0.86584     |

**Table 39. Normalized Applied Loads for L=5 ft. and  $\overline{T} = 0.1$**

| $\overline{T}$ | $\overline{P}$ | $\overline{M}_x$ | $\overline{M}_y$ | $\overline{V}_x$ | $\overline{V}_y$ | $\phi, deg.$ | $\overline{T}$ | $\overline{P}$ | $\overline{M}_x$ | $\overline{M}_y$ | $IR_{ASCE}$ |
|----------------|----------------|------------------|------------------|------------------|------------------|--------------|----------------|----------------|------------------|------------------|-------------|
| 0.1            | 0              | 0.72631          | 0.999784         | 0.010989         | 0.043958         | 7.983589     | 0.1            | 0              | 0.679            | 0.781888         | 1.470888    |
| 0.1            | 0              | 0.86175          | 0.345753         | 0.002769         | 0.055371         | 4.327484     | 0.1            | 0              | 0.85529          | 0.196978         | 1.062268    |
| 0.1            | 0              | 0.83826          | 0.455001         | 0.004017         | 0.053555         | 5.089176     | 0.1            | 0              | 0.82724          | 0.285777         | 1.123017    |
| $\overline{T}$ | $\overline{P}$ | $\overline{M}_x$ | $\overline{M}_y$ | $\overline{V}_x$ | $\overline{V}_y$ | $\phi, deg.$ | $\overline{T}$ | $\overline{P}$ | $\overline{M}_x$ | $\overline{M}_y$ | $IR_{ASCE}$ |
| 0.1            | 0.2            | 0.85717          | 0.248973         | 0.001382         | 0.055281         | 4.388968     | 0.1            | 0.2            | 0.8539           | 0.098329         | 1.162229    |
| 0.1            | 0.2            | 0.8301           | 0.36723          | 0.002662         | 0.05324          | 5.379644     | 0.1            | 0.2            | 0.82238          | 0.189399         | 1.221779    |
| 0.1            | 0.2            | 0.80684          | 0.471502         | 0.003855         | 0.051403         | 6.179041     | 0.1            | 0.2            | 0.794            | 0.274294         | 1.278294    |
| $\overline{T}$ | $\overline{P}$ | $\overline{M}_x$ | $\overline{M}_y$ | $\overline{V}_x$ | $\overline{V}_y$ | $\phi, deg.$ | $\overline{T}$ | $\overline{P}$ | $\overline{M}_x$ | $\overline{M}_y$ | $IR_{ASCE}$ |
| 0.1            | 0.3            | 0.8724           | 0.129552         | 0                | 0.056479         | 3.694428     | 0.1            | 0.3            | 0.8724           | 0                | 1.1824      |
| 0.1            | 0.3            | 0.83965          | 0.264686         | 0.001353         | 0.054121         | 5.011964     | 0.1            | 0.3            | 0.83599          | 0.096267         | 1.242257    |
| 0.1            | 0.3            | 0.81257          | 0.380206         | 0.002603         | 0.052057         | 6.03366      | 0.1            | 0.3            | 0.8041           | 0.185189         | 1.299289    |

**Table 40. Normalized Applied Load for L=9 ft. and  $\bar{T} = 0.1$** 

| $\bar{T}$ | $\bar{P}$ | $\bar{M}_x$ | $\bar{M}_y$ | $\bar{V}_x$ | $\bar{V}_y$ | $\phi, deg.$ | $\bar{T}$ | $\bar{P}$ | $\bar{M}_x$ | $\bar{M}_y$ | $IR_{ASCE}$ |
|-----------|-----------|-------------|-------------|-------------|-------------|--------------|-----------|-----------|-------------|-------------|-------------|
| 0.1       | 0         | 1           | 0.06971051  | 0           | 0.015981    | 3.958635     | 0.1       | 0         | 0.99        | 0           | 1           |
| 0.1       | 0         | 0.9998743   | 0.15066615  | 0.000398    | 0.015901    | 5.613632     | 0.1       | 0         | 0.995       | 0.050909    | 1.055909    |
| 0.1       | 0         | 0.9921595   | 0.22471061  | 0.000783    | 0.015661    | 7.109087     | 0.1       | 0         | 0.98        | 0.100283    | 1.090283    |
| $\bar{T}$ | $\bar{P}$ | $\bar{M}_x$ | $\bar{M}_y$ | $\bar{V}_x$ | $\bar{V}_y$ | $\phi, deg.$ | $\bar{T}$ | $\bar{P}$ | $\bar{M}_x$ | $\bar{M}_y$ | $IR_{ASCE}$ |
| 0.1       | 0.1       | 0.99999     | 0.08313304  | 0           | 0.01598     | 4.654793     | 0.1       | 0.1       | 0.99999     | 0           | 1.10999     |
| 0.1       | 0.1       | 0.9997217   | 0.16795787  | 0.000397    | 0.015885    | 6.596196     | 0.1       | 0.1       | 0.994       | 0.050858    | 1.154858    |
| 0.1       | 0.1       | 0.9996344   | 0.32437968  | 0.001167    | 0.015565    | 10.05298     | 0.1       | 0.1       | 0.974       | 0.149503    | 1.233503    |
| $\bar{T}$ | $\bar{P}$ | $\bar{M}_x$ | $\bar{M}_y$ | $\bar{V}_x$ | $\bar{V}_y$ | $\phi, deg.$ | $\bar{T}$ | $\bar{P}$ | $\bar{M}_x$ | $\bar{M}_y$ | $IR_{ASCE}$ |
| 0.1       | 0.2       | 1           | 0.10063301  | 0           | 0.015981    | 5.634597     | 0.1       | 0.2       | 1           | 0           | 1.21        |
| 0.1       | 0.2       | 0.9998211   | 0.19040709  | 0.000397    | 0.015869    | 7.871551     | 0.1       | 0.2       | 0.993       | 0.050807    | 1.253807    |
| 0.1       | 0.2       | 0.9968266   | 0.2724681   | 0.000783    | 0.015661    | 9.837675     | 0.1       | 0.2       | 0.98        | 0.100283    | 1.290283    |

### 5.3 Interaction Relation Comparisons

Presented herein is a comparison between the results from the proposed interaction relations of Equations 192 and 193 and the one from ASCE/Sei 74-23 Standard, Reference [33] for different loadings and lengths of 1 ft, 3 ft, 5 ft which correspond to slenderness ratios,  $\frac{L}{r_y}$ , 17, 51, and 85, respectively.

**Table 41. Interaction Relation for  $\frac{L}{r_y} = 17$** 

| $\bar{M}_x$ | $\bar{M}_y$ | $\bar{V}_x$ | $\bar{V}_y$ | $\bar{P}$ | $\bar{T}_{ASCE}$ | $\bar{T}_{No\_Shear}$ | $\bar{T}_{with\_Shear}$ |
|-------------|-------------|-------------|-------------|-----------|------------------|-----------------------|-------------------------|
| 0.4         | 0.4         | 0.056       | 0.171       | 0         | 0.447214         | 0.428668              | 0.2195213               |
| 0.4         | 0.4         | 0.056       | 0.171       | 0.05      | 0.387298         | 0.3684375             | 0.159606                |
| 0.4         | 0.4         | 0.056       | 0.171       | 0.1       | 0.316228         | 0.2976351             | 0.0885355               |
| 0.4         | 0.4         | 0.056       | 0.171       | 0.15      | 0.223607         | 0.2066557             | -0.0040855              |
| 0.4         | 0.4         | 0.056       | 0.171       | 0.2       | 3.16E-05         | 1.833E-05             |                         |

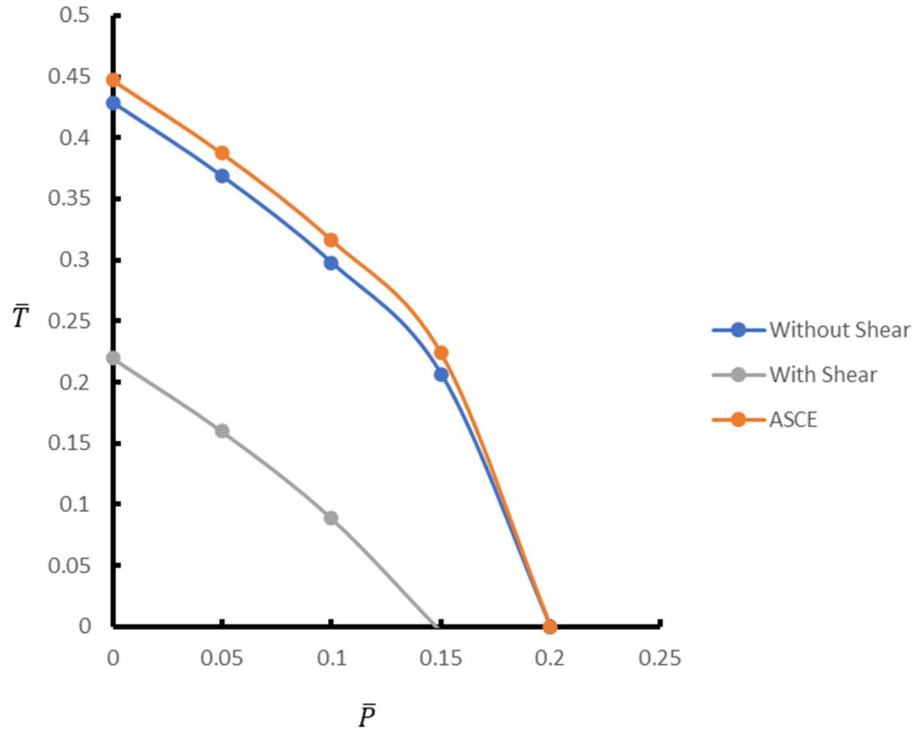


Figure 115. Interaction Relation for  $\frac{L}{r_y} = 17$

Table 42. Interaction Relation for  $\frac{L}{r_y} = 17$

| $\bar{M}_x$ | $\bar{M}_y$ | $\bar{V}_x$ | $\bar{V}_y$ | $\bar{P}$ | $\bar{T}_{ASCE}$ | $\bar{T}_{No\_Shear}$ | $\bar{T}_{with\_Shear}$ |
|-------------|-------------|-------------|-------------|-----------|------------------|-----------------------|-------------------------|
| 0.3         | 0.4         | 0.056       | 0.128       | 0         | 0.547723         | 0.5306408             | 0.3628508               |
| 0.3         | 0.4         | 0.056       | 0.128       | 0.05      | 0.5              | 0.482088              | 0.3151282               |
| 0.3         | 0.4         | 0.056       | 0.128       | 0.1       | 0.447214         | 0.428668              | 0.2623418               |
| 0.3         | 0.4         | 0.056       | 0.128       | 0.15      | 0.387298         | 0.3684375             | 0.2024265               |
| 0.3         | 0.4         | 0.056       | 0.128       | 0.2       | 0.316228         | 0.2976351             | 0.131356                |
| 0.3         | 0.4         | 0.056       | 0.128       | 0.25      | 0.223607         | 0.2066557             | 0.038735                |
| 0.3         | 0.4         | 0.056       | 0.128       | 0.2755    | 0.156525         | 0.1419687             | -0.028347               |
| 0.3         | 0.4         | 0.056       | 0.128       | 0.3       | 1E-05            | 5.456E-06             |                         |

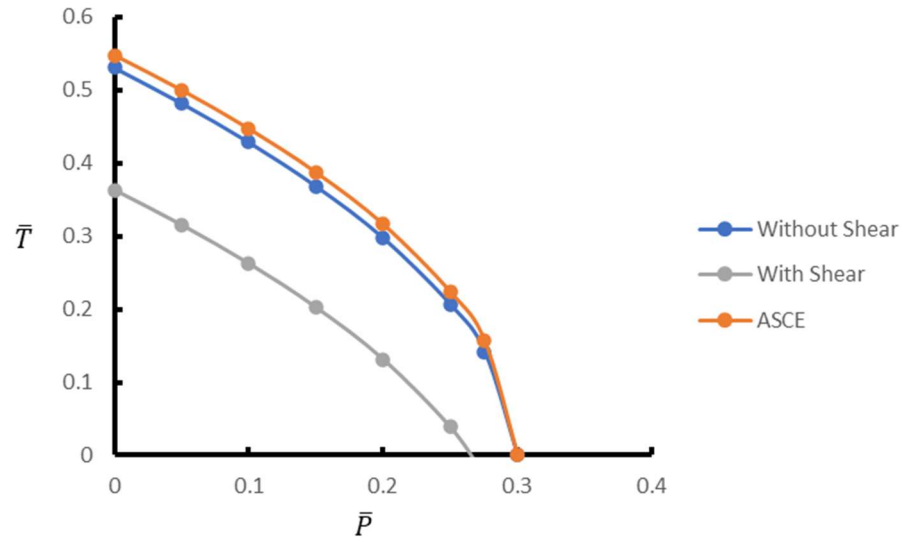
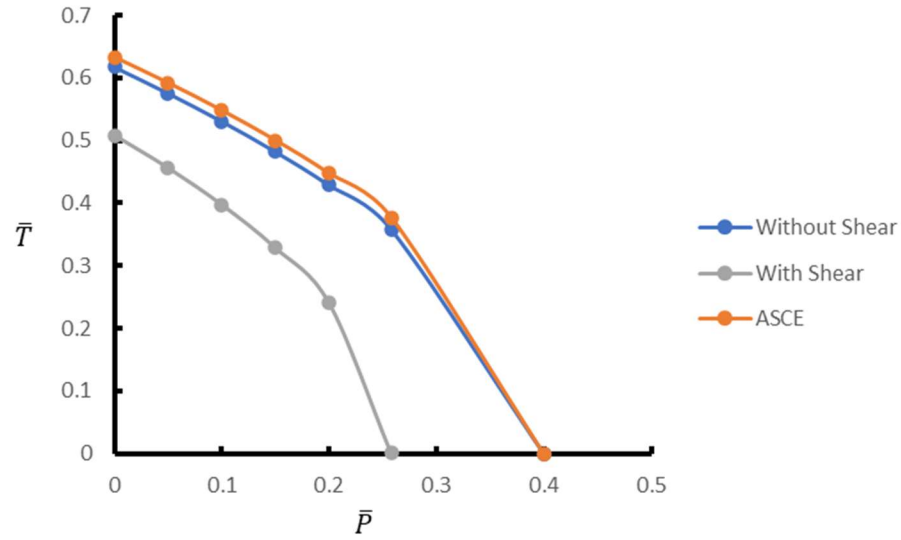


Figure 116. Interaction Relation for  $\frac{L}{r_y} = 17$

Table 43. Interaction Relation for  $\frac{L}{r_y} = 17$

| $\overline{M}_x$ | $\overline{M}_y$ | $\overline{V}_x$ | $\overline{V}_y$ | $\overline{P}$ | $\overline{T}_{ASCE}$ | $\overline{T}_{No\_Shear}$ | $\overline{T}_{with\_Shear}$ |
|------------------|------------------|------------------|------------------|----------------|-----------------------|----------------------------|------------------------------|
| 0.2              | 0.4              | 0.056            | 0.086            | 0              | 0.632456              | 0.6173876                  | 0.5078865                    |
| 0.2              | 0.4              | 0.056            | 0.086            | 0.05           | 0.591608              | 0.5754874                  | 0.4560139                    |
| 0.2              | 0.4              | 0.056            | 0.086            | 0.1            | 0.547723              | 0.5306408                  | 0.3974276                    |
| 0.2              | 0.4              | 0.056            | 0.086            | 0.15           | 0.5                   | 0.482088                   | 0.3285555                    |
| 0.2              | 0.4              | 0.056            | 0.086            | 0.2            | 0.447214              | 0.428668                   | 0.2407254                    |
| 0.2              | 0.4              | 0.056            | 0.086            | 0.2579         | 0.376898              | 0.3580303                  | 0.0009044                    |
| 0.2              | 0.4              | 0.056            | 0.086            | 0.4            | 0                     | 0                          |                              |



**Figure 117. Interaction Relation for  $\frac{L}{r_y} = 17$ .**

**Table 44. Interaction Relation for  $\frac{L}{r_y} = 17$**

| $\overline{M}_x$ | $\overline{M}_y$ | $\overline{V}_x$ | $\overline{V}_y$ | $\overline{P}$ | $\overline{T}_{ASCE}$ | $\overline{T}_{No\_Shear}$ | $\overline{T}_{with\_Shear}$ |
|------------------|------------------|------------------|------------------|----------------|-----------------------|----------------------------|------------------------------|
| 0.2              | 0.2              | 0.028            | 0.086            | 0              | 0.774597              | 0.7642536                  | 0.6608454                    |
| 0.2              | 0.2              | 0.028            | 0.086            | 0.1            | 0.707107              | 0.6943256                  | 0.5933555                    |
| 0.2              | 0.2              | 0.028            | 0.086            | 0.2            | 0.632456              | 0.6173876                  | 0.5187042                    |
| 0.2              | 0.2              | 0.028            | 0.086            | 0.3            | 0.547723              | 0.5306408                  | 0.4339713                    |
| 0.2              | 0.2              | 0.028            | 0.086            | 0.4            | 0.447214              | 0.428668                   | 0.3334623                    |
| 0.2              | 0.2              | 0.028            | 0.086            | 0.5            | 0.316228              | 0.2976351                  | 0.2024765                    |
| 0.2              | 0.2              | 0.028            | 0.086            | 0.587          | 0.114018              | 0.1017041                  | 0.0002663                    |
| 0.2              | 0.2              | 0.028            | 0.086            | 0.6            | 0.000316              | 0.0002069                  |                              |

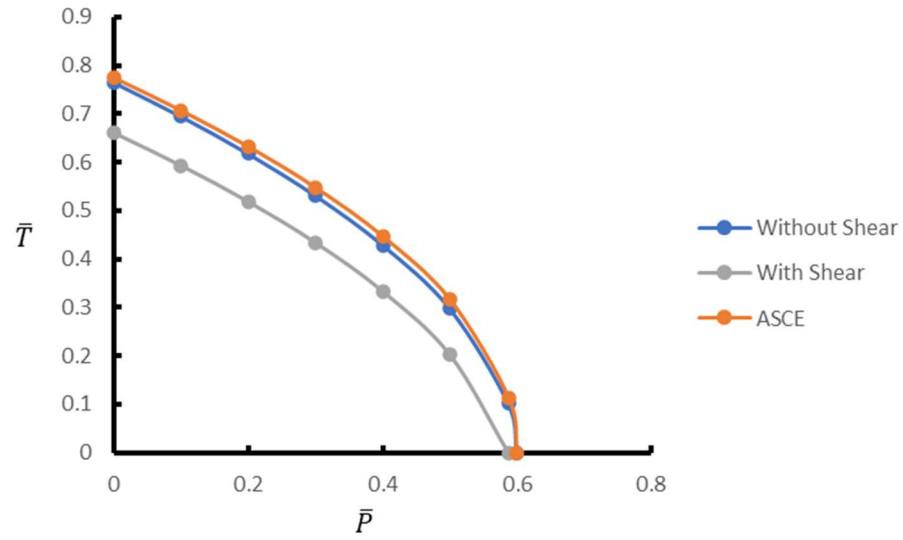


Figure 118. Interaction Relation for  $\frac{L}{r_y} = 17$

Table 45. Interaction Relation for  $\frac{L}{r_y} = 51$

| $\overline{M}_x$ | $\overline{M}_y$ | $\overline{V}_x$ | $\overline{V}_y$ | $\overline{P}$ | $\overline{T}_{ASCE}$ | $\overline{T}_{No\_Shear}$ | $\overline{T}_{with\_Shear}$ |
|------------------|------------------|------------------|------------------|----------------|-----------------------|----------------------------|------------------------------|
| 0.2              | 0.2              | 0.009            | 0.022            | 0              | 0.774597              | 0.7642536                  | 0.74335165                   |
| 0.2              | 0.2              | 0.009            | 0.022            | 0.1            | 0.707107              | 0.6943256                  | 0.67586177                   |
| 0.2              | 0.2              | 0.009            | 0.022            | 0.2            | 0.632456              | 0.6173876                  | 0.60121052                   |
| 0.2              | 0.2              | 0.009            | 0.022            | 0.3            | 0.547723              | 0.5306408                  | 0.51647754                   |
| 0.2              | 0.2              | 0.009            | 0.022            | 0.4            | 0.447214              | 0.428668                   | 0.41596858                   |
| 0.2              | 0.2              | 0.009            | 0.022            | 0.5            | 0.316228              | 0.2976351                  | 0.28498275                   |
| 0.2              | 0.2              | 0.009            | 0.022            | 0.599          | 0.031623              | 0.0263665                  | 0.00037776                   |
| 0.2              | 0.2              | 0.009            | 0.022            | 0.6            | 1.05E-08              | 4.007E-09                  |                              |

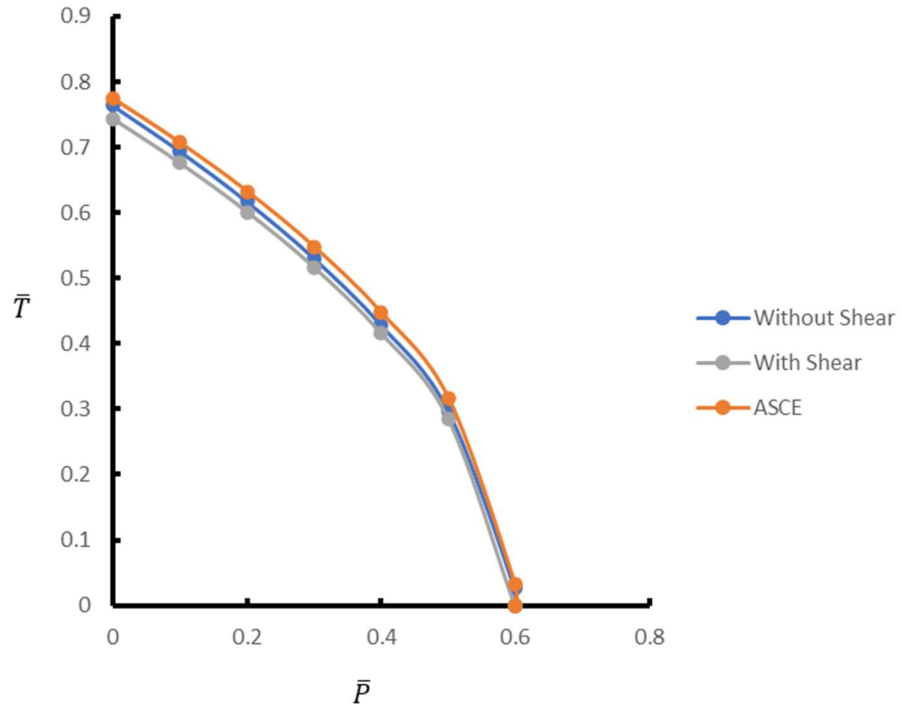


Figure 119. Interaction Relation for  $\frac{L}{r_y} = 51$

Table 46. Interaction Relation for  $\frac{L}{r_y} = 51$

| $\overline{M}_x$ | $\overline{M}_y$ | $\overline{V}_x$ | $\overline{V}_y$ | $\overline{P}$ | $\overline{T}_{ASCE}$ | $\overline{T}_{No\_Shear}$ | $\overline{T}_{with\_Shear}$ |
|------------------|------------------|------------------|------------------|----------------|-----------------------|----------------------------|------------------------------|
| 0.2              | 0.4              | 0.019            | 0.022            | 0              | 0.632456              | 0.6173876                  | 0.59180881                   |
| 0.2              | 0.4              | 0.019            | 0.022            | 0.1            | 0.547723              | 0.5306408                  | 0.50707583                   |
| 0.2              | 0.4              | 0.019            | 0.022            | 0.2            | 0.447214              | 0.428668                   | 0.40656687                   |
| 0.2              | 0.4              | 0.019            | 0.022            | 0.3            | 0.316228              | 0.2976351                  | 0.27558104                   |
| 0.2              | 0.4              | 0.019            | 0.022            | 0.399          | 0.031623              | 0.0263665                  | -0.0090239                   |
| 0.2              | 0.4              | 0.019            | 0.022            | 0.4            | 0                     | 0                          |                              |

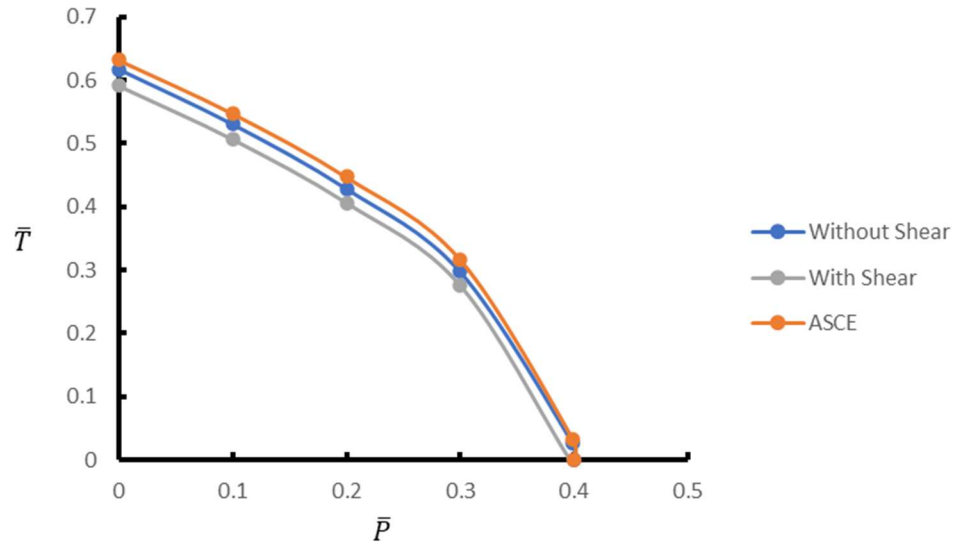


Figure 120. Interaction Relation for  $\frac{L}{r_y} = 51$

Table 47. Interaction Relation for  $\frac{L}{r_y} = 51$

| $\bar{M}_x$ | $\bar{M}_y$ | $\bar{V}_x$ | $\bar{V}_y$ | $\bar{P}$ | $\bar{T}_{ASCE}$ | $\bar{T}_{No\_Shear}$ | $\bar{T}_{with\_Shear}$ |
|-------------|-------------|-------------|-------------|-----------|------------------|-----------------------|-------------------------|
| 0.4         | 0.4         | 0.019       | 0.044       | 0         | 0.447214         | 0.428668              | 0.38472357              |
| 0.4         | 0.4         | 0.019       | 0.044       | 0.025     | 0.41833          | 0.3995756             | 0.35583998              |
| 0.4         | 0.4         | 0.019       | 0.044       | 0.05      | 0.387298         | 0.3684375             | 0.32480831              |
| 0.4         | 0.4         | 0.019       | 0.044       | 0.075     | 0.353553         | 0.334726              | 0.29106336              |
| 0.4         | 0.4         | 0.019       | 0.044       | 0.1       | 0.316228         | 0.2976351             | 0.25373774              |
| 0.4         | 0.4         | 0.019       | 0.044       | 0.125     | 0.273861         | 0.2558156             | 0.21137125              |
| 0.4         | 0.4         | 0.019       | 0.044       | 0.15      | 0.223607         | 0.2066557             | 0.16111677              |
| 0.4         | 0.4         | 0.019       | 0.044       | 0.197     | 0.054772         | 0.0470077             | -0.0077178              |
| 0.4         | 0.4         | 0.019       | 0.044       | 0.2       | 1E-05            | 5.456E-06             |                         |



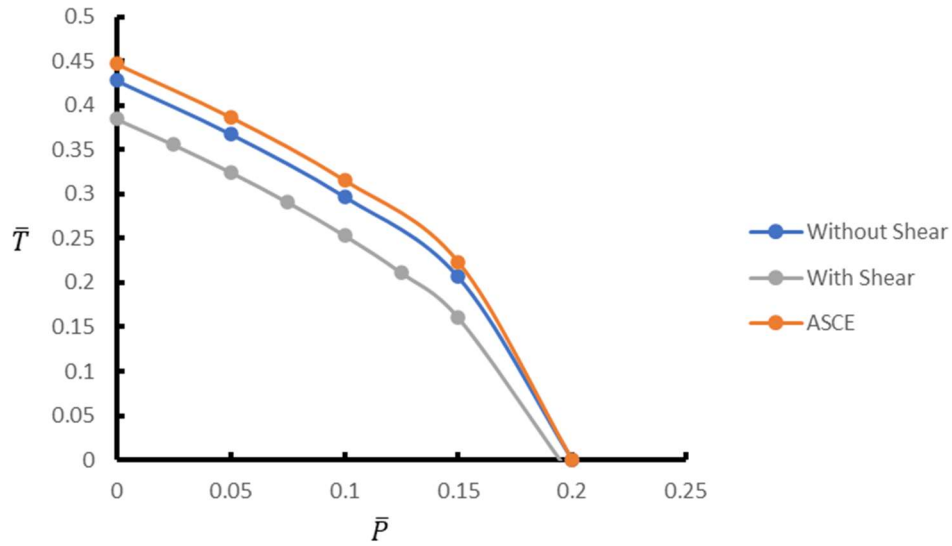


Figure 121. Interaction Relation for  $\frac{L}{r_y} = 51$

Table 48. Interaction Relation for  $\frac{L}{r_y} = 85$

| $\overline{M}_x$ | $\overline{M}_y$ | $\overline{V}_x$ | $\overline{V}_y$ | $\overline{P}$ | $\overline{T}_{ASCE}$ | $\overline{T}_{No\_Shear}$ | $\overline{T}_{with\_Shear}$ |
|------------------|------------------|------------------|------------------|----------------|-----------------------|----------------------------|------------------------------|
| 0.3              | 0.4              | 0.011            | 0.01             | 0              | 0.547723              | 0.5306408                  | 0.5268251                    |
| 0.3              | 0.4              | 0.011            | 0.01             | 0.05           | 0.5                   | 0.482088                   | 0.4791026                    |
| 0.3              | 0.4              | 0.011            | 0.01             | 0.1            | 0.447214              | 0.428668                   | 0.4263162                    |
| 0.3              | 0.4              | 0.011            | 0.01             | 0.15           | 0.387298              | 0.3684375                  | 0.3664009                    |
| 0.3              | 0.4              | 0.011            | 0.01             | 0.2            | 0.316228              | 0.2976351                  | 0.2953303                    |
| 0.3              | 0.4              | 0.011            | 0.01             | 0.2996         | 0.02                  | 0.0162784                  | -0.0008974                   |
| 0.3              | 0.4              | 0.011            | 0.01             | 0.3            | 1E-05                 | 5.456E-06                  |                              |

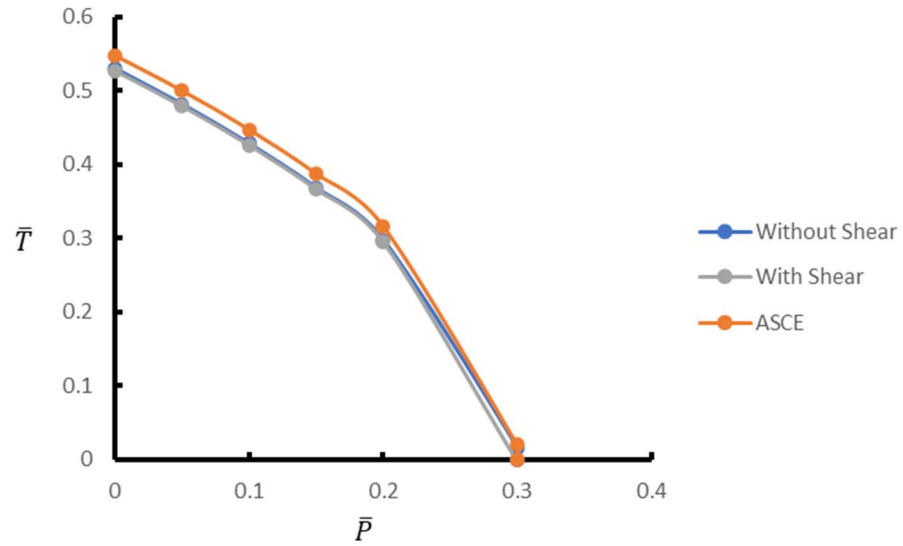


Figure 122. Interaction Relation for  $\frac{L}{r_y} = 85$ .

Table 49. Interaction Relation for  $\frac{L}{r_y} = 85$

| $\bar{M}_x$ | $\bar{M}_y$ | $\bar{V}_x$ | $\bar{V}_y$ | $\bar{P}$ | $\bar{T}_{ASCE}$ | $\bar{T}_{No\_Shear}$ | $\bar{T}_{with\_Shear}$ |
|-------------|-------------|-------------|-------------|-----------|------------------|-----------------------|-------------------------|
| 0.4         | 0.4         | 0.011       | 0.013       | 0         | 0.447214         | 0.428668              | 0.423111                |
| 0.4         | 0.4         | 0.011       | 0.013       | 0.05      | 0.387298         | 0.3684375             | 0.3631958               |
| 0.4         | 0.4         | 0.011       | 0.013       | 0.075     | 0.353553         | 0.334726              | 0.3294508               |
| 0.4         | 0.4         | 0.011       | 0.013       | 0.1       | 0.316228         | 0.2976351             | 0.2921252               |
| 0.4         | 0.4         | 0.011       | 0.013       | 0.125     | 0.273861         | 0.2558156             | 0.2497587               |
| 0.4         | 0.4         | 0.011       | 0.013       | 0.15      | 0.223607         | 0.2066557             | 0.1995042               |
| 0.4         | 0.4         | 0.011       | 0.013       | 0.175     | 0.158114         | 0.1434863             | 0.1340113               |
| 0.4         | 0.4         | 0.011       | 0.013       | 0.19941   | 0.02429          | 0.0199732             | 0.0001874               |
| 0.4         | 0.4         | 0.011       | 0.013       | 0.2       | 1E-04            | 6.158E-05             |                         |

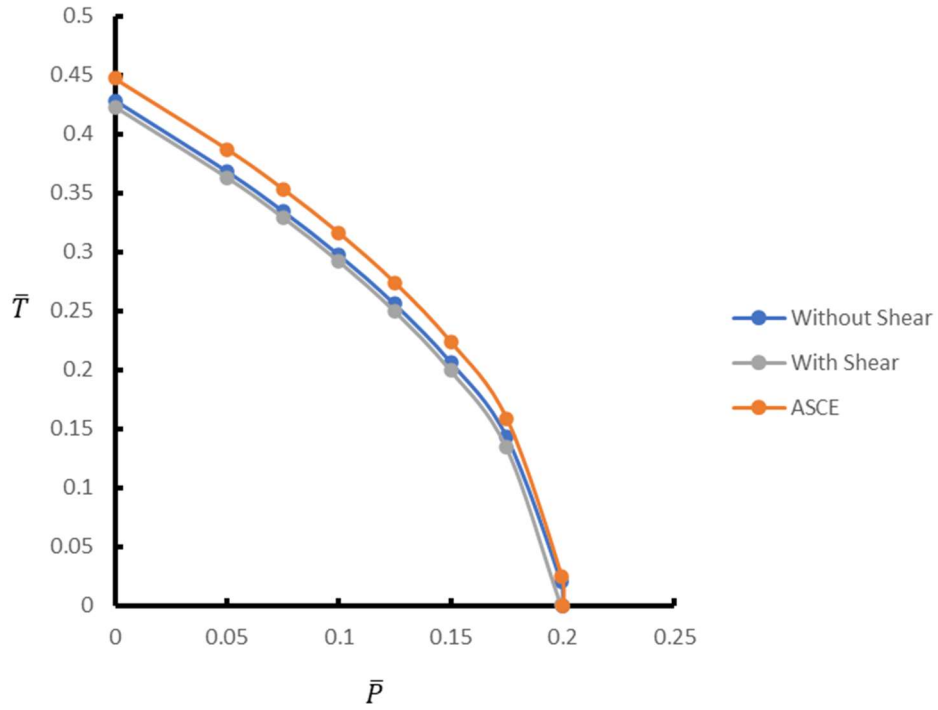
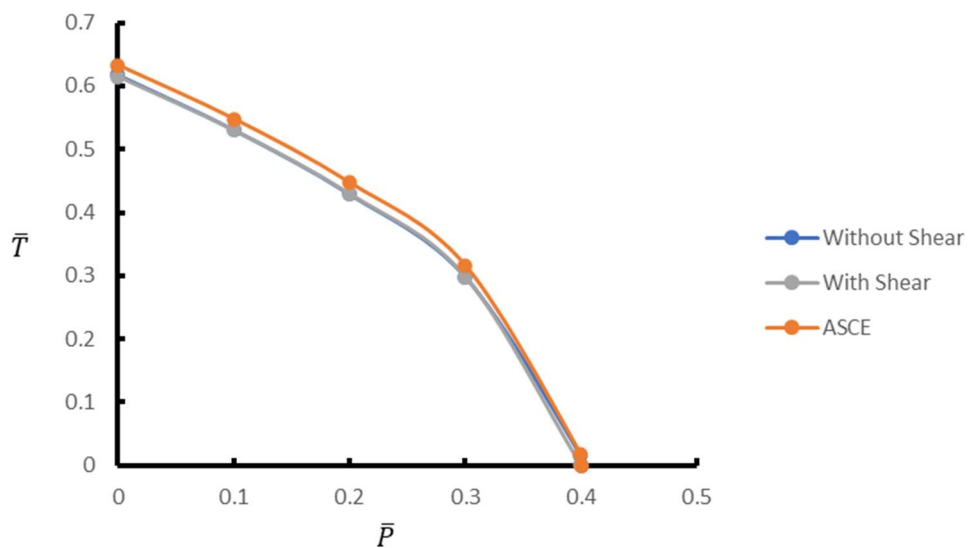


Figure 123. Interaction Relation for  $\frac{L}{r_y} = 85$

Table 50. Interaction Relation for  $\frac{L}{r_y} = 85$

| $\bar{M}_x$ | $\bar{M}_y$ | $\bar{V}_x$ | $\bar{V}_y$ | $\bar{P}$ | $\bar{T}_{ASCE}$ | $\bar{T}_{No\_Shear}$ | $\bar{T}_{with\_Shear}$ |
|-------------|-------------|-------------|-------------|-----------|------------------|-----------------------|-------------------------|
| 0.2         | 0.4         | 0.011       | 0.006       | 0         | 0.632456         | 0.6173876             | 0.6147632               |
| 0.2         | 0.4         | 0.011       | 0.006       | 0.1       | 0.547723         | 0.5306408             | 0.5300302               |
| 0.2         | 0.4         | 0.011       | 0.006       | 0.2       | 0.447214         | 0.428668              | 0.4295213               |
| 0.2         | 0.4         | 0.011       | 0.006       | 0.3       | 0.316228         | 0.2976351             | 0.2985355               |
| 0.2         | 0.4         | 0.011       | 0.006       | 0.39966   | 0.01852          | 0.0150131             | 0.000828                |
| 0.2         | 0.4         | 0.011       | 0.006       | 0.4       | 0                | 0                     |                         |



**Figure 124. Interaction Relation for  $\frac{L}{r_y} = 85$**

As anticipated, shorter members tend to experience greater shear forces. When incorporating this force into the interaction relation, it leads to increased deviation from the ASCE-LRFD Pre-Standard Equation 164, in addition to the impact of the neglected warping effect.

## CHAPTER 6

### CONCLUSIONS AND FUTURE RESEARCH

#### 6.1 Conclusions

Within the range of the geometric and material variables considered, and the results from the experimental and theoretical study of the behavior of the biaxially loaded glass fiber reinforced polymer (glass FRP) beam-columns with applied torque presented in this dissertation, the following conclusions are drawn.

1. The theoretically predicted applied torsional moment versus the maximum angle of twist relationship is found to be practically identical to that based on the experimental results up to 2.6 degrees whereafter the test member eventually develops an angle of twist larger than 45 degrees and exhibits a geometrically nonlinear response without developing any cracking.
2. The theoretical axial load-carrying capacity agrees well with that observed experimentally and is found to be only 1.8 percent less than that found experimentally.
3. The experimental load-deflection response of the members under combined axial load, bending moments, and torsional loading schemes resulted in nearly the same stiffness characteristics in the elastic range as predicted theoretically; however, the ultimate loads could not be achieved experimentally due to excessive cracking in and around the flange connection-holes at the member bottom end.
4. The interaction expression formulated in this dissertation including both warping and shear deformations effects is found to be more conservative than that given in the ASCE-LRFD Pre-Standard.

5. In the presence of biaxial bending moments and an absence of the axial load, the ASCE-LRFD interaction expression results in up to a 204 percent unconservative estimate for the member torsional moment capacity.
6. Whereas the torsional moment capacity is found to be zero in the presence of biaxial bending moments including warping and shear deformation effects in the theory presented, the ASCE-LRFD expression un-conservatively predicts a torsional moment capacity of up to 23.2 percent.
7. The influence of the shear deformation effects on the member load-carrying capacity gradually decreases as its slenderness ratio increases.

In summary, the study reveals the combined influence of both warping and shear deformations on the strength of FRP beam-columns with applied torsion and culminates in the formulation of an interaction expression of possible use by analysts and designers. The results also show that the current ASCE-LRFD Pre-Standard is providing unconservative ultimate strength estimates for the type of combined loading considered herein.

## **6.2 Future Research**

Future studies can include the development of load-moment-shear-torsion interaction relations for members with singly-symmetric and unsymmetric cross sections. A number of corresponding experimental investigations also need to be conducted to validate the theoretical predictions.

## REFERENCES

1. Sirjani, M., and Razzaq, Z., “Lateral-Torsional Buckling of FRP I-Section Beams.” *Global Journal of Research in Engineering: Civil and Structural Engineering* 16, no. 5 (2016).
2. Lin, Z., D. Polyzois, and A. Shah. “Stability of Thin-Walled Pultruded Structural Members by the Finite Element Method.” Elsevier Science Limited, *Thin-Walled Structures*, 24 (February 28, 1995): 1–18.
3. Cardoso, D., Harries A K., and Batista M. E., “Compressive Strength Equation for GFRP Square Tube Columns.” *Composites Part B: Engineering* 59 (March 2014): 1–11.
4. Ascione, F., Lamberti M., and Razaqpur G., “Modifications of Standard GFRP Sections Shape and Proportions for Improved Stiffness and Lateral-Torsional Stability.” *Composite Structures* 132 (November 2015)
5. Razzaq, Z., Prabhakaran R., and Mike M. Sirjani. “Load and Resistance Factor Design (LRFD) Approach for Reinforced-Plastic Channel Beam Buckling.” *Composites Part B: Engineering* 27, no. 3–4 (January 1996): 361–69.
6. Konate, M., and Razzaq. Z., “Failure Modes For I-Section GFRP Beams.” *Global Journal of Research in Engineering*, January 6, 2016.
7. Nunes, F., M. Correia, J.R. Correia, N. Silvestre, and A. Moreira. “Experimental and Numerical Study on the Structural Behavior of Eccentrically Loaded GFRP Columns.” *Thin-Walled Structures* 72 (November 2013): 175–87.
8. Barbero, E. J., and DeVivo L. “Beam-Column Design Equations for Wide-Flange Pultruded Structural Shapes.” *Journal of Composites for Construction* 3, no. 4 (November 1999): 185–91.

9. Davalos, J. F., Pizhong Q., and Hani A. S. "Flexural-Torsional Buckling of Pultruded Fiber Reinforced Plastic Composite I-Beams: Experimental and Analytical Evaluations." *Composite Structures* 38, no. 1–4 (May 1997): 241–50.
10. Brooks, R.J., and G.J. Thrvey. "Lateral Buckling of Pultruded GRP I-Section Cantilevers." *Composite Structures* 32, no. 1–4 (January 1995): 203–15,
11. Yoon, S., Jung, J., & Jang, W. (1993). Elastic Web Buckling Strength of Pultruded Flexural Members. *KEM Key Engineering Materials*, 621-626.
12. Barbero, E., & Yiannis, R., I. Lateral and distortional buckling of pultruded I-beams. *Composite Structures*, 261-268.
13. Kubiak, T. "Numerical Model of Post buckling Behavior of GFRP Beams Subjected to Pure Bending." *International Journal for Computational Methods in Engineering Science and Mechanics* 18, no. 1 (January 2, 2017).
14. Smith, S.J., and L.C. Bank. "Modifications to Beam Theory for Bending and Twisting of Open-Section Composite Beams — Experimental Verification." *Composite Structures* 22, no. 3 (January 1992): 169–77.
15. Giosuè, B., Casalegno C., Russo S., and J. Toby Mottram. "Buckling of Built-Up Columns of Pultruded Fiber-Reinforced Polymer C-Sections." *Journal of Composites for Construction* 18, no. 4 (August 2014): 04013050.
16. Yang, Z., Wu, G., and Harries, K. A. "Determination of Critical Load for Global Flexural Buckling in Concentrically Loaded Pultruded FRP Structural Struts." *Engineering Structures* 158 (March 2018): 1–12.



17. Sirjani, M. B., and Razzaq, Z. "Stability of FRP Beams under Three-Point Loading and LRFD Approach." *Journal of Reinforced Plastics and Composites* 24, no. 18 (December 2005): 1921–27.
18. Lawrence C. B., Yin J., and Nadipelli M. "Local Buckling of Pultruded Beams — Nonlinearity, Anisotropy and Inhomogeneity." *Construction and Building Materials* 9, no. 6 (December 1995): 325–31.
19. Vanevenhoven, L. M., Carol K. Shield, and Bank, C. L. Bank. "LRFD Factors for Pultruded Wide-Flange Columns." *Journal of Structural Engineering* 136, no. 5 (May 2010): 554–64.
20. Ever, B. "Structural Design Equation for FRP Column." *Materials Engineering* 6 (1995): 197–210.
21. Chen, W., & Atsuta, T. *Space behavior and design* (Vol. 2). New York USA: McGraw-Hill. 1977
22. Galambos, T. *Structural members and frames*. Englewood Cliffs, N.J.: Prentice-Hall, 1968.
23. Heins, C.P. *Bending and Torsional Design in Structural Members*. First edition. Lexington, Massachusetts: Lexington Books, 1975.
24. Timoshenko, S., & Gere, J. *Theory of elastic stability*. Second edition. Mineola, N.Y.: Dover Publications, 1961.
25. Horne, M. R. & Merchant, W. *The Stability of Frames*. First edition. London: Pergamon Press Ltd., 1965
26. Chen, W.F. & Lui, E.M., *Stability Design of Steel Frames*. First edition. USA: CRC Press Inc. 1991.
27. Timoshenko, S., & Gere, J. *Mechanics of Materials*. Fourth edition: PWS Publishing Company. 1990.

28. Mario, S and Melvin, B. Numerical Methods in Engineering. Second edition. Englewood Cliffs, N.J.: Prentice-Hall, Inc. July 1962.
29. Vlasov, V. Z. Thin-Walled Elastic Beams (Second Edition).: National Science Foundation. 1961.
30. Kollbrunner, C. F., & Basler, K. Torsion in Structures: An Engineering Approach (1st ed.): Springer-Verlag. 1969.
31. Timoshenko, S., & Gere, J. Theory of Elasticity. Fourth edition: McGraw-Hill Book Co., New York, 1951.
32. Boresi, A., Sidebottom, O., Seely, F. & Smith, J. Advanced Mechanics of Materials. Third edition: John Wiley and Sons. New York. 1978.
33. ASCE 74-23 Standard for Load & Resistance Factor Design (LRFD) of Pultruded Fiber Reinforced Polymer (FRP) Structures : American Society of Civil Engineers. 2003.
34. The Pultex Pultrusion Design Manual (Imperial Version): Creative Pultrusion, Inc. 2004
35. Ziemian, R. Guide to stability design criteria for metal structures (6th ed.). Hoboken, N.J.: John Wiley & Sons. 2010.
36. Steel construction manual (14.th Ed.). Milwaukee, WI: AISC. 2014.
37. Timoshenko, Strength of Materials, Part I, Elementary Theory and Problems. Second Edition: D. Van Nostrand Company, Inc. 1940.
38. Wang, C. M., Reddy, J. N., & Lee, K. H. Shear Deformable Beams and Plates, Relationships with Classical Solutions: Elsevier 2005.
39. Irving, S., and Dym C. Energy and Finite Element Methods in Structural Mechanics. First. New York: CRC Press, 1985.

40. Sirjani, M. Fiber-Reinforced Plastic Composite Beam Stability and Load and Resistance Factor Design Approach. PhD Dissertation: ODU.1998.
41. Hampton, W. Lateral-Torsional Instability and Biaxial Flexure of Continuous GFRP Beams Including Warping and Shear Deformations. PhD Dissertation: ODU. 2020.
42. Knorowski, J. Behavior of FRP I-Beam Members Subjected to Biaxial Bending Various Reference Load Heights, and Kevlar Fabric Retrofit. Master's Thesis: ODU. 2012.
43. AL-Huazi, A. Experimental and Predicted Behavior of FRP Beam-Columns Including Retrofitting. Master's Thesis: ODU. 2015.
44. The Pultex Pultrusion Design Manual of Standard and Customer Fiber Reinforced Polymer Structural Profiles. Volume 5, Revision 11: Creative Pultrusions, Inc. 2020.

## VITA AUCTORIS

Emad M. Amin was born on June 6, 1968, in Baghdad, Iraq. He received his B.S. in Civil Engineering from the University of Technology in Baghdad, Iraq, in 1991. After graduation, he joined the Military Engineering Corps and contributed to infrastructure rebuilding efforts. He later worked with several engineering firms in both Baghdad, Iraq, Amman, Jordan, and Richmond, VA. He pursued further education, obtaining an MBA in Accounting and Finance from South University in 2005. In 2015, he earned his M.S in Structural Engineering from Old Dominion University and continued to pursue a Ph.D. degree in Structural Engineering. Currently, he is a senior engineer at Dominion Energy – Civil Design Group and a member of ASCE 4 Task Committee on Dynamic Analysis of Nuclear Structures.

10916 Rickey Court  
Glen Allen, VA 23060